# Dynamics and Synchrony of Pancreatic beta-cells and Islets

**Pedersen, Morten Gram; Sørensen, Mads Peter**

*Publication date:*
2006

*Document Version*
Publisher's PDF, also known as Version of record

# Dynamics and Synchrony of Pancreatic $\beta$-cells and Islets

Morten Gram Pedersen

June 23, 2006

# Summary

Pancreatic $\beta$-cells secrete insulin in response to raised glucose levels. Malfunctioning of this system plays an important role in the metabolic disease diabetes. The biological steps from a glucose stimulus to the final release of insulin are incompletely understood, and a more complete description of these processes and their interactions would provide important input in the search for a better treatment of the disease.

This thesis describes several aspects of mathematical modeling of $\beta$-cells relevant for the understanding of glucose stimulated insulin secretion. It consists of an introductory part with successive chapters tying together the ten original articles, which I have (co-) published, or submitted for publication, during my ph.d. studies. These papers consist the last and most substantial part of the thesis. Besides the results presented in the articles, I have included new, preliminary results in chapters 3, 4 and 5 concerning, respectively, stochastic events in $\beta$-cells, excitation wave propagation and entrainment of insulin pulses to a periodic glucose stimulus.

The title of the thesis indicates that it provides a study of dynamic aspects of $\beta$-cell biology with attention to the difference between single cell behavior and the synchronized behavior of many coupled $\beta$-cells as well as to the synchrony of islets. Rather than developing new biophysical models, I have studied existing models, their integration and simplifications, and analyzed the corresponding dynamics, in order to use these models for investigating biological hypotheses. Thus, the reader who looks for models of so-far unexploited parts of $\beta$-cell biology will look in vain. Rather, I have aimed at harvesting the advantage of models compared to real biology: The precise description of the underlying assumptions and mechanisms, which allows us to test well-defined hypotheses without confounding 'unknowns' in the system.

The questions addressed are: Quasi-steady-state approximations of enzyme reactions (Chapter 2, *Paper V* and *Papers VIII-X*), the effect of noise on bursting electrical behavior (Chapter 3, *Paper III* and *Paper VI*), excitation wave propagation in pancreatic islets (Chapter 4, *Paper I* and *Paper II*), intra- and inter-islet synchronization and pulsatile insulin secretion (Chapter 5 and *Paper IV*), and mitochondrial dynamics (Chapter 6 and *Paper VII*). Finally, I suggest future directions for $\beta$-cell modeling in Chapter 7.

# Preface

I got introduced to mathematical biology as an exchange student at the Department of Mathematics, University of Columbia, Vancouver, Canada, where Professor Robert Miura gave a course on the topic during the fall of 1999. As the final course project, he suggested me to work on models of $\beta$-cells, since he knew that researchers in Denmark had been, and are still, working on the subject. When I finished my Master of Science at the University of Copenhagen and was looking for a possible ph.d. project on mathematical biology, I contacted Professor Miura, who kindly suggested me to contact my ph.d. supervisor, Mads Peter Sørensen.

Mads Peter has let me develop freely starting off from his previous work on wave propagation. I thank him for always believing in my ideas based on the phrase (I quote him from my memory): "Don't interfere with a project that is going well". To have this freedom and support has been invaluable during my many travels and collaborations around the globe. At the same time, Mads Peter never left me alone, but was always interested in my work, and had always time for a discussion about an idea or a manuscript.

Besides him, I would like to thank a number of people, who have made these last four years during which I have worked on the project a truly enjoyable time.

Here it would be appropriate to mention that I have had a year of leave, thus explaining the *four* years, due to receiving the amazing scholarship "Rejselegat for matematikere" (Travelling Scholarship for Mathematicians), which was used to spend time at research laboratories in Rome, Italy, Rio de Janeiro, Brazil and Bethesda, Maryland, USA. I thank warmly late Valdemar Julius Andersen and his wife, Else Andersen, for founding such an scholarship, hoping that all wealthy people would think like they did. Let me thank Andrea De Gaetano, IASI, CNR, Rome, Marcelo Viana, IMPA, Rio de Janeiro and Arthur Sherman, NIH, Bethesda for letting me stay and work at their respective institutes during the travel.

Tom Høholdt, the responsible faculty member for the ph.d. students at MAT, receives a warm thought for not only supporting but encouraging my staying in Italy for extended periods. Rather than keeping the department or the mathematician at center stage, Tom is ready to support the person inside the mathematician. A great human capacity!

Also thanks to Alberto Bersani for having me visiting DMMM, Università La Sapienza, Rome, and to Alberto and Enrico for their warm and friendly personalities, which have made my stays in Rome really wonderful. *Ringrazio particularmente "Il Baretto" su Viale Ippocrate per sostegno e svago.*

My stay in Padova has also been a truly memorable one. To visit the great capacities of Professors Claudio Cobelli and Gianna Toffolo, Bioengineering group, University of Padova, is a pleasure for any young researcher in this area. I am happy to be able to say that from January, I will again stay in Padova for a Post. Doc. project with Prof. Cobelli as supervisor.

Let me also mention and thank Professor Erik Mosekilde and Anne Marie Clemensen, FYS, DTU, coordinator and administrator, respectively, of the European Network of Excellence BioSim. First of all for offering me a Post. Doc. position for the fall 2006. It is a privilege to have a job immediately after finishing my ph.d. But more importantly for creating a focus point for European mathematical biology right here at DTU.

But above all these people shines my star, whom I met at the very first days of my ph.d. in the beautiful town of Urbino, Italy. You have lived with traveling, long periods far from each other, staying away from your friends and family, but have always done what was possible in order for me to pursue my professional goals. To have a support like yours is more than I could ever ask for, and it has taught me that work and career, intellectual stimuli and conquests, are nothing and meaningless compared to the true beauty. Grazie, amore mio.

Morten Gram Pedersen

Copenhagen, June 2006

# Contents

# List of papers

This thesis is based on the following papers referred to by roman numerals.

# Chapter 1

# Glucose, insulin and diabetes

Glucose (sugar) is an utmost important energy source for the human body. The brain works almost exclusively on glucose and requires large amounts of this substrate. An insufficient concentration of glucose in the blood (plasma glucose) can lead to drowsiness, fainting, coma and even death. On the other hand, too high glucose levels are also dangerous leading to kidney failure, heart diseases and other serious complications.

Our body has developed a finely tuned control system to keep the plasma glucose concentration in a fairly narrow range (4-7 mM), and the failure of this system is what characterizes diabetes. Diabetes is one of the western worlds most widespread diseases, and the World Health Organization (WHO) has described the current development as a "diabetes epidemic" (Wild et al., 2004). This has lead to extensive research in the reasons for and implications of the disease.

This chapter gives the necessary biological background for the following, more mathematical chapters.

## 1.1 The glucose/insulin feedback system

The discovery of insulin by Frederick Banting and Charles Best in Toronto in 1921 opened up for an understanding and treatment of diabetes. Insulin is a hormone secreted from the pancreas into the blood in response to glucose and other stimuli, and its main effect is to signal to cells in the body that they should increase the uptake of glucose. The glucose is then either used as a fuel, for example in muscles, or stored as glycogen in the liver for later use, in this way decreasing plasma glucose levels. On the other hand, low glucose levels reduce the amount of insulin released such that the body uses less glucose, keeping the glucose supply for the brain at sufficient levels. Hence, the glucose/insulin system constitutes a classical negative feedback system as, e.g., a normal thermostat. It should be noted that the glucose consumption in the brain is unaffected by insulin since a steady supply of sugar is so crucial for the brain.

Insulin controls the blood sugar levels in concert with other hormones of which glucagon plays an important role. This hormone is also secreted from the pancreas, but it has the opposite effect of insulin. It is secreted in response to low glucose levels, and promotes breakdown of glycogen to glucose in the liver in this way raising the plasma glucose

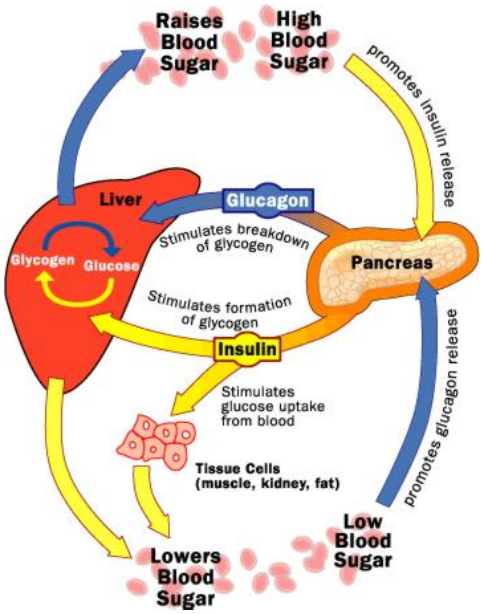


Figure 1.1: Glucose is controlled by glucagon and insulin through feedback processes (from http://health.howstuffworks.com).

concentration. This effect of glucagon is counteracted by insulin, see Fig. 1.1.

Diabetes occurs as the result of either insufficient production and secretion of insulin (type I diabetes), or as an insufficient efficacy of insulin signaling in the target cells despite of fairly high plasma insulin levels, a phenomenon known as insulin resistance. Insulin resistance is the main symptom in type II diabetes, which is by far the most common type in the western world. Usually people develop insulin resistance before entering the diabetic state of the disease. This is because at the beginning of the disease the pancreas is still able to compensate for the insulin resistance by releasing more insulin. If the disease is not reversed, the pancreas can eventually not keep up to the demand and diabetes develops.

### 1.1.1 Plasma glucose and insulin oscillations

The dynamics of plasma glucose and insulin is complex and far from static. Glucose is known to fluctuate on at least two time scales. The so-called *ultradian* oscillations have a period of 80-170 minutes, and are believed to be a result of the glucose/insulin feedback system (Sturis et al., 1991). Superimposed on these slow oscillations are faster fluctuations with a period of 4-10 minutes, which are paralleled by insulin oscillations with a similar time scale (Lang et al., 1979; Goodner et al., 1982; Sturis et al., 1993; Pørksen et al., 2000; Pørksen, 2002). In contrast to the ultradian oscillations, the fast insulin oscillations do not seem to be a result of systemic feedback mechanisms, but are believed to be a result of pulsatile insulin secretion (Chou and Ipp, 1990; Sturis et al., 1994; Ritzel et al., 2003; Pørksen, 2002). However, it is plausible that the fast glucose and insulin fluctuations interact to provide a synchronization mechanism (Sturis et al., 1994; Pørksen, 2002) as studied in *Paper IV*.

## 1.2 The islet of Langerhans

As mentioned above insulin is released from the pancreas. The hormone secreting endocrine cells constitute a very small part of the pancreas, and are located in some millions micro-organs called pancreatic islets of Langerhans. The islets consist of four kinds of cells; insulin-secreting $\beta$-cells, glucagon-releasing $\alpha$-cells, somatostatin-producing $\delta$-cells and pancreatic polypeptide-containing PP-cells, and each islet contains of the order of 2000-4000 cells (Kulkarni, 2004). In rodents the relative distribution in an islet is approximately 65-90 % $\beta$-cells, 15-20 % $\alpha$-cells, 3-10 % $\delta$-cells and 1 % PP-cells (Brissova et al., 2005; Kulkarni, 2004; Ashcroft and Rorsman, 1989; Cabrera et al., 2006), but humans have a quite different distribution with approximately 55 % $\beta$-cells, 35 % $\alpha$-cells and 10 % $\delta$-cells, and have a greater inter-subject variation, as well as a different architecture of the islet, compared to mice (Brissova et al., 2005; Cabrera et al., 2006). This thesis study the insulin secreting $\beta$-cells, which are directly coupled within an islet by gap junctions (Meissner, 1976; Eddlestone et al., 1984), which are small pores in the plasma membrane that allows diffusion of ions and even small molecules between the cytoplasm of the coupled cells. However, $\beta$-cells do not seem to be coupled electrically to the other types of islet cells, nor are these other cells coupled among each other, but paracrine (cell signaling in which the target cell is close to the signal releasing cell) interactions between the different groups of cells do exist (Nadal et al., 1999; Göpel et al., 1999b).

## 1.3 Glucose Stimulated Insulin Secretion (GSIS)

Although several physiological and pharmacological stimuli, such as glyceraldehyde, glucagon and sulphonylureas, lead to insulin release from $\beta$-cells, glucose is by far the most important of these (Ashcroft and Rorsman, 1989).

Insulin release is the last step of the process starting with insulin synthesis, packaging of insulin in secretory granules, granule trafficking between different pools, docking and priming of granules in the membrane and finally the exocytotic process, where insulin is released into the blood (Orci, 1985; Rorsman et al., 2000). Little is known of this movement or about the dynamics of docked granules, but due to improved experimental techniques, this has been changing recently (Niki et al., 2003; Kwan and Gaisano, 2005).

It is widely accepted that glucose stimulate insulin secretion through both triggering and amplifying pathways (Henquin, 2000). The triggering pathways are characterized by leading to the signal that triggers insulin release, namely an increased intracellular calcium concentration. The main pathway through which this occurs in glucose stimulated insulin secretion (GSIS) is described as follows (Ashcroft and Rorsman, 1989; Henquin, 2000). Glucose is broken down glycolytically, and the resulting pyruvate is further metabolized in the mitochondria. Through oxidative phosphorylation ATP is produced, and the increase in the ATP/ADP ratio closes ATP-sensitive potassium channels (K(ATP) channels) in the plasma membrane. The cell then depolarizes, thus opening voltage sensitive $Ca^{2+}$ -channels through which calcium enters the cell finally triggering insulin release. This is summarized in Fig. 1.2. The amplifying pathways

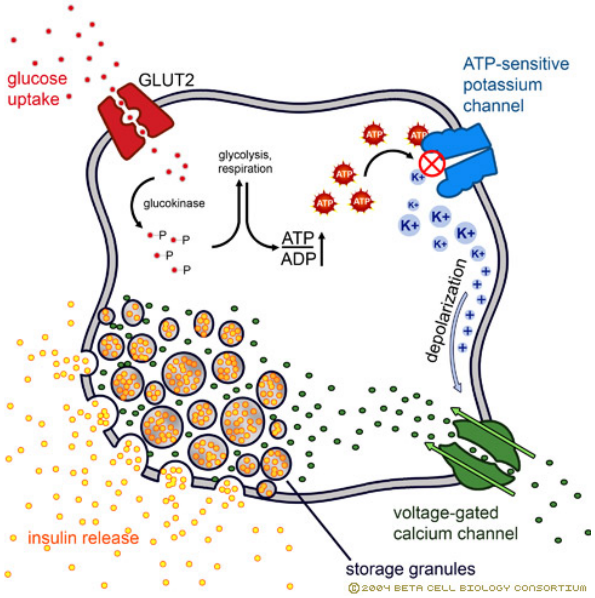


Figure 1.2: The main triggering pathway in glucose stimulated insulin secretion (from the Beta Cell Biology Consortium, http://www.betacell.org).

are less understood, but are believed to result in higher calcium sensitivity of the exocytory machinery, in this way amplifying the action of calcium on insulin release.

### 1.3.1 Bursting electrical activity

When the $\beta$-cell is subjected to a sufficiently high glucose concentration, the electrical potential across the cell membrane, the membrane potential, exhibits a characteristic electrical behavior known as *bursting* (Ashcroft and Rorsman, 1989). Bursting consist of a periodic variation between a silent phase where the cell is hyperpolarized at approximately -70 mV, and an active phase where the membrane potential shows spiking activity with an amplitude of the order of 40 mV, rising from a plateau of approximately -50 mV, see Fig. 1.3. A burst consists of a silent phase followed by an active one, and the burst period in intact islets range from tens of seconds to a few minutes (as in Fig. 1.3). The cytoplasmic calcium concentration varies in synchrony with bursting electrical activity and correlates with pulsatile insulin secretion (Santos et al., 1991; Barbosa et al., 1998; Henquin, 2000). The plateau fraction is defined as the ratio of the length of the active phase to the total burst period. When the glucose challenge increases, the plateau fraction also increases, and insulin secretion correlates well with the plateau fraction (Meissner and Schmelz, 1974). Hence, understanding what controls bursting electrical activity is of great importance for an insight in the mechanisms behind proper insulin secretion.

The electrical potential across the cell membrane is due to concentration differences of ions between the extracellular (outside) and intracellular, cytoplasmic side of the cell membrane. These differences are a result of ion fluxes and pumping through the plasma membrane. The membrane contains a series of channels and ATP consuming

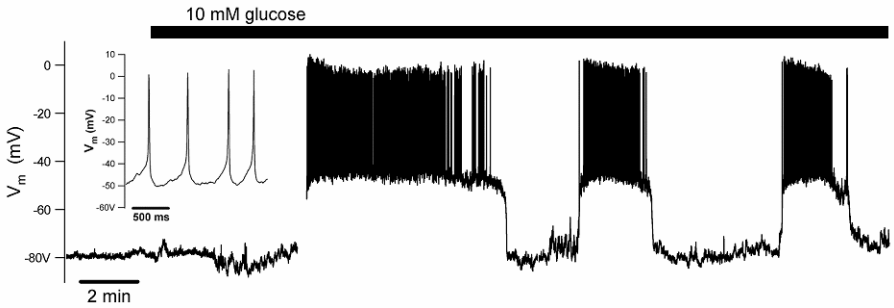


Figure 1.3: Bursting of membrane potential in mouse $\beta$-cell stimulated with 10 mM glucose. Insert: Details of the initial action potential spikes of the first burst. (From Luciani (2004)).

pumps, and the periodic activation and inactivation of a series of these channels are believed to underlie bursting electrical activity (Ashcroft and Rorsman, 1989).

The channels change their conductivity (activity) in response to changes in the membrane potential and the concentrations of various ions and molecules. One can think of the channels having *gates* that open or close depending on the controlling factors for that particular type of channel. Moreover, the gates open and close stochastically, for example because of thermal fluctuations (Atwater et al., 1983; Sherman et al., 1988).

### Single cells vs. islet behavior

It is remarkable that single, isolated $\beta$-cells in general behave very differently from intact islets (Rorsman and Trube, 1986; Göpel et al., 1999a; Larsson et al., 1996). In a large study (Kinard et al., 1999) it was found that isolated cells can be divided into three categories based on the behavior of the membrane potential: Cells with repetitive spikes (*spikers*; 33 % of the population studied), cells with small spikes superimposed upon brief (less than 5 seconds) plateau depolarizations (*fast bursters*; 52 %), and cells with periodic plateaus of longer duration (10-20 seconds) with small fluctuations on top (*plateau cells*; 15 %). The same group confirmed that this distinction is reflected in the intracellular calcium dynamics, which show small and fast oscillations reflecting the electrical activity of the cell (Zhang et al., 2003). It should be noted that other groups have found isolated cells to be very slow, especially when measuring intracellular $Ca^{2+}$ (Jonkers et al., 1999; Larsson et al., 1996), but also very slow membrane potential bursting has occasionally been observed (Larsson et al., 1996; Bertram et al., 2000). Noteworthy is also the recent study with islets from genetically modified mice lacking gap junctions (Ravier et al., 2005). When monitoring cells located in a cluster, but uncoupled to neighboring cells due to the loss of gap junctions, asynchronous slow $Ca^{2+}$ oscillations were seen in some but not all of the cells. Unfortunately, the authors did not measure the electrical activity of these cells and not of single, uncoupled cells in intact islets.

Thus, it seems that single, isolated cells are either much faster or significantly slower than intact islets or clusters of $\beta$-cells. Moreover, going from isolated cells to clusters to islets the orderliness increases, both when considering the electrical behavior (Rors-

man and Trube, 1986; Zhang et al., 2003) and the $Ca^{2+}$ oscillations (Jonkers et al., 1999; Zhang et al., 2003).

Several hypotheses have been proposed to explain the discrepancy between isolated cells and islets. Atwater et al. (1983) suggested that stochastic fluctuations of ion channels disrupt the bursting behavior in single cells. When the cells are coupled they effectively share the ion channels, and hence the stochastic fluctuation have less influence on the individual cell. This is known as the *channel sharing hypothesis*, and can explain how bursters are transformed to spikers or fast bursters when isolated.

The *heterogeneity hypothesis* (Smolen et al., 1993) is based on the fact that since $\beta$-cells have heterogeneous properties, some of them will be spikers or fast bursters, while other will be slow bursters, but very few will have a medium bursting pattern as seen in islets. The coupling between the heterogeneous cell population will change the dynamics of the population such that they become medium bursters.

In the islet, paracrine interactions from $\alpha$- and $\delta$-cells could play a role, and such stimulus, which could be crucial for obtaining bursting behavior, would of course be lost when removing the $\beta$-cells from their natural neighbors. However, clusters of $\beta$-cells, without or with very few $\alpha$- or $\delta$-cells, often show bursting and $Ca^{2+}$ oscillations (Rorsman and Trube, 1986; Jonkers et al., 1999).

Finally, the biophysical properties such as ion channel conductances of islet cells have been claimed to be changed after the isolation procedure (Göpel et al., 1999a), and hence, the isolated $\beta$-cells could be spikers only because of human intervention. If it was possible to isolate the $\beta$-cells, for example by blocking gap junction without interfering with the single cell physiology, we should, in the light of this idea, still be able to observe bursting. Indeed, such an experiment would be the ideal test of the different hypotheses. Genetically modified cells with reduced gap junction expression (Calabrese et al., 2003; Ravier et al., 2005) could be an alternative approach, although these cells might maintain a low degree of coupling (Calabrese et al., 2003). It should be noted that other studies could not confirm that isolated cells have channel conductances differing greatly from cells located in the islet, thus questioning this idea (Goforth et al., 2002).

These questions and hypotheses have inspired a great deal of mathematical studies, which are discussed further in chapter 3.

### 1.3.2 Calcium homeostasis

Calcium provides the triggering signal for insulin release from the $\beta$-cells. The intracellular calcium concentration increases during the active phase of the burst due to calcium influx through voltage-gated calcium channels, which open when the cell membrane is depolarized. During the silent phase $Ca^{2+}$ is cleared from the cell by ATP-consuming pumps and the $Na^{+}$-$Ca^{2+}$ -exchanger (Chen et al., 2003; Chay and Kang, 1988). Thus, calcium oscillates in phase with the membrane potential (Valdeolmillos et al., 1989; Zhang et al., 2003), often in a mixed pattern with slow waves with a period of approximately 5 minutes having faster fluctuations riding upon them. This pattern has been suggested to be a result of *compound bursting*, a pattern composed of clusters of bursts separated by silent phases (Bertram et al., 2004). This was recently

confirmed experimentally (Beauvois et al., 2006).

Intracellular calcium is sequestrated by the endoplasmic reticulum (ER) stores and the mitochondria. $Ca^{2+}$ enters the ER through ATP-consuming SERCA pumps, while the flux out of the ER is mainly through inositol 1,4,5-triphosphate ($IP_3$) sensitive channels or by passive leak. The ER stores plays an important role in shaping the $Ca^{2+}$ oscillations (Arredouani et al., 2002; Tengholm et al., 2001; Bertram and Sherman, 2004b). The way of entry into the mitochondria is provided by the $Ca^{2+}$ uniporter, while the exit is mainly by the mitochondrial $Na^{+}$-$Ca^{2+}$ -exchanger (McCormack et al., 1990; Rizzuto et al., 2000). The role of calcium in the mitochondria is described below.

### 1.3.3 Glycolysis

Glycolysis has a crucial role in GSIS of the $\beta$-cell. It is an ubiquitous pathway consisting of a series of enzymatic reactions, which break down each molecule of glucose entering the pathway into two molecules of pyruvate along with two molecules of ATP and NADH (reduced nicotinamide adenine dinucleotide). Pyruvate in then further metabolized in the mitochondria.

The $\beta$-cell has some kinetic peculiarities, which plays an important role in GSIS. First, the initial phosphorylation of glucose is catalyzed by glucokinase (GK), and, second, the phosphofructokinase (PFK), catalyzing phosphorylation of fructose 6-phosphate (F6P) to fructose 1,6-biphosphate (FBP), is of the muscle type (PFK-M).

GK has been regarded as the $\beta$-cell 'glucose sensor', mainly since the glucose phosphorylation of glucose by GK is rate limiting for glucose usage in $\beta$-cells, and it follows a sigmoidal relation similar to the dose-response curve of GSIS (Matschinsky et al., 1998).

PFK-M is another important regulator of glycolytic flux. It is inhibited by ATP, the final product of glucose metabolism, but activated by its product FBP, and by the nucleotides AMP and ADP. Due to these feedback mechanisms, it mediates oscillations in glycolysis in skeletal muscle extracts (Tornheim and Lowenstein, 1974). Hence, glycolytic oscillations in $\beta$-cells should also be possible, and this has indeed been supported by oscillations in glucose consumption (Jung et al., 2000) and G6P (Nilsson et al., 1996). Indirect support is given from oscillations in oxygen levels (Longo et al., 1991; Jung et al., 2000), NAD(P)H (Luciani et al., 2006) and ATP levels (Ainscow and Rutter, 2002), but we should keep in mind that these oscillations could be the result of periodic metabolism in the mitochondria, not in glycolysis.

Since oscillations in glycolysis typically have a time scale of approximately 5 minutes, they have been suggested to underlie pulsatile insulin secretion due to the similar period (Tornheim, 1997). The mechanism would be that oscillating glycolysis provides oscillating input for the mitochondria, which in turn synthesizes ATP periodically. This leads to rhythmic closure of K(ATP) channels, depolarization and $Ca^{2+}$ influx finally triggering pulsatile insulin secretion. These steps have been incorporated in a mathematical model (Bertram et al., 2004), which is used in *Paper IV*.

One might speculate that the slow bursts and $Ca^{2+}$ oscillations observed in isolated $\beta$-cells are glycolytic in nature. If the resulting ATP/ADP changes are sufficiently large,

they will overcome stochastic channel openings. Thus, the slow periodic pattern will persist but be less regular when going from islets to single $\beta$-cells (Jonkers et al., 1999), while a medium bursting pattern will be disrupted by the fluctuations in isolated cells as hypothesized in the channel sharing hypothesis. Thus, the mechanisms underlying the oscillations on various time scales are important for single cell versus islet behavior (see chapter 3 for a further discussion on this idea).

### 1.3.4 The mitochondria

The end product of glycolysis, pyruvate, is further metabolized in the mitochondria through oxidative phosphorylation. After being transported into the matrix of mitochondria, pyruvate is decarboxylated by pyruvate dehydrogenase (PDH) forming acetyl-coenzyme A (acetyl-CoA). In this process NADH is produced, but more importantly the generated acetyl-CoA is oxydized in the tricarboxylic acid (TCA) cycle yielding even more NADH and $FADH_2$ (reduced flavin adenine dinucleotide). Most NADH originates from the TCA cycle, but there is also an indirect transfer from the cytosol through two shuttle complexes, the malate-aspartate and the glycerol phosphate shuttles.

NADH and $FADH_2$ are carriers of energy rich electrons, which are delivered to the electron transport chain (ETC) when NADH and $FADH_2$ are metabolized. The energy in the electrons is harvested for pumping protons out of the mitochondrial matrix, and the proton gradient created is then used for driving the ATP synthase, which is the enzyme phosphorylating ADP, thus producing ATP, the end product of glucose metabolism in the $\beta$-cell. The produced ATP is finally exchanged with cytosolic ADP through the adenine nucleotide transporter.

The proton gradient created by the ETC results in an electric potential across the mitochondrial inner membrane, $\Delta\Psi_m$ of approximately 150 mV. It is this potential that drives, besides the ATP synthase, e.g., the pyruvate transporter, the adenine nucleotide transporter and uptake of $Ca^{2+}$ through the uniporter. The flux of $Ca^{2+}$ into the mitochondria has two opposing effects. Mitochondrial $Ca^{2+}$ stimulates several dehydrogenases, thus enhancing NADH production and eventually ATP production (McCormack et al., 1990). On the other hand the current introduced from the flux of the positive calcium ions lowers $\Delta\Psi_m$ and thus ATP synthesis (Magnus and Keizer, 1998a). The competition between these two opposing effects is the question treated in *Paper VII*.

See chapter 6 for more about the role and function of the mitochondria.

### 1.3.5 Inter-islet synchrony

$\beta$-cells are coupled through gap-junctions, and it has been established that the islet responds to stimulatory glucose levels as a functional syncytium, since electrical and calcium oscillations are quasi-synchronized across an islet (Meissner, 1976; Eddlestone et al., 1984; Santos et al., 1991; Aslanidi et al., 2001; Valdeolmillos et al., 1996). However, small phase-shifts of up to 2 seconds across the islet can be observed, which is due to the calcium signal spreading across the islet in the form of an excitation wave (Bertuzzi et al., 1999; Aslanidi et al., 2001). Also, metabolic synchronization was

demonstrated by Jung et al. (2000), who showed that oxygen levels measured at two different sites in an islet were synchronized. We showed in *Paper IV* that surprisingly electrical coupling is sufficient also for metabolic synchrony.

Genetically modified mice without gap junctions lose the synchronization (Calabrese et al., 2003; Ravier et al., 2005) such that the overall $Ca^{2+}$ signal is flat even though oscillations can be seen in smaller areas of the islet and in single cells. This flat signal is reflected in constant insulin secretion in contrast to pulsatile secretion from control islets (Ravier et al., 2005), underlining the importance of gap junction communication.

Synchronization has very recently been questioned to hold in human islets, maybe because of the unique architecture of human islets (Cabrera et al., 2006). That study did not find oscillations in calcium when imaging intact human islets, but only in small areas within the islet or in isolated cells. The authors proposed, but did not show directly, that the lack of communication between $\beta$-cells led to phase-shifts between different areas of the islet, and thus the local oscillatory signals were masked when averaged over the entire islet. However, these observations are in direct contrast to previous results, which showed a clear oscillatory calcium signal from human islets (Martin and Soria, 1996; Kindmark et al., 1991, 1994), which was found to be synchronized between different regions of the islet (Martin and Soria, 1996). Moreover, oscillatory insulin secretion from human islets speaks in favor of overall oscillatory calcium levels on the islet level (Song et al., 2002; Ritzel et al., 2003, 2006).

### 1.3.6 Pulsatile insulin release

As mentioned above, plasma insulin is oscillatory with a period of 4-10 minutes, which is believed to be a result of pulsatile insulin secretion from the pancreas. The ability to release insulin periodically resides in the individual islet, where is correlates with oscillatory $Ca^{2+}$ levels, a result of synchronized oscillations in the $\beta$-cell population in the islet. Both oscillatory $Ca^{2+}$ and pulsatile insulin secretion are lost in islets lacking gap junctions as a result of the lack of intra-islet synchronization (Ravier et al., 2005).

In order to see an overall pulsatile insulin profile from the pancreas it is furthermore necessary that the millions of islets are synchronized (inter-islet synchronization). The mechanisms underlying this synchrony are far from understood, but two hypotheses have been suggested.

One hypothesis is that an intrapancreatic neural pacemaker may be responsible for inducing periodic insulin release from the population of islets (Stagner et al., 1980; Pørksen, 2002; Gilon et al., 2002). However, pulsatile insulin secretion has been observed in individual islets (Westerlund and Bergsten, 2001; Sturis et al., 1994; Ritzel et al., 2003; Ravier et al., 2005) demonstrating that such a pacemaker has at most a synchronizing function. It has also been shown that groups of islets (Chou and Ipp, 1990; Berman et al., 1993; Sturis et al., 1994) and pieces of pancreas containing electrically silent nerves (ganglia) (Sha et al., 2001) exhibit oscillatory release of the hormone. Hence, there must be additional synchronizing mechanisms.

An alternate synchronization mechanism has been postulated based on data showing that plasma glucose levels fluctuate on the timescale of pulsatile insulin release as mentioned above (Sturis et al., 1994; Pørksen, 2002). This is the mechanism studied

in *Paper IV*, which can be summarized as follows. The insulin pulses from the islets interact with the liver and other tissues to produce the glucose fluctuations, which on the other hand entrain the islets and in this way synchronize the insulin pulses. The islets are from this point of view globally coupled oscillators interacting through the liver and plasma glucose. This idea is supported by the ability of oscillatory glucose to entrain insulin secretion *in vitro* (Chou and Ipp, 1990; Sturis et al., 1994; Ritzel et al., 2006) and *in vivo* (Mao et al., 1999; Pørksen et al., 2000), as well as entrainment of metabolism and $Ca^{2+}$ (Luciani, 2004). However, pulsatile secretion has been observed even when the glucose concentration was held constant. This has been observed *in vitro* for the perifused pancreas (Stagner et al., 1980) as well as *in vivo* when plasma glucose was clamped (Song et al., 2002). Thus, it seems plausible that both mechanisms, an intrapancreatic pacemaker and feedback from glucose, are at play. Such redundancy is not uncommon in biological systems.

# Chapter 2

# Enzyme kinetics

All cells, and thus also the $\beta$-cells, transduce information arriving to the cell membrane through a complex network of enzyme reactions. The first network that is activated in glucose stimulated insulin secretion in the $\beta$-cell, is that of glycolysis which break down glucose to pyruvate entering the mitochondria for further metabolism.

Henri (1901a,b, 1902) and Michaelis and Menten (1913) laid the foundation of the description of enzyme reactions. This formulation considers a reaction where a substrate $S$ binds reversibly to an enzyme $E$ to form a complex $C$. The complex can decay irreversibly to a product $P$ and the enzyme, which is then free to bind another substrate molecule. This is summarized in the scheme

$$E + S \underset{k_{-1}}{\overset{k_1}{\rightleftarrows}} C \xrightarrow{k_2} E + P, \tag{2.1}$$

where $k_1, k_{-1}$ and $k_2$ are kinetic parameters (supposed constant) associated with the reaction rates.

The reaction (2.1) can be described by a system of two nonlinear ordinary differential equations. Assuming that the complex is in a quasi-steady-state leads to the Michaelis-Menten-Briggs-Haldane approximation (Briggs and Haldane, 1925; Segel, 1988; Segel and Slemrod, 1989)

$$\frac{d\,S}{dt} \approx -\frac{V_{max} S}{K_M + S}, \quad S(0) = S_0, \tag{2.2}$$

Here $V_{max} = k_2\, E_0 = k_2\, E(0)$ is the maximal reaction rate and $K_M = \frac{k_{-1}+k_2}{k_1}$ is the Michaelis constant, identifying the substrate concentration giving the half-max reaction rate, i.e., $K_M$ reflects the substrate affinity of the enzyme.

The Michaelis-Menten-Briggs-Haldane approximation (2.2), also known as the standard quasi-steady-state approximation (sQSSA), is widely used, although it is known that it holds only when the enzyme concentration is much lower than either the substrate concentration or the Michaelis constant, $K_M$, as stated in the relation (Segel, 1988; Segel and Slemrod, 1989)

$$E_0 \ll S_0 + K_M. \tag{2.3}$$

This criterion is not satisfied in a wide range of intracellular situations, and hence the sQSSA (2.2) is sometimes inappropriate, in particular in glycolysis (Albe et al., 1990).

One should therefore model either each step of the reaction (2.1) or find approximations valid in a wider setting. One very promising candidate for such a new approximation is the total quasi-steady-state approximation (tQSSA) (Borghans et al., 1996; Tzafriri, 2003), which is summarized in *Paper IX* and *Paper X*.

In *Paper X* we studied the importance of using a valid approximation when estimating unknown parameters in a biochemical system. A common method to obtain these parameters is to fit a mathematical model to experimentally obtained data, for example by least square methods. This is often referred to as reverse engineering. However, a model formulated with the sQSSA can not be expected to be a good representation of the full system as discussed above. As for most other approaches, the use of the sQSSA produces excellent goodness of fit. But for the sQSSA such a good fit will necessarily correspond to parameter values far from the true ones. Indeed, inserting the true values in the sQSSA model does, in general, not approximate the full system. Instead, we expect that the tQSSA will reduce this problem consistently. This was confirmed for the simple reaction (2.1) in *Paper X*.

The newer approximations such as the tQSSA have so far only been found for isolated reactions. However, *in vivo* the reactions are coupled in complex networks or cascades of intermediate, second messengers with successive reactions, competition between substrates, feedback loops etc. In *Paper V*, we found an extension of the tQSSA to enzymes with competing substrates; in *Paper VIII*, *Paper IX* and *Paper X* we investigated the use of the tQSSA in phosphorylation cycles; and in *Paper VIII* and *Paper IX* in the mitogen activated protein kinase (MAPK) cascade.

This ubiquitous cascade is also present in the $\beta$-cells, where it is activated by glucose. The calcium dependent activation of the MAP kinases ERK1 and ERK2 promotes transcription of the insulin gene, but has little effect on insulin secretion. Thus, it seems to be involved on a relatively slow time scale to maintain appropriate insulin production (Khoo et al., 2004). The next chapters deal with processes on a faster time scale, and taking the MAPK cascade into account does not seem necessary for what follows.

# Chapter 3

# Modeling $\beta$-cell electrophysiology

The foundation to our present models of bursting electrical activity in $\beta$-cells was laid by Atwater et al. (1980), on which Chay and Keizer (1983) formulated the first mathematical model based on the Hodgkin-Huxley formalism. Virtually all models of the $\beta$-cells since then are variations of this model.

The main characteristics of the models are a fast subsystem, consisting of the membrane potential and at least one fast gating variable, usually of delayed rectifying potassium channels, and one or more slow variables, which make up the slow subsystem. 'Fast' and 'slow' refer to the timescales of the subsystems. The fast subsystem generates the spikes during the active phase, while the slow subsystem is responsible for switching between the active and silent phases.

## 3.1 Early models

The first models are characterized by having one slow variable as in the first $\beta$-cell model by Chay and Keizer (1983). Following the proposal by Atwater et al. (1980) this model was based on $Ca^{2+}$ being the slow variable modulating a calcium sensitive potassium current, K(Ca), and it predicted that $Ca^{2+}$ would show a sawtooth oscillation. This hypothesis was proven wrong when better methods for measuring $Ca^{2+}$ were invented, which showed that $Ca^{2+}$ is closer to having square wave oscillations (Valdeolmillos et al., 1989). Thus, $Ca^{2+}$ levels change not quite slow enough to pace bursts with a period of tens of seconds. For this reason, $Ca^{2+}$ was for many years considered unlikely to drive bursting (Sherman, 1997). However, a novel slowly activating calcium dependent potassium current, $K_{slow}$, has reintroduced $Ca^{2+}$ as a potential candidate for the slow variable (Göpel et al., 1999a). This has been supported by a mathematical model with two slow variables (Goforth et al., 2002; Zhang et al., 2003), which is a so-called *phantom burster model*, see the following section. Other proposed candidates for the slow variable have included cytosolic ATP/ADP ratio (Keizer and Magnus, 1989; Magnus and Keizer, 1998a) and the concentration in the endoplasmic reticulum (ER) (Chay, 1997). Moreover, the underlying dynamics of these models have been reproduced in a minimal, polynomial model (Pernarowski, 1994), which is the model used in *Paper VI*.

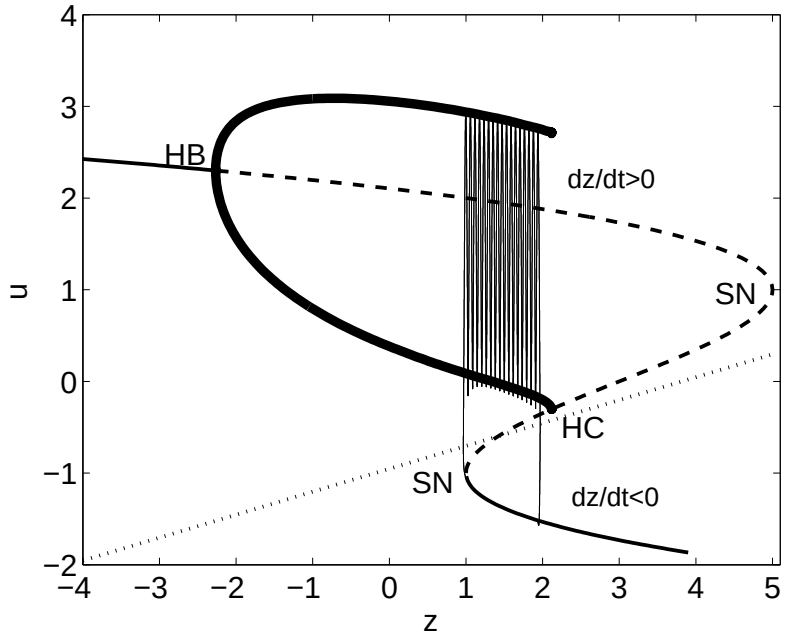


Figure 3.1: Bifurcation diagram of the fast subsystem with $z$ as the bifurcation parameter. Thin, full curves indicate stable fixpoints; thin, broken curve correspond to unstable fixpoints and the thick, full curve shows the extrema of periodic solutions. The dotted curve shows the $z$-nullcline, $\frac{dz}{dt} = 0$. A simulation of the deterministic system is projected onto the $z - u$ plane for comparison. See the text for more details.

In the case of one slow variable, Rinzel (1985) elegantly explained the mechanism underlying bursting using a bifurcation diagram of the fast subsystem with the slow variable as the bifurcation parameter. This fundamental analysis is reproduced here (taken from *Paper VI*).

We denote the slow variable by $z$, and the membrane potential is mimicked by $u$. The fixpoints of the fast system fall on a Z-shaped curve, see Fig. 3.1. The fast system is stable for low $z$ values, but increasing $z$, this stability is lost in a Hopf-bifurcation (HB). The fixpoints on the middle branch of the Z-shaped curve are saddle-points, while they are stable on the lower branch. The middle-branch meets the upper and lower branch in saddle-node bifurcations (SN). The Hopf-bifurcation gives rise to stable periodic solutions around the unstable fixpoints on the upper branch, but these periodics disappear in a homoclinic bifurcation (HC) for sufficiently large $z$. The mechanism underlying bursting is based on the bistability between the stable fixpoints on the lower branch and the stable periodics for a range of $z$-values. When we reintroduce the slow variation of $z$, we can explain bursting. When the system is near the lower branch, it moves slowly to the left since $u$ is low and thus $\frac{dz}{dt} < 0$ here. This continues until the stable branch disappears in the left saddle-node bifurcation. The system now leaves the lower branch (silent phase) and goes to the stable periodics (active phase), where $u$ is high and $\frac{dz}{dt} > 0$. Hence, the system now moves to the right until it meets the homoclinic bifurcation and the stable periodics disappear. The system then leaves the active phase and settles on the lower branch and the scenario is repeated.

## 3.2 Phantom bursting

Isolated $\beta$-cells show a wide range of behavior, with the majority showing either spiking or very fast bursting activity (Kinard et al., 1999; Zhang et al., 2003). However, bursting slower than observed in islet is also seen, especially in $Ca^{2+}$ measurements (Zhang et al., 2003; Jonkers et al., 1999). Only rarely do isolated cells burst with a period of tens of seconds (medium bursting) as observed in intact bursting islets. Furthermore, no convincing slow variable, which changes on a time scale of tens of seconds has been found. As mentioned above, $Ca^{2+}$ reacts to fast, and the K(Ca) current has a time scale of less than 10 seconds (Göpel et al., 1999a). The ATP/ADP ratio on the other hand seems to change too slowly (Nilsson et al., 1996; Ainscow and Rutter, 2002), while the ER $Ca^{2+}$ concentration is insufficient in explaining bursting, since bursting and $Ca^{2+}$ oscillations can persist, although with a changed profile, when ER stores are emptied by the SERCA pump blocker thapsigargin (Tg) (Bertram et al., 1995; Tamarina et al., 2005; Gilon et al., 1999; Miura et al., 1997). However, it is also often seen that Tg converts bursting and $Ca^{2+}$ oscillations to continuous spiking and stable, raised $Ca^{2+}$ (Kanno et al., 2002; Gilon et al., 1999; Miura et al., 1997)

These problems of finding an appropriate slow variable led to the development of the phantom burster model (Bertram et al., 2000). The idea is to combine a slow variable, $z_1$, with a rather small time constant of the order of a few seconds, with a very slow variable, $z_2$, with a time constant of more than a minute. The interplay between these two slow processes yield a slow modulation of the fast subsystem on an intermediate time scale of tens of seconds. Besides, depending on the relative strength of the two slow processes the system can exhibit either fast or slow bursting, while medium bursting occurs when both slow processes contribute to the dynamics. Thus, the model can account for the full spectrum of observed burst periods.

I have constructed a minimal polynomial phantom burster model based on the model by Pernarowski (1994) as follows (compare with Eq. 2.2 in *Paper VI*):

$$\frac{d^2u}{dt^2} + F(u)\frac{d\,u}{dt} + G(u) + \rho_z z_1 + z_2 = \tag{3.1a}$$
$$-(h_1(u) - z_1)/\tau_1 - (h_2(u) - z_2)/\tau_2 - \sigma\Gamma_t,$$
$$\frac{d\,z_1}{dt} = (h_1(u) - z_1)/\tau_1, \tag{3.1b}$$
$$\frac{d\,z_2}{dt} = (h_2(u) - z_2)/\tau_2, \tag{3.1c}$$

The fastest of the two slow variables $z_1$ has a time scale of $\tau_1 = 40$ time units, while the slowest variable $z_2$ has a time scale of $\tau_2 = 2000$. The functions $h_i, i = 1, 2$, are both linear, but with different parameters, and $F$ and $G$ are as in *Paper VI*. Introducing a parameter $\rho_z$, which modifies the relative strength of $z_1$ versus $z_2$ enables us to switch from slow phantom bursting with a period greater than, e.g., 1000 time units ($\rho_z \approx 0.7$) to medium (period of 200-1000, $\rho_z \approx 1.1$) to fast (period less than 200, $\rho_z \approx 2.5$, see the black curve in Fig. 3.4A. This polynomial phantom burster is also used in the following section when studying the influence of noise modelled by the term $\sigma\Gamma_t$, but for now we consider the deterministic case, $\sigma = 0$.

To explain the mechanism behind phantom bursting we take advantage of the bifur-

cation diagram from the previous section (Fig. 3.1) with $z_1$ playing the role of $z$. We consider $z_2$ constant. The Z-curve is given by $\frac{d^2u}{dt^2} = \frac{du}{dt} = 0$ yielding

$$z_1 = -\frac{G(u) + z_2}{\rho_z}. \tag{3.2}$$

$z_2$ then effectively moves the Z-curve horizontally: for large $z_2$ it is shifted to the left, and for smaller $z_2$ to the right.

Now, if the $z_1$-nullcline is steeper than in Fig. 3.1 such that it always has at least one intersection with either the upper or the lower branch of the Z-curve with $z_1$ between the values of the left saddle-node and the homoclinic bifurcation (more precisely, it is not the intersection with the Z-curve that matters in the active phase, rather with the average of $u$ over a spike period, i.e., the appropriate intersection with the periodic), then, for constant $z_2$, the system will come to rest in either a constantly spiking state (when intersecting the periodic) or a silent state (when intersecting the lower branch).

The bifurcation diagram for the model with $\rho_z = 1$ is shown in Fig. 3.2. We explain phantom bursting as follows. Assume that the system is at rest in the silent state and that $z_2$ now behaves similarly to $z_1$ but much slower. Since $u$ is low, $z_2$ decreases, and the Z-curve moves to the right (Fig. 3.2, right panel). At a certain point the $z_1$-nullcline no longer intersects the lower branch of the Z-curve and the fast subsystem escapes to the active phase. Now $z_1$ increases until it reaches the point where its nullcline intersects the periodic where it then stalls (Fig. 3.2, left panel). $z_2$ now increases slowly moving the Z-curve to the left, and at a certain point the intersection of the $z_1$-nullcline and the periodics passes the homoclinic bifurcation and the fast subsystem jumps to the silent phase. Here $z_1$ decreases finally reaching the reintroduced intersection between the $z_1$-nullcline and the lower branch, and again it stalls waiting for $z_2$ to decrease sufficiently (Fig. 3.2, right panel). The scenario is then repeated.

Increasing (respectively decreasing) $\rho_z$ compresses (respectively stretches) the Z-curve as seen from (3.2). Hence, for large $\rho_z$ the system will never be trapped and we get fast bursting driven almost exclusively by $z_1$. For small $\rho_z$ the situation is the opposite, since $z_2$ now has to change a lot before the system escapes, and thus we get slow bursting driven almost exclusively by $z_2$. See the black, full curve with squares in Fig. 3.4, upper, left panel, for the influence of $\rho_z$ on the burst period.

Examples of physiological phantom bursters, all having cytosolic calcium as the fastest slow feedback variable $z_1$, differ by having either the ER calcium concentration (Goforth et al., 2002; Zhang et al., 2003) or the ATP/ADP ratio (Bertram and Sherman, 2004a) as the slowest variable. The latter is the model used for the electrophysiological and calcium handling part of the model in *Paper IV*.

## 3.3 Stochastic fluctuations

As mentioned, isolated single cells behave differently from coupled cells, and usually either spike or have very short bursts (Kinard et al., 1999). It was suggested by Atwater et al. (1983) that stochastic fluctuations (noise) of ion channels destroy the bursting pattern, but that these fluctuations are less influential on the individual cell when it is

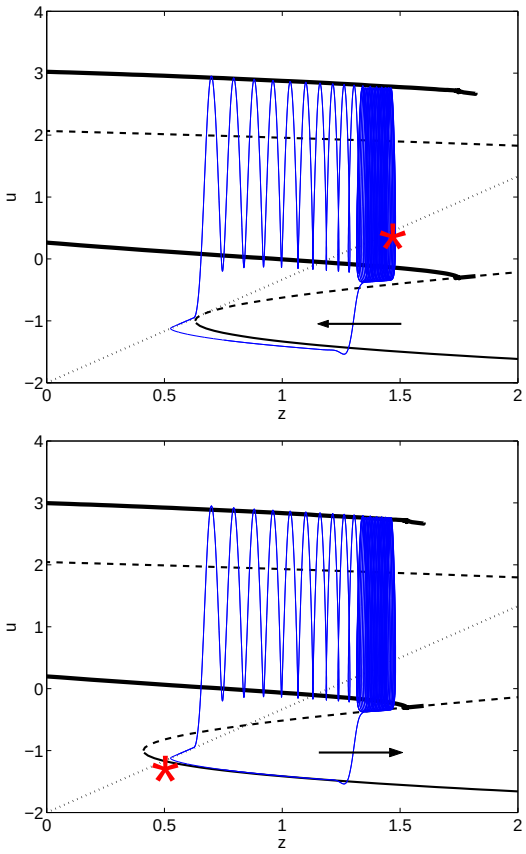


Figure 3.2: Bifurcation diagram explaining phantom bursting. The first panel shows the bifurcation diagram from Fig. 3.1 shifted 0.37 ($\sim z_2$) to the left, corresponding to the beginning of the active phase. A numerical solution for the entire burst trajectory superimposed (blue). The red asterisk indicates that the system becomes trapped in the active phase until $z_2$ has grown sufficiently such that the underlying Z-curve has moved sufficiently to the left, and the system meets the homoclinic bifurcation. This happens for a shift of 0.57 ($\sim z_2$, second panel). The system is then trapped in the silent phase where the $z_1$-nullcline intersect the lower branch of the Z-curve (red asterisk). The time series is shown in Fig. 3.3A, where it is also seen that $z_1$ reaches a constant value where it stays until $z_2$ has grown sufficiently.

coupled to other cells, since the channels are effectively shared between cells. This idea, known as *the channel sharing hypothesis*, was investigated using computer simulations by Chay and Kang (1988) and Sherman et al. (1988).

In *Paper VI*, we analyzed the influence of noise from a more analytical point of view. More specifically, we showed that the bifurcations that determine the burst period, i.e., the left saddle-node bifurcation and the homoclinic bifurcation (see Fig. 3.1) can be followed for varying noise strength using a collective coordinate method for the exit from the silent phase at the saddle-node bifurcation, and a stochastic Melnikov method for determining the homoclinic bifurcation, which ends the active phase. We found that noise effectively moves the homoclinic bifurcation to the left, see *Paper VI*.

When introducing noise into a phantom bursting model, the effect on the burst period is much more dramatic than in the case of a standard bursting model, i.e., a model with only one slow variable, see Fig. 3.3. I have used the model (3.1) introduced above. A medium phantom burster with a period of roughly 400 time units (Fig. 3.3A) is converted to a fast burster with a period of approximately 150 time units by even extremely low noise intensity ($\sigma = 0.01$, Fig. 3.3B). A standard burster with a period similar to the phantom burster (Fig. 3.3C) is influenced very little by such a low noise intensity (Fig. 3.4, lower, left panel), and even the stronger intensity $\sigma = 0.05$ only shortens the burst period to approximately 300 time units (Fig. 3.3D). This pattern is consistent: Noise is more efficient at shortening the period of slow and medium phantom bursters than of standard bursters and fast phantom bursters (Fig. 3.4). Fast phantom bursting is effectively driven by only one slow variable, and hence, it comes as no surprise that noise has little effect on this kind compared to medium and slow bursting, since moving the homoclinic bifurcation does not have the ability to change the type of phantom bursting. Note that for strong noise there is almost no dependence on $\rho_z$ indicating that the stochastic fluctuations have disrupted the bifurcation structure and the effect of the slowest variable $z_2$ (Fig. 3.4, upper left panel, dash-dotted curve).

The dramatic noise dependence is due to the fact that moving the homoclinic bifurcation to the left will shorten the time that the system is stalled in the active phase, and for a larger shift it can even be expected that the system will follow the fastest of the two slow time scales since it will never be trapped in the active phase. Alternatively, it can be explained by noticing that while the system is stalled, it is near the $z$-nullcline, and thus small perturbations are sufficient to push the system into the basin of attraction for the silent branch. This scenario is reflected in the large flux factor $\Phi_{stoch}$ near the deterministic homoclinic bifurcation, see *Paper VI*, Fig. 4.2, and is more important for low noise strengths since the homoclinic bifurcation is moved much less to the left than for larger noise intensities. In the standard bursting model the system is only near the $z$-nullcline in a relatively small fraction of the active phase. The same holds true for the end of the silent phase although to a less degree (*Paper VI*). The effect on burst period in relation to the relative time that the system is stalled taking into account the Melnikov process and flux factor, would merit a more thorough study.

These simulations speak against the proposed role of phantom bursting in creating either fast or slow bursters when considering isolated cells, since the ever present stochastic effects in single cell will tend to make all the cells rather fast. In other words, the mechanism behind the channel sharing hypothesis will shorten the burst

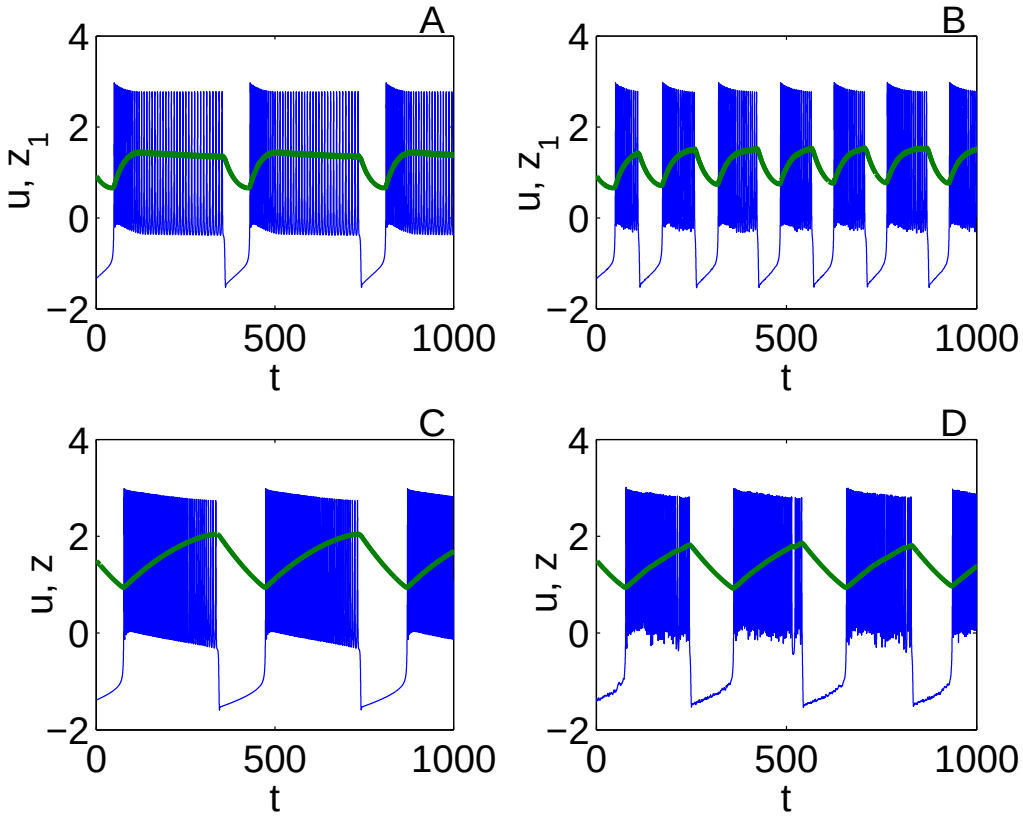


Figure 3.3: Noise has a stronger effect on phantom bursters than on regular bursters. Panel A shows a medium phantom burster without noise. Panel C is a standard burster with a period similar to the phantom burster in panel A. When subjected to noise ($\sigma = 0.01$) the burst period of the phantom burster shortens significantly (panel B), and more than for the standard burster with stronger noise influence ($\sigma = 0.05$, panel D). The blue curves show the membrane potential $u$, while the red curves are in panels A & B (respectively, C & D) the fastest of the two slow variables $z_1$ (respectively, the slow variable $z$).

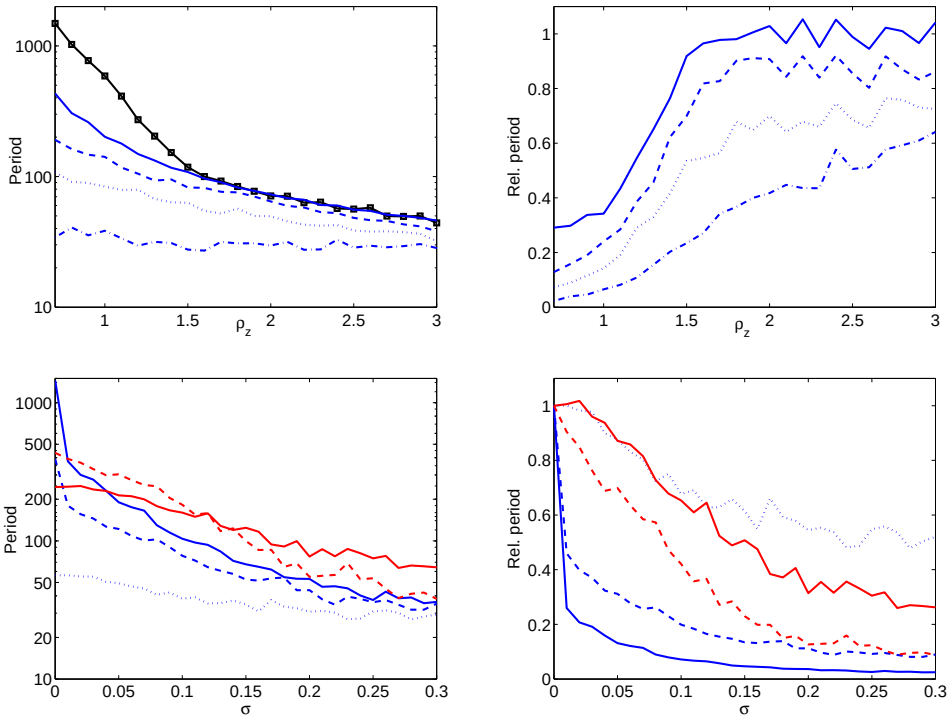


Figure 3.4: Burst periods for various type of bursters and noise strengths. Upper, left panel: Period of phantom bursters as a function of $\rho_z$ for various noise strengths ($\sigma = 0$, full, black curve with squares; $\sigma = 0.01$, full, blue curve; $\sigma = 0.05$, dashed curve; $\sigma = 0.1$, dotted curve; $\sigma = 0.3$, dash-dotted curve). Note the logarithmic scale on the $y$-axis. Upper right panel: Relative period (compared to the deterministic case $\sigma = 0$) for the curves from the upper, left panel with same legends. Lower, left panel: Burst period as a function of noise intensity $\sigma$ for a slow phantom burster (blue, full curve), a medium phantom burster (blue, dashed curve), a fast phantom burster (blue, dotted curve), a standard burster as in Fig. 3.3, panels C and D (red, dashed curve), and the standard burster investigated in *Paper VI* (red, full curve). Note the logarithmic scale on the $y$-axis. Lower, right panel: Relative periods for the curves in the lower, left panel with respect to the deterministic case ($\sigma = 0$) for each of the curves.

period dramatically in single cells in contrast to several experiments, e.g., by Jonkers et al. (1999), who found single cells to show mainly slow $Ca^{2+}$ oscillations that increased in regularity when coupled in cell clusters. These authors found that $\sim$25% of single cells did not show oscillations, while $\sim$10% ($\sim$13% of all oscillating cells) showed a mixed pattern of fast oscillations on top of slow oscillations and the remaining $\sim$65% had only slow oscillations In islets, the distribution of the various patterns is in contrast $\sim$40% of islets showing oscillating $Ca^{2+}$ levels have slow oscillations, $\sim$35% fast oscillations (corresponding to medium bursting) and 25-30% have a mixed pattern (Bergsten et al., 1994; Liu et al., 1998). Thus, mixed oscillations are seen mostly in islets, indicating that compound bursting is rarely seen in single islets, since the mixed $Ca^{2+}$ pattern has been shown to be a consequence of compound bursting (Beauvois et al., 2006).

These observations would be explained by a scenario where the slow envelope is controlled by glycolysis and the individual bursts by a phantom mechanism (Bertram et al., 2004). When the cell is isolated, noise will disrupt the phantom bursting, while the glycolytic oscillations will continue. In contrast, intermediate islet phantom bursting will be changed to fast, noisy bursting as in the channel sharing hypothesis. Thus, where islets show intermediate, compound or slow glycolytic bursting, individual cells should mainly show fast bursting or spiking with a relatively flat $Ca^{2+}$ signal (corresponding to an islet with intermediate bursting) or slow bursting and $Ca^{2+}$ oscillations (corresponding to compound or glycolytic bursting). Interestingly, the numbers for the distribution of various $Ca^{2+}$ patterns cited above correspond quite well to this hypothesis, although it would be even better to have data from the same group using identical experimental settings for the isolated cells and islets. The only group that, to my knowledge, compared islets and isolated cells found that isolated cells are either fast bursters or spikers and correspondingly show very fast (<5 sec) $Ca^{2+}$ oscillations (Zhang et al., 2003). Thus, their study does not provide any insight in the mechanism behind slow bursting and $Ca^{2+}$ oscillations in isolated cells. For comparison, these authors found that 47% of islet show fast $Ca^{2+}$ oscillations (corresponding to medium bursting), 11% have slow oscillations, and the remaining 42% show a mixed pattern (Zhang et al., 2003).

I am currently investigating this idea of combining the channel sharing hypothesis and the role of glycolytic oscillations using modeling. As shown in Fig. 3.5, the above considerations seem to be well represented by preliminary simulations of a stochastic version of the model by Bertram et al. (2004), which is the model used in *Paper IV*. The noise term is included as a stochastic K(ATP) channel as in De Vries and Sherman (2000) and *Paper III*. The $Ca^{2+}$ response is even more convincing as seen in Fig. 3.6, where I show a 5 second moving average of the $Ca^{2+}$ level for comparison with experiments such as by Jonkers et al. (1999) to include non-continuous image sampling, buffering, possible slower responding subspaces (Zhang et al., 2003), etc. The case with a low number of K(ATP)-channels corresponding to a single cell does indeed show a slow $Ca^{2+}$ oscillations, while the "islet" with many K(ATP)-channels show mixed oscillations.

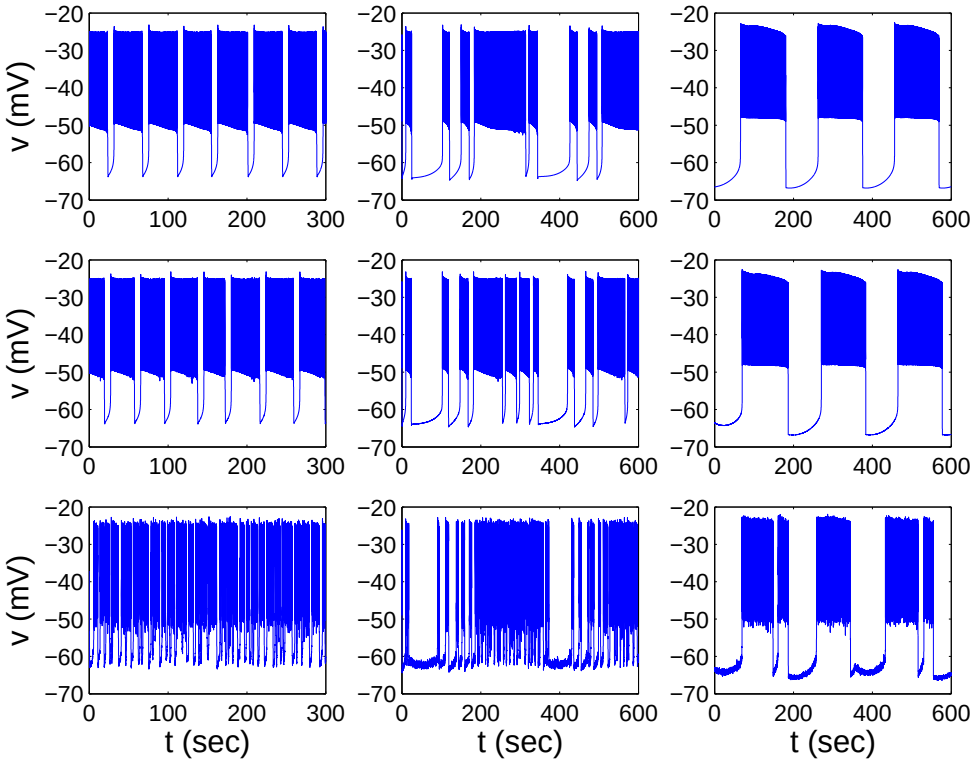


Figure 3.5: Simulations of a stochastic version of the model by Bertram et al. (2004). The upper panels show the deterministic version for medium (left; parameters $J_{gk} = 0.4$, $g_{k,ca} = 400$ pS, $\lambda = 0.005$), compound (center; $J_{gk} = 0.2$, $g_{k,ca} = 400$ pS, $\lambda = 0.005$), and slow bursting (right; $J_{gk} = 0.2$, $g_{k,ca} = 80$ pS, $\lambda = 0.01$). The corresponding stochastic versions are shown below, with the number of K(ATP)-channels given by $N_{K(ATP)} = 100000$ and $N_{K(ATP)} = 100$ in the middle and lower row, respectively. A lower number of channels correspond to a stronger noise term (De Vries and Sherman, 2000).

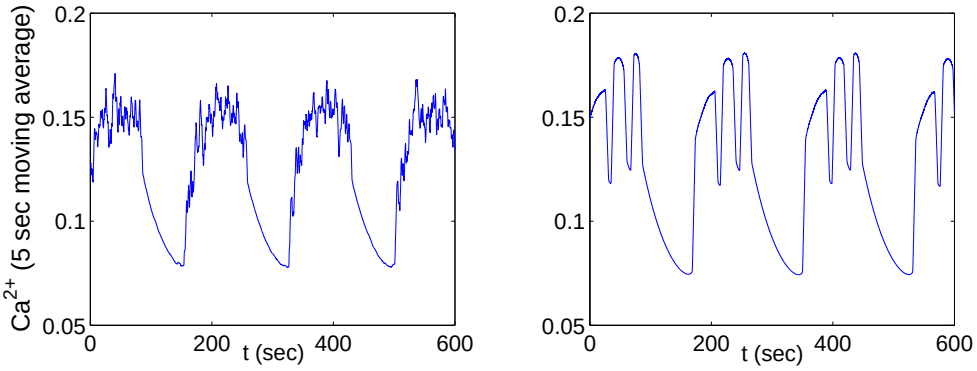


Figure 3.6: Simulations of a stochastic version of compound bursting in the model by Bertram et al. (2004) as in Fig. 3.5, center panels. The figures show $Ca^{2+}$ levels, smoothed by averaging over 5 sec windows. Parameters are as in Fig. 3.5, center panels, except $\bar{g}_{K(ATP)} = 1700$ pS, $\lambda = 0.01$, and the number of K(ATP)-channels is given by $N_{K(ATP)} = 20$ (left panel) and $N_{K(ATP)} = 100000$ (right panel).

## 3.4 Two coupled cells

Puzzling to understand the difference between isolated and coupled cells, researchers have modeled just two coupled cells, where the bifurcation structure of the system can be analyzed similarly to the case of one cell. It has been shown that cells that spike when isolated can become bursters when coupled (Sherman and Rinzel, 1991). This observation has been reported to be more robust when the cells have heterogeneous properties (De Vries and Sherman, 2001), or when they are subjected to noise (De Vries and Sherman, 2000). *Paper III* shows that it is necessary that the two cells have different stochastic perturbations, and suggests that it is the effective heterogeneity induced by the two noise sources that change the spikers to bursters. Thus, heterogeneity, even when masqueraded as noise, can robustly make spiking cells burst. It should be interesting to apply the methods from *Paper VI* to coupled, noisy cells, especially with the scope to further understand the result from *Paper III*, i.e., how precisely does the noise-induced heterogeneity break the symmetry such that the bursting behavior occurs.

Bertram et al. (2000) showed that when coupling slow and fast phantom bursters they synchronize in a medium bursting pattern. Moreover, when two fast phantom bursters are weakly coupled a medium bursting pattern can be obtained (R. Bertram, unpublished results). Zimliki et al. (2004) simulated larger populations of coupled phantom bursters, and they found that when moderately coupled, medium bursting can arise from cells that are either all fast, all slow or a mixture of the two. It would be interesting to thoroughly investigate the bifurcation structure and the effect of noise in coupled phantom bursters.

# Chapter 4

# Excitation waves in pancreatic islets

Nonlinear waves is a commonly observed phenomenon in excitable media. Since the $\beta$-cells are electrically excitable, and coupled through gap-junctions, it could be envisaged that wave propagation would occur in the islets of Langerhans. This has indeed been observed as mentioned below, and using mathematical modeling it has been suggested to be nonlinear waves similar in nature to those arising from the Nagumo equation (sometimes referred to as Fisher's equation, although Fisher (1937) studied a second degree polynomial)

$$u_t = u_{xx} - u(u-1)(u-a), \tag{4.1}$$

where subscripts denote differentiation and $0 < a < 1$, see Aslanidi et al. (2001) and *Paper I* and *Paper II*.

## 4.1 Experimental facts

*In vitro* experiments have shown that calcium waves propagate through glucose stimulated pancreatic islets and monolayers of insulin secreting cells (Bertuzzi et al., 1999; Cao et al., 1997; Aslanidi et al., 2001; Rocheleau et al., 2004). Also electrical activity is slightly out of synchrony such that a burst starts with a time difference of a few seconds at different cells in the islet, again indicating that an electrical wave is propagating across the islet (Eddlestone et al., 1984; Palti et al., 1996). These excitation waves are likely to be a synchronization mechanism by which the $\beta$-cells in an islet secrete insulin almost simultaneously. Moreover, it could be a mechanisms by which cells that become active and secrete insulin in response to an elevated glucose stimulus, could signal to otherwise non-responding cells in order to activate them (Aslanidi et al., 2001). The opposite could also be envisaged; that hyperactive cells, i.e., because of a permanently closed K(ATP)-channel, could behave normally when coupled to normally functioning cells. This has been supported recently (Rocheleau et al., 2006).

When imposing a glucose gradient across the islet, wave propagation is again observed, but now the waves pass only partly across the islet (Rocheleau et al., 2004).

When the wave enters the region where the $\beta$-cells would be silent if uncoupled, it progresses slightly further than the active (when uncoupled) region, but then it stops (see also simulations below). Hence, excitation waves might function as a triggering signal from active to silent cells, but only over limited ranges.

The waves have been hypothesized to be a result of electrical and/or chemical coupling through gap junctions, or to be mediated by diffusion of some messenger in the extracellular medium. As in many other biological systems, there is here some redundancy where several mechanisms can serve the same purpose. A likely extracellular messengers could be ATP, which is secreted together with insulin from the granules (Cao et al., 1997; Hellman et al., 2004). The idea of a diffusing messenger came mainly from the fact that groups of cells that are not physically coupled have the ability to communicate, such that an excitation wave can jump the physical gap between the clusters (Cao et al., 1997; Bertuzzi et al., 1999). However, these diffusion waves are much slower that the ones seen in intact islets (Bertuzzi et al., 1999; Aslanidi et al., 2001), and thus, electrical communication is more likely to be the main mechanism for wave propagation in intact islets. This is also supported by the asynchronous calcium oscillations in islets from genetically modified mice lacking gap junctions (Ravier et al., 2005), since if the diffusible messenger was able to synchronize the cells, then the lack of gap junctions should not disrupt the coordinated periodic behavior. The response in intact islets thus seems to be different from that of monolayers of insulin secreting cells, where gap junction communication is not crucial for wave propagation (Cao et al., 1997; Bertuzzi et al., 1999).

## 4.2 Modeling

These experimental facts were studied using mathematical modeling (Aslanidi et al., 2001). It was found that electrical coupling is indeed enough to see excitation waves propagate, but the model used in that study predicted too fast waves in comparison to the experimentally found wave speeds. The authors suggested that a lower glucose concentration in the center of the islet, due to slow diffusion of glucose, would explain this discrepancy. This was based on theoretical considerations. Lower glucose concentration was modelled by a higher conductance of the K(ATP) channels, $g_{K(ATP)}$, and it was argued that this would lower the wave speed.

However, in *Paper II* I showed both by simulations and theoretical considerations, that changing the value of $g_{K(ATP)}$ should have minimal effect on the speed of the waves. I suggested in *Paper I* that heterogeneous coupling strength could explain the discrepancy between experimental and simulated wave speed. This was supported by a homogenization procedure (Bensoussan et al., 2002).

We note here that this homogenization procedure does not interfere with the assumptions leading to the Nagumo-like equation (personal communication, M. Amar, La Sapienza University of Rome). More specifically, in *Paper I* a model equivalent to the

following was considered for $\epsilon > 0$,

$$\begin{aligned} u_t^\epsilon &= I(u^\epsilon, n^\epsilon, s^\epsilon) + (\kappa(\frac{x}{\epsilon})u_x^\epsilon)_x, \\ n_t^\epsilon &= \frac{n_\infty(v^\epsilon) - n^\epsilon}{\tau_n}, \\ s_t^\epsilon &= \frac{s_\infty(v^\epsilon) - s^\epsilon}{\tau_s}, \end{aligned} \tag{4.2}$$

and following Aslanidi et al. (2001) it was assumed that $n^\epsilon = n_\infty(u^\epsilon)$ and $s^\epsilon = s_*$ (constant). This results in a single Nagumo-like equation for $u^\epsilon$ which is then homogenized by letting $\epsilon \to 0$, see *Paper I*, yielding the homogenized equation, say for $u_0$. If instead, we homogenize (4.2) directly by letting $\epsilon \to 0$, we get a system similar to (4.2), say for $u^0, n^0$ and $s^0$. If we then assume $n^0 = n_\infty(u^0)$ and $s^0 = s_*$, we obtain again a Nagumo-like equation for $u^0$, which is identical to the one for $u_0$, i.e., $u^0 = u_0$, and thus the homogenization method commutes with the procedure leading to the Nagumo-like equation.

I studied further the influence of oscillating gap junction conductance on wave propagation (*Paper II*). Andreu et al. (1997) reported that the conductances of gap junctions oscillate in phase with the bursting phenomena of the $\beta$-cells such that during the active phase the conductance is almost four times greater than in the silent phase. The gap junctions are not voltage sensitive, so such an oscillation would have to be mediated by other messengers. It should be noted that the results presented by Andreu et al. (1997) should be interpreted with care, since the authors used very strong currents in their experiments, likely to interfere with the normal electrophysiological behavior of the $\beta$-cells (A. Sherman, NIH, personal communications). However, from a theoretical point of view there is nothing that hinders the investigation of oscillating gap junction conductance. I showed in *Paper II* that this scenario can be studied along the lines of the case of constant gap junction conductance described above, now leading to a density dependent Nagumo diffusion equation. Moreover, using a simple transformation I found a new expression for the wave speed of such density dependent Nagumo diffusion equations.

Rocheleau et al. (2004) imposed a glucose gradient across an islet and observed wave propagation, but only across a part of the islet. To simulate this scenario, I have used the model from *Paper I* of a line of 20 $\beta$-cells coupled with constant gap-junction conductance. The glucose gradient is imposed by letting $g_{K,ATP}$ decrease linearly across the islet, such that cell no. 1 has $g_{K,ATP} = 292$ pS (low glucose concentration), while cell no. 20 has $g_{K,ATP} = 140$ pS (high glucose concentration). As seen in Fig. 4.1, a calcium wave propagates from the cell with the highest glucose stimulus, but stops in the middle of the islet. However, the wave travels into the region where the cells would be silent if uncoupled (here cell no. < 15) as observed experimentally. In collaboration with M.P. Sørensen, I am currently investigating this phenomenon along the lines of *Paper I* and *Paper II*.

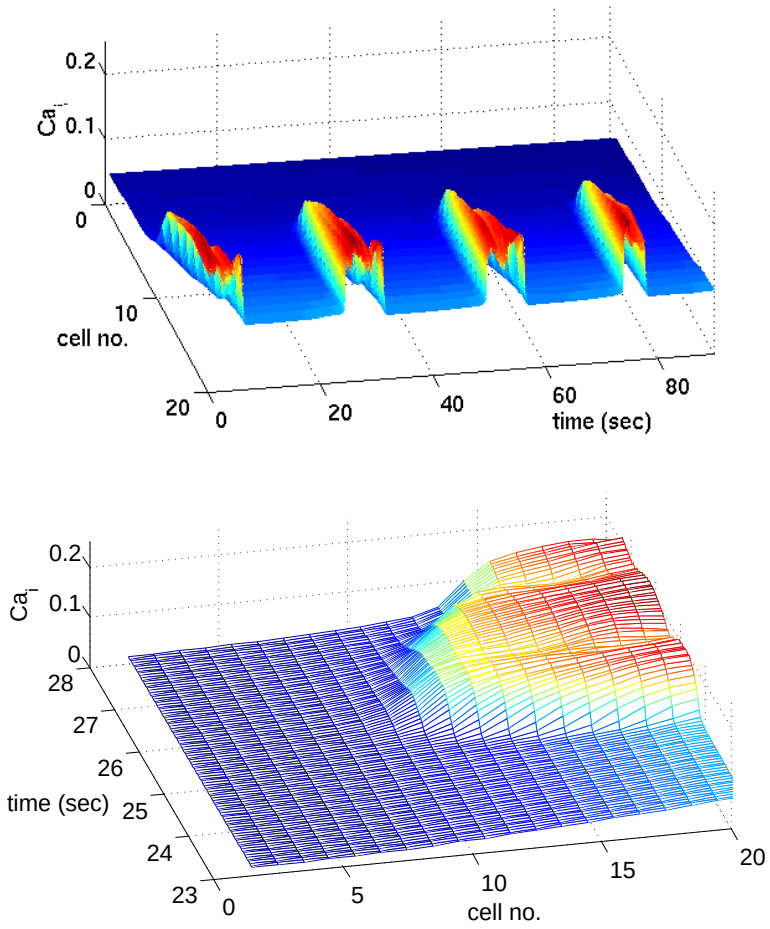


Figure 4.1: Simulation of wave propagation in an islet with an imposed glucose gradient. Upper panel: Several burst episodes leading to wave propagation. Lower panel: Close up of a wave front. The figure has been turned 90 degrees counter-clock wise compared to the upper panel.

# Chapter 5

# Entrainment and synchrony of pulsatile insulin secretion

## 5.1 Background

Insulin is secreted in pulses with a period of 4-10 minutes, both when measured *in vitro* from single islets (Westerlund and Bergsten, 2001; Ritzel et al., 2003; Sturis et al., 1994), groups of islets (Chou and Ipp, 1990; Sturis et al., 1994; Song et al., 2002) or the pancreas (Stagner et al., 1980), or *in vivo* from the blood immediately after the pancreas in the portal vein (Song et al., 2000; Pørksen et al., 2002). These pulses are believed to underlie oscillatory plasma insulin levels (Sturis et al., 1994; Pørksen, 2002). In humans more than 70-75 % of the total insulin secretion is released in bursts (Pørksen et al., 1997; Song et al., 2000; Pørksen et al., 2002), and it is primarily the amplitude of the pulsatile insulin secretion, rather than the period, that is affected by changes in glucose concentration (Song et al., 2000; Ritzel et al., 2003; Pørksen et al., 2002; Song et al., 2002; Pørksen, 2002).

It has been suggested that glycolytic oscillations drive the periodic insulin release pattern through periodic modulation of bursting electrical activity (Tornheim, 1997). Bertram et al. (2004) described a model, where the glycolytic subsystem has the ability to oscillate due to positive product feedback onto the glycolytic enzyme PFK. The oscillatory glycolysis leads to oscillations in ATP production which drive periodic activity of K(ATP)-channels. This slow rhythm interacts with the faster activity-dependent $Ca^{2+}$ rhythm that drives simple bursting. The possible outcome of the interaction can occur as clusters or episodes of bursts followed by long silent phases ("compound bursting"), very slow bursting driven entirely by glycolysis ("glycolytic bursting"), or as a periodic variation in the plateau fraction ("accordion bursting"). These various forms of bursting have in common a slow modulation of the intracellular calcium concentration, and consequent pulsatile insulin secretion (Bertram et al., 2004).

To observe an overall oscillatory insulin profile it is necessary that the insulin secretion from individual $\beta$-cells is synchronized within islets (intra-islet synchronization), and that the population of islets is also synchronized (inter-islet synchronization). If the cells or islets were not synchronized we would observe a flat, averaged signal even

though the single cells and islets released insulin in pulses.

## 5.2 Intra-islet synchrony

In *Paper IV* we showed how electrical coupling through gap-junctions can be sufficient to synchronize not only membrane potentials and $Ca^{2+}$ levels, but more surprisingly, also metabolic oscillations within an islet. Thus, diffusion by glycolytic intermediates or other metabolic messengers does not seem to be strictly necessary for intra-islet synchronization. It should be noted that because of the sizes of the molecules, diffusion of ATP or the glycolytic intermediate FBP through gap-junctions is unlikely, while diffusion of G6P is expected to happen. Diffusion of either FBP or G6P synchronizes slow oscillations, but sufficiently strong coupling through G6P can kill glycolytic oscillations (Tsaneva-Atanasova et al., 2006). Thus, glycolytic oscillations can be synchronized by gap-junction coupling, thus explaining the intra-islet synchrony of oxygen consumption (Jung et al., 2000). Since the slow metabolic oscillations are hypothesized to underlie pulsatile insulin secretion, the islet should then release clear insulin pulses as observed experimentally (Sturis et al., 1994; Westerlund and Bergsten, 2001; Ritzel et al., 2003). The next question at hand, which is studied in the following section, is then how groups of isolated islets or the millions of islet in the pancreas are synchronized.

In *Paper IV* we showed that if glycolysis is not synchronized, there is less insulin secretion (Figs. 4 and 5). The positive effects of glycolytic synchronization would be accentuated by any K(ATP)-independent, amplifying pathway (Henquin, 2000), since amplifying signals would plausibly be in phase with the glycolytic oscillator, since they are believed to result from mitochondrial metabolism (MacDonald et al., 2005). If the calcium levels in different cells were in synchrony, but the glycolytic components were not, then the amplifying signals would not be synchronized, and thus would not have maximal effect.

## 5.3 Entrainment by glucose oscillations

It has been shown that pulsatile insulin secretion can be entrained by a periodic glucose stimulus in islets from healthy rats (Chou and Ipp, 1990; Sturis et al., 1994) and humans (Ritzel et al., 2006), as well as in healthy humans *in vivo* (Mao et al., 1999; Pørksen et al., 2000). Moreover, slow NAD(P)H, $Ca^{2+}$ and mitochondrial membrane potential oscillations, which are thought to underlie pulsatile insulin release, can be entrained in mouse islets (Luciani, 2004). The entrainment is impaired in ZDF rats (Sturis et al., 1994) and diabetic humans (Mao et al., 1999; Hollingdal et al., 2000), pointing to a possibly crucial mechanism for normal overall pulsatility. Similar results have been obtained for entrainment of the slower ultradian oscillations (Sturis et al., 1991, 1995).

As shown in *Paper IV*, the modified model by Bertram et al. (2004) can be entrained. Also, an earlier model (Magnus and Keizer, 1998a) shows entrainment (Luciani, 2004), but this model seems too sensitive as seen by the extremely wide Arnold tongue

(Fig. 5.1).

The model used in *Paper IV* can undergo 2:1 entrainment, meaning that for each period of the glucose oscillations we have two $Ca^{2+}$ oscillations and pulses of insulin release (Fig. 5.2). 2:1 entrainment is a general phenomenon of forced oscillatory systems and is also observed in the model by Magnus and Keizer (1998a) as shown by Luciani (2004). Such 2:1 entrainment was recently observed for entrainment of insulin pulses from human islets (Ritzel et al., 2006), and of NAD(P)H, $Ca^{2+}$ and mitochondrial membrane potential oscillations (Luciani, 2004). It was also seen in an *in vivo* study with human patients (Mao et al., 1999). Moreover, the phenomenon is observed for ultradian oscillations (Sturis et al., 1995).

## 5.4 Inter-islet synchrony

The entrainment phenomena has been suggested to be a mechanism by which pulsatile insulin secretion is coordinated between islets (Sturis et al., 1994; Ritzel et al., 2006). Luciani (2004) showed very convincingly that endogenous $Ca^{2+}$ oscillations adjust both their phase and amplitude to a periodic glucose stimulus. Since plasma glucose levels fluctuate *in vivo*, it has been suggested that they are responsible for synchronizing insulin pulses from the dispersed islets and letting the overall pulsatile release pattern from the pancreas appear (Sturis et al., 1994; Pørksen, 2002; Goodner et al., 1991; Gilon et al., 2002). Moreover, *in vivo*, hepatic glucose production follows plasma insulin oscillations (Goodner et al., 1982), which suggests a mechanism by which pulsatile insulin release leads to periodic glucose production and plasma glucose levels. Hence, we have a scenario where pulsatile insulin secretion leads to fluctuations in plasma glucose, which might be able to synchronize the pulses from individual islets thus reinforcing the signal to the liver and plasma glucose. This is the mechanism investigated in *Paper IV* by adding a simplified "liver". We showed that this mechanism of globally coupled oscillators (islets) is indeed able to provide inter-islet synchrony. As mentioned in chapter 1, this feedback scenario is likely to work in parallel with neural synchronizing signals (Stagner et al., 1980; Pørksen, 2002; Gilon et al., 2002).

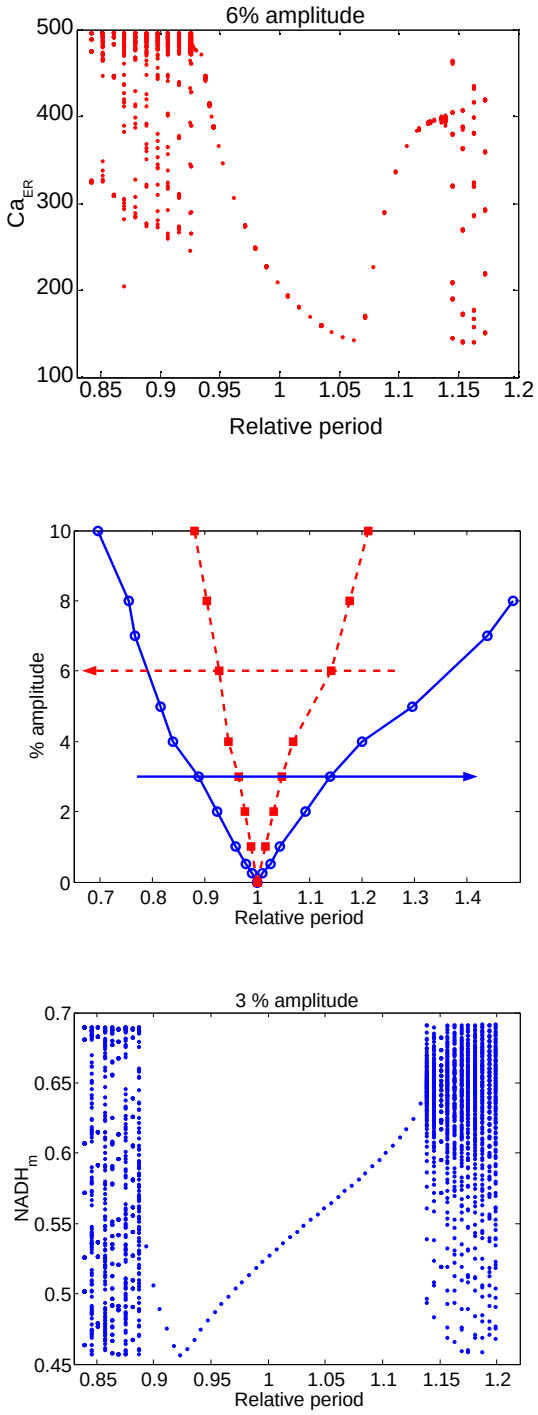


Figure 5.1: Both the models from *Paper IV* (red, upper panel) and Magnus and Keizer (1998a) (blue, lower panel) are entrainable to an oscillating glucose concentration around 10 mM. Upper and lower panels show brute force scans (stroboscopic Poincaré section) through the 1:1 Arnold tongue (middle panel).

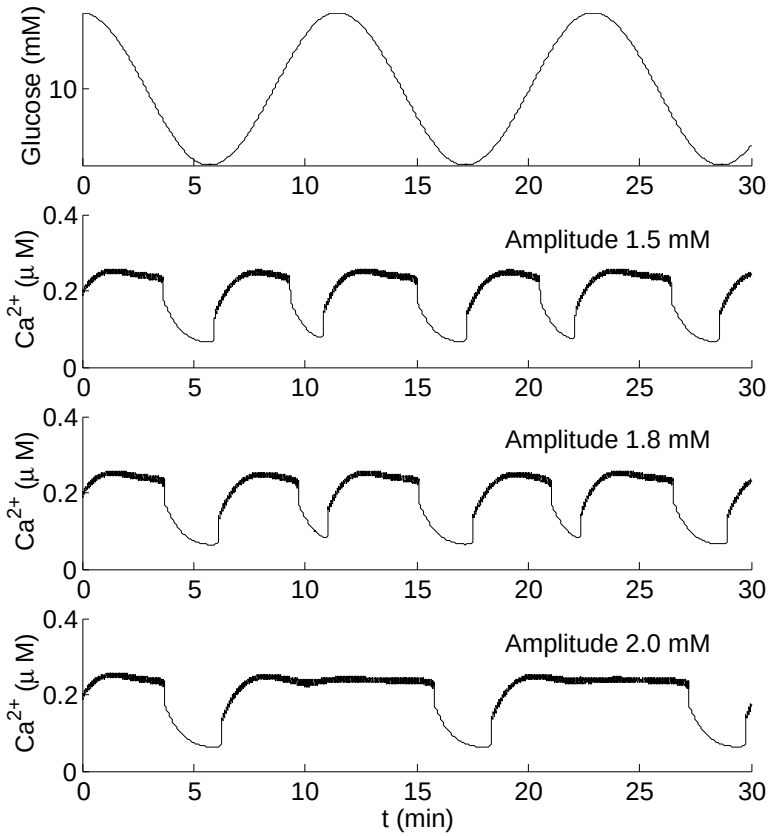


Figure 5.2: 2:1 entrainment of forced $Ca^{2+}$ oscillations. For sufficiently large amplitude, the $Ca^{2+}$ patterns changes to an apparent 1:1 entrainment pattern.

# Chapter 6

# Mitochondria

## 6.1 Structure and function in GSIS

The mitochondria, which are present in the cells of virtually all organisms (including fungi, animals, and plants), are responsible for the production of the majority of the "energy currency" molecule ATP. They are surrounded by double membranes, the inner of which is organized in folds, where aerobic respiration takes place. This inner membrane bounds the compartment called the *mitochondrial matrix*. Mitochondria contain their own DNA and are only formed by the fission of other mitochondria, and are in some sense independent organisms living in symbiosis with the host cell (Alberts et al., 2002).

### 6.1.1 ATP production

The primary function of the mitochondria, which is also its main role in GSIS of $\beta$-cells, is the production of ATP. This is done by metabolizing the major products of glycolysis, pyruvate and NADH, as summarized in Fig. 6.1.

Each pyruvate molecule produced by glycolysis is actively transported across the inner mitochondrial membrane, and into the matrix where it forms acetyl-CoA, which is fed into the tricarboxylic acid (TCA) cycle, also known as the citric acid cycle or the Krebs cycle. This process creates 3 molecules of NADH and 1 molecule of $FADH_2$, which go on to participate in the electron transport chain (ETC). Also NADH from glycolysis is transported into the mitochondrial matrix by a shuttle system.

The energy from NADH and $FADH_2$ is transferred to oxygen in several steps via the electron transfer chain. The protein complexes in the inner membrane that perform the transfer use the released energy to pump protons against a gradient (the concentration of protons in the intermembrane space is higher than that in the matrix). As the proton concentration increases in the intermembrane space, a strong concentration gradient is built up, as well as a large hyperpolarization of the inner membrane. The main exit from the intermembrane space for these protons is through the ATP synthase complex. By transporting protons back into the matrix, the ATP synthase complex can make ATP from ADP and inorganic phosphate ($P_i$). The produced ATP is then exchanged

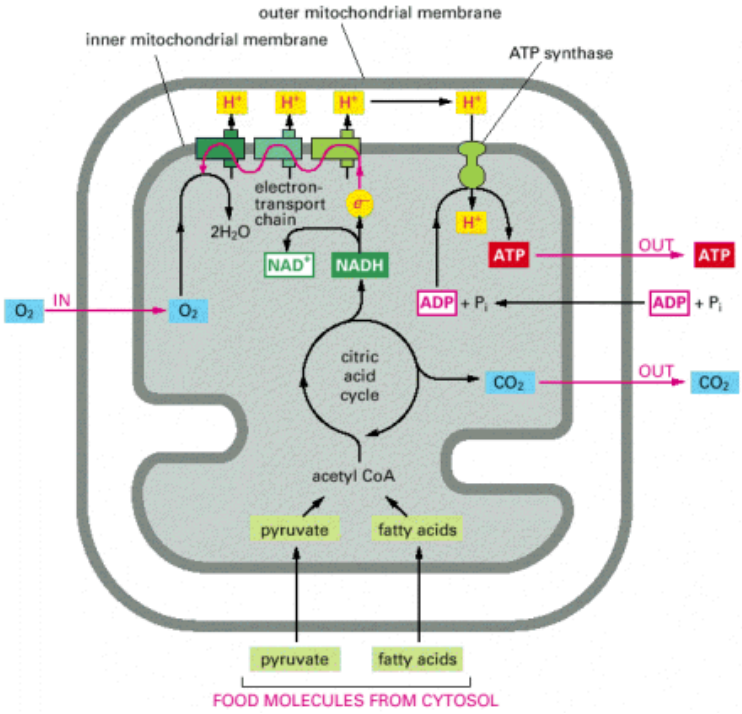


Figure 6.1: Schematics of mitochondrial ATP production. (From Alberts et al. (2002))

with cytosolic ADP.

### 6.1.2 Role of $Ca^{2+}$

The flux of $Ca^{2+}$ into the mitochondria has to opposing effects. Mitochondrial $Ca^{2+}$ stimulates several dehydrogenases, thus enhancing NADH production and leading to hyperpolarization of the inner membrane and eventually ATP production (McCormack et al., 1990). On the other hand the current introduced from the flux of the positive calcium ions through the uniporter lowers the proton motive force and thus ATP synthesis (Magnus and Keizer, 1998a; Krippeit-Drews et al., 2000; Kindmark et al., 2001). These competing effects are studied in *Paper VII*.

### 6.1.3 Anaplerotic products and signaling

$\beta$-cells show remarkedly high levels of the enzyme pyruvate carboxylase (PC), which produces the TCA cycle intermediate oxaloacetate from pyruvate, rather than acetyl-CoA produced by pyruvate dehydrogenase (PDH). The carboxylation pathway can increase the levels of TCA cycle intermediates due to a net input of carbon atoms, while decarboxylation by PDH does not raise the net levels of intermediates. It has been shown that approximately 50% of glucose-derived pyruvate enters mitochondrial metabolism via carboxylation by PC, thus quantitatively equaling the metabolism of acetyl-CoA in the TCA cycle. Anaplerosis, the net synthesis of TCA cycle intermediates, has been suggested to be important in GSIS in the $\beta$-cell, since the excess

amounts of intermediates is exported from the mitochondria to the cytosol for specific purposes, such as signaling and supporting insulin secretion (Schuit et al., 1997; MacDonald et al., 2005). A recent study showed that inhibition of PC, and thus anaplerosis, lowered both first and second phase insulin secretion, possibly by lowering the ATP/ADP ratio, which was attributed to decreased pyruvate cycling in the mitochondria (Fransson et al., 2006).

Malate and citrate levels increase in response to glucose and pyruvate, and the export of malate and citrate to the cytosol by mitochondrial shuttles, permits the export of NADPH equivalents from the mitochondria. Cytosolic NADPH has multiple signaling roles, including stimulating insulin production and secretion (MacDonald et al., 2005).

Exported citrate has another putative messenger role besides being involved in the pyruvate-citrate shuttle and NADPH export. In the cytosol, it is converted into cytosolic acetyl-CoA, which can be carboxylated to malonyl-CoA. Malonyl-CoA itself is believed to have a signaling role, because it is should raise the level of long-chain acyl-CoAs in the cytosol, which has been proposed to influence K(ATP) channels, glucokinase, ATPases and trafficking of insulin granules (Corkey et al., 2000; MacDonald et al., 2005).

Interestingly, citrate oscillates both in isolated mitochondria and in intact insulin secreting INS-1 cells (MacDonald et al., 2003). This demonstrates that besides oscillations in glycolysis and electrical activity, the mitochondria have the ability to oscillate by themselves. A possible mechanism could be the inhibition of citrate production by citrate itself and by succinyl-CoA, another TCA cycle intermediate.

Synchronization between mitochondria within a cell could be achieved by glycolytic oscillations and $Ca^{2+}$ feedback in the spirit of *Paper IV*, but in addition by citrate oscillations due to the inhibition of its own production (MacDonald et al., 2005). Moreover, citrate inhibits PFK, as does ATP, providing feedback from mitochondria to glycolysis and a mechanisms for synchrony.

## 6.2 Modeling

Magnus and Keizer (1997) summarized the most important components of mitochondrial $Ca^{2+}$ handling and ATP production in a minimal model including proton pumping via respiration and proton uptake by the ATP synthase complex, a proton leak, ADP/ATP exchange, the $Ca^{2+}$ uniporter and $Na^{+}/Ca^{2+}$ exchange. The main result was that in the absence of significant $Ca^{2+}$ activation of mitochondrial dehydrogenases, $Ca^{2+}$ uptake would reduce the ATP production rate substantially by reducing the proton motive force, thus suggesting a potential role for mitochondrial $Ca^{2+}$ handling in determining the ATP/ADP ratio in $\beta$-cells by a negative feedback loop. The model was later improved and extended to include the TCA cycle for a study of cardiac mitochondria (Cortassa et al., 2003).

In *Paper VII* we simplified the extremely complex Magnus-Keizer expressions, and used the simple model to study the competing effects of $Ca^{2+}$ in the mitochondria; stimulus of dehydrogenases and lowering of the mitochondrial membrane potential.

Magnus and Keizer (1998a,b) incorporated their mitochondrial model into a elec-

trophysiological model of the cell membrane, and showed that the combined model exhibits bursting electrical behavior. They proposed in line with their earlier article (Keizer and Magnus, 1989), that the negative feedback from $Ca^{2+}$ on ATP/ADP was the mechanism initiating and terminating the active phase of a burst.

In collaboration with R. Bertram, D.S. Luciani and A. Sherman, I coupled the original Magnus and Keizer (1997) model of the mitochondria to the model used in *Paper IV* in order to investigate the effect of coupling the glycolytic system to a detailed model of ATP production and $Ca^{2+}$ handling. This was what led us to simplify the Magnus and Keizer (1997) model as done in *Paper VII*. We are currently working on coupling our simplified mitochondria model (*Paper VII*) to the $\beta$-cell model from *Paper IV*. A main motive for this is the possibility of comparing simulations to experimental observations of mitochondrial variables such as NAD(P)H, mitochondrial membrane potential and oxygen consumption. Our results so far indicate that the model describes these variables appropriately. For example, NAD(P)H leads slow $Ca^{2+}$ oscillations (Luciani, 2004), and intracellular $Ca^{2+}$ concentrations are out of phase with extracellular oxygen levels (Jung et al., 2000), both of which are reproduced accurately by the model. Moreover, it provides an explanation for the termination of oscillations in oxygen consumption and NAD(P)H levels by plasma membrane hyperpolarization. We suggest that the drop in $Ca^{2+}$ induced by hyperpolarization reduces ATP hydrolysis by pumps and increases mitochondrial ATP production. The resulting increase in ATP concentration inhibits PFK and in this way terminates glycolytic oscillations.

Other aspects of mitochondrial functions in $\beta$-cells have also been modeled, such as the NADH shuttles and the TCA cycle (Westermark, 2005). This model was used to analyze the production of the potential messengers in the amplifying pathway, NADPH and malonyl-CoA, besides ATP production. It also reproduced the findings that blocking the NADH shuttles attenuates ATP production while retaining the rate of glucose oxidation (Eto et al., 1999). Modeling the citrate oscillations seen by MacDonald et al. (2003) and investigating synchronization of individual mitochondria would be another interesting task to pursue.

# Chapter 7

# Outlook

A scenario where the global response and dynamics of a population of enzymes, cells or islets are created from the individual properties, is at the core of the fashionable *system biology*. The parts constitute the whole. Such a hierarchy was followed in the present thesis, which started off by studying the correct formulation of enzyme kinetics, moving on to the electrical behavior of individual $\beta$-cell behavior where stochastic effects are important. The electrophysiological descriptions were then complemented by models of glycolysis and mitochondria. At a higher level the cells are synchronized within an islet, and I investigated the role of excitation waves and synchrony of metabolic oscillations. Finally the overall signal from the pancreas in the form of pulsatile secretion with importance for whole body glucose homeostasis, was studied.

$\beta$-cell modeling has helped in clarifying the dynamics underlying mainly bursting electrical activity, which were the topics of *Paper III* and *Paper VI*. Also, excitation wave propagation has been supported by modeling within the framework of nonlinear partial differential equations as in *Paper I* and *Paper II*. I presented preliminary simulations showing waves propagating only partly through an islet in chapter 4, and we are currently trying to understand this phenomena from a mathematical point of view. These models have, roughly speaking, been spurred by the relatively well-understood triggering pathway where electrophysiological behavior is crucial for the $Ca^{2+}$ rise leading to insulin release.

The future questions to be addressed by $\beta$-cell modeling will be phenomena within the cell, such as glycolysis and mitochondrial metabolism. This was initiated in the work by Magnus and Keizer (1997, 1998a,b), and we have made further steps in this direction in *Paper IV* and *Paper VII*. I would also like to mention the work by Westermark (2005) on both glycolysis and NADH shuttles and the TCA cycle in the mitochondria. The scope here is two fold. 1) To understand how metabolism interacts with $Ca^{2+}$ dynamics in shaping various bursting patterns and pulsatile insulin release as in *Paper IV*, and, 2) to include the amplifying pathway, which is believed to include metabolic signals, for example derived from anaplerosis. Modeling could help in gaining a better understanding of the less well-characterized amplifying pathway.

Interestingly, the last and medically most important step, insulin release by exocytosis following granule trafficking and priming, has been in great parts neglected by model-

ing efforts. Grodsky and co-workers (Grodsky et al., 1970; Grodsky, 1972; O'Connor et al., 1980), made a relatively crude two-compartmental model, but since then it appears that no one has attempted to make a more detailed model of these crucial last steps of GSIS including the biological facts obtained since Grodsky's work in the seventies. This fact is highly related to the lack of modeling of the amplifying pathway, which is thought to act on the mechanisms controlling the dynamics of the insulin granules such as trafficking, docking, priming and exocytosis. It is now known that granule movement is not directly controlled by calcium in contrast to insulin release, but rather by various kinases such as protein kinases A and C, and by calmodulin phosphorylation of myosin light chains (Niki et al., 2003) in addition to cAMP-mediated enhancement of mobilization and priming of secretory granules (Kwan and Gaisano, 2005). Moreover, ATP levels and other mitochondrial products are involved in controlling priming (MacDonald et al., 2005) and mobilization (Rorsman et al., 2000). Thus, several putative pathways seem to interact in establishing the amplifying signal controlling insulin granule dynamics. Mathematical modeling would help investigate the relative strength of the different signals. I have received a one-year Post. Doc. grant for a project going in this direction, which will be carried out in Prof. C. Cobelli's group at the University of Padova, Italy.

A result that still needs explanation, is the fact that islets from SUR-deficient mice lacking functional K(ATP)-channels show compound bursting (Düfer et al., 2004). Islets from these mice show very little dependence on the extracellular glucose concentration, emphasizing that the ATP/ADP ratio does not play a significant role for the bursting activity due to the dysfunctional K(ATP)-channels. Plausibly, bursting is driven by the $Ca^{2+}$ dependent $K_{slow}$ channels described by Göpel et al. (1999a) (Haspel et al., 2005). But the glycolytic mechanism that we have proposed to underlie the clustering of individual burst can not be at play since periodic ATP/ADP ratio and K(ATP)-channels activity would play no role. A speculative idea could be that oscillating ATP concentration would drive the SERCA pumps, and thus the ER $Ca^{2+}$ concentration, rhythmically with a period of several minutes. This could then yield periodic activation of the $K_{slow}$ channels. Mathematically modeling could be used to test such an idea and give suggestions for experiments to support it.

A more fundamental issue is the use of correct approximations when modeling biochemical reaction as discussed in *Paper VIII* and *Paper X*. As shown in *Paper VIII* the use of an invalid approximation could predict, e.g., oscillations while the original system shows stable behavior, and could lead to incorrectly estimated parameter values as shown in *Paper X*. This might lead our research off track when studying the system further, for example with the scope to look for drugs changing the behavior of the system. I refer to the discussions in *Paper VIII* and *Paper X* for further comments on these aspects. Besides this, there is the question of stochastic versus deterministic simulations and the underlying assumption of a well-stirred media as commented on in the discussion of *Paper V*. It is known that high local $Ca^{2+}$ gradients, so-called microdomains or hot-spots, are present for example near the mitochondrial $Ca^{2+}$ uniporter (Rizzuto et al., 2000). $Ca^{2+}$ microgradients have also been directly observed under the plasma membrane in mouse $\beta$-cells, where they are believed to be important for exocytosis (Bokvist et al., 1995; Quesada et al., 2000). New models, not only for the $\beta$-cell, should take spatial and stochastic effects into account, but only where

appropriate. Thus, we should not forget Einstein's principle of keeping the models simple, but not too simple.

# *Paper I*

*Journal of Biological Physics* **30:** 285–303, 2004.



# Homogenization of Heterogeneously Coupled Bistable ODE's—Applied to Excitation Waves in Pancreatic Islets of Langerhans

MORTEN GRAM PEDERSEN
*Informatics and Mathematical Modelling, The Technical University of Denmark, DK-2800 Lyngby, Denmark*
*(e-mail: mgp@imm.dtu.dk)*

**Abstract.** We consider a lattice of coupled identical differential equations. The coupling is between nearest neighbors and of resistance type, but the strength of coupling varies from site to site. Such a lattice can, for example, model an islet of Langerhans, where the sites in the lattice model individual but identical $\beta$-cells, and the coupling between cells is made of gap junctions.

By using a homogenization technique we approximate the coupled discrete equations by a PDE, basically a nonlinear heat equation (a Fisher equation). For appropriate parameters this equation is known to have wave-solutions. Of importance is the fact, that the resulting diffusion coefficient does not only depend on the average of the coupling, but also on the variance of the strength. This means that the heterogeneity of the coupling strength influences the wave velocity—the greater the variance, the slower is the wave. This result is illustrated by simulations, both of a simple prototype equation, and for a full model of coupled beta-cells in both one and two dimensions, and implies that the natural heterogeneity in the islets of Langerhans should be taken into account.

**Key words:** homogenization, calcium waves, excitation waves, propagation speed, coupled pancreatic $\beta$-cells, gap-junctions

## 1. Introduction

The pancreatic islets of Langerhans consist of thousands of coupled cells, among these the $\beta$-cells produce insulin. To have a proper functioning and insulin production, it is very important that the $\beta$-cells co-operate in a synchronized manner, and the coupling between cells made up of gap junctions seems to be crucial for this synchronization ([3, 5] and references herein). In [1] it was shown experimentally that calcium waves could provide a way to synchronize the cells. Using a mathematical model of the $\beta$-cells the authors showed that the gap junctions indeed could result in waves of the observed kind. However, the simulated speed was significantly faster (about 200 $\mu$m/s) than the experimentally observed speeds (30–100 $\mu$m/s), if standard values were used in the model. The authors gave possible

explanations for this speed difference, all involving modifying parameter values.

It was assumed in [1] that the coupling strength was constant from site to site. This is known not to be the case, indeed there is a natural variance of the coupling strengths [7, 5].

We show here that if the authors of [1] had taken into account the natural variance of the coupling strengths of the gap-junctions, they would have seen significantly lower wave-speeds—in some cases—even in the experimentally observed region.

To understand why the average (the arithmetic mean) of the coupling strength is not enough to estimate the propagation speed of the waves, we need the mathematical discipline *homogenization* theory (see [2]), which shows that, it is the *harmonic mean* that determines the velocity—and this will explain why the variance is important.

The paper is organized as follows. In the next section we look at the general case, and see that the homogenization theory can indeed be applied, and the harmonic mean determines the wave speed. This is then used for the Fisher equation (Section 3) to see that the theory estimates the simulated wave-speed very well. We then move on to compare it with the $\beta$-cell model, obtaining the results mentioned above. Finally, two-dimensional simulations show that similar conclusions can be made in both the case of the Fisher equations and the $\beta$-cell model in 2D. We discuss the results in Section 6. A detailed description of the $\beta$-cell model is given in the Appendix.

## 2. The Model and Homogenization—The Continuum Limit

We consider an finite line of cells modeled by ($j = 0, \ldots, N$)

$$\frac{dv_j}{dt} = f(v_j) + g_{j+1} \cdot (v_{j+1} - v_j) + g_j \cdot (v_{j-1} - v_j). \tag{1}$$

The relevance for $\beta$-cells is similar for Eqs. (5) and (6) in [1]. This is discussed further in Section 4.

The distance between neighbors is set to be $\epsilon$ such that $v_j = v(j\epsilon)$, and we observe the behavior when $\epsilon \to 0$. Let us first consider the simple case of equal connections, where every $g_i = g = \epsilon^{-2}D$ for a constant D (see also [1]). With $x = j\epsilon$, we get

$$\frac{\partial v}{\partial t}(x) = f(v(x)) + g \cdot (v(x+\epsilon) + v(x-\epsilon) - 2v(x)),$$

or, using a Taylor approximation and letting $\epsilon \to 0$,

$$\frac{\partial v}{\partial t}(x) = f(v) + D\frac{\partial^2 v}{\partial x^2}, \tag{2}$$

which is known to have wave solutions for appropriate $f$, with propagation velocity proportional to $\sqrt{D}$ [1].

Now, we assume that the connection varies from site to site as described by (1). Let $\kappa_\epsilon$ be a family of differentiable functions with $||\kappa_\epsilon||_\infty$ independent of $\epsilon$. With $g_j = g(j\epsilon) = \epsilon^{-2}\kappa_\epsilon(x)$, $x = j\epsilon$ we get as above:

$$\begin{aligned}\frac{\partial v}{\partial t} &= f(v) + \left(g + \epsilon\frac{\partial g}{\partial x} + o(1)\right)\left(\epsilon\frac{\partial v}{\partial x} + \frac{\epsilon^2}{2}\frac{\partial^2 v}{\partial x^2} + o(\epsilon^3)\right) \\ &\quad + g\cdot\left(-\epsilon\frac{\partial v}{\partial x} + \frac{\epsilon^2}{2}\frac{\partial^2 v}{\partial x^2} + o(\epsilon^3)\right) \\ &= f(v) + \kappa_\epsilon(x)\frac{\partial^2 v}{\partial x^2} + \frac{\partial \kappa_\epsilon}{\partial x}\frac{\partial v}{\partial x} + o(\epsilon) \\ &= f(v) + \frac{\partial}{\partial x}\left(\kappa_\epsilon(x)\frac{\partial v}{\partial x}\right) + o(\epsilon).\end{aligned} \tag{3}$$

## 2.1. PERIODIC COUPLING

We hold the total length constant, $N\epsilon = L$, and assume that the coupling strength is periodic, $g_j = g_{j+J}$ for some $J$. This can be incorporated in (3) without any loss of generality by assuming that $\kappa_\epsilon(x) = \kappa(\frac{x}{\epsilon})$, where $\kappa$ is a periodic function of period 1 with $0 < \kappa_1 \le \kappa \le \kappa_2$ for constants $\kappa_1, \kappa_2$. Then we obtain

$$\frac{\partial v}{\partial t} = f(v) + \frac{\partial}{\partial x}\left(\kappa\left(\frac{x}{\epsilon}\right)\frac{\partial v}{\partial x}\right) + o(\epsilon). \tag{4}$$

The theory of such equations in the limit $\epsilon \to 0$ is understood well from material science modeling of a periodic structure and is rigorously covered by the mathematical discipline of *homogenization theory* (see [2]).

In the limit $\epsilon \to 0$ we get the equation [2]:

$$\frac{\partial v}{\partial t} = f(v) + \kappa^*\frac{\partial^2 v}{\partial x} \tag{5}$$

where $\kappa^*$ *is not* the average of $\kappa$, $E(\kappa)$, as one might expect from a first guess, but instead is the *harmonic mean*

$$\kappa^* = \left(E(1/\kappa)\right)^{-1}. \tag{6}$$

We expect that the solution to the discrete Eq. (1) behaves similar to the solution of Eq. (5). Of course, if $\kappa(x) = D$ is constant, we obtain Eq. (2) again.

To understand the implications for the heterogenous case, we consider the simplest case, where

$$\kappa(x) = \begin{cases} g_1 & \text{for } 0 \leq x \leq 0.5, \\ g_2 & \text{for } 0.5 \leq x < 1, \end{cases} \tag{7}$$

$g_2 > g_1$, modeling interchangingly strong and weak coupling.[1] The unique part is that it is not the average $E(g) = \frac{g_1+g_2}{2}$ that determines the wave velocity, but instead

$$\left(\frac{g_1^{-1} + g_2^{-1}}{2}\right)^{-1} = 2 \cdot \frac{g_1 g_2}{g_1 + g_2} = \frac{(E(g) - \sigma(g))(E(g) + \sigma(g))}{E(g)} = E(g) - \frac{\sigma(g)^2}{E(g)},$$

where $\sigma(g) = \frac{g_2-g_1}{2}$ is related to a kind of "standard deviation" of $g$, i.e., the degree of heterogeneity of the couplings.

In general, we have

$$\kappa^* = (E(1/\kappa))^{-1} \leq E(\kappa),$$

and we expect that in the case of wave propagation, a greater variance will lead to slower waves.

### 2.2. Randomly distributed connections

In the proof of the above [2] the periodicity of $\kappa$ is not explicitly used—only that

$$\frac{1}{\kappa_\epsilon} \to E(1/\kappa) \text{ weak star in } L_\infty.$$

This should also be true if we choose the connections $g_j$ randomly from a fixed distribution $F$, i.e., as data coming from a stochastic variable $X$ with distribution $F$. For sufficiently multiple connections (i.e., $\epsilon$ small enough) integrating $\frac{1}{\kappa_\epsilon}$ should be near the average of, not the original distribution, but $E(1/X)$. This would be a consequence of the Law of Large Numbers for weighted averages. Hence, the theory should also work in this case.

## 3. Numerical Simulations of a Simple Model

### 3.1. Periodic coupling

We consider a line of 500 cells connected with interchangingly weak and strong connections as indicated in Eq. (7), and with a no-flux boundary condition

($v_0 = v_1, v_{501} = v_{500}$). We observe that the propagation velocity, $c$, should not depend on the average of the connections, $E(g)$, but instead, we have

$$c_{\text{th}} = K \cdot \sqrt{(E(1/\kappa))^{-1}} = K \cdot \sqrt{E(g) - \frac{\sigma^2}{E(g)}}, \tag{8}$$

where $K$ is a constant, which we can find from the homogeneous case, $\sigma = 0$.

We choose a simple model, the *Fisher equation*, with

$$f(v) = -v(v - a)(v - 1).$$

It is well known [8] that the wave speed in the homogeneous case $\sigma = 0$ is

$$c_{\text{th}}^0 = \sqrt{\frac{D}{2}}(1 - 2a) = \sqrt{\frac{E(g)}{2}}(1 - 2a), \tag{9}$$

so that

$$c_{\text{th}} = \frac{1 - 2a}{\sqrt{2}} \sqrt{E(g) - \frac{\sigma^2}{E(g)}}. \tag{10}$$

We hold $a = 0.1$, $E(g) = 2$ is fixed and $\sigma$ varies from 0 to 1.9. The initial conditions are $v_j = 0$ for all $j$. We start a wave by instantaneously rising $v_1 = 1$. Then the time is measured when respectively $v_{100}$ and $v_{500}$ reach the value 0.9, from which we can calculate the speed, $c$. We see in Figure 1 that the theory indeed

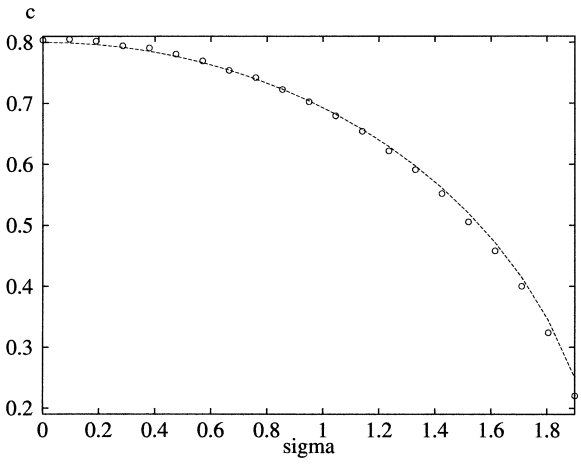


*Figure 1.* Comparison between theoretical propagation velocities ($c_{\text{th}}$, the curve) and the simulations ($c$, the circles) as a function of the "deviation", $\sigma$, for the Fisher equation with *periodic coupling* is shown. Here, $a = 0.1$ and $E(g) = 2$ so that $c_{\text{th}}^0 = 0.8$.

estimates the simulated speed very well, especially if the variance is not too big, and also get the right speed for the homogeneous case $\sigma = 0$, $c_{\text{th}}^0 = \frac{1-2\cdot 0.1}{\sqrt{2}}\sqrt{2} = 0.8$.

Varying $E(g)$ and $a$ does not seem to change this conclusion as long as the parameters initiate a wave.

### 3.2. Randomly chosen coupling

Again we simulate a line of 500 cells modeled as given in the previous subsection. However, now the coupling strength is chosen randomly from a gamma-distribution $GAMMA(a, b)$. The reasons for choosing the gamma-distribution (and not for example a normal distribution) are that we know the average of the inverse gamma-distribution, and will always have a positive coupling strength. We have for $X \sim GAMMA(a, b)$,

$$E(X) = ab, \quad \text{Var}(X) = ab^2, \tag{11}$$

and

$$\left(E\left(\frac{1}{X}\right)\right)^{-1} = (a-1)b = E(X) - \frac{\text{Var}(X)}{E(X)}. \tag{12}$$

So, also in this case we expect that the propagation velocity decreases with increasing variance following

$$c_{\text{th}}^{\text{Gamma}} = K\sqrt{E(X) - \frac{\sigma^2}{E(X)}}. \tag{13}$$

We hold $E(X) = 2$ constant as above, and vary $\sigma^2 = \text{Var}\,(X)$. Figure 2 shows that the theory predicts the simulated speed well.

The fit is not so good as in the periodic case because of the random factor. Comparing with the so-called *semi-theoretical* speed

$$c_{\text{semi}} = K\sqrt{\left(\frac{1}{400}\sum_{i=101}^{500}\frac{1}{g_i}\right)^{-1}}, \tag{14}$$

obtained from the actual coupling used in the simulation, we get a better fit. In this manner, we see that a large part of the difference between simulated and theoretical speeds arises from the random choice of coupling strengths rather than from a gap in the theory. Again, repeating the simulations does not change the conclusion, and of course, the average of many such simulation should fit the theoretical curve well.

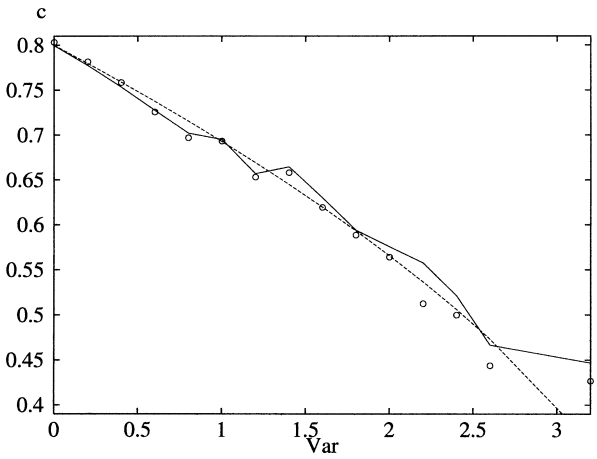


*Figure 2.* Comparison is shown between theoretical propagation velocities ($c_{\text{th}}^{\text{Gamma}}$, the punctuated, smooth curve), the semi-theoretical velocities ($c_{\text{semi}}$, the rugged curve) and the simulations (the circles) as a function of the variance, Var $= \sigma^2$, now for *Gamma-distributed* couplings. Again $c_{\text{th}}^0 = 0.8$. For Var > 2.6 most of these specific coupling strengths and initial conditions do not initiate a wave.

## 4. A Line of $\beta$-Cells

We simulate a line of $\beta$-cells using the same model as given in [1]. However, we choose the coupling strengths randomly, so that they vary along the line. This is in contrast to the simulations given in [1] where an identical coupling was assumed. We show how the propagation speed depends on the variance of the couplings. In particular, it is shown that the heterogeneity can provide another explanation why the simulations in [1] gave very high wave speeds.

### 4.1. Model and method

The model is taken from [9] and is given as follows with $j = 1,\ldots, 20$:

$$c_m \cdot \frac{dv_j}{dt} = I\left(v_j, n_j, s_j, Ca_j^i, Ca_j^{er}\right) + g_j(v_{j-1} - v_j) + g_{j+1}(v_{j+1} - v_j), \quad (15)$$

$$\frac{dn_j}{dt} = \frac{n_\infty(v_j) - n_j}{\tau_n}, \quad (16)$$

$$\frac{ds_j}{dt} = \frac{s_\infty(v_j) - s_j}{\tau_s}, \quad (17)$$

$$\frac{dCa_j^i}{dt} = f \cdot \left(\alpha I_{Ca}(v_j) - k_c Ca_j^i\right) + (J_{\text{out}} - J_{\text{in}}), \quad (18)$$

$$\frac{dCa_j^{er}}{dt} = \frac{J_{\text{in}} - J_{\text{out}}}{\rho}. \quad (19)$$

Here, $v_j$ is the membrance potential, $n_j$ and $s_j$ are, respectively, fast and slow gating variables, $Ca^i_j$ is the intra-cellular calcium concentration and $Ca^{er}_j$ is the calcium concentration in the ER calcium stores for the $j'$th cell. The $j'$th cell is coupled through gap junctions to the neighboring cells $j-1$ with conductance $g_j$ and $(j+1)$ with conductance $g_{j+1}$. The function $I$ is the total membrance current, and $I_{Ca}$ is one of these currents, a voltage-dependent calcium current. $J_{\text{in}}$ and $J_{\text{out}}$ are the currents going in and coming out of the ER stores, $c_m$ is the total membrance capacity, $n_\infty$ and $s_\infty$ are steady states depending on $v$, $\tau_n$ and $\tau_s$ are time constants and $f$, $\alpha$, $k_c$ and $\rho$ are constants. We impose the no-flux boundary condition, $v_0 = v_1, v_{21} = v_{20}$. For details see [9, 1] or Appendix for detailed expressions and parameter values.

The relation to Eq. (1) is given as follows (see also [1]). On the wave front we can uncouple the variables $Ca^i$ and $Ca^{er}$, assuming that $s$ is constant while $n = n_\infty(v)$ leaves only

$$c_m \cdot \frac{dv_j}{dt} = I(v_j, n_\infty(v_j); s) + g_j(v_{j-1} - v_j) + g_{j+1}(v_{j+1} - v_j),$$

of the same form as (1).

Simulations now result in similar conclusions as seen for the Fisher equation in Section 3: As the variance increases, the wave speed decreases.

Imposing a random initial condition on $v_j$ results in a wave pattern after a very short transient period. The speed is found as the length between the center of the first and the last cell, $L = 20 \times 10$ $\mu$m, divided by the (absolute) difference of the times when $v_1$, respectively, $v_{20}$ increases through $-60$ mV signifying the beginning of an active period. Hence we count waves starting from either side of the line. To ensure that we do not count "false" beginnings we require that $s_1$, $s_{20}$, is less than 0.45 at the same time. This value was found empirically.

Now we take the average speed of many successive waves (until $t = 1000$ s), but only counting speeds between 30 and 500 $\mu$m/s (the typical simulated value is 100–250 $\mu$m/s, in experiments it is 30–100 $\mu$m/s). Hence, we rule out very fast waves because these are probably waves starting almost simultaneously from both sides, and very slow speeds because these are probably coming from errors in the measure method. For example, one could imagine that for a brief moment $v_1$ passes above $-60$ mV without starting a wave. However, the time is recorded, so when $v_{20}$ increases above $-60$ mV much later, we will obtain a very small number for the speed. Such phenomena should of course be ruled out.

### 4.2. SIMULATIONS

Simulations of periodic coupling with $g_i = 100$ pS $+ (-1)^i \cdot \sigma$ as given in Section 3.1 are shown in Figure 3, where the simulated average wave speed is

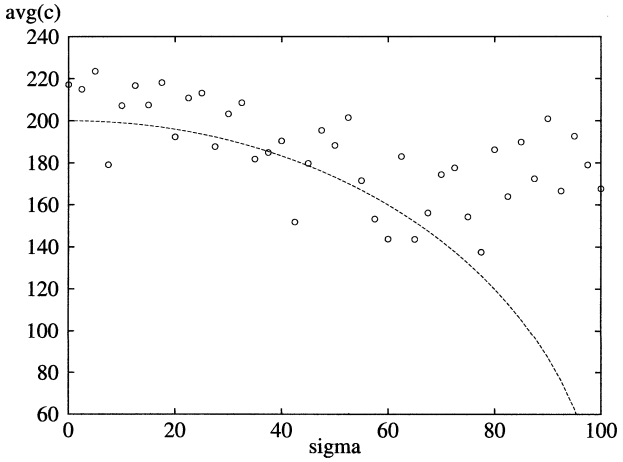


*Figure 3.* Comparison is shown between theoretical propagation velocities ($c_{\text{th}}$, the curve) and the simulations (the circles) as a function of the "variance," $\sigma$, for the $\beta$-cell model with periodic coupling, $g_i = 100\ \text{pS} + (-1)^i\sigma$.

compared with the theoretically expected value

$$c_{\text{th}} = 200\ \mu\text{m/s}\sqrt{1 - \left(\frac{\sigma}{100\ \text{pS}}\right)^2},$$

where 100 pS is the average coupling strength, and the value of 200 $\mu$m/s is chosen for obtaining a reasonable fit. This speed coincides with the speed found in [1]. We see that for $\sigma$ below approximately 70 pS, the simulated and the theoretical values coincide pretty well, although there are large deviations. We claim, that at least the tendency seems to be, that for larger $\sigma$ the wave is slower.

We repeat the simulation, but now with coupling strengths randomly chosen from a uniform distribution on $(\mu - d, \mu + d)$, i.e. coming from a stochastic variable $X \sim UNIF(\mu - d, \mu + d)$. The simulated wave speeds should be compared with

$$c_{\text{th}} = K\sqrt{E(1/X)^{-1}} = K\sqrt{\frac{2d}{\ln\left(\frac{\mu+\text{d}}{\mu-\text{d}}\right)1\text{pS}}}. \tag{20}$$

To distinguish whether the differences between the simulated speed and the speed coming from the limit equation is due to the actual chosen coupling strengths, we also compare with the semitheoretical value

$$c_{\text{semi}} = K\sqrt{\left(\frac{1}{19}\sum_{i=2}^{20}\frac{1\ \text{pS}}{g_i}\right)}. \tag{21}$$

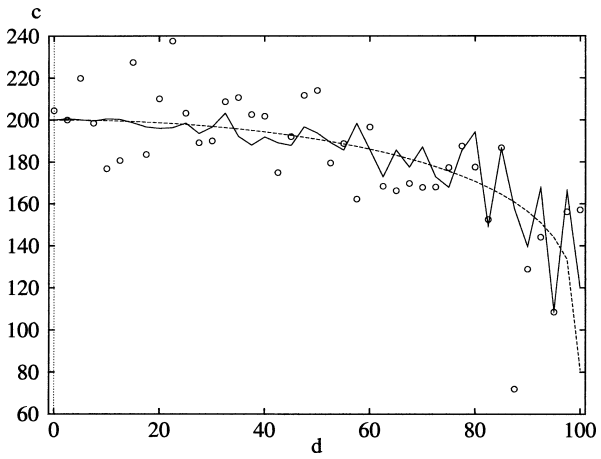


*Figure 4.* Comparison is shown between theoretical propagation velocities ($c_{\text{th}}$, the punctuated, smooth curve), the semi-theoretical velocities ($c_{\text{semi}}$, the rugged curve) and the simulations (the circles) as a function of $d$ for the $\beta$-cell model with uniformly, randomly chosen coupling, *UNIF*(100 pS $-d$, 100 pS $+ d$). We know that the relation between $d$ and the variance is Var $= \frac{d^2}{3}$. Here $K = 20$ $\mu$m/s, corresponding to a homogeneous velocity of 200 $\mu$m/s, is chosen to obtain a good fit.

Again, we hold $\mu = 100$ pS as fixed and vary $d$. Figure 4 shows that the simulated values are predicted well by the theoretical and the semitheoretical speeds, $c_{\text{th}}$ and $c_{\text{semi}}$. Also, we see that these two values coincides well, and hence the simulated speeds are not different from the theoretical values because of a wrong predicted value for the relevant $(E(1/X))^{-1}$. This corresponds to the fact that we have discrepancies between the simulated and predicted speed even in the perfect periodic case.

By using the gamma-distribution the same conclusion is yielded as shown in Figure 5. Again we get a reasonable fit with the expected theoretical wave speed from Eq. (13), at least for Var $< 8000$ (pS)$^2$, or even better also for higher values of Var by using the semitheoretical values from Eq. (21).

The simulations with a normal distribution confirm the general picture, as shown in Figure 6. In this case we do not have a simple theoretical expression to compare the speed with. Instead, after many simulations, we found that the average decreases approximately from 210 $\mu$m/s to 150 $\mu$m/s. Because the normal distribution can result in negative values, we take special care in setting these couplings to 0, signifying no connection between the two cells (indicated with a dot in Figure 6). This should of course prohibit wave propagation. However, because the cells are self-excitory, we can get two independent waves on each side of the point without connection so that the overall picture could imitate a true wave. These cases should be ruled out which results in a slightly greater average speed (the speeds quoted above) than if these cases were included.

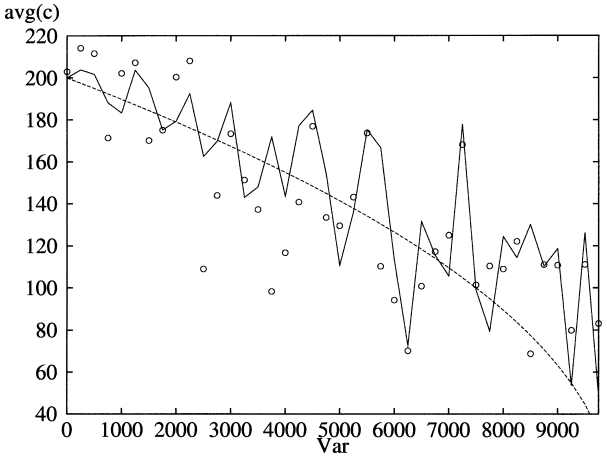


*Figure 5.* Comparison is shown between theoretical propagation velocities ($c_{\text{th}}$, the punctuated, smooth curve), the semi-theoretical velocities ($c_{\text{semi}}$ the rugged curve) and the simulations (the circles) as a function of the variance, Var, for the $\beta$-cell model with randomly chosen coupling from a Gamma-distribution, $GAMMA(a, b)$ with $a = \frac{\mu^2}{\text{Var}}$, $b = \frac{\text{Var}}{\mu}$, where $\mu = 100$ pS is the average. Again we use the value 200 $\mu$m/s for the homogeneous case.

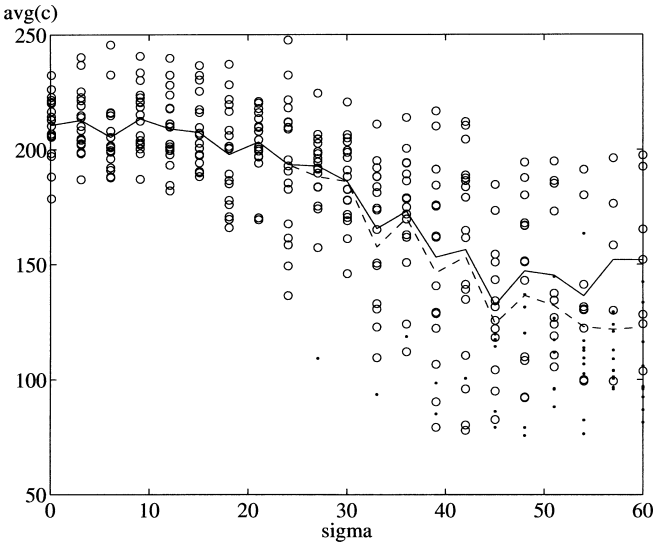


*Figure 6.* Several simulations were done of the wave speed for the line of $\beta$-cells with couplings chosen from a normal distribution $N(100 \text{ pS}, \sigma^2)$. For each choice of $\sigma$ we did 18 simulations applying different configurations of the couplings. The circle indicates a simulation where all the couplings were positive, the dot indicates a simulation where one or more of the couplings were zero so that the line was not connected. The solid line indicates the average for the connected lines (the circles), the dashed line the average of all the simulations (the circles as well as the dots).

Note that we get average speeds as low as 80 $\mu$m/s for sufficiently large Var $= \sigma^2$ in all three cases. This is in the experimental range of (30–100 $\mu$m/s), hence we observe, as previously mentioned, another possible explanation for the fact that Aslanidi *et al.* found too large wave speeds in [1]—they did not consider the natural variance between the coupling strengths in an islet.

## 5. The Two-Dimensional Case

We have successfully simulated two-dimensional wave propagation. We considered a square lattice of 13 by 13 cells, each cell coupled to four nearest neighbors (N, S, E and W) with a no-flux boundary condition.

Using the Fisher equation and choosing random couplings, leads to similar conclusions as obtained in the one-dimensional case – for greater heterogeneity we find lower propagation speed, as shown in Figure 7. The speed was found over the center cells to rule out (part of) boundary phenomena and the fact that we start the wave in a corner, which influences the speed measured over the first few cells. In this case the speed is slightly higher than in the one-dimensional case (0.98 instead of 0.8 for $\sigma = 0$). We expect that this stems from boundary phenomena.

For the $\beta$-cell model, we used the simpler $(v, n, s)$-system from Eqs. (15)–(17), following Sherman [9]. We imposed heterogeneity by choosing the $g_j$'s from a normal distribution $N(100 \text{ pS}, \sigma^2)$. Examples of two waves from our simulations are shown in Figure 8.

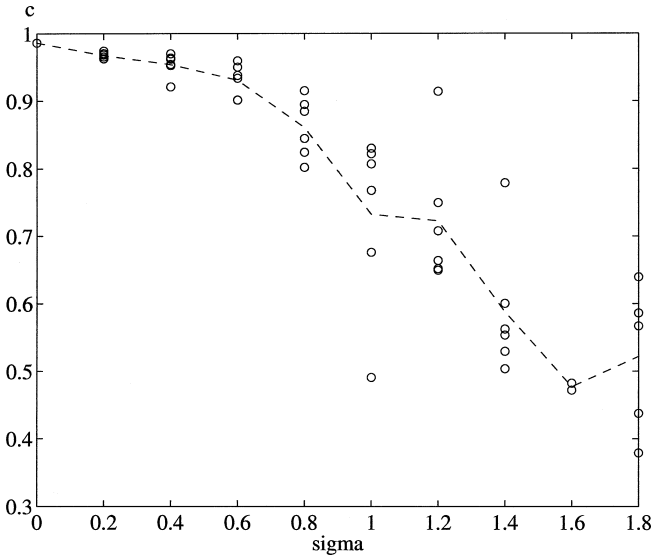


*Figure 7.* Six simulations for each choice of $\sigma$, of the two-dimensional Fisher equation with coupling strengths chosen from a normal distribution $N(2, \sigma^2)$, showing the speed as a function of the standard deviation $\sigma$. The curve shows the average speed of these six simulations.

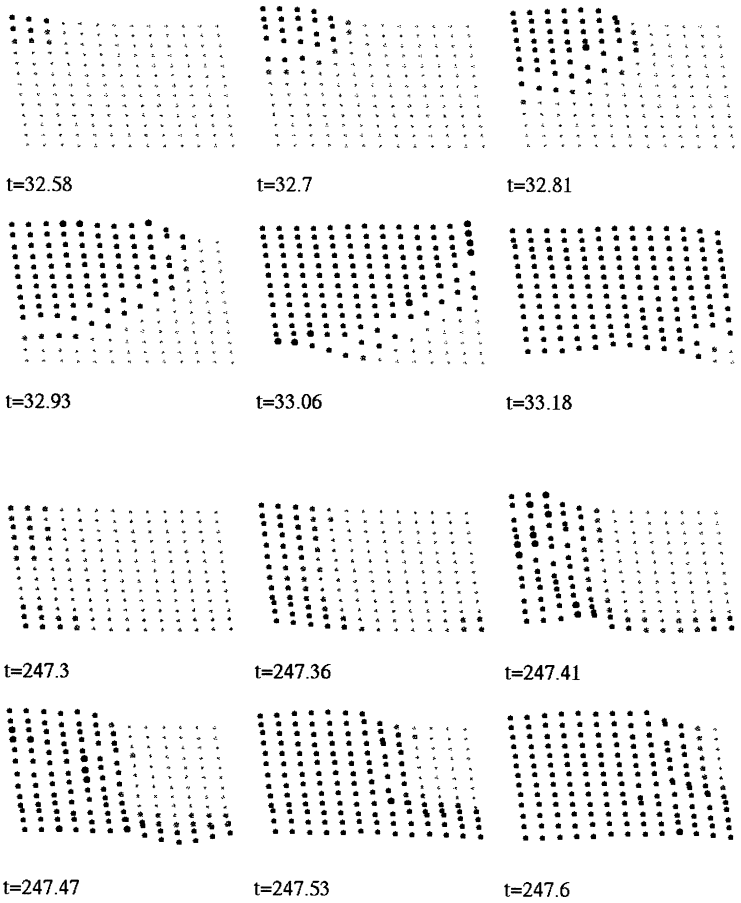


*Figure 8.* Two typical two-dimensional waves obtained from the $(v, n, s)$-subsystem of the $\beta$-cell model. In this simulation the coupling is chosen from a normal distribution, $N(100\text{ pS}, (53\text{ pS})^2)$. The upper figures show the most typical case, where the wave starts from just one corner. The lower ones show the case where the wave starts almost simultaneously from two corners (SW, NW), with a third (SE) starting "independently" slightly later. This results in a much higher measured wave speed.

The speed was found by requiring that all four corner cells should enter the active phase. The time from when this happened to the first, to the time it happened to the last of these cells, was recorded and the diameter of the "islet", $L = 12\sqrt{2} \times 10\ \mu\text{m} = 170\ \mu\text{m}$, was used as the distance the wave had traveled. In the two-dimensional case we do not rule out those cases where one or more of the $g_j$'s have negative value; instead, we used the value 0, which implies that the two involved cells are not coupled. This indeed is the case for about 33% of cell pairs in an islet [7], but the wave can still propagate, using other couplings.

Again varying $\text{Var} = \sigma^2$ seems to have the same effect as seen in the one-dimensional case–for larger $\sigma$, the propagation velocity is lower, as shown in

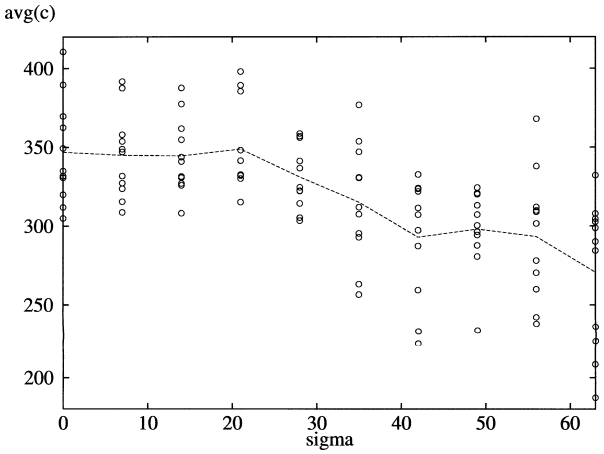


*Figure 9.* Propagation speeds from the $(v, n, s)$-subsystem of the $\beta$-cell model with coupling chosen from a $N(100, \sigma^2)$-distribution. For each choice of $\sigma$ we did 11 simulations applying different configurations of the couplings. The circles indicate each such simulation and the curve shows the average of these 11 simulations, which decreased from 347 $\mu$m/s to 270 $\mu$m/s almost monotonously over the range from $\sigma = 0$ pS to $\sigma = 63$ pS.

Figure 9. Note that the wave speed is significantly greater, about 1.5–2 times as great as in the one-dimensional case.

## 6. Discussion

The main outcome of this paper is the fact that heterogeneity plays an important role in determining the wave speed of an excitation wave. In natural systems such as the islet of Langerhans, the cells are always coupled in a heterogenous manner. So far models have applied the average coupling strength found in experiments as a prototype coupling strength and then, assumed that the coupling was homogenous.

Here we have shown that for estimating the propagation velocity the variance of the coupling strengths plays a crucial role, both in the (pure mathematical) Fisher equation (Figures 1, 2 and 7) and in a standard model for the $\beta$-cells in an islet of Langerhans (Figures 3–6 and 9), for both the case periodic case (Figures 1 and 3) and the random case (Figures 2, 4–7 and 9), and further, both in the one- and two-dimensional cases. To the best of our knowledge, this is the first published literature on simulations of two-dimensional waves in a lattice model of an islet of Langerhans.

The dependence of the coupling on the variance was explained theoretically using the homogenization theory, which gave theoretic predictions of the propagation velocities using harmonic mean $(E(1/g))^{-1}$ instead of the average (arithmetic mean) $E(g)$. This theoretic result coincided well with the simulated speeds, especially when we took into account the deviations arising from the random choices

of coupling strengths using the semitheoretical speed. We believe that the use of the homogenization theory in modeling the $\beta$-cells is a new application. It has been used for a model of the cardiac tissue in [4]. However, from a different perspective, investigating propagation failure and the case of varying gap junctions is not considered explicitly. The heterogeneity there stems from the difference between the resistance in the cells and the resistance of the gap junctions.

However, we obtained excellent fits which simulated the theoretical results only for the Fisher equation. For the $\beta$-cell model the difference between the predicted and simulated velocities was greater. We suggest several possible explanations.

The first explanation could be that we used 500 "cells" for the simulation of the Fisher equation whereas only 20 cells were used for the $\beta$-cell model. Hence, we are closer to the continuum limit of $\epsilon \to 0$ given in the homogenization theory. In Figure 10, we see a simulation of the Fisher equation for 20 cells, and observe that the fit is still decent when we calculate the speed over the center cells (between cell numbers 8 and 12). The deviation for low variance seems to stem from boundary phenomena; when we calculated the speed over all the cells the deviation was found to be significantly greater. Similar boundary phenomena were found in the case of 500 cells, if we calculated the speed over the last 20 cells. Hence, this boundary phenomenon might explain some of the deviation for the $\beta$-cell, but the low number of cells do not matter directly if we take their boundaries into the account. This also explains why we found higher speeds from in the 2D-case (since the boundary is much larger here).

However, even for the periodic case of the $\beta$-cell in Figure 3, we did not obtain regular results. The boundary phenomena result in a nice pattern for the Fisher equation, and hence the same should be expected for the full $\beta$-cell model. The

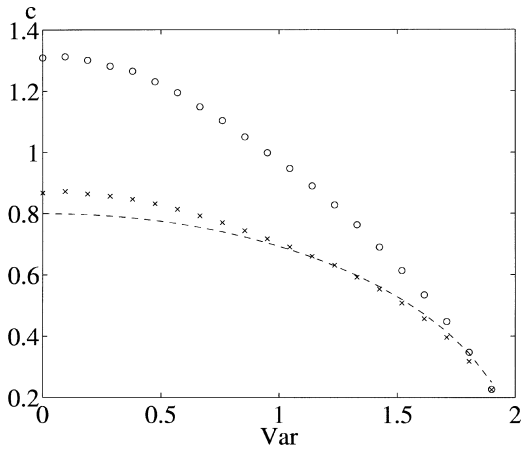


*Figure 10.* Simulated speeds from the Fisher equation, similar to Figure 1, but for 20 cells. The circles are simulated speed calculated as the speed over all the cells whereas the crosses are speeds (of the same waves) calculated over the center cells. The punctuated curve is obtained from the theoretical curve by using the theoretical result $c_{\text{th}}^0 = 0.8$.

$\beta$-cell model is known to admit chaos, even for a single cell [6], and the complex situation with 20 or more coupled cells should be expected to behave irregularly. The above fact complicates the calculation of the simulated wave speeds. The method chosen to find the speed in the simulations could indeed be doubted. We have done control simulations, going through the simulation in detail, and it seems that, in general, the automatic method described in Section 4.1 obtain the same result as a detailed "hands-on" calculation.

The simulations of the one-dimensional $\beta$-cell model showed that heterogeneity alone was sufficient to obtain velocities in the experimental region, and we claim that the fact that Aslanidi *et al.* in [1] used a homogenous coupling can explain the major reason why they obtained too high speeds.

Interestingly, in the case of a normal distribution, which is probably the most "natural" for a physical islet, these low velocities happen around the standard deviation $\sigma = 50$, i.e., for $\sigma$ about half of the mean. Perez-Armendariz *et al.* [7] found experimentally that 67% of cell pairs were coupled with $g_j = 215 \pm 110$ pS, i.e., the standard deviation was about half of the average value. This might be an optimal ratio for proper islet functioning. If the variance is less, the waves are very fast, and if the variance is higher, too many cells will be uncoupled leading to insufficient synchronization. A low variance and/or fast waves could result in a lower responsiveness of the islet on glucose stimulation, as seen in experiments with gene-manipulated cell in the islet expressing abnormally strong connections [3]. The idea is that all the cells in the islets responded even to low glucose stimulations whereas in a normal islet only parts of the islet respond at low glucose levels, and that more cells are entrained for greater glucose stimulation. Naturally, a variating coupling strength would help in having such a behavior.

However, our two-dimensional simulations raised a new question: why do we obtain very high wave speeds in the 2D case but not in the 1D case? Indeed the experiments in [1] and elsewhere were practically two-dimensional, and hence the 2D case is of greater interest.

The fact that the wave is more likely to start independently at two corners (see Figure 8, lower part), so that it has to travel a shorter distance, can explain this. However, for the simulation shown in Figure 8 only 1 out of 15 waves started from two (or more) corners, and in none of the cases where the wave started from one corner did we find wave speeds less than 200 $\mu$m/s.

We also did one-dimensional control simulation of the reduced $(v, n, s)$-system, which gave results similar to the full system, that ruled out the possibility that the $(Ca^i, Ca^{er})$-variables are important.

As mentioned above boundary phenomena, which are more important in two dimensions because more cells are near the boundary, seem to be a plausible explanation. Indeed, we see in Figure 10 that the boundary phenomena can explain a rise of the wave speed of up to 50%, similar to the increased speed between one- and two-dimensional simulations for the $\beta$-cell model. If this is so, then there might be a property of the islet or some condition in the experiments might exist, so that

the no-flux boundary condition become inappropriate. Indeed, the center of an islet has a different structure than the parts near the surface ([5] and references therein). Or maybe, we simply require simulation of greater assemblies of cells—we did the simulations for $13^2 = 169$ cells. But in an islet there are of the order of 2000 cells, so if the cells were squished down to 2D with a height of e.g. three cells, we should simulate $26^2$ cells, i.e., four times as many. Mads Peter Sørensen (personal communications) pointed out another possibility, which is that the curvature of the wave front might result in faster waves. We should pursue this possibility further. Finally, the 3D-case should be of interest—indeed $2000 \simeq 13^3$ so that the simulations presented here have a relevant size for this case.

In summary, the heterogeneity of the islet seems to have an important role in the control of insulin secretion in response to glucose stimulation. Here we have shown that the excitation waves spreading through the islet are modulated by the heterogeneity of the coupling strength, thereby suggesting a way of expressing the heterogeneity. Similar behavior should be expected in other organs consisting of heterogeneously coupled cells, or in ecology modeling having interactions on a smaller scale than that which is relevant for the full problem.

## Acknowledgements

The author thanks "Rejselegat for Matematikere" (Travelling scholarship for Mathematicians) for financial support, "The Biomathematics Laboratory at IASI "A. Ruberti," CNR', Roma, Italy, for kindly letting me visit the Lab, where this work was carried out and Mads Peter Sørensen, IMM, Technical University of Denmark, for fruitful discussions.

## Note

1. It seems reasonable to choose $\kappa$ to be piece-wise constant if $\kappa$ should model gap junctions, and this will be done in what follows. However, then $\kappa$ is not differentiable so to justify the calculations leading to the PDE (3), we should use e.g. a smooth approximation of $\kappa$.

## Appendix: The Equations and Parameters for The $\beta$-Cell Model

The functions and parameters of the Eqs. (15)–(19) are as follows:

$$
\begin{aligned}
I(v, n, s, Ca^i, Ca^{er}) &= I_s(v, s) + I_{\mathrm{Ca}}(v) + I_K(v, n) + I_{K,\mathrm{atp}}(v) \\
&\quad + I_{\mathrm{K,Ca}}(v, Ca^i) + I_{\mathrm{CRAC}}(v, Ca^{er}) \\
I_s(v, s) &= g_s \cdot s \cdot (v - v_k) \\
I_{\mathrm{Ca}}(v) &= g_{\mathrm{Ca}} \cdot m_\infty(v) \cdot (v - v_{\mathrm{Ca}}) \\
I_K(v, n) &= g_K \cdot n \cdot (v - v_k) \\
I_{K,\mathrm{atp}}(v) &= g_{K,\mathrm{atp}} \cdot (v - v_k)
\end{aligned}
$$

$$I_{K,\mathrm{Ca}}(v, Ca^i) = g_{K,\mathrm{Ca}} \cdot (v - v_k) \cdot \frac{(Ca^i)^5}{(Ca^i)^5 + k_d^5}$$

$$\begin{aligned}
I_{\mathrm{CRAC}}(v, Ca^{er}) &= g_{\mathrm{CRAC}} \cdot z_\infty(Ca^{er}) \cdot (v - v_{\mathrm{CRAC}}) \\
m_\infty(v) &= \frac{1}{(1 + \exp((v_m - v)/s_m))} \\
n_\infty(v) &= \frac{1}{1 + \exp((v_n - v)/s_n)} \\
s_\infty(v) &= \frac{1}{1 + \exp((v_s - v)/s_s)} \\
z_\infty(Ca^{er}) &= \frac{1}{1 + \exp((Ca^{er} - \bar{c}_{ER})/s_z)} \\
J_{\mathrm{in}}(Ca^i) &= \frac{v_p}{\mu} \cdot \frac{(Ca^i)^2}{(Ca^i)^2 + k_p^2} \\
J_{\mathrm{out}}(Ca^i, Ca^{er}) &= \frac{p_1}{\mu}(Ca^{er} - Ca^i)
\end{aligned}$$

The parameters used through out the work are:

$$\begin{aligned}
&g_{\mathrm{Ca}} = 1000 \text{ pS}, g_K = 2700 \text{ pS}, g_s = 200 \text{ pS}, g_{K,\mathrm{atp}} = 120 \text{ pS}, \\
&g_{K,\mathrm{Ca}} = 1000 \text{ pS}, g_{\mathrm{CRAC}} = 40 \text{ pS}, \\
&v_{\mathrm{Ca}} = 25 \text{ mV}, v_k = -75 \text{ mV}, v_m = -20 \text{ mV}, v_n = -16 \text{ mV}, v_s = -52 \text{ mV}, \\
&v_{\mathrm{CRAC}} = -30 \text{ mV}, s_m = 12 \text{ mV}, s_n = 5.6 \text{ mV}, s_s = 5 \text{ mV}, \\
&c_m = 5300 \text{ fF}, \tau_n = 20 \text{ ms}, \tau_s = 20000 \text{ ms}, \mu = 250 \text{ ms}, \\
&f = 0.01, k_c = 0.2 \text{ ms}^{-1}, \alpha = -4.5 \cdot 10^{-6} \mu\text{M}/(fA \cdot \text{ms},) \\
&k_d = 0.6,\ k_p = 0.1\ \mu\text{M}, v_p = 0.24\ \mu\text{M}, \bar{c}_{ER} = 4\ \mu\text{M}, s_z = 1\ \mu\text{M}, \rho = 5, p_1 = 0.02.
\end{aligned}$$

The diameter of a $\beta$-cell was set at 10 $\mu$m.

In the two-dimensional simulations we uncoupled $(Ca^i, Ca^{er})$ by neglecting $I_{K,\mathrm{Ca}}$ and $I_{\mathrm{CRAC}}$. All parameters were left unchanged.

All simulations were done using the banded version of the CVODE solver of the program XPPAUT with standard tolerances.

## References

1. Aslanidi, O.V., Mornev, O.A., Skyggebjerg, O., Arkhammar, P., Thastrup, O., Sørensen, M.P., Christiansen, P.L., Conradsen, K. and Scott, A.C.: Excitation Wave Propagation as a Possible Mechanism for Signal Transmission in Pancreatic Islets of Langerhans, *Biophys. J.* **80** (2001), 1195–1209.
2. Bensoussan, A., Lions, J.L. and Papanicolaou, G.C.: *Asymptotic Analysis for Periodic Structures*, North Holland, New York, 1978.
3. Charollais, A., Gjinovci, A., Huarte, J., Bauquis, J., Nadal, A., Martín, F., Andreu, E., Sánchez-Andrés, J.V., Calabrese, A., Bosco, D., Soria, B., Wollheim, C.B., Herrera, P.L. and Meda, P.:

Junctional Communication of Pancreatic $\beta$ Cells Contributes to the Control of Insulin Secretion and Glucose Tolerance, *J. Clin. Invest.* **106** (2000), 235–243.

4. Keener, J.P.: 'Homogenization and Propagation in the Bistable Equation', *Physica D* **136** (2000), 1–17.
5. Mears, D., Sheppard, N., Atwater, I. and Rojas, E.: 'Magnitude and Modulation of Pancreatic $\beta$-Cell Gap Junction Electrical Conductance *In Situ'*, *J. Membr. Biol.* **146** (1995), 163–176.
6. Mosekilde, E., Maistrenko, Y. and Postnov, D.: *Chaotic Synchronization—Applications to Living Systems,* World Scientific, Singapore, 2002.
7. Perez-Armendariz, M., Roy, C., Spray, D.C. and Bennett, M.V.: Biophysical Properties of Gap Junctions Between Freshly Dispersed Pairs of Mouse Pancreatic Beta Cells, *Biophys. J.* **59** 1991, 76–92.
8. Scott, A.C.: *Nonlinear Science: Emergence and Dynamics of Coherent Structures,* Oxford University Press, Oxford, 1999.
9. Sherman, A.: Calcium and membrane potential oscillations in pancreatic $\beta$-cells in H.G. Othmer, F.R. Adler, M.A. Lewis and J.C. Dallon (eds.) *Case Studies in Mathematical Modeling: Ecology, Physiology, and Cell Biology,* Prentice-Hall, New York, 1997, pp. 199–217.

# *Paper II*

J. Math. Biol. (2004)
Digital Object Identifier (DOI):
10.1007/s00285-004-0304-4

**Mathematical Biology**

Morten Gram Pedersen

# Wave speeds of density dependent Nagumo diffusion equations – inspired by oscillating gap-junction conductance in the islets of Langerhans

Received: 27 October 2003 / Revised version: 1 October 2004 /
Published online: 20 December 2004 – 

**Abstract.** The equation $u_t = (D(u)u_x)_x + f(u)$ arises in several biological examples and is known to have wave solutions for appropriate $D$ and $f$. We give here a new formula for finding an approximation to the wave speed, relevant for comparing experiments with model simulations. This is done in details for the simple example $D(u) = u + k$ and an N-shaped $f$, derived from a model of coupled pancreatic $\beta$-cells, where the coupling conductance follows the electrical activity as it is found in experiments. On the way, we claim that the wave speed does not depend on the parameter $g_{K,ATP}$, mimicking the glucose concentration in the islet, in sharp contrast to the claim set forth in the article by Aslanidi *et al.* [4].

## 1. Introduction

Malfunctioning of the insulin secretory system is a major factor in diabetes. The pancreatic islets of Langerhans consist of thousands of coupled cells, among these the $\beta$-cells, which secrete insulin in response to several stimuli with glucose being the physiologically most important. A pivotal component of the glucose stimulus-secretion coupling is the closure of ATP-sensitive $K^+$ channels, leading to bursting electrical activity and calcium influx [21,16,3,20].

To have a proper functioning and insulin secretion, it is of great importance that the $\beta$-cells co-operate in a synchronized manner, and the coupling between cells made of gap-junctions seems to be crucial for this synchronization ([7,6,15] and references herein).

In [4] it was shown experimentally that calcium waves could provide a way to synchronize the cells. Using a mathematical model of the $\beta$-cells the authors showed that the gap-junctions indeed could result in waves of the observed kind. Furthermore, the calcium waves seem to be a result of electric waves [4,10,25], so to understand the wave phenomena it is in great parts enough to consider the membrane potentials. One way to compare model simulations with experiments is to compare the wave speeds. In [4] it was found that the simulated waves were significantly faster (approximately 200 $\mu$m/s) than the experimental waves (speeds

M. G. Pedersen: Department of Mathematics, The Technical University of Denmark, 2800 Kgs. Lyngby, Denmark. e-mail: m.g.pedersen@mat.dtu.dk

*Key words or phrases:* Wave speed – Density dependent diffusion – Excitation wave – Coupled $\beta$-cells – Gap junctions

of 30–100 $\mu$m/s). The authors suggested that a lower glucose concentration was to be expected in the center of the islet, and that this would lead to slower waves.

Andreu *et al.* [1] found that gap-junction conductance oscillates in phase with the bursting electrical activity of the $\beta$-cells. The significance of this behavior has not been investigated, and in this paper we will explore theoretically whether the wave propagation is altered by an oscillating gap-junction conductance with special focus on the wave speeds.

We modify a standard $\beta$-cell model [4,24] by assuming that the coupling conductance between two cells is a linear function of the average of the two relevant membrane potentials. The model includes an ATP-dependent potassium channel with conductance $g_{K,ATP}$, which models the coupling from glucose metabolism to the electrical behavior of the $\beta$-cell [14,24,11] where $g_{K,ATP}$ is inversely related to the glucose concentration.

Simulations of the model show that it has propagating wave solutions. As mentioned above, it was claimed in [4] that a higher $g_{K,ATP}$-value (lower glucose concentration) results in lower speeds. However, the simulations of the $\beta$-cell model presented here show that the wave speed does not decrease for higher $g_{K,ATP}$-values. Furthermore, control simulations show that this is not a property of the voltage dependent coupling; it also happens in the case of constant coupling strength. The results presented in [4] seem to be a transient phenomena arising from biologically unrealistic initial conditions.

To understand why the model with voltage dependent coupling has wave solutions and to investigate the wave speed more closely, we look only at the wave front as in [4] and go to the continuum limit, where the model becomes a one-dimensional *density dependent diffusion Nagumo equation*. Similar models occur in population models, and have been shown to have wave solutions [12,2,22].

Because no explicit expression for the wave speed $c$ exists, precise estimates are important. Using a simple transformation, first described in [13,8], we arrive at another nonlinear heat equation which gives us a way of finding the approximate wave speed of the wave front using the formula derived by Mornev [17,4]. This estimate for the speed of density dependent Nagumo equations is new and is illustrated by simulations of a standard density dependent Nagumo equation and the full $\beta$-cell model.

To understand why the wave speed should not depend on the parameter $g_{K,ATP}$, we will be more careful than what was done in [4] when looking at the wave front. This will show that the reaction part of the density dependent Nagumo equation is *independent* of $g_{K,ATP}$, i.e., the glucose concentration. This is somewhat exactly the opposite conclusion than what was found and used in [4,5]. We follow this up in the discussion.

The paper is organized as follows. The model for a line of $\beta$-cells is introduced in section 2 and we demonstrate wave propagation and find the speed of the first wave as in [4] and of the biologically more realistic successive waves, which is found to be independent of $g_{K,ATP}$. In section 3 the continuum equation is found. This equation is analyzed in section 4 and in particular the formula for the wave speed is found. The theoretical formulas are compared with computer simulations, and it is then shown in section 5 why the wave speed is to be independent of $g_{K,ATP}$.

Finally, we will discuss the results in section 6. A detailed description of the $\beta$-cell model is given in appendix A.

## 2. Simulations of the $\beta$-cell model

We consider a model of a finite line of $\beta$-cells taken from [24] and given by ($j = 1, \ldots, N$)

$$c_m \cdot \frac{dv_j}{dt} = I(v_j, n_j, s_j, Ca_j^i, Ca_j^{er}) + g_c(v_{j-1} - v_j) + g_c(v_{j+1} - v_j), \quad (1)$$

$$\frac{dn_j}{dt} = \frac{n_\infty(v_j) - n_j}{\tau_n}, \quad (2)$$

$$\frac{ds_j}{dt} = \frac{s_\infty(v_j) - s_j}{\tau_s}, \quad (3)$$

$$\frac{dCa_j^i}{dt} = f \cdot (\alpha I_{Ca}(v_j) - k_c Ca_j^i) + (J_{out} - J_{in}), \quad (4)$$

$$\frac{dCa_j^{er}}{dt} = \frac{J_{in} - J_{out}}{\rho}. \quad (5)$$

Here $v_j$ is the membrane potential, $n_j$ and $s_j$ are fast and slow gating variables respectively, $Ca_j^i$ is the intra-cellular calcium concentration and $Ca_j^{er}$ is the calcium concentration in the endoplasmic reticulum (ER) calcium stores for the $j$'th cell. The $j$'th cell is coupled through gap-junctions to the neighboring cells $j-1$ and $j+1$ with conductances $g_c$. The function $I$ is the total membrane current, and $I_{Ca}$ is one of these currents, a voltage dependent calcium current. $J_{in}$ and $J_{out}$ are currents in and out of the ER, $c_m$ is the total membrane capacitance, $n_\infty$ and $s_\infty$ are steady-states depending on $v$, $\tau_n$ and $\tau_s$ are time constants and $f, \alpha, k_c$ and $\rho$ are other constants. We impose the no-flux boundary condition, $v_0 = v_1,\ v_{N+1} = v_N$. For details see [24,4] or appendix A for detailed expressions and parameter values.

When the cells are uncoupled, $g_c = 0$, the membrane potential $v$ exhibits characteristic periodic *bursting* consisting of active phases where the membrane potential spikes from a plateau of approximately $-50$ mV to a maximum of approximately $-25$ mV, interrupted by silent phases where the cell is hyperpolarized with $v \simeq -65$ mV [24]. The average membrane potential during the active phase is approximately $-40$ mV. When coupled, the plateau of the active phase increases to around $-45$ mV and the average membrane potential during the active phase to approximately $-35$ mV [24,4].

Usually people have assumed that $g_c$ is constant over time, but in the light of the results of [1], where it was found that the conductance is more than three times greater in the active phase compared to the silent one ($514 \pm 137$ pS, respectively $149 \pm 41$ pS), we will let $g_c$ follow the membrane potential of the two cells that the gap junction couples. Although the conductance is known not to be voltage dependent [7,19], it seems to be the easiest way to incorporate the fact that the coupling strength actually follows the membrane potential, even though this might be mediated through oscillating calcium, cAMP or other chemical concentrations [1]. Furthermore, it captures the fact that the coupling conductance decreases slightly

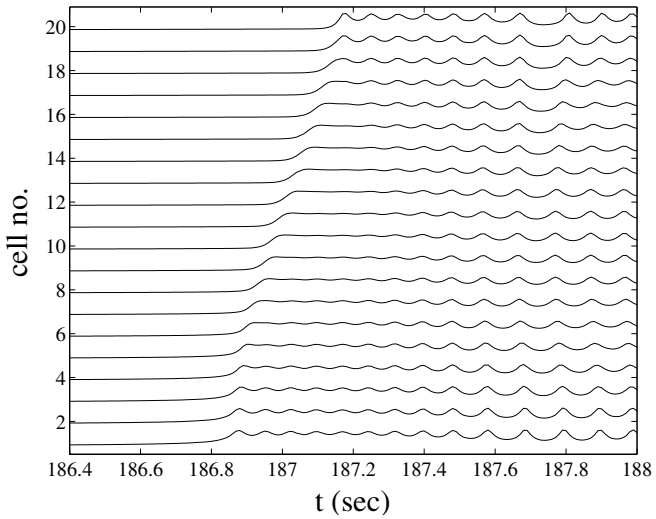


**Fig. 1.** A front wave propagating from the bottom (cell no. 1) to the top (cell no. 20) through a line of $\beta$-cells modeled by equations (1)–(6). Each curve shows for the corresponding cell, the membrane potential. The curves have been scaled and translated for clarity of the figure. We get a speed of 464 $\mu$m/s in this case.

during the active period [15], since the membrane potential does so. The gap junction conductance as a function of the membrane potentials is assumed to be linear, since this is the simplest way to fit the data from [1]. So we set

$$g_c(v_i - v_j) = \bar{g}_c(\frac{v_i + v_j}{2} + \kappa)(v_i - v_j), \quad i = j \pm 1, \tag{6}$$

where $\bar{g}_c$ models the slope of the voltage-conductance relation, and $\kappa$ is a parameter determining the basic conductance.

To obtain conductances similar to the ones found in [1] we assume that during the active phase $v = -35$ mV and during the silent phase $v = -65$ mV. This leads to the parameters

$$\bar{g}_c = 12 \text{ pS/mV}, \quad \kappa = 77.25 \text{ mV}. \tag{7}$$

A simulation of this system (1)–(6) shows a train of excitation waves propagate through the line of cells, as it was found for the case of constant coupling [4]. One of these successive wave fronts is shown in Fig. 1.

Let us first look at the speed of the first wave as it was done in [4]. This wave is initiated by setting initial conditions such that the two cells in one end of the line enter the active phase, see appendix A. These two cells will then pull the neighbors into the active phase and in this way start a wave. To avoid boundary phenomena we calculate the speed only over the 10 center cells from the time when cell number 6 enter the active phase, defined as $v_6$ passing through $-55$ mV, to the time when cell number 15 becomes active.

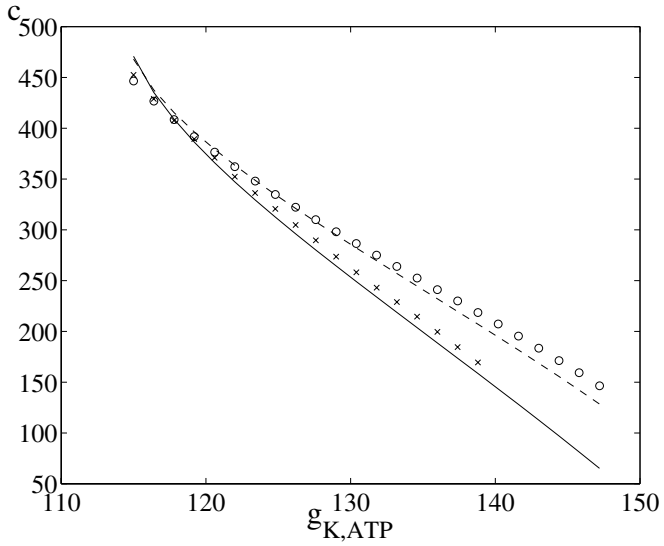


**Fig. 2.** The simulated speed of the first wave measured in $\mu$m/s as a function of $g_{K,ATP}$ in the case of constant coupling conductance $g_c = 312$ pS (x's), and density dependent coupling with parameters as in (7) (circles). The theoretical expected values from formula (18) are given by the solid line for the case of constant coupling with $\lambda = 1.45$, and by the broken line for density dependent coupling with $\lambda = 1.3$.

We see in Fig. 2 that the velocity decreases rapidly as $g_{K,ATP}$ increases, both in the case of constant (as found in [4]) and density dependent coupling, but fastest for the constant coupling. The reason for this as well as the estimated speeds indicated by the curves in Fig. 2 will be explained in section 4. We have used the value $g_c = 312$ pS for the constant coupling, which corresponds to the mean of the values found in [1] and which is higher than what was used in [4] resulting in higher speeds than in that paper.

We now regard the successive waves occurring after a transient period of 50 seconds, in the case of constant coupling with $g_c = 312$ pS, and with non-constant coupling with the parameters from (7). The simulations are repeated with random initial conditions, see appendix A, to rule out the dependence on initial conditions, and to avoid boundary phenomena the speed is again found over the 10 center cells. The successive waves have different speeds, i.e., the train of waves is not perfectly periodic, indicating that the system of coupled cells is chaotic.

This also leads to difficulties in determining the velocity of the wave front. We neglect cases where the time measurement results in very small time differences (apparent speeds greater than 1000 $\mu$m/s) between the instants when cells number 6 and 15 enter the active phase, since these are probably waves starting almost simultaneously from both sides. Also, we neglect very large time differences (apparent speeds less than 10 $\mu$m/s). For example one could imagine that for a brief moment $v_6$ passes above the threshold of $-55$ mV without starting a wave. However the

time is recorded, so when $v_{15}$ much later increases above $-55$ mV, we will obtain a very small value for the speed. Such phenomena should of course be ruled out.

We see an almost constant speed in both cases, in sharp contrast to when we looked at the first wave, compare Fig. 3 with Fig. 2. The waves in the case of non-constant coupling are in general faster than the waves arising from constant coupling, as it could be expected from Fig. 2, and the average wave speeds are in both cases faster than the speeds of the first wave.

## 3. The limit PDE

To analyze the observed wave phenomena for the voltage dependent coupling we obtain a single PDE from (1)–(6) following the idea in [4]. On the wave front we can uncouple the variables $Ca^i$ and $Ca^{er}$, and assuming that $s = s_*$ is constant while $n = n_\infty(v)$ leaves only

$$\begin{aligned} c_m \cdot \frac{dv_j}{dt} &= I(v_j, n_\infty(v_j); s_*) + g_c(v_{j-1} - v_j) + g_c(v_{j+1} - v_j) \\ &= \Phi(v_j) + g_c(v_{j-1} - v_j) + g_c(v_{j+1} - v_j). \end{aligned} \tag{8}$$

We note that $\Phi$ is *N-shaped* for standard parameters [4], i.e.,

$$\begin{gathered} \Phi \text{ has three zeros, } v_0 < v_a < v_1, \text{ and} \\ \Phi(v) < 0 \text{ for } v_0 < v < v_a, \quad \Phi(v) > 0 \text{ for } v_a < v < v_1. \end{gathered} \tag{9}$$

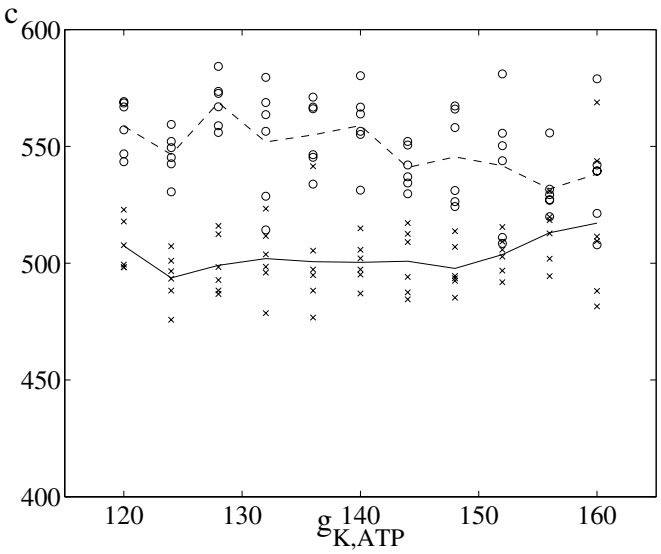


**Fig. 3.** Six simulations, each with different initial conditions, showing the average wave speed in $\mu$m/s of several successive waves as a function of $g_{K,ATP}$ in the case of non-constant coupling conductance with $\bar{g}$ and $\kappa$ as in (7) (circles; the average of the six simulations is showed by the dashed line), and the case of constant coupling $g_c = 312$ pS (x's and solid line).

Using (6) we now get

$$\begin{aligned} c_m \cdot \frac{dv_j}{dt} &= \Phi(v_j) + \bar{g}_c(\frac{v_{j-1}+v_j}{2} + \kappa)(v_{j-1} - v_j) \\ &\quad + \bar{g}_c(\frac{v_{j+1}+v_j}{2} + \kappa)(v_{j+1} - v_j) \\ &= \Phi(v_j) + \frac{\bar{g}_c}{2}(v_{j+1}^2 + v_{j-1}^2 - 2v_j^2) + \bar{g}_c\kappa(v_{j+1} + v_{j-1} - 2v_j). \end{aligned} \tag{10}$$

We assume that the distance between neighbors is $\epsilon$ (the diameter of a $\beta$-cell) and that $\bar{g}_c = \epsilon^{-2} c_m D$ for a constant $D$. Letting $x$ be the spatial coordinate such that $v_j = v(j\epsilon) = v(x)$, we obtain by letting $\epsilon \to 0$

$$\begin{aligned} v_t &= \frac{D}{2}(v^2)_{xx} + \kappa D v_{xx} + F(v) \\ &= D((v+\kappa)v_x)_x + F(v), \end{aligned} \tag{11}$$

where $F = \Phi/c_m$ is an N-shaped function. In (11) and the following subscripts denote differentiation with respect to the variable. The boundary conditions are

$$v(-\infty, t) = v_1, \quad v(\infty, t) = v_0, \tag{12}$$

since we are looking at the front where the system leaves the silent phase (corresponding to $v = v_0$) and enters the active phase (corresponding to $v = v_1$), see Fig. 1.

## 4. Analysis of the density dependent diffusion equation

We apply the transformation

$$\begin{aligned} u &= \frac{v - v_0}{v_1 - v_0}, \quad s = \frac{t}{v_1 - v_0}, \quad y = \frac{x}{(v_1 - v_0)\sqrt{D}}, \\ k &= \frac{v_0 + \kappa}{v_1 - v_0}, \quad f(u) = F(v_0 + (v_1 - v_0)u), \end{aligned} \tag{13}$$

so that (11) becomes

$$u_s = ((u+k)u_y)_y + f(u). \tag{14}$$

Note that $f$ is N-shaped with zeros in 0, 1 and $a = \frac{v_a - v_0}{v_1 - v_0} \in (0, 1)$, and for $\kappa \geq -v_0$ (as in (7)) we get $k \geq 0$. The boundary conditions are now

$$u(-\infty, t) = 1, \quad u(\infty, t) = 0. \tag{15}$$

We are looking for traveling wave solutions to (14), $u(y, s) = U(y - cs) = U(\xi)$. Let

$$\mathcal{D} = \int_0^1 (u+k) f(u) du.$$

For $\mathcal{D} > 0$, $k \geq 0$ there is a unique positive value of $c$ such that the PDE (14)–(15) has a wave solution [12, 2, 22]. For $k = 0$ the *density dependent Nagumo equation*

(14) is called *degenerate*, and in this case the wave is *sharp* [2,22], which comes from the fact that the diffusion vanishes at $u = 0$. That the wave is sharp means that there exists a $\xi_0$ such that $U(\xi) = 0$ for $\xi > \xi_0$ and the derivative $U'(\xi)$ is discontinuous at $\xi_0$. This means biologically that disturbances in the membrane potential propagate with finite speed as opposed to the cases with $k > 0$ or constant coupling strength where the disturbances propagate with infinite speed.

The Hadeler-Engler transformation [13,8] says that (14) is equivalent to

$$u_s = u_{yy} + (u + k) f(u), \tag{16}$$

in the sense that we have a wave solution to (14)-(15) if and only if we have one to (15)–(16) and the solutions will have the same speed $c$.

There exists no exact expression for the speed of wave solutions to (14), (16) or the general Nagumo equation

$$u_s = Du_{yy} + g(u), \tag{17}$$

where $D$ is a constant and $g$ satisfies (9) with zeros in $u_0 < u_a < u_1$, except in special cases. Mornev [17,4] found an approximation to the speed of (17) given by

$$c = \lambda \frac{\Delta g}{u_1 - u_0} \sqrt{\frac{D}{\Pi + \Delta g}}, \tag{18}$$

where $\lambda$ is a constant of order 1 [4],

$$\Pi = \frac{1}{u_1 - u_0} \int_{u_0}^{u_1} \int_{u_0}^{u} g(u') du' du,$$

and

$$\Delta g = \int_{u_0}^{u_1} g(u) du.$$

We now note that if $f$ satisfies (9) with zeros in $0 < a < 1$, then for any $k \geq 0$,

$$g : u \mapsto (u + k) f(u)$$

does as well and therefore formula (18) provides a formula for finding the wave speed of equation (16) and hence our original equation (14), for which (18) becomes

$$c = \lambda \mathcal{D} \sqrt{\frac{1}{\Pi + \mathcal{D}}}, \tag{19}$$

showing why $\mathcal{D}$ enters the picture.

To compare directly with our simulations of the $\beta$-cells, we must transform back to $v(x, t)$. Then $v$ must satisfy

$$v_t = D(v_1 - v_0) v_{xx} + \frac{v + \kappa}{v_1 - v_0} \cdot F(v), \tag{20}$$

or equivalently, using again the Hadeler-Engler transformation,

$$v_t = v_{xx} + D \cdot (v + \kappa) \cdot F(v), \tag{21}$$

so using (18) on

$$G : v \mapsto D \cdot (v + \kappa) \cdot F(v) \tag{22}$$

yields the wave speed of equation (11).

Since the parameter $\lambda$ is undetermined, we have some degree of freedom. However, the formula provides a way to investigate how the speed depends on the parameters defining the system, and is of value in this way rather than just for a single experiment or simulation.

We finally note that all of the above can be done for the general non-linear diffusion Nagumo equations studied in [12,13,22,8],

$$u_t = (D(u)u_x)_x + f(u),$$

which gives a formula for the speed of the wave solutions to these equations.

### *4.1. Comparison between estimates and simulations*

The theoretical expression (19) for equation (14) with $k = 0$ and the standard cubic function

$$f(u) = u(1-u)(u-a), \quad 0 < a < 1, \tag{23}$$

is now compared to simulations of the equation. From (19) we can obtain an analytic expression for the speed as a function of the parameter $a$ given by

$$c = \lambda \left( \frac{1}{10} - \frac{a}{6} \right) \sqrt{\frac{15}{1-a}}. \tag{24}$$

Varying $a$ results in Fig. 4, where we have chosen $\lambda = 1.17$ to obtain a good fit to the simulations, and we see that the formula indeed estimates the speed very well. We regard only $0 \leq a < 0.6$ which insures that $\mathcal{D} > 0$ and that the formula is valid.

Also the simulations of the first wave in the voltage dependent $\beta$-cell model (1)–(6) are estimated very well by the formula (18) used on $G$ from (22) with $s_* = 0.4$ (the initial value), see Fig. 2. Note that $g_{K,ATP}$ plays a role similar to $a$ in Fig. 4.

It is interesting to compare the expression (24) with the well-known speed for the case with constant diffusion constant (constant coupling)

$$u_t = \frac{1}{2} u_{xx} + f(u),$$

where we have chosen the diffusion constant $\frac{1}{2}$ equal to the mean of $u$, i.e., the mean density dependent coupling. The speed is in this case given by [23]

$$cc = \frac{1}{2} - a. \tag{25}$$

We see in Fig. 4 that for small $a$ the case with constant coupling has greater wave speed, while for higher values of $a$ the model with density dependent coupling

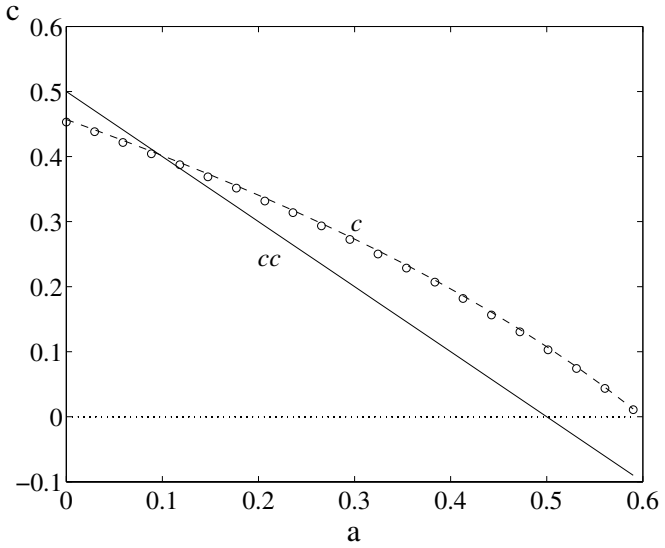


**Fig. 4.** A simulation (circles) of a line of 100 cells approximating equation (14) with $k = 0$ and $f(u) = u(1-u)(u-a)$ is compared to the theoretical expressions for density dependent coupling ($c$ from (24) with $\lambda = 1.17$, broken line) and for constant coupling ($cc$ from (25), solid line) for varying $a$. We look only at $a$'s such that $\mathcal{D}$ and hence $c$ is positive.

has faster waves, even allowing propagation with positive $c$ for $0.5 < a < 0.6$, where there can be no propagation of this kind in the model with constant coupling. This explains the observation from Fig. 2 where we saw that for higher $g_{K,ATP}$ the voltage dependent coupling resulted in faster waves than the constant coupling.

## 5. The wave speed is independent of the glucose concentration

In [4] it was claimed that a lower glucose concentration (modeled by a higher value of $g_{K,ATP}$) will decrease the speed of the excitation waves. This could then give an explanation why the authors found too high simulated speeds compared to experiments; the parameter $g_{K,ATP}$ would be higher in the center of the islet, and the average wave speed would therefore be lower. This conclusion carries apparently over to the case of non-constant coupling if one regards the first wave, see Fig. 2. However, we found that when looking at many successive waves the speed in nearly constant as a function of $g_{K,ATP}$, see Fig. 3.

In [4] and Fig. 2, when analyzing the function $F$, the value for $s_*$ in (8) was set to the initial condition $s(0) = 0.4$. This explains the speed of the first wave since $s \simeq s(0)$ is a good approximation. However, over time $s$ will in general *not* be near $s(0)$ at the beginning of the active phase, so when we look at not the first but at successive waves we will not get a good estimate if we use $s_* = s(0)$.

The value of $s$ when the system leaves the silent and enters the active phase can be estimated as follows. When we regard just one cell, we can (after neglecting the calcium currents) separate the $(v, n, s)$-system into a fast $(v, n)$-subsystem and a slow $s$-subsystem, see e.g. [24]. Treating $s$ as a parameter in the fast subsystem, we obtain a bifurcation diagram where the fixpoints lie on a N-shaped curve in $(v, s)$ space given by solving $I(v, n_\infty(v); s) = 0$ for $s$ leading to

$$s(v) = -\frac{1}{g_s}\left(\frac{I_{Ca}(v)}{v - v_K} + g_K n_\infty(v) + g_{K,ATP}\right).$$

The relevant value for $s_*$ is the value at the local minimum near $v = -60$, see Fig. 5, which is easily found numerically. Of importance is the fact that the point $v_*$, at which we have the local minimum, is independent of $g_{K,ATP}$ so that $s_*$ depends linearly on $g_{K,ATP}$,

$$s_* = \sigma_* - \frac{g_{K,ATP}}{g_s}, \tag{26}$$

where $\sigma_* \simeq 1$ is the value of $s_*$ for $g_{K,ATP} = 0$ pS.

When we plug $s_*$ into $\Phi$ we find that

$$\begin{aligned}\Phi(v) =& I(v, n_\infty(v); s_*)\\ =& -\big(I_{Ca}(v) + g_K n_\infty(v)(v - v_K) + g_s\sigma_*(v - v_K)\big),\end{aligned} \tag{27}$$

which is independent of $g_{K,ATP}$. Hence, in the full realistic system $g_{K,ATP}$ should not have any importance for the analysis of (11) and hence for the wave speed!

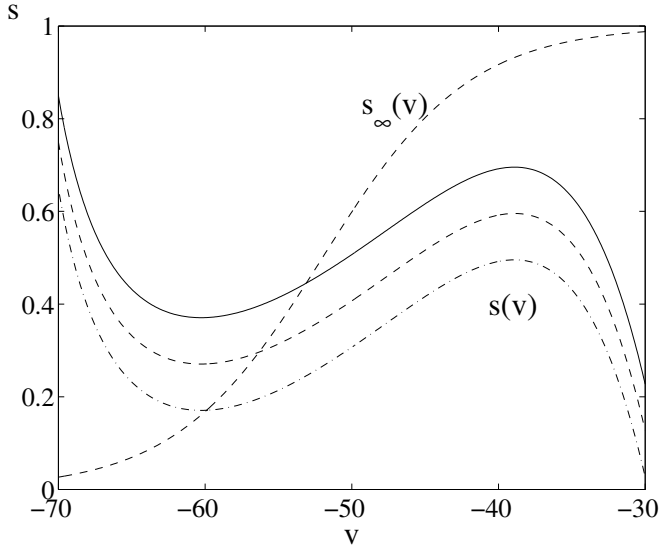


**Fig. 5.** The function $s(v)$ for three different values of $g_{K,ATP}$ Starting with the uppermost the values are 120, 140 and 160 pS, respectively, and the $s$-nullcline $s_\infty(v)$.

Let us note that this analysis of the model in this paper carries over to, for example, the more recent model from [11], where the current of the 'artificial' slow variable $I_s$ is replaced by a slow calcium dependent potassium current, simply by letting

$$s = \frac{[Ca^{2+}]^q}{[Ca^{2+}]^q + K_d^q}.$$

Hence, the claim that the wave speed does not depend on the glucose concentration is not model specific; the above can be done for any reasonable model with an ATP-dependent potassium channel and some slow potassium channel.

## 6. Discussion

Our original idea was to investigate how the wave phenomena are influenced by an oscillating gap junction conductance, in particular if the claim that the wave speed decreases for lower glucose concentrations would still hold. Including the voltage dependent coupling strength, we still observe waves, and the speed of the system with voltage dependent coupling is similar to the speed in the case of constant coupling (Figs. 2 and 3). Hence, including the oscillating coupling strength does not lead to biologically significant conclusions. However, it shows another example of how the density dependent Nagumo equation can arise in biology, and that these equations can be analyzed in the same way as the case with constant diffusion. In particular, it led us to find a new estimate of the speed of wave solutions to such equations.

This new estimate arose using the transformation from [13,8], and the formula from [17], and we showed that the formula predicts the simulated speeds very well, see Figs. 2 and 4. The big advantage of the new estimate presented here is that it is immediate to compute in contrast to earlier estimates [12,9] based on extrema values, which are much harder to find. Since the density dependent Nagumo equation arises in other contexts in mathematical biology the formula for the wave speed given here by (18) used for $g : u \mapsto D(u)f(u)$, should be of general interest, for example in ecological populations models [2,22]. Also, in any model of coupled cells where the coupling strength is modified by one of the relevant variables (e.g., membrane potential, calcium, cAMP), would an analysis as the one done here be of relevance when investigating wave phenomena.

When simulating the full $\beta$-cell model we found that the wave speed does not depend on the parameter $g_{K,ATP}$ as claimed in [4], in both the case of constant and oscillating coupling, when looking at successive waves, compare Figs. 2 and 3. We explained why the analysis done in [4] makes a biologically unrealistic assumption when changing $g_{K,ATP}$ without adjusting $s_*$ correspondently, and how such an adjustment leads to the conclusion that $F$ and hence the wave speed should be completely independent from $g_{K,ATP}$. Note that the formula from [17] can explain the case of constant coupling, but that we need the newfound formula for the non-constant coupling.

We see in Fig. 3 that the waves in the model with non-constant coupling have higher speeds than the ones in the case of constant coupling, which could be

expected from Figs. 2 and 4. Also, the successive waves (Fig. 3) are faster than the the first wave (Fig. 2). We believe that this is due to the high degree of synchronization of the cells; they are all very near to entering the active phase when the wave starts, even without an impulse from the wave. So the wave propagation should be facilitated in contrast to the first wave where $s$ is not near the value where the cells would have entered the active phase if there was no stimulation from the wave. This synchronization can be seen in Fig. 1, where the cells near the bottom (no. 1-4) enter the active phase almost simultaneously compared to the cells in the upper half (no. 10-20). Moreover, it results in waves starting independently from both sides almost simultaneously. We calculated the speed over the ten center cells (no. 6-15) to minimize this problem as well as boundary phenomena, and neglected unrealisticly high apparent wave speeds.

It would be natural to investigate experimentally how the wave speed depends on glucose; we suggest here that there should be almost no dependence. But then, the explanation why [4] found too fast waves can not be that there is a lower glucose concentration in the center of islet. Also, we have seen that the oscillating gap junction conductance results in yet faster waves than for the constant coupling (Fig. 3), so non-constant coupling can also not help us. We have in [18] showed that the natural heterogeneity of the gap junctions results in slower waves than when one just uses the average coupling strength, which can provide one explanation of why we get too fast waves – we must take the heterogeneity into account. Another question that one can ask in this context is 'what is the right value for $g_c$?' Since the speed is proportional to $\sqrt{g_c}$ this choice has a strong influence on the wave speed. In [4,5,18] the (mean) value $g_c = 100$ pS was used, which is near the lower value of the experimental results in [19] and of the silent phase conductance in [1]. We have here used the average of the silent and active conductances from [1] leading to the value $g_c = 312$ pS, which is near the upper value from [19], but corresponds well to the value from [15]. Anyway, the simulated speeds of discretely coupled $\beta$-cells have all been faster than experimentally observed, except a few in [18].

In conclusion, we have given an investigation of the significance of the voltage dependent gap-junction for the wave propagation in pancreatic islets of Langerhans leading to a new estimate for wave speeds of density dependent Nagumo equations. From a biological point of view, the main result is that the wave speeds are independent of $g_{K,ATP}$ and hence glucose.

*Acknowledgements.* The author thanks 'Rejselegat for Matematikere' (Travelling Scholarship for Mathematicians) for financial support, and 'Associação Instituto Nacional de Matemática Pura e Aplicada (IMPA)', Rio de Janeiro, Brazil, for kindly letting me visit the institute, where this work was carried out. Also, thanks to anonymous reviewers for constructive comments and Mads Peter Sørensen, MAT, Technical University of Denmark, for fruitful discussions on this manuscript.

## A. The equations and parameters for the $\beta$-cell model

The functions and parameters of the equations (1)-(5) are as follows.

$$\begin{aligned}
I(v,n,s,Ca^i,Ca^{er}) &= -\big(I_s(v,s)+I_{Ca}(v)+I_K(v,n)+I_{K,ATP}(v)\\
&\quad +I_{K,Ca}(v,Ca^i)+I_{CRAC}(v,Ca^{er})\big)\\
I_s(v,s) &= g_s\cdot s\cdot(v-v_K)\\
I_{Ca}(v) &= g_{Ca}\cdot m_\infty(v)\cdot(v-v_{Ca})\\
I_K(v,n) &= g_K\cdot n\cdot(v-v_K)\\
I_{K,ATP}(v) &= g_{K,ATP}\cdot(v-v_K)\\
I_{K,Ca}(v,Ca^i) &= g_{K,Ca}\cdot(v-v_K)\cdot\frac{(Ca^i)^5}{(Ca^i)^5+k_d^5}\\
I_{CRAC}(v,Ca^{er}) &= g_{CRAC}\cdot z_\infty(Ca^{er})\cdot(v-v_{CRAC})\\
m_\infty(v) &= \frac{1}{(1+\exp((v_m-v)/s_m))}\\
n_\infty(v) &= \frac{1}{1+\exp((v_n-v)/s_n)}\\
s_\infty(v) &= \frac{1}{1+\exp((v_s-v)/s_s)}\\
z_\infty(Ca^{er}) &= \frac{1}{1+\exp((Ca^{er}-\bar{c}_{ER})/s_z)}\\
J_{in}(Ca^i) &= \frac{v_p}{\mu}\cdot\frac{(Ca^i)^2}{(Ca^i)^2+k_p^2}\\
J_{out}(Ca^i,Ca^{er}) &= \frac{p_1}{\mu}(Ca^{er}-Ca^i)
\end{aligned}$$

The parameters used are

$g_{Ca}=1000$ pS, $g_K=2700$ pS, $g_s=200$ pS, $g_{K,Ca}=1000$ pS, $g_{CRAC}=40$ pS,
$v_{Ca}=25$ mV, $v_K=-75$ mV, $v_m=-20$ mV, $v_n=-16$ mV, $v_s=-52$ mV,
$v_{CRAC}=-30$ mV, $s_m=12$ mV, $s_n=5.6$ mV, $s_s=5$ mV,
$c_m=5300$ fF, $\tau_n=20$ ms, $\tau_s=20000$ ms, $\mu=250$ ms,
$f=0.01$, $k_c=0.2$ ms$^{-1}$, $\alpha=-4.5\cdot10^{-6}\mu$M/(fA·ms),
$k_d=0.6$, $k_p=0.1\,\mu$M, $v_p=0.24\,\mu$M, $\bar{c}_{ER}=4\,\mu$M, $s_z=1\,\mu$M, $\rho=5$, $p_1=0.02$.

The diameter of a $\beta$-cell was set to be 10 $\mu$m.

Initial conditions are (for all $j$) $n_j(0)=0.0001$, $s_j(0)=0.4$, $Ca^i_j(0)=0.1\mu$M, $Ca^{er}_j(0)=10\mu$M. For Fig. 2 we used $v_1(0)=v_2(0)=-40$ mV, $v_3(0)=\cdots=v_{20}(0)=-65$ mV. For Fig. 3 we chose $v_j(0)$ randomly from a uniform distribution on $[-65,-55]$ mV and we had a transient time of 50 seconds.

All simulations were done using the banded version of the CVODE solver of the program XPPAUT with standard tolerances.

## References

1. Andreu, E., Bernat, S., Sanchez-Andres, J.V.: Oscillation of gap junction electrical coupling in the mouse pancreatic islets of Langerhans, J. Physiol. **498**, 753–761 (1997)

2. Aronson, D.G.: Density-Dependent Interaction-Diffusion Systems, in W.E. Stewart, W.H. Ray and C.C. Conley (eds.): Dynamics and Modelling of Reactive Systems, (Academic Press, New York 1980) pp. 161–176
3. Ashcroft, F.M., Rorsman, P.: Electrophysiology of the pancreatic $\beta$-cell, Prog. Biophys. Mol. Biol. **54**, 87–143 (1989)
4. Aslanidi, O.V., Mornev, O.A., Skyggebjerg, O., Arkhammar, P., Thastrup, O., Sørensen, M.P., Christiansen, P.L., Conradsen, K., Scott, A.C.: Excitation Wave Propagation as a Possible Mechanism for Signal Transmission in Pancreatic Islets of Langerhans. Biophys. J. **80**, 1195–1209 (2001)
5. Aslanidi, O.V., Mornev, O.A., Vesterager, M., Sørensen, M.P., Christiansen, P.L.: A Model for Glucose-induced Wave Propagation in Pancreatic Islets of Langerhans. J. Theor. Biol. **215**, 273–286 (2002)
6. Charollais, A., Gjinovci, A., Huarte, J., Bauquis, J., Nadal, A., Martín, F., Andreu, E., Sáfnchez-Andrés, J.V., Calabrese, A., Bosco, D., Soria, B., Wollheim, C.B., Herrera, P.L., Meda, P.: Junctional communication of pancreatic $\beta$ cells contributes to the control of insulin secretion and glucose tolerance, J. Clin. Invest. **106**, 235–243 (2000)
7. Eddlestone, G.T., Goncalves, A., Bangham, J.A.: Electrical coupling between cells in islets of Langerhans from mouse. J. Membr. Biol. **77**, 1–14 (1984)
8. Engler, H.: Relations Between Travelling Wave Solutions of Quasilinear Parabolic Equations, Proc. Am. Math. Soc. **93**, 297–302 (1985)
9. Gilding, B.H., Kersner, R.: Travelling waves in nonlinear diffusion-convection-reaction. (Memorandum No. 1585, Faculty of Mathematical Sciences, University of Twente 2001)
10. Gilon, P., Henquin, J.-C.: Influence of Membrane Potential Changes on Cytoplasmic $Ca^{2+}$ Concentration in an Electrically Excitable Cell, the Insulin-secreting Pancreatic B-cell, J. Biol. Chem. **267**, 20713–20720 (1992)
11. Goforth, P.B., Bertram, R., Khan, F.A., Zhang, M., Sherman, A., Satin, L.S.: Calcium-activated $K^+$ Channels of Mouse $\beta$-cells are controlled by Both Store and Cytoplasmic $Ca^{2+}$: Experimental ad Theoretical Studies, J. Gen. Physiol. **120**, 307–322 (2002)
12. Hadeler, K.P.: Travelling fronts and free boundary value problems, in Albrecht, J., Collatz, L., and Hoffmann, K.-H.: Numerical Treatment of Free Boundary Value Problems (Birkhauser Verlag, Basel, 1982) pp. 90–107
13. Hadeler, K.P.: Free boundary problems in biological models, in Fasano, A., and Primicerio, M. (eds.): Free Boundary Problems: Theory and Applications, Volume II. (Pitman Advanced Publishing Program, Boston, 1983) pp. 664–671
14. Keizer, J., Magnus, G.: ATP-sensitive potassium channel and bursting in the pancreatic beta cell. A theoretical study. Biophys. J. **56**, 229–242 (1989)
15. Mears, D., Sheppard, N., Atwater, I., Rojas, E.: Magnitude and Modulation of Pancreatic $\beta$-Cell Gap Junction Electrical Conductance *In Situ*, J. Membr. Biol. **146**, 163–176 (1995)
16. Misler, S., Falke, L.C., Gillis, K., McDaniel, M.L.: A metabolite-regulated potassium channel in rat pancreatic B cells, PNAS **83**, 7119–7123 (1986)
17. Mornev, O.A.: Modification of the Biot method on the basis of the principle of minimum dissipation (with an application to the problem of propagation of nonlinear concentration waves in an autocatalytic medium), Russian J. Phys. Chem. **72**, 112–118 (1998)
18. Pedersen, M.G.: Homogenization of heterogeneously coupled bistable ODE's - applied to excitation waves in pancreatic isles of Langerhans, J. Biol. Phys. *In press*.
19. Perez-Armendariz, M., Roy, C., Spray, D.C., Bennett, M.V.: Biophysical properties of gap junctions between freshly dispersed pairs of mouse pancreatic beta cells, Biophys. J. **59**, 76–92 (1991)

20. Prentki, M., Matschinsky, F.M.: $Ca^{2+}$, cAMP, and Phospholipid-Derived Messengers in Coupling Mechanisms of Insulin Secretion, Physiol. Rev. **67**, 1185–1248 (1987)
21. Rutter, G.A.: Nutrient secretion coupling in the pancreatic islet $\beta$-cell: recent advances, Mol Aspects Med. **22**, 247–284 (2001)
22. Sánchez-Garduño, F., Maini, P.K.: Travelling wave phenomena in non-linear diffusion degenerate Nagumo equations, J. Math. Biol. **35**, 713–728 (1997)
23. Scott, A.C.: Nonlinear Science: Emergence and Dynamics of Coherent Structures. (Oxford University Press, Oxford 1999)
24. Sherman, A.: Calcium and membrane potential oscillations in pancreatic $\beta$-cells, in Othmer, H.G., Adler, F.R., Lewis, M.A., and Dallon, J.C. (eds.): Case Studies in Mathematical Modeling: Ecology, Physiology, and Cell Biology. (Prentice-Hall, New York 1997) pp. 199-217
25. Valdeolmillos, M., Santos, R.M., Contreras, D. Soria, B., Rosario, L.M.: Glucose-induced oscillations of intracellular $Ca^{2+}$ concentration resembling bursting electrical activity in single mouse islets of Langerhans, FEBS Lett. **259**, 19–23 (1989)

# *Paper III*

Available online at www.sciencedirect.com
SCIENCE DIRECT®
Journal of Theoretical Biology 235 (2005) 1–3
Journal of Theoretical Biology
www.elsevier.com/locate/yjtbi

Letter to the Editor

## A comment on noise enhanced bursting in pancreatic β-cells

De Vries and Sherman (2000) study the electrical behavior of coupled pancreatic $\beta$-cells with focus on the beneficial influence of noise. When subjected to glucose the $\beta$-cells produce and secrete insulin, and the amount of secreted insulin correlates with the intracellular calcium levels (Jonas et al., 1998). Early recordings of single, isolated pancreatic $\beta$-cells showed that the membrane potential exhibits noisy spiking activity. On the other hand, the $\beta$-cells are electrically coupled in the islets of Langerhans where they show bursting electrical activity. Bursting consists of the membrane potential alternating between a silent hyperpolarized phase, and an active phase of spiking rising from a depolarized plateau. The importance of bursting is that it leads to higher average intracellular $Ca^{2+}$concentrations and insulin secretion than continuous spiking (De Vries and Sherman, 2000, and references herein). The question under investigation is whether the electrical coupling between the $\beta$-cells is enough to change the behavior from spiking to bursting. It had previously been shown that weak coupling between identical cells can induce bursting (Sherman and Rinzel, 1991), and it is known that heterogeneous but spiking cells start to burst when coupled with physiologically realistic coupling strengths (De Vries and Sherman, 2001). The main result presented by De Vries and Sherman (2000) is that noise dramatically increases the interval of coupling strengths for which bursting is seen for identical cells, and this observation was supported by analyzing a bifurcation diagram. This letter will show that the beneficial influence is more likely through heterogeneity masqueraded as noise, and that the explanation of the enhancement of emergent bursting must be modified accordingly.

The single cell model (De Vries and Sherman, 2000) is

$$\tau \frac{dv}{dt} = -I_{Ca}(v) - I_K(v,n) - I_s(v,s) - I_{K(ATP)}(v,p), \quad (1)$$

$$\tau \frac{dn}{dt} = \lambda(n_\infty(v) - n), \quad (2)$$

$$\tau_s \frac{ds}{dt} = s_\infty(v) - s, \quad (3)$$

$$\frac{dp}{dt} = \frac{1}{\tau_p}(\alpha_p(1-p) - \beta_p p) + g_p(t), \quad (4)$$

where $g_p(t)$ is a Gaussian zero mean white-noise process with mean square

$$\langle g_p(t) g_p(t') \rangle = \frac{\alpha_p(1-p) + \beta_p p}{\tau_p N_{K(ATP)}} \delta(t - t'). \quad (5)$$

Eq. (1) describes the membrane potential, $v$. $I_{Ca}, I_K, I_s, I_{K(ATP)}$ are ion-currents through the membrane controlled by $v$, the fast gating variable $n$ (Eq. (2)), the slow gating variable $s$ (Eq. (3)) and noisy opening and closing of ATP sensitive $K^+$-channels modeled by the Stratonovich stochastic differential equation (4). For details see De Vries and Sherman (2000). We note that in all simulations (De Vries and Sherman, 2000) the opening ($\alpha_p$) and closing ($\beta_p$) probabilities are assumed identical, $\alpha_p = \beta_p = 1$, and in this case the Stratonovich and Itô interpretation coincide since the mean square of $g_p(t)$ in Eq. (5) is constant. This model for a single cell produces noisy spiking (De Vries and Sherman, 2000, Fig. 3) arising from the spiking solution of the corresponding deterministic system with $p = 0.5$ constant.

The model is extended to two coupled cells by adding the term $-g_c(v_i - v_j)$ to Eq. (1) for cell $i$, where $j \neq i$. Although not explicitly stated, De Vries and Sherman (2000) use two independent white-noise processes, $p_1$ and $p_2$, for the two cells, which makes perfect sense biologically. They show that the inclusion of noise enhances the interval of coupling strengths inducing bursting (De Vries and Sherman, 2000, Figs. 4 and 5). For example, for $g_c = 0.08$ they obtain a very clear bursting profile (Fig. 5(c)). However, a simulation with identical noise $p_1 = p_2$ does not produce bursting for $g_c = 0.08$, see Fig. 1. In fact, the interval of coupling strengths resulting in bursting is not significantly larger than the deterministic case when $p_1 = p_2$. This indicates that the heterogeneity introduced by $p_1 \neq p_2$ is of great importance in explaining the phenomena.

De Vries and Sherman (2000) explain the emergent bursting from the bifurcation diagram of the fast $(v,n)$-subsystem for the deterministic case $p_1 = p_2 = 0.5$. As

0022-5193/$ - see front matter 
doi:10.1016/j.jtbi.2005.01.025

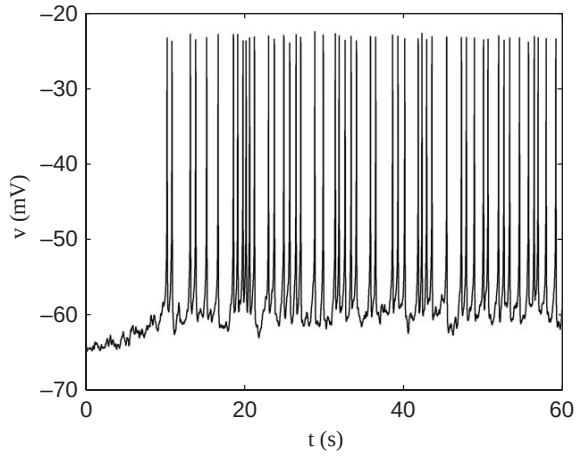


Fig. 1. Identical noise in the two cells does not induce bursting. As De Vries and Sherman (2000, Fig. 5(c)), but with $p_1 = p_2$.

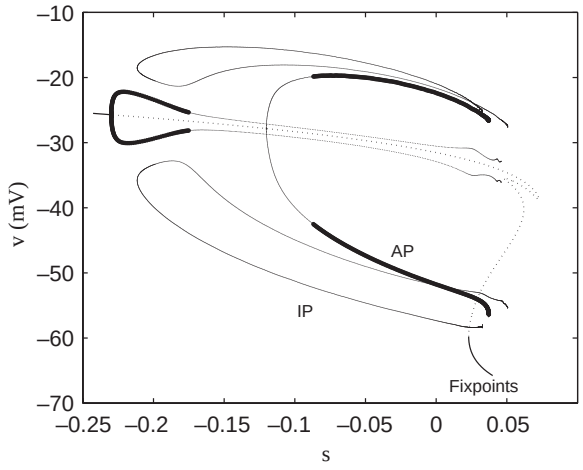


Fig. 2. The bifurcation diagram for $p_1 = 0.5, p_2 = 0.5115$. The Z-shaped curve are fixpoints where the full line indicate stable and the dotted line unstable fixpoints. The other curves are periodic solutions where the fat lines indicate stable periodics and the fine curves unstable periodics.

mentioned above this deterministic, homogenous case has a spiking solution which corresponds to a stable periodic solution of the fast subsystem. (De Vries and Sherman, 2000, Fig. 6(c)). According to De Vries and Sherman (2000) the noise "shakes" the bifurcation diagram forcing the system to leave the in phase (IP) periodic branch and instead follow another periodic branch, the anti-phase (AP) branch, resulting in bursting. However, as seen in Fig. 1 the "shaking" by noise alone is not enough to make the system burst. Instead we propose that the heterogeneity introduced by the two independent processes $p_1 \neq p_2$ changes the bifurcation diagram making the stable part of the IP branch unstable, so that the system settles on the AP branch, and in this way induces bursting.

As a measure of the heterogeneity we found that on average $|p_1 - p_2| \approx 0.0115$. That is, 1000 time series, $d^j(t) := |p_1(t) - p_2(t)|, j = 1, \ldots, 1000$, were calculated, and it was seen that $\sum_{j=1}^{1000} d^j(t)/1000$ is approximately constant and equal to 0.0115. A simulation of the deterministic case with $p_1 = 0.5$, $p_2 = 0.5115$ confirms that heterogeneity of this order in the $p$ variables induce bursting similar to the full stochastic system (simulation not shown). Moreover, the bifurcation diagram for the heterogeneous, deterministic case $p_1 = 0.5$, $p_2 = 0.5115$ confirms that the IP branch has lost its stability, see Fig. 2. For the homogeneous case, $p_1 = p_2 = 0.5$, a pitchfork-of-periodics (PFP) bifurcation exists for $s \approx -0.22$ on the IP branch (De Vries and Sherman, 2000, Fig. 6(a)). We note that this PFP bifurcation "unfolds" into a saddle-node bifurcation of periodics, one of which is the IP branch. Since the stable part of the IP branch near the saddle-node on invariant circle (SNIC) bifurcation, which result in spiking in the homogeneous case, is born in another PFP bifurcation (De Vries and Sherman, 2000, Fig. 6(c)) we expect that the unfolding of this other PFP bifurcation is underlying the disappearance of the stable periodic solution resulting in spiking, and consequently, the appearance of bursting. Such unfoldings of pitchfork bifurcations are well-known to happen when a system loses its symmetry, in this case $p_1 \neq p_2$, and are often called *imperfect bifurcations* (Strogatz, 1994, Ch. 3.6).

In summary, two spiking, noisy cells are transformed into bursters when coupled only in the case when the noise in the two cells is independent. The reason for the emergence of bursting is not the "shaking" of the bifurcation diagram. Instead, the heterogeneity introduced by the noise makes the cells burst. This highlights the idea (De Vries and Sherman, 2001) that heterogeneity of cell properties (Kinard et al., 1999; Pipeleers et al., 1994) is more important than noise in transforming spikers into bursters.

All simulations and bifurcation diagrams were done using XPPAUT (Ermentrout, 2002).

## Acknowledgements

Partially supported by 'Rejselegat for Matematikere' (Travelling Scholarship for Mathematicians). The author thanks IMPA, Rio de Janeiro, Brazil, for letting him visit the institute, where this work was initiated.

## References

De Vries, G., Sherman, A., 2000. Channel sharing in pancreatic $\beta$-cells revisited: enhancement of emergent bursting by noise. J. Theor. Biol. 207, 513–530.

De Vries, G., Sherman, A., 2001. From spikers to bursters via coupling: help from heterogeneity. Bull. Math. Biol. 63, 371–391.

Ermentrout, G.B., 2002. Simulating, Analyzing, and Animating Dynamical Systems: A Guide to XPPAUT for Researchers and Students. SIAM Books, Philadelphia.

Jonas, J.C., Gilon, P., Henquin, J.C., 1998. Temporal and quantitative correlation between insulin secretion and stably elevated or oscillatory cytoplasmic $Ca^{2+}$in mouse pancreatic $\beta$-cells. Diabetes 47, 1266–1273.

Kinard, T.A., De Vries, G., Sherman, A., Satin, L.S., 1999. Modulation of the bursting properties of single mouse pancreatic beta-cells by artificial conductances. Biophys. J. 76, 1423–1435.

Pipeleers, D., Kiekens, R., Ling, Z., Wilikens, A., Schuit, F., 1994. Physiologic relevance of heterogeneity in the pancreatic beta-cell population. Diabetologia 37, S57–S64.

Sherman, A., Rinzel, J., 1991. Model for synchronization of pancreatic beta-cells by gap junction coupling. Biophys. J. 59, 547–559.

Strogatz, S.H., 1994. Nonlinear Dynamics and Chaos, with Applications to Physics, Biology, Chemistry, and Engineering. Addison-Wesley, Reading, MA.

Morten Gram Pedersen*

*Department of Mathematics, Technical University of Denmark, Matematiktorvet, Building 303, DK-2800 Kgs. Lyngby, Denmark*

*E-mail address:* m.g.pedersen@mat.dtu.dk

*Fax: (+45) 4588 1399.

# *Paper IV*

Biophysical Journal Volume 89 July 2005 107–119 

# Intra- and Inter-Islet Synchronization of Metabolically Driven Insulin Secretion

Morten Gram Pedersen,* Richard Bertram,† and Arthur Sherman‡
*Department of Mathematics, Technical University of Denmark, Kgs. Lyngby, Denmark; †Department of Mathematics and Institute of Molecular Biophysics, Florida State University, Tallahassee, Florida; and ‡Laboratory of Biological Modeling, National Institute of Diabetes and Digestive and Kidney Diseases, National Institutes of Health, Bethesda, Maryland

ABSTRACT Insulin secretion from pancreatic $\beta$-cells is pulsatile with a period of 5–10 min and is believed to be responsible for plasma insulin oscillations with similar frequency. To observe an overall oscillatory insulin profile it is necessary that the insulin secretion from individual $\beta$-cells is synchronized within islets, and that the population of islets is also synchronized. We have recently developed a model in which pulsatile insulin secretion is produced as a result of calcium-driven electrical oscillations in combination with oscillations in glycolysis. We use this model to investigate possible mechanisms for intra-islet and inter-islet synchronization. We show that electrical coupling is sufficient to synchronize both electrical bursting activity and metabolic oscillations. We also demonstrate that islets can synchronize by mutually entraining each other by their effects on a simple model "liver," which responds to the level of insulin secretion by adjusting the blood glucose concentration in an appropriate way. Since all islets are exposed to the blood, the distributed islet-liver system can synchronize the individual islet insulin oscillations. Thus, we demonstrate how intra-islet and inter-islet synchronization of insulin oscillations may be achieved.

## INTRODUCTION

Insulin secretion from pancreatic $\beta$-cells, located in the islets of Langerhans, is pulsatile with a period of 5–10 min and is believed to be responsible for in vivo pulsatility with similar frequency (1–3). It has been suggested that this is due to oscillations in glycolysis mediated by the allosteric enzyme phosphofructokinase (PFK), resulting in rhythmic activity of ATP-dependent potassium channels (K(ATP)-channels) (3–6). Insulin pulsatility is impaired in diabetic humans (7), their relatives (8,9) and in animal models such as ob/ob mice (10) and ZDF rats (2). Moreover, target tissues are more sensitive to pulsatile insulin levels than to constant levels (11–14). Hence, understanding the mechanisms underlying pulsatile insulin secretion is important for a potential medical treatment of diabetes.

The link between metabolism and $Ca^{2+}$ influx leading to insulin secretion is provided by the electrical activity of the $\beta$-cells, which has a characteristic behavior known as ''bursting.'' A burst consists of an active phase of spiking followed by a silent phase of hyperpolarization. During the active phase $Ca^{2+}$ enters the cell through voltage-gated calcium channels leading to an elevated cytosolic $Ca^{2+}$ concentration and the consequent release of insulin. During the silent phase $Ca^{2+}$ is cleared by $Ca^{2+}$ ATPases. When the glucose concentration is increased, increasing the strength of the metabolic stimulus, K(ATP)-channels close and the plateau fraction increases, i.e., the active phases become longer compared to the silent phases. In this way, glucose increases the average $Ca^{2+}$ concentration, which increases the rate of insulin release (15). The period of this ''simple'' bursting is often tens of seconds.

Another form of bursting called ''compound bursting'' consists of clusters or episodes of bursts followed by long silent phases (6). Compound bursting has often been observed in electrical and calcium recordings from $\beta$-cells in islets (6,16–18). The period of a compound burst is several minutes, considerably longer than a single simple burst. It has been suggested that compound bursts are responsible for pulsatile insulin secretion (6).

In Bertram et al. (6) a potential mechanism for compound bursting was described. In this model, the glycolytic subsystem has the ability to oscillate due to positive product feedback onto the glycolytic enzyme PFK. The oscillatory glycolysis leads to oscillations in ATP production which lead to periodic activity of K(ATP)-channels. This slow rhythm interacts with the faster activity-dependent $Ca^{2+}$ rhythm that drives simple bursting, producing episodes of bursting followed by long silent phases. In addition to compound bursting, oscillations in glycolysis were shown to have other possible effects. These include production of a very slow form of bursting driven purely by glycolysis (''glycolytic bursting''), and a periodic variation in the plateau fraction (''accordion bursting''). These various forms of bursting have in common a slow modulation of the intracellular calcium concentration, and consequent pulsatile insulin secretion.

To observe an overall oscillatory insulin profile it is necessary that the insulin secretion from individual $\beta$-cells is synchronized within islets (intra-islet synchronization), and that the population of islets is also synchronized (inter-islet synchronization). If the cells or islets were not synchronized we would observe a flat, averaged signal even though the single cells and islets released insulin in pulses. This raises the questions

*Submitted November 8, 2004, and accepted for publication April 6, 2005.*
Address reprint requests to Arthur Sherman, Tel.: 301-496-4325; E-mail: asherman@nih.gov.

0006-3495/05/07/107/13 $2.00
doi: 10.1529/biophysj.104.055681

of how metabolic oscillations are synchronized within and among islets. These questions are the focus of this report.

Insulin secretion from the isolated pancreas is pulsatile (19,20), and this has lead to the hypothesis that an intrapancreatic neural pacemaker may be responsible for inducing periodic insulin release from the population of islets (3,19,21). However, pulsatile insulin secretion has been observed in individual $\beta$-cells (22) and islets (1,2,23), demonstrating that such a pacemaker has, at most, a synchronizing function. It has also been shown that groups of islets (2,24) and pieces of pancreas containing electrically silent ganglia (25) exhibit oscillatory release of the hormone. Hence, there must be additional synchronizing mechanisms.

An alternate synchronization mechanism has been postulated based on data showing that plasma glucose levels fluctuate on the timescale of pulsatile insulin release (26–30). According to this mechanism, classical glucose/insulin feedback pathways account for the synchronization of the islets (2,3,20,21). We stress that this is a synchronization mechanism only, since the ability to secrete in 5–10 min pulses resides within the individual cells and islets. This is in contrast to the slower ultradian oscillations of insulin which have periods of hours. Here the feedback between the islets and the liver is believed to create the oscillations, not just synchronize those that are already present in the islets (31).

The possibility that oscillations in glucose feed back onto the 5–10 min insulin pulses is supported by the following facts. It has been shown that pulsatile insulin secretion can be entrained by a periodic glucose stimulus in healthy rats (1,2) as well as in healthy humans (29,30). Moreover, slow NAD(P)H, $Ca^{2+}$, and mitochondrial membrane potential oscillations, which are thought to underlie pulsatile insulin release, can be entrained in mouse islets (32). The entrainment is impaired in ZDF rats (2) and diabetic humans (29,33), pointing to a possibly crucial mechanism for normal overall pulsatility. Similar results have been obtained for entrainment of the slower ultradian oscillations (31,34).

Not all data support the glucose/insulin feedback mechanism for synchronization. For example, pulsatile secretion has been observed even when the glucose concentration was held constant. This has been observed in vitro for the perfused pancreas (19) as well as in vivo when plasma glucose was clamped (35). Our aim here is not to reconcile all of the in vitro and in vivo data, but rather to test the plausibility that insulin oscillations can be produced and coordinated in the absence of an intrapancreatic neural pacemaker.

Using the model of Bertram et al. (6), we investigate possible mechanisms for intra-islet and inter-islet synchronization. We show that, surprisingly, electrical coupling is sufficient to synchronize both electrical bursting activity and metabolic oscillations. We also demonstrate that inter-islet synchronization is possible through the glucose/insulin feedback mechanism described above, here modeled by the interaction of $\beta$-cells with a ''liver.'' The simple model liver responds to the level of insulin secretion by adjusting the external glucose concentration in an appropriate way. Furthermore, we show that some degree of pulsatile secretion from groups of islets can be expected even when glucose is kept constant. Thus, intra-islet and inter-islet synchronization are possible for a model $\beta$-cell in which pulsatile insulin secretion is produced through compound bursts involving glycolytic oscillations.

## MATERIALS AND METHODS

### Modeling

We use the model developed by Bertram et al. (6), which combines a model for electrical and $Ca^{2+}$ dynamics from Bertram and Sherman (36) with a model for glycolysis that is modified from Smolen (37). To this model we add a first-order equation for insulin secretion. The link between glycolysis and the electrical/ $Ca^{2+}$ component of the model is provided by the adenine nucleotides adenosine monophosphate (AMP), adenosine diphosphate (ADP), and adenosine triphosphate (ATP) (3,4,6). The model is summarized in Fig. 1.

The glycolytic component of the model (*left side* of Fig. 1) is modified from an earlier model for glycolytic oscillations in muscle extracts (37). The key player in glycolysis for the production of oscillations is the allosteric enzyme phosphofructokinase (PFK). This is activated by its product fructose 1-6-bisphosphate (FBP) and by adenosine monophosphate, and inhibited by ATP. The main difference from the recent model by Westermark and Lansner (38) is that their model does not include feedback of ATP and AMP onto PFK.

The glycolysis model consists of equations for intracellular glucose ($G_i$), glucose 6-phosphate (G6P) and FBP,

$$\frac{dG_i}{dt} = J_{glut} - J_{gk}, \tag{1}$$

$$\frac{dG6P}{dt} = \kappa(J_{gk} - J_{PFK}), \tag{2}$$

$$\frac{dFBP}{dt} = \kappa(J_{PFK} - \frac{1}{2}J_{GPDH}). \tag{3}$$

The concentrations of G6P and fructose 6-phosphate (F6P) are assumed to be in equilibrium through rapid catalytic activity of the enzyme phosphoglucose isomerase. They satisfy the equilibrium relation F6P = 0.3 G6P.

The parameter $\kappa = 0.005$ (in 2–3) converts milliseconds to seconds and increases the frequency of glycolytic oscillations by a factor of 5 with respect to the earlier Smolen model (37). $J_{glut}$ is the rate of the GLUT-2 facilitated glucose transporter (39),

$$J_{glut} = V_{glut}\frac{(G_e - G_i)K_{glut}}{(K_{glut} + G_e)(K_{glut} + G_i)}, \tag{4}$$

where $G_e$ is the extracellular glucose concentration, $V_{glut}$ is the maximal rate, and $K_{glut}$ is a constant. The value $J_{gk}$ is the glucokinase reaction rate, which is described by a Hill function of $G_i$ (40), where it is assumed that the reaction is irreversible:

$$J_{gk} = V_{gk}\frac{G_i^{n_{gk}}}{K_{gk}^{n_{gk}} + G_i^{n_{gk}}}. \tag{5}$$

Furthermore,

$$J_{GPDH} = 0.2\sqrt{\frac{FBP}{1\,\mu M}}\mu M s^{-1} \tag{6}$$

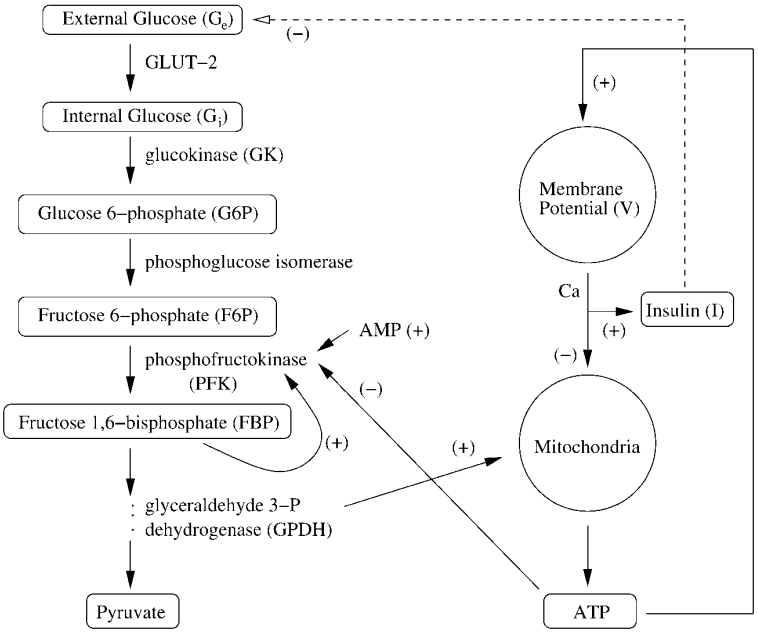


FIGURE 1 An overview of the pathways in the model. Glucose enters the $\beta$-cell through GLUT-2 transporters, and is broken down during glycolysis. (*Left column*) Part of the glycolytic pathway, highlighting the enzyme PFK and its regulators. The products of glycolysis feed into the mitochondria where ATP is produced. ATP links the glycolytic component to the electrical component (*right column*) by regulating K(ATP)-channels. These, in turn, regulate membrane potential and $Ca^{2+}$ flow leading to insulin secretion. The electrical/$Ca^{2+}$ component is linked back to glycolysis through $Ca^{2+}$ regulation of ATP production and AMP/ATP feedback onto PFK. (*Dashed line*) Function of insulin to lower the plasma glucose concentration through the actions of the liver. The negative insulin feedback is added to the model when in vivo synchronization is discussed.

is the glyceraldehyde 3-P dehydrogenase (GPDH) reaction rate. The PFK reaction rate, $J_{PFK}$, reflects the binding of activators (AMP and FBP), an inhibitor (ATP), and the substrate F6P (= 0.3 G6P). ATP is both a substrate and an inhibitor of PFK. As substrate, it is assumed to be saturating, so it is not explicitly included in the model. The PFK reaction rate function is given by

$$J_{PFK} = V_{max}\frac{(1-\lambda)w_{1110} + \lambda\sum_{ijl} w_{ij11}}{\sum_{ijkl} w_{ijkl}}, \tag{7}$$

where $i$, $j$, $k$, $l$ take value 0 or 1, and

$$w_{ijkl} = \frac{1}{f_{13}^{ik} f_{23}^{jk} f_{41}^{il} f_{42}^{jl} f_{43}^{kl}}\left(\frac{AMP}{K_1}\right)^{i}\left(\frac{FBP}{K_2}\right)^{j}\left(\frac{F6P^2}{K_3}\right)^{k}\left(\frac{ATP^2}{K_4}\right)^{l}. \tag{8}$$

We refer to Smolen (37) for a discussion of these expressions.

We assume that the total concentration of adenine nucleotides is conserved, and that the adenylate kinase reaction, which converts two molecules of ADP to one molecule of AMP and one of ATP, is at equilibrium $AMP + ADP + ATP = A_{tot}$, $AMP \times ATP = ADP^2$.

Glycolysis provides input to the mitochondria. Magnus and Keizer (41) developed a model for the mitochondrial production of ATP, in which the production rate decreases with the concentration of free cytosolic $Ca^{2+}$. In Bertram et al. (6) the Keizer-Magnus model was modified by including the time dynamics of glycolysis. The GPDH reaction rate, $J_{GPDH}$, is used as a measure of the time-varying input to the mitochondria.

The differential equation for the ADP concentration includes the effects of cytosolic $Ca^{2+}$ concentration ($Ca$), and the effects of glycolysis:

$$\frac{dADP}{dt} = \frac{1}{\tau_a}\left[ATP - ADP\exp\left((r+\gamma)(1-\frac{Ca}{r_1})\right)\right]. \tag{9}$$

The $Ca^{2+}$ effect is through the factor $(1 - (Ca/r_1))$; increases in $Ca^{2+}$ concentration lead to increases in ADP. The total substrate-dependent rate is $r + \gamma$. Input from glycolysis is incorporated through the function $\gamma$, which depends on the GPDH rate. We describe this with a sigmoidal function of Michaelis-Menten form,

$$\gamma = \frac{\nu_\gamma J_{GPDH}}{k_\gamma + J_{GPDH}}, \tag{10}$$

where $\nu_\gamma$ and $k_\gamma$ are constants. The dependence of ADP on $\gamma$ (and thus on FBP) is the means through which glycolytic oscillations are transduced into oscillations in nucleotide production. In the earlier Keizer-Magnus model the factor $\gamma$ was not included (42). The parameter $\tau_a = 5$ min is a slow time constant.

The electrical and $Ca^{2+}$ handling components of the model are based on an earlier $\beta$-cell model in which bursting is driven by calcium-dependent oscillations in the K(Ca) current and the K(ATP) current (36). The K(Ca) current is directly activated by calcium. The K(ATP) current conductance is dependent on the concentrations of ADP and ATP; the conductance is lower for higher values of the ratio ATP/ADP. Changes in the cytosolic $Ca^{2+}$ concentration ($Ca$) take place on a moderately slow timescale (a few seconds to tens of seconds), whereas changes in ADP and ATP occur on a slower timescale (tens of seconds to minutes). The interaction of these two slow processes with disparate timescales can give rise to bursting with periods ranging from a few seconds to a few minutes. This is an example of a phantom bursting model (36,43). The equation for the membrane potential ($v$) is

$$c_m\frac{dv}{dt} = -(I_K + I_{Ca} + I_{K(Ca)} + I_{K(ATP)}), \tag{11}$$

where $c_m$ is the membrane capacitance, $I_K$ is a $v$-dependent $K^+$ current, $I_{Ca}$ is a $v$-dependent $Ca^{2+}$ current, $I_{K(Ca)}$ is a calcium-activated $K^+$ current, and $I_{K(ATP)}$ is an ATP-sensitive $K^+$ current, $I_K = \bar{g}_K n(v - v_K)$, $I_{Ca} = \bar{g}_{Ca} m_\infty(v)(v - v_{Ca})$, $I_{K(Ca)} = g_{K(Ca)}(v - v_K)$, and $I_{K(ATP)} = g_{K(ATP)}(v - v_K)$, where $g_{K(Ca)} = \bar{g}_{K(Ca)}(Ca^2/K_D^2 + Ca^2)$, $g_{K(ATP)} = \bar{g}_{K(ATP)} o_\infty(ADP, ATP)$.

The equation for the $I_K$ activation variable is

$$\frac{dn}{dt} = \frac{n_\infty(v) - n}{\tau_n(v)}, \tag{12}$$

where $\tau_n(v) = (1/0.035 \cdot \cosh((v + 16)/22.4))$ is the timescale and $n_\infty(v)$ is the equilibrium value of $n$, $n_\infty(v) = (1/1 + \exp(-(v + 16)/5.6))$. Activation of $Ca^{2+}$ current is assumed to be instantaneous, with equilibrium function $m_\infty(v) = (1/1 + \exp(-(v + 20)/12))$.

The K(ATP) conductance is assumed to adjust instantaneously to the concentrations of ADP and ATP, and the form of the conductance function ($o_\infty$) is described in detail in Magnus and Keizer (41). We use the Magnus-Keizer expression for $o_\infty$ without modification:

$$o_\infty(ADP,ATP) = \frac{0.08\left(1+\frac{2\mathrm{MgADP}^-}{17\mu\mathrm{M}}\right)+0.89\left(\frac{\mathrm{MgADP}^-}{17\mu\mathrm{M}}\right)^2}{\left(1+\frac{\mathrm{MgADP}^-}{17\mu\mathrm{M}}\right)^2\left(1+\frac{\mathrm{ADP}^{3-}}{26\mu\mathrm{M}}+\frac{\mathrm{ATP}^{4-}}{1\,\mu\mathrm{M}}\right)}. \quad (13)$$

As discussed in Magnus and Keizer (41), the nucleotide concentrations are related to the total concentrations of ADP and ATP by $MgADP^{2-} = 0.165\ ADP$, $ADP^{3-} = 0.135\ ADP$, and $ATP^{4-} = 0.005\ ATP$.

The equation for the free cytosolic $Ca^{2+}$ concentration is

$$\frac{dCa}{dt} = f_{\mathrm{cyt}}(J_{\mathrm{mem}} + J_{\mathrm{er}}), \quad (14)$$

where $f_{\mathrm{cyt}}$ is the fraction of free to total cytosolic $Ca^{2+}$, $J_{\mathrm{mem}}$ is the $Ca^{2+}$ flux across the plasma membrane, and $J_{\mathrm{er}}$ is the $Ca^{2+}$ flux out of the endoplasmic reticulum (ER). The plasma membrane flux term is given by $J_{\mathrm{mem}} = -(\alpha I_{\mathrm{Ca}} + k_{\mathrm{PMCA}}Ca)$, where $\alpha$ converts current to flux, and $k_{\mathrm{PMCA}}$ is the $Ca^{2+}$ pump rate. We do not consider the actions of IP3-generating muscarinic agonists, so flux out of the ER is due only to leakage ($J_{\mathrm{leak}}$). $Ca^{2+}$ flux into the ER is through SERCA pumps ($J_{\mathrm{SERCA}}$): $J_{\mathrm{er}} = J_{\mathrm{leak}} - J_{\mathrm{SERCA}}$, where $J_{\mathrm{leak}} = p_{\mathrm{leak}}(Ca_{\mathrm{er}} - Ca)$, $J_{\mathrm{SERCA}} = k_{\mathrm{SERCA}}Ca$, and $p_{\mathrm{leak}}$ is the leakage permeability and $k_{\mathrm{SERCA}}$ is the SERCA pump rate. The differential equation for the $Ca^{2+}$ concentration in the ER is

$$\frac{dCa_{\mathrm{er}}}{dt} = -f_{\mathrm{er}}(V_{\mathrm{cyt}}/V_{\mathrm{er}})J_{\mathrm{er}}, \quad (15)$$

where $f_{\mathrm{er}}$ is analogous to $f_{\mathrm{cyt}}$, and $V_{\mathrm{cyt}}$, $V_{\mathrm{er}}$ are the volumes of the cytosolic and ER compartments, respectively.

Finally, we add an equation for insulin secretion to the model from Bertram et al. (6). We describe the rate of insulin secretion, $I$, by a first-order relation

$$\frac{dI}{dt} = \frac{I_\infty(Ca) - I}{\tau_{\mathrm{I}}}, \quad (16)$$

where $\tau_{\mathrm{I}}$ is a time constant. $I_\infty(Ca)$ is the equilibrium secretion rate, modeled as a linear function of $Ca^{2+}$ (44) by

$$I_\infty(Ca) = \begin{cases} I_{\mathrm{slope}}(Ca - Ca_{\mathrm{null}}) & \text{for} \quad Ca \geq Ca_{\mathrm{null}} \\ 0 & \text{for} \quad Ca < Ca_{\mathrm{null}} \end{cases},$$

where $Ca_{\mathrm{null}}$ is the minimal $Ca^{2+}$ concentration necessary for insulin release, and $I_{\mathrm{slope}}$ measures the $Ca^{2+}$ sensitivity of secretion. The simple Eq. 16 is motivated by the fact that the most important trigger of insulin release is cytosolic calcium (44–46). For simplicity we do not include the amplifying (K(ATP)-independent) pathway, nor vesicle transportation between different pools. $I$ is measured in arbitrary units.

Values of all parameters used in the model are given in Table 1. Details of the model not described here and discussion of parameters can be found in Bertram et al. (6), Bertram and Sherman (36), Smolen (37), and Magnus and Keizer (41). The differential equations were integrated numerically with the CVODE solver in the software package XPPAUT (47). The computer code for the model can be downloaded from http://www.math.fsu.edu/~bertram or http://mrb.niddk.nih.gov/sherman.

## RESULTS

### Single-cell simulations

As discussed in Bertram et al. (6), the model can give rise to pulsatile insulin secretion through compound bursting (Fig. 2) with a natural period of ~5 min. The slowest component of the compound bursting is due to oscillatory glycolysis, reflected by an oscillatory FBP concentration (Fig. 2 *A*). This causes slow oscillations in ADP, which superimpose with the faster ADP oscillations driven by $Ca^{2+}$ (Fig. 2 *B*). This multimodal ADP rhythm leads to oscillations in the conductance $g_{\mathrm{K(ATP)}}$ of the ATP-dependent potassium channel, which drives the burst episodes of the membrane potential, $v$ (Fig. 2 *C*). This then gives compound bursting of intracellular calcium (Fig. 2 *D*), leading to pulsatile insulin secretion (Fig. 2 *E*). We show the one-minute moving average of the insulin secretion (Fig. 2 *F*) to facilitate comparison with insulin measurements such as in Sturis et al. (2), where insulin is sampled only about once per minute.

We will be varying the glucose sensitivity parameter $V_{\mathrm{gk}}$. Glycolysis oscillates for intermediate values of this parameter. For $V_{\mathrm{gk}}$ too small or too large the glycolytic subsystem is stationary (6). The oscillation period for a range of $V_{\mathrm{gk}}$ values is shown in Fig. 3. We note that the period is relatively insensitive to changes in the value of $V_{\mathrm{gk}}$. Importantly, the period is always on the order of several minutes, consistent with data on pulsatile insulin secretion.

Fig. 3 is constructed by finding the period for some $V_{\mathrm{gk}}$, and then we use the endpoint of the previous solution as initial condition for a new solution with $V_{\mathrm{gk}}$ slightly changed.

**TABLE 1 Parameter values used in the model, except where noted**

| | | | |
|---|---|---|---|
| $V_{\mathrm{glut}} = 8$ mM/ms | $K_{\mathrm{glut}} = 7$ mM | $V_{\mathrm{gk}} = 0.8$ mM/ms | $K_{\mathrm{gk}} = 7$ mM |
| $n_{\mathrm{gk}} = 4$ | $V_{\mathrm{max}} = 2\ \mu$M/ms | $\lambda = 0.06$ | $K_1 = 30\ \mu$M |
| $K_2 = 1\ \mu$M | $K_3 = 50{,}000\ \mu$M | $K_4 = 1000\ \mu$M | $f_{13} = 0.02$ |
| $f_{23} = 0.2$ | $f_{41} = 20$ | $f_{42} = 20$ | $f_{43} = 20$ |
| $A_{\mathrm{tot}} = 3000\ \mu$M | $\nu_\gamma = 2.2$ | $k_\gamma = 0.1\ \mu$M/ms | $\tau_{\mathrm{a}} = 300{,}000$ ms |
| $r = 0.5$ | $r_1 = 0.35\ \mu$M | $\bar{g}_{\mathrm{K}} = 2700$ pS | $v_{\mathrm{K}} = -75$ mV |
| $\bar{g}_{\mathrm{Ca}} = 1000$ pS | $v_{\mathrm{Ca}} = 25$ mV | $\bar{g}_{\mathrm{K(Ca)}} = 400$ pS | $K_{\mathrm{D}} = 0.5\ \mu$M |
| $\bar{g}_{\mathrm{K(ATP)}} = 40{,}000$ pS | $c_{\mathrm{m}} = 5300$ fF | $V_{\mathrm{cyt}}/V_{\mathrm{er}} = 31$ | $p_{\mathrm{leak}} = 0.0002\ \mathrm{ms}^{-1}$ |
| $f_{\mathrm{cyt}} = 0.01$ | $f_{\mathrm{er}} = 0.01$ | $k_{\mathrm{PMCA}} = 0.18\ \mathrm{ms}^{-1}$ | $k_{\mathrm{SERCA}} = 0.4\ \mathrm{ms}^{-1}$ |
| $\tau_{\mathrm{I}} = 10{,}000$ ms | $I_{\mathrm{slope}} = 210\ \mu\mathrm{M}^{-1}$ | $Ca_{\mathrm{null}} = 0.055\ \mu$M | $\kappa = 0.005$ |
| $\alpha = 4.5 \cdot 10^{-6}\ \mu$M/ms | | | |

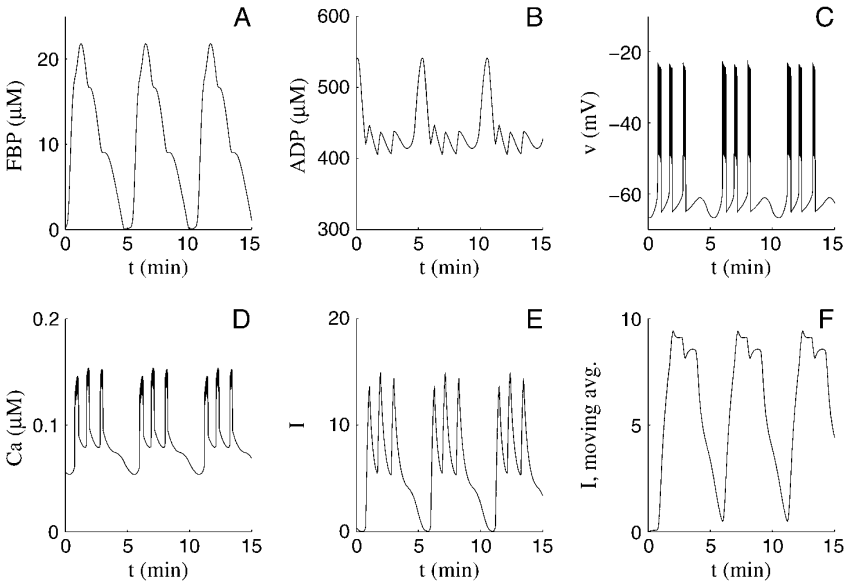


FIGURE 2 Compound bursting leading to pulsatile insulin secretion for a constant glucose stimulus, $G_e = 7$ mM, with $V_{gk} = 0.8$ mM/ms. The period of the pulses is 5.2 min.

When increasing $V_{gk}$ (Fig. 3, *solid curve*) the system follows a branch of stable periodic solutions, corresponding to pulsatile insulin secretion, until such a periodic solution no longer exists at $V_{gk} = 0.84$ mM/ms. The system then follows the branch of steady states, corresponding to constant insulin release with small oscillations that reflect simple bursting. For decreasing $V_{gk}$ (Fig. 3, *dashed curve*) the system follows this branch of steady states until the steady state loses its stability at $V_{gk} = 0.74$ mM/ms. The system then follows the branch of periodic solutions for lower $V_{gk}$ values.

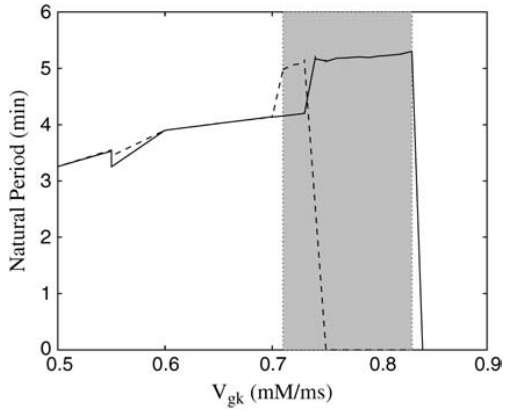


FIGURE 3 The natural period of the pulsatile insulin secretion as a function of the glucose sensitivity parameter $V_{gk}$. The solid curve is produced by increasing $V_{gk}$, using the previous solution as initial conditions, whereas the dashed line is generated by decreasing $V_{gk}$. The shaded area indicates the region of bistability between stationary glycolysis and oscillatory glycolysis.

Note that there is bistability for $V_{gk}$ between 0.71 and 0.83 mM/ms. Thus, pulsatile insulin release patterns and constant release patterns coexist, corresponding to a coexisting periodic solution and a stable stationary state of the glycolytic subsystem. The values of the initial conditions determine which behavior is produced. This model prediction was confirmed experimentally in Bertram et al. (6). We also note that another type of bistability, consisting of two coexisting periodic solutions, is present for $V_{gk}$ near 0.71 mM/ms. We hypothesize that this corresponds to an S-shaped periodic branch where the two stable branches shown in Fig. 3 with periods ~4 and 5 min, respectively, are connected with a branch of unstable periodic solutions, which is created and destroyed in two saddle-node bifurcations.

## Intra-islet synchronization

It is well established that electrical and $Ca^{2+}$ oscillations of $\beta$-cells are synchronized within an islet (10,48–51), a necessary fact in order to see a pulsatile insulin signal from an islet. This synchronization is impaired in islets from ob/ob mice (10). If glycolysis is driving pulsatile secretion, then metabolism should be synchronized throughout the islet. This metabolic synchronization was demonstrated by Jung et al. (52), who showed that oxygen levels measured at two different sites in an islet were synchronized.

Although it is generally believed that gap junctions synchronize cells via electrical coupling, it is also possible that gap junctions are permeable to glycolytic intermediaries. By allowing FBP to diffuse between two cells, we can easily obtain synchronization of both insulin secretion and glycolysis. This is possible even for very low diffusion rates and without electrical coupling (simulations not shown). On the

other hand, electrical oscillations can be synchronized by electrical coupling through gap junctions (53).

More surprisingly, we now show that electrical coupling alone can synchronize glycolytic oscillations without the need for the diffusion of glycolytic intermediates. We model the electrical coupling between two cells by adding

$$-g_c(v_i - v_j) \tag{17}$$

to Eq. 11 for cell $i = 1, 2, j \neq i$.

In this case $v$ and $c$ are synchronized by the electrical coupling (not shown), leading to synchronized secretion (Fig. 4 *A*). Surprisingly, glycolytic oscillations also synchronize when the two cells are electrically coupled (Fig. 4 *B*). The figure also illustrates that the average insulin secretion signal is not clearly pulsatile when the cells are uncoupled, since the two glycolytic oscillations are often out of phase. This lack of phasing would be more pronounced with more cells.

The mechanism behind the synchronization is that the coupling rapidly synchronizes electrical activity. This then synchronizes $Ca^{2+}$ levels and, consequently, insulin release (Fig. 4 *A*). Synchronization of metabolism takes longer to achieve (Fig. 4 *B*), due to the indirect manner in which $Ca^{2+}$ affects the glycolytic oscillator. The $Ca^{2+}$ inhibits mitochondrial ATP production, thus disinhibiting PFK activity. Without $Ca^{2+}$ feedback onto ATP production, or ATP and AMP feedback onto PFK, synchronization of glycolysis would not occur, even though gap junctions could synchronize electrical activity. This is illustrated for the case of no $Ca^{2+}$ feedback in Fig. 5, where the glycolytic oscillator drives pulsatile insulin release. The electrical subsystem synchronizes when the cells are coupled leading to synchronized insulin secretion (Fig. 5 *A*) but the glycolytic subsystems do not synchronize (Fig. 5 *B*).

Interestingly, in Fig. 4 there is virtually no insulin secretion at $\sim t = 20$ min, even though the average FBP concentration is fairly high. The FBP concentrations of the two cells are out of phase, and one is low at $t = 20$ min. So, if uncoupled at any time at $\sim t = 20$ min, one of the cells would be silent and the other one would be active. Fig. 4 shows that the silent cell is enough to terminate the (synchronized) insulin secretion. The same phenomenon is seen in Fig. 5. This points to the importance of having synchronized glycolysis, since insulin release is lower when glycolysis is out of phase.

The period of the coupled cells is similar to that of the faster of the two uncoupled cells. Thus, the faster cell drives the slow cell when coupled.

## Entrainment by a rhythmic glucose stimulus

Several labs have examined the entrainability of insulin secretion from the perfused pancreas, groups of islets, and single islets (1,2). They found that in all three cases it is possible to entrain the insulin secretion to an oscillating glucose stimulus. Moreover, slow NAD(P)H, $Ca^{2+}$, and mitochondrial membrane potential oscillations, which are thought to underlie pulsatile insulin release, can be entrained in mouse islets (32). Finally, it has been confirmed in vivo that pulsatile insulin release can be entrained to a periodic glucose infusion (29,30). We next demonstrate that it is possible to entrain our model cells with a low-amplitude glucose stimulus, and that the period of the entrained oscillation can be lower or greater than the natural period.

Sturis et al. (2) showed that pulsatile insulin secretion from an isolated pancreas and from isolated islets can be entrained by a sinusoidal glucose stimulus with amplitude as low as 5% of the mean. The present model describes the behavior of a representative cell located in an islet, and indeed, applying a sinusoidal external glucose stimulus to the model entrains the insulin secretion (Fig. 6). In Fig. 6 *A*, the natural pulsatility for $V_{gk} = 0.8$ mM/ms with a period of $\sim$5 min is

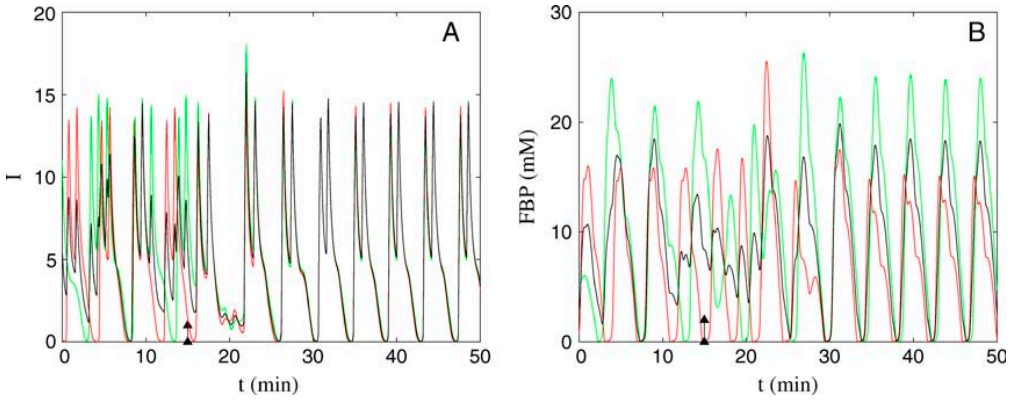


FIGURE 4 Two cells become synchronized when electrically coupled. Parameters as in Fig. 2, except $V_{gk,\,1} = 0.6$ mM/ms, $V_{gk,\,2} = 0.8$ mM/ms, and $g_c$ is raised from 0 pS to 100 pS at $t = 15$ min (*arrow*). (*A*) Rapid synchronization of insulin secretion. Red is the faster $I_1$, green is the slower $I_2$, and black is the average insulin secretion $\bar{I}$ from the two cells. (*B*) Slower synchronization of glycolysis. Red is $FBP_1$, green is $FBP_2$, and black is the average of the two cells.

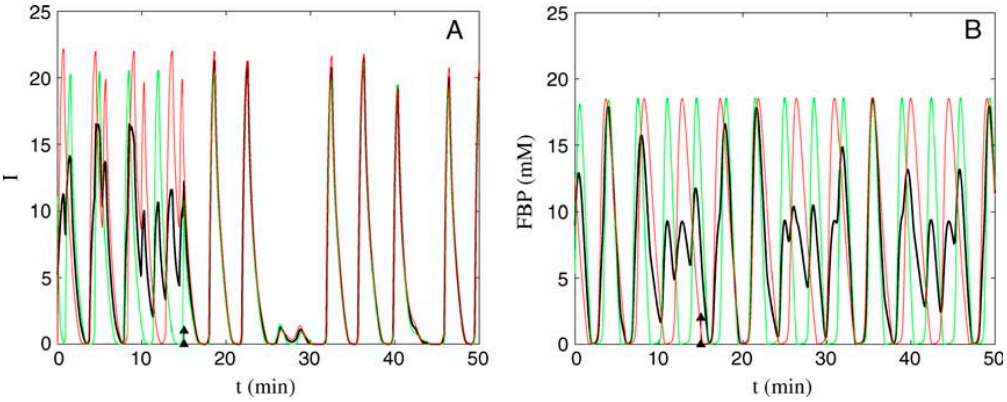


FIGURE 5 Without $Ca^{2+}$ feedback the cells do not synchronize glycolysis when electrically coupled. The absence of feedback is attained by keeping $Ca = 0.1\ \mu$M constant in Eq. 9. The parameters are as in Table 1 except $V_{gk,\,1} = 0.6$ mM/ms, $V_{gk,\,2} = 0.5$ mM/ms, $\kappa_1 = 0.003$, $\kappa_2 = 0.004$, $\bar{g}_{K,\,ATP} = 37{,}000$ pS, and $g_c$ is raised from 0 pS to 100 pS at $t = 15$ min (*arrow*). (*A*) Rapid synchronization of insulin secretion. Red is the slower $I_1$, green is the faster $I_2$, and black is the average insulin secretion $\bar{I}$ from the two cells. (*B*) Lack of synchronization of glycolysis. Red is $FBP_1$, green is $FBP_2$, and black is the average of the two cells.

shown. This pulsatile secretion is entrained to a faster (4-min period, Fig. 6 *B*) as well as to a slower (7-min period, Fig. 6 *C*) periodic glucose stimulus. However, for $V_{gk} = 0.6$ mM/ms the entrainment is impaired; the pulses are no longer entrainable to a glucose signal with period of 7 min (Fig. 6 *D*). In all cases, the external glucose concentration oscillates at ~7 mM on average, with 1-mM amplitude. The insulin pulses are in phase with the maximal glucose concentrations when forced by slower glucose oscillations as found by Sturis et al. (2).

As demonstrated in Fig. 6, it is possible to entrain the model $\beta$-cells at periods shorter or longer than the natural period. The entrainment window depends on the amplitude of the glucose oscillations and on the glucose sensitivity parameter $V_{gk}$. Fig. 7 shows the entrainment windows for a range of values of $V_{gk}$, with the glucose oscillation amplitude fixed at 1 mM. Note that the range of entrainment periods is larger when we enter the region with bistability ($V_{gk} > 0.7$ mM/ms, see Fig. 3) and larger yet in the region with no unforced glycolytic oscillations. In this region, the forced system has a clearly pulsatile behavior even though the unforced system does not. This is because the varying glucose concentration, which is similar to varying $V_{gk}$, pushes the system into the region with oscillatory glycolysis.

Electrical coupling between cells within an islet facilitates the entrainment of the heterogeneous cell population of the islet. Cell number one (*red*) in Fig. 4 with $V_{gk} = 0.6$ mM/ms is difficult to entrain, i.e., the cell is only entrainable in a narrow interval of forcing periods, see Fig. 6 *D* and Fig. 7. However, when coupled to cell number two (*green*), which is easier to entrain ($V_{gk} = 0.8$ mM/ms), the cell pair is entrainable (Fig. 8), even though one of the two cells was not entrainable when uncoupled. In this way, the coupling between cells not only synchronizes the secretion within the islet but also helps the islet to synchronize to an external glucose signal. If the cells were uncoupled, some would not follow the external signal because of heterogeneity of cell properties, and the overall response from the collection of cells (the islet) would not follow the glucose stimulus as nicely as shown in Fig. 8.

We can regard the pancreas as an assembly of many uncoupled islets, and the mechanism for the entrainment of the pancreas could be the following. With a constant glucose concentration the islets drift with respect to each other, so that even though each islet gives a pulsatile insulin signal, the total signal will be relatively flat; it has been averaged over all the islets. But when the glucose concentration oscillates, the islets synchronize their insulin secretion so that the total signal will be clearly pulsatile.

To illustrate this, we simulate 20 uncoupled islets with different glucose sensitivity ($V_{gk}$ chosen from a uniform distribution between 0.6 and 0.9 mM/ms) with glucose concentration first constant, then oscillatory, and then constant again. (Here and in the following we represent each islet as a single cell whose properties are the average of those in the islet.) Fig. 9 shows that the islets start off desynchronized and the average signal consists of small irregular pulses. When the glucose stimulus oscillates, the islets synchronize and the average signal becomes clearly pulsatile.

## In vivo inter-islet synchronization

Several in vivo studies have shown that in healthy humans, pulsatile insulin secretion can be entrained to rhythmic glucose stimuli with periods of 7–12 min (30) or, yielding a more complex pattern, to pulses every 29 min (29), demonstrating that the pancreas is tightly controlled by the fast oscillations in plasma glucose levels that occur in vivo (26–30). Although ultradian oscillations are also entrained to

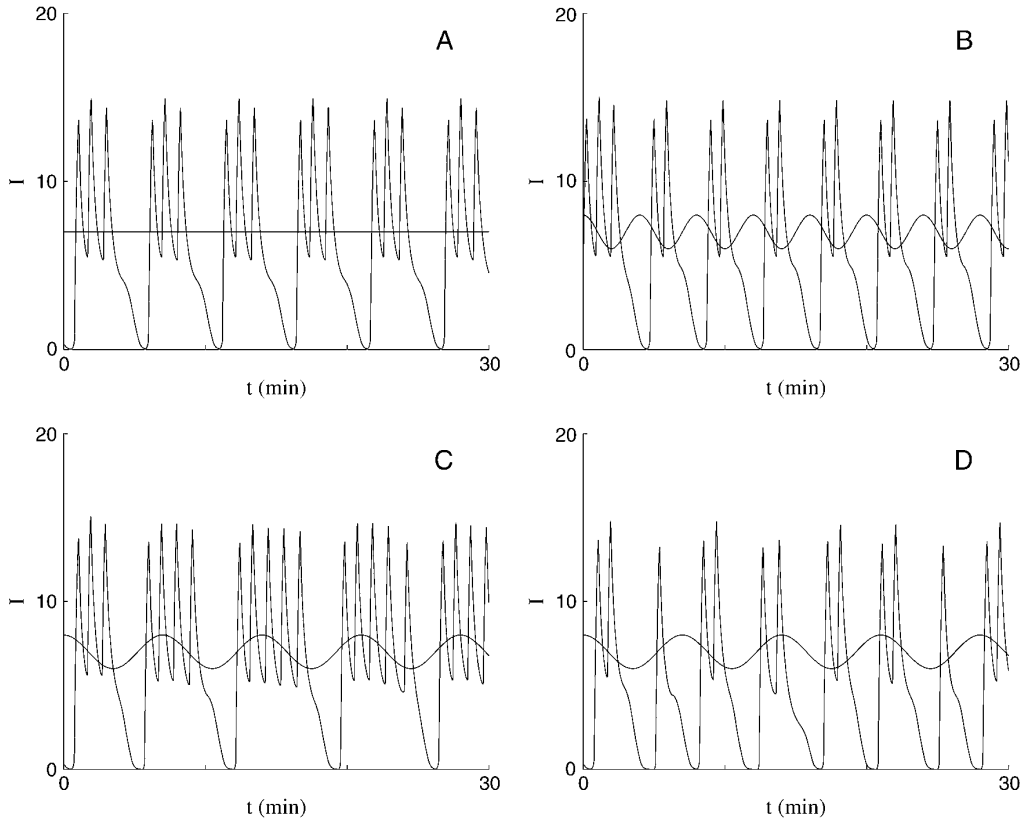


FIGURE 6 Entrainment of the pulsatile insulin secretion to a sinusoidal glucose stimulus. (*A*) The natural pulsatile insulin secretion with $V_{gk} = 0.8$ mM/ms and constant $G_e = 7$ mM. The period of the pulses is ~5 min. (*B*) Entrainment to a faster oscillating glucose stimulus with a period of 4 min. $V_{gk} = 0.8$ mM/ms. (*C*) Entrainment to a slower oscillating glucose stimulus with a period of 7 min. $V_{gk} = 0.8$ mM/ms. (*D*) Lack of entrainment to a glucose stimulus with a period of 7 min when $V_{gk}$ is reduced to 0.6 mM/ms. All glucose oscillations are centered at $\sim G_e = 7$ mM with 1 mM amplitude.

periodic infusions (31), the underlying mechanisms seem to be different. Ultradian oscillations are believed to be created by glucose/insulin feedback (31,54), and the infusions interact directly with this feedback system. For the faster insulin pulses under investigation here, the glucose stimulus rather seems to have a synchronizing role of the oscillating secretion from individual cells and islets.

We have shown that oscillations in the extracellular glucose concentration can synchronize insulin secretion. In vivo, hepatic glucose production follows plasma insulin oscillations (27), which suggests a mechanism by which pulsatile insulin release leads to periodic glucose production and plasma glucose levels. We investigate next whether insulin itself, through its action on the liver, could produce oscillations in the glucose concentration that could then entrain insulin secretion from the islets, as proposed by several authors (2,3,20,21).

To our model system we add a very simple representation of the liver, modeled by a first order equation for the dynamic response of plasma glucose, $G_e$, to the average insulin secretion $\bar{I}$,

$$\frac{dG_e}{dt} = \frac{G_\infty(\bar{I}) - G_e}{\tau_G}, \tag{18}$$

where $G_\infty$ is a decreasing sigmoidal function,

$$G_\infty(\bar{I}) = G_{min} + \frac{G_{max} - G_{min}}{1 + \exp\left(\dfrac{\mathrm{I} - \hat{\mathrm{I}}}{\mathrm{S_G}}\right)}. \tag{19}$$

Here $G_{min}$ corresponds to a very high insulin concentration, whereas $G_{max}$ corresponds to a very low insulin concentration. The value $\hat{I}$ is the insulin secretion, which gives the half-maximal glucose level, $G_e = (1/2)(G_{max} + G_{min})$. The parameters are listed in Table 2. Note that the timescale set by $\tau_G = 7.5$ min allows the liver to respond to changes in insulin release on a scale of minutes. This is in contrast to the much slower response time used in the models of ultradian oscillations (34,54).

In Fig. 10 *A* we see that we can synchronize 20 islets using this model for the external glucose feedback, even though the islets are not directly (e.g., electrically) coupled to each

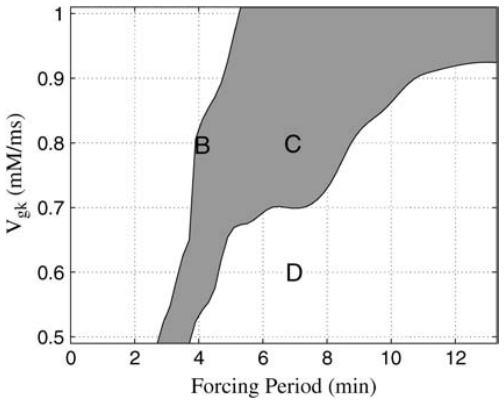


FIGURE 7 The entrainment window (*shaded*) for a range of values of $V_{gk}$ and period of the $G_e$ oscillations (*Forcing Period*). Glucose oscillations are 1 mM in amplitude, with an approximate mean value of 7 mM. *B–D* correspond to the panels in Fig. 6.

other. We begin by keeping $G_e$ constant, and then at time $t = 20$ min we let $G_e$ vary according to Eq. 18. Soon afterwards the previously unsynchronized islets become synchronized, resulting in a clearly pulsatile insulin signal, even though the individual bursts are out of phase as found in vivo (51); only the burst episodes are in phase. This is reflected in the lack of large-amplitude spikes on top of the slow pulses in the average insulin release (Fig. 10 *A*), in contrast to the intra-islet synchronization (Fig. 4 *A*).

Synchronization by feedback from the liver is possible even for islets that would not give pulsatile secretion in constant glucose, but when the glucose begins to oscillate they become entrained, which results in a pulsatile signal. Fig. 10 *B* shows a simulation of nine islets with $V_{gk} \geq 0.87$ mM/ms. Glycolysis does not oscillate in any of these islets when $G_e = 7$ mM is constant. At time $t = 10$ min we let $G_e$ vary as before and now a pulsatile insulin signal emerges. Note that, in constant glucose, the islets release insulin in fast pulses as observed experimentally in vitro (55,56). These fast fluctuations are driven by bursting electrical activity since glycolysis is stable. They are of much smaller amplitude than the slower pulses driven by glycolysis, due to the lack of synchrony of individual bursts between islets. Thus, bursting electrical activity can drive insulin oscillations, but it is not likely to drive the slower insulin pulsatility with a period of several minutes.

The difference between dynamic and constant extracellular glucose is even clearer in Fig. 11 *A*, where the smoothed insulin secretion from Fig. 10 *A* is compared with the secretion with a fixed glucose concentration. The power spectrum of the two curves beyond the point where the glucose concentration is allowed to vary (after a 10-min transient phase) confirms that the insulin secretion is much more pulsatile when $G_e$ is allowed to vary and the islets synchronize (Fig. 11 *B*). However, even in constant glucose the average insulin secretion oscillates. This is due to the fact that the drifting between the islets leads to times when some of the islets are nearly in phase, resulting in pulses of insulin secretion.

These observations could mean that pulsatile insulin secretion would be seen more often and be more regular in vivo than in vitro, where $G_e$ is usually kept constant. This observation is confirmed by the fact that, in vivo, >70–75% of the total insulin secretion is released in bursts (35,57,58), whereas the corresponding fraction in vitro is <40% (23,59). Moreover, the in vitro pulses from the perfused pancreas are less regular than the in vivo pulses when analyzed by autocorrelation (20).

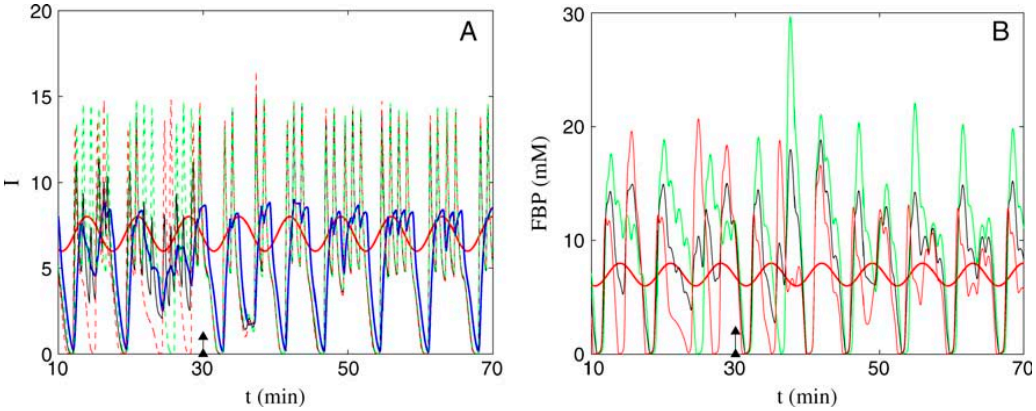


FIGURE 8 Two cells are entrainable to a stimulus with a larger period when coupled. Parameters as in Fig. 4, except $g_c$ is raised from 0 pS to 100 pS at $t = 30$ min (*arrow*). The glucose concentration (*sinusoidal red curves*) oscillates with a period of 7 min and amplitude of 1 mM. (*A*) Entrainment of insulin secretion. Red is the faster non-entrainable cell, green is the slower entrainable cell, and black is the average insulin secretion $\bar{I}$ from the two cells. The blue curve is the 1-min moving average of $\bar{I}$. (*B*) Entrainment of glycolysis. The color scheme is the same as in *A*.

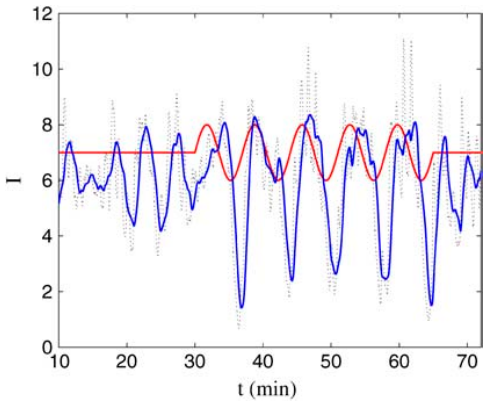


FIGURE 9 A population of 20 islets becomes synchronized by an oscillatory glucose stimulus, resulting in pulsatile insulin secretion. The figure shows the insulin secretion averaged over the 20 islets (*dotted black line*), the average insulin secretion smoothed using a 1-min moving average (*blue*), and the glucose concentration (*red*), which is either constant or oscillatory with a period of 7 min and an amplitude of 1 mM. $V_{gk,\,i}$, $i = 1, \ldots,$ 20 are randomly chosen from a uniform distribution over [0.6, 0.9] mM/ms.

## DISCUSSION

The role of the glycolytic oscillator could be to add a component slower than that driving bursting so that $\beta$-cells are capable of resonating with a feedback signal (glucose) from the body. The timescale of insulin signaling in the liver is on the order of 5–15 min (12–14,60,61), and the sensitivity of the liver to pulsatile insulin is frequency-dependent (14), which indicates that, for optimal functioning, the $\beta$-cells would need a system sensing as well as secreting on the timescale of insulin signaling. The glycolytic pathway is ideal for sensing glucose feedback, since glucose is a substrate for glycolysis. Furthermore, the period of the glycolytic oscillator is relatively insensitive to changes in plasma glucose concentration (Fig. 3). This frequency-insensitivity is consistent with studies that have shown that it is primarily the amplitude of the pulsatile insulin secretion, rather than the period, that is affected by changes in the glucose concentration (3,23,35,58,59).

In this scenario, the glycolytic oscillator produces insulin pulses with a period of 5 min, which is of the ideal timescale for optimal insulin sensitivity in the liver. The liver responds to the insulin pulses so that the plasma glucose concentration oscillates, which then entrains the population of islets, in this way regularizing and amplifying the insulin release pattern (Figs. 10 and 11). For this to work, the entrainability of each islet is crucial. The model presented here can be entrained by both faster and slower glucose oscillations (Fig. 6), and this mechanism indeed synchronizes the insulin pulses from uncoupled islets (Fig. 9).

**TABLE 2 Parameter values defining the response of plasma glucose, $G_e$, to the average insulin secretion $\bar{I}$**

| | | | | |
|---|---|---|---|---|
| $G_{min} = 1$ mM | $G_{max} = 15$ mM | $\tau_G = 450{,}000$ ms | $S_G = 1$ | $\hat{I} = 5$ |

In contrast, it has been suggested that an intrapancreatic, neuronal pacemaker is responsible for synchronizing the pulsatile insulin secretion from the many islets in the pancreas (3,19,25). However, as mentioned, and studied previously (2,24,39), this would not explain how single islets or groups of islets can be entrained. If a pancreatic pacemaker was solely responsible for the entrainment, then this effect would be lost when the islets were separated from the pancreas. Furthermore, in Sha et al. (25) pulsatile insulin secretion was observed from a piece of the pancreas, even though the intrapancreatic ganglion nerves were electrically silent, showing that neuronal activity is not essential for at least some degree of synchrony and pulsatile release. We showed that the entrainability of each cell, and hence each islet, is sufficient to provide the synchronization mechanism (Figs. 10 and 11). However, it cannot be ruled out that a neuronal pacemaker mechanism enhances this effect in vivo. Indeed, pulsatile insulin secretion has been observed in conditions of constant glucose (19,35), arguing for a role of a neuronal pacemaker.

The first step toward a pulsatile signal from the pancreas is the pulsatile secretion from the individual islets. Fig. 4 showed that electrical coupling of the cells through gap junctions is enough to synchronize not only the membrane potential, intracellular calcium, and insulin secretion, but the glycolytic oscillations as well. Two essential elements for synchronization in our model are the feedback of $Ca^{2+}$ onto the mitochondria (Fig. 5) and the feedback of AMP and ATP onto PFK. Without these feedback pathways the membrane potential, which is coupled to the membrane potential of neighboring cells through gap junctions, could not be communicated to the glycolytic subsystem, and it would not be possible for electrical coupling to synchronize glycolytic oscillations. Our simulations showed that if glycolysis is not synchronized, there is less insulin secretion (Figs. 4 and 5). The positive effects of glycolytic synchronization would be accentuated by any K(ATP)-independent glucose pathway (45), since amplifying signals would plausibly be in phase with the glycolytic oscillator. If the calcium levels in different cells were in synchrony, but the glycolytic components were not, then the amplifying signals would not be synchronized, and thus would not have maximal effect. Finally, we do not count out the possibility that synchronization of glycolytic oscillations could be aided by the diffusion through gap junctions of glycolytic intermediates, ATP, or other signaling molecules.

It was demonstrated in Fig. 4 that gap-junctional coupling between cells leads to a pulsatile secretion with a period close to that of the fastest of the cells. Moreover, this coupling enhances the entrainability of the islets to plasma glucose feedback (Fig. 8). This shows an advantage of having the cells clustered into islets and not scattered around in the pancreas as single cells.

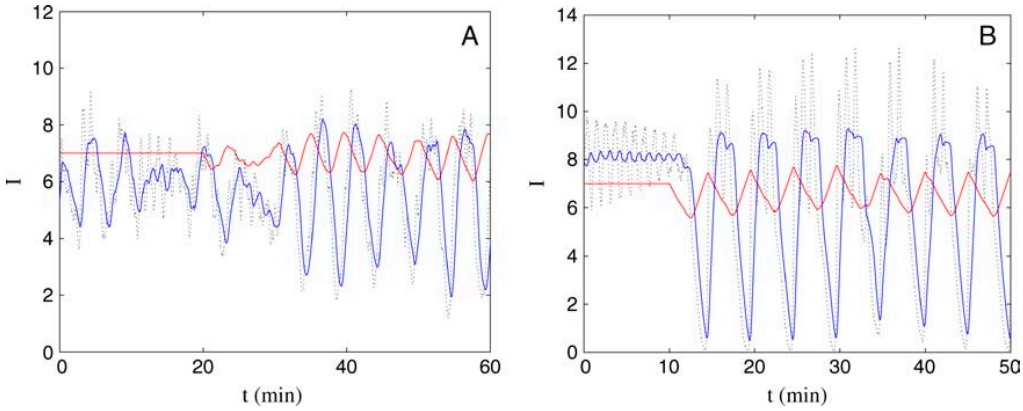


FIGURE 10 (*A*) 20 islets become synchronized when coupled through the plasma glucose concentration. The value $G_e$ is dynamic from $t = 20$ min. Legends and $V_{gk,\,i}$ as in Fig. 9. (*B*) Islets without pulsatile secretion can become pulsatile when coupled through the plasma glucose concentration. The value $G_e$ is dynamic from $t = 10$ min. $V_{gk,\,i} = 0.85 + 0.02i$ mM/ms, $i = 1, \ldots, 9$.

The present model can undergo 2:1 entrainment, meaning that for each period of the glucose oscillations we have two pulses of insulin release (simulations not shown). The 2:1 entrainment is a general phenomenon of forced oscillatory systems and is also observed for ultradian oscillations (34). Such 2:1 entrainment was recently observed for entrainment of NAD(P)H, $Ca^{2+}$, and mitochondrial membrane potential oscillations (32). It was also observed in an in vivo study with human patients (29). We will continue the investigation of various kinds of entrainment in a future article.

We have previously proposed ''the metronome model'' for insulin secretion (6). The idea is that, whereas the glycolytic component is responsible for setting the period of the insulin pulses (the metronome), the electrical component is responsible for the pulse mass (the amplitude of the beat of the metronome). Although the period of the metronome is relatively insensitive to the glucose level, the amplitude is highly sensitive, and is adjusted by modulating the plateau fraction of bursting in response to changes in the glucose level. The K(ATP)-independent, amplifying pathway could further accentuate the effects of glucose on the pulse amplitude. This model provides a way for the $\beta$-cells to meet two demands: matching the frequency to the timescale of the target issues and being able to adjust the insulin secretion level to match the demands of the body. It also gives a *raison d'être* for both the glycolytic oscillator and for the electrical bursting behavior. We have shown here that the metronome model is consistent with the experimental findings that $\beta$-cells are synchronized within an islet, that islets can be entrained by sinusoidal glucose oscillations, and that insulin secretion is oscillatory in vivo.

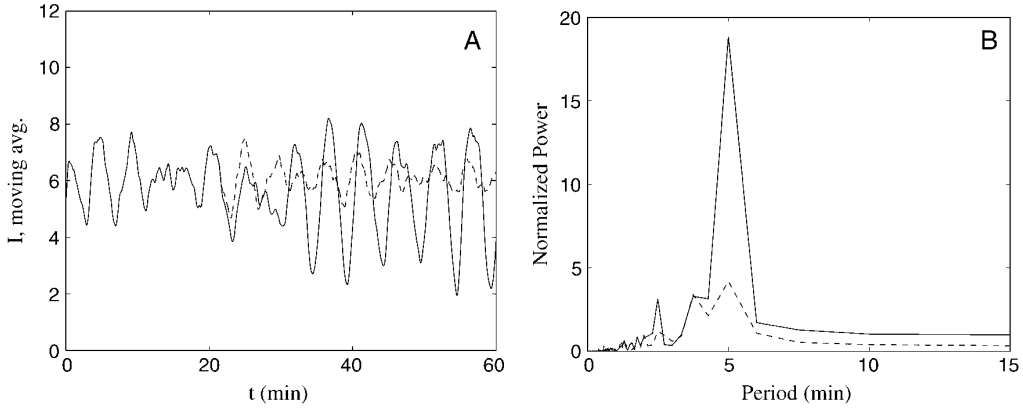


FIGURE 11 (*A*) The smoothed insulin signal from Fig. 10 *A* (*blue curve*) is compared to the smoothed insulin signal when the glucose concentration remains fixed (*black dashed curve*). (*B*) The normalized power spectra of the two signals from the last 30 min (*t* from 30 to 60 min) of *A* with dynamic (*blue curve*) or fixed (*black dashed curve*) glucose concentration.

M.G.P. thanks the Laboratory of Biological Modeling, National Institute of Diabetes and Digestive and Kidney Diseases, National Institutes of Health, for letting him visit the lab, where this work was initiated.

M.G.P. was partially supported by ''Rejselegat for Matematikere'' (Travelling Scholarship for Mathematicians). R.B. was supported by National Science Foundation grant No. DMS-0311856.

## REFERENCES

1. Chou, H. F., and E. Ipp. 1990. Pulsatile insulin secretion in isolated Rat islets. *Diabetes.* 39:112–117.
2. Sturis, J., W. L. Pugh, J. Tang, D. M. Ostrega, J. S. Polonsky, and K. S. Polonsky. 1994. Alterations in pulsatile insulin secretion in the Zucker diabetic fatty rat. *Am. J. Physiol. Endocrinol. Metab.* 267:E250–E259.
3. Pørksen, N. 2002. The in vivo regulation of pulsatile insulin secretion. *Diabetologia.* 45:3–20.
4. Longo, E. A., K. Tornheim, J. T. Deeney, B. A. Varnum, D. Tillotson, M. Prentki, and B. E. Corkey. 1991. Oscillations in cytosolic free $Ca^{2+}$, oxygen consumption, and insulin secretion in glucose-stimulated Rat pancreatic islets. *J. Biol. Chem.* 266:9314–9319.
5. Tornheim, K. 1997. Are metabolic oscillations responsible for normal oscillatory insulin secretion? *Diabetes.* 46:1375–1380.
6. Bertram, R., L. Satin, M. Zhang, P. Smolen, and A. Sherman. 2004. Calcium and glycolysis mediate multiple bursting modes in pancreatic islets. *Biophys. J.* 87:3074–3087.
7. Lang, D. A., D. R. Matthews, M. Burnet, and R. C. Turner. 1981. Brief, irregular oscillations of basal plasma insulin and glucose concentrations in diabetic man. *Diabetes.* 30:435–439.
8. O'Rahilly, S., R. C. Turner, and D. R. Matthews. 1988. Impaired pulsatile secretion of insulin in relatives of patients with non-insulin-dependent diabetes. *N. Engl. J. Med.* 318:1225–1230.
9. Schmitz, O., N. Pørksen, B. Nyholm, C. Skjærbæk, P. C. Butler, J. D. Veldhuis, and S. M. Pincus. 1997. Disorderly and nonstationary insulin secretion in relatives of patients with NIDDM. *Am. J. Physiol. Endocrinol. Metab.* 272:E218–E226.
10. Ravier, M. A., J. Sehlin, and J. C. Henquin. 2002. Disorganization of cytoplasmic $Ca^{2+}$ oscillations and pulsatile insulin secretion in islets from ob/ob mice. *Diabetologia.* 45:1154–1163.
11. Matthews, D. R., B. A. Naylor, R. G. Jones, G. M. Ward, and R. C. Turner. 1983. Pulsatile insulin has greater hypoglycemic effect than continuous delivery. *Diabetes.* 32:617–621.
12. Bratusch-Marrain, P. R., M. Komjati, and W. K. Waldhausl. 1986. Efficacy of pulsatile versus continuous insulin administration on hepatic glucose production and glucose utilization in type I diabetic humans. *Diabetes.* 35:922–926.
13. Komjati, M., P. Bratusch-Marrain, and W. Waldhausl. 1986. Superior efficacy of pulsatile versus continuous hormone exposure on hepatic glucose production in vitro. *Endocrinology.* 118:312–319.
14. Paolisso, G., A. J. Scheen, D. Giugliano, S. Sgambato, A. Albert, M. Varricchio, F. D'Onofrio, and P. J. Lefebvre. 1991. Pulsatile insulin delivery has greater metabolic effects than continuous hormone administration in man: importance of pulse frequency. *J. Clin. Endocrinol. Metab.* 72:607–615.
15. Ashcroft, F. M., and P. Rorsman. 1989. Electrophysiology of the pancreatic $\beta$-cell. *Prog. Biophys. Mol. Biol.* 54:87–143.
16. Cook, D. L. 1983. Isolated islets of Langerhans have slow oscillations of electrical activity. *Metabolism.* 32:681–685.
17. Henquin, J. C., H. P. Meissner, and W. Schmeer. 1982. Cyclic variations of glucose-induced electrical activity in pancreatic B cells. *Pflugers Arch.* 393:322–327.
18. Zhang, M., P. Goforth, R. Bertram, A. Sherman, and L. Satin. 2003. The $Ca^{2+}$ dynamics of isolated Mouse $\beta$-cells and islets: implications for mathematical models. *Biophys. J.* 84:2852–2870.
19. Stagner, J. I., E. Samols, and G. C. Weir. 1980. Sustained oscillations of insulin, glucagon, and somatostatin from the isolated canine pancreas during exposure to a constant glucose concentration. *J. Clin. Invest.* 65:939–942.
20. Goodner, C. J., D. J. Koerker, J. I. Stagner, and E. Samols. 1991. In vitro pancreatic hormonal pulses are less regular and more frequent than in vivo. *Am. J. Physiol. Endocrinol. Metab.* 260:E422–E429.
21. Gilon, P., M. A. Ravier, J. C. Jonas, and J. C. Henquin. 2002. Control mechanisms of the oscillations of insulin secretion in vitro and in vivo. *Diabetes.* 51:S144–S151.
22. Westerlund, J., and P. Bergsten. 2001. Glucose metabolism and pulsatile insulin release from isolated islets. *Diabetes.* 50:1785–1790.
23. Ritzel, R. A., J. D. Veldhuis, and P. C. Butler. 2003. Glucose stimulates pulsatile insulin secretion from human pancreatic islets by increasing secretory burst mass: dose-response relationships. *J. Clin. Endocrinol. Metab.* 88:742–747.
24. Berman, N., H. F. Chou, A. Berman, and E. Ipp. 1993. A mathematical model of oscillatory insulin secretion. *Am. J. Physiol.* 264:R839–R851.
25. Sha, L., J. Westerlund, J. H. Szurszewski, and P. Bergsten. 2001. Amplitude modulation of pulsatile insulin secretion by intrapancreatic ganglion neurons. *Diabetes.* 50:51–55.
26. Lang, D. A., D. R. Matthews, J. Peto, and R. C. Turner. 1979. Cyclic oscillations of basal plasma glucose and insulin concentrations in human beings. *N. Engl. J. Med.* 301:1023–1027.
27. Goodner, C. J., F. G. Hom, and D. J. Koerker. 1982. Hepatic glucose production oscillates in synchrony with the islet secretory cycle in fasting rhesus monkeys. *Science.* 215:1257–1260.
28. Sturis, J., N. M. O'Meara, E. T. Shapiro, J. D. Blackman, H. Tillil, K. S. Polonsky, and E. Van Cauter. 1993. Differential effects of glucose stimulation upon rapid pulses and ultradian oscillations of insulin secretion. *J. Clin. Endocrinol. Metab.* 76:895–901.
29. Mao, C. S., N. Berman, K. Roberts, and E. Ipp. 1999. Glucose entrainment of high-frequency plasma insulin oscillations in control and type 2 diabetic subjects. *Diabetes.* 48:714–721.
30. Pørksen, N., C. Juhl, M. Hollingdal, S. M. Pincus, J. Sturis, J. D. Veldhuis, and O. Schmitz. 2000. Concordant induction of rapid in vivo pulsatile insulin secretion by recurrent punctuated glucose infusions. *Am. J. Physiol. Endocrinol. Metab.* 278:E162–E170.
31. Sturis, J., E. Van Cauter, J. D. Blackman, and K. S. Polonsky. 1991. Entrainment of pulsatile insulin secretion by oscillatory glucose infusion. *J. Clin. Invest.* 87:439–445.
32. Luciani, D. S. 2004. Oscillations of cytosolic $Ca^{2+}$ and metabolism studied in murine pancreatic islets. Ph.D. thesis. Department of Physics, The Technical University of Denmark, Kgs. Lyngby, Denmark.
33. Hollingdal, M., C. B. Juhl, S. M. Pincus, J. Sturis, J. D. Veldhuis, K. S. Polonsky, N. Pørksen, and O. Schmitz. 2000. Failure of physiological plasma glucose excursions to entrain high-frequency pulsatile insulin secretion in type 2 diabetes. *Diabetes.* 49:1334–1340.
34. Sturis, J., C. Knudsen, N. M. O'Meara, J. S. Thomsen, E. Mosekilde, E. Van Cauter, and K. S. Polonsky. 1995. Phase-locking regions in a forced model of slow insulin and glucose oscillations. *Chaos.* 5:193–199.
35. Song, H. S., S. S. McIntyre, H. Shah, J. D. Veldhuis, P. C. Hayes, and P. C. Butler. 2000. Direct measurement of pulsatile insulin secretion from the portal vein in human subjects. *J. Clin. Endocrinol. Metab.* 85:4491–4499.
36. Bertram, R., and A. Sherman. 2004. A calcium-based phantom bursting model for pancreatic islets. *Bull. Math. Biol.* 66:1313–1344.
37. Smolen, P. 1995. A model for glycolytic oscillations based on skeletal muscle phosphofructokinase kinetics. *J. Theor. Biol.* 174:137–148.
38. Westermark, P. O., and A. Lansner. 2003. A model of phosphofructokinase and glycolytic oscillations in the pancreatic $\beta$-cell. *Biophys. J.* 85:126–139.
39. Maki, L. W., and J. Keizer. 1995. Analysis of possible mechanisms for in vitro oscillations of insulin secretion. *Am. J. Physiol. Cell Physiol.* 268:C780–C791.

40. Matschinsky, F. M., B. Glaser, and M. A. Magnuson. 1998. Pancreatic $\beta$-cell glucokinase: closing the gap between theoretical concepts and experimental realities. *Diabetes*. 47:307–315.

41. Magnus, G., and J. Keizer. 1998. Model of $\beta$-cell mitochondrial calcium handling and electrical activity. I. Cytoplasmic variables. *Am. J. Physiol. Cell Physiol.* 274:C1158–C1173.

42. Keizer, J., and G. Magnus. 1989. ATP-sensitive potassium channel and bursting in the pancreatic $\beta$-cell. A theoretical study. *Biophys. J.* 56: 229–242.

43. Bertram, R., J. Previte, A. Sherman, T. A. Kinard, and L. S. Satin. 2000. The phantom burster model for pancreatic $\beta$-cells. *Biophys. J.* 79:2880–2892.

44. Jonas, J. C., P. Gilon, and J. C. Henquin. 1998. Temporal and quantitative correlation between insulin secretion and stably elevated or oscillatory cytoplasmic $Ca^{2+}$ in Mouse pancreatic $\beta$-cells. *Diabetes.* 47:1266–1273.

45. Henquin, J. C. 2000. Triggering and amplifying pathways of regulation of insulin secretion by glucose. *Diabetes*. 49:1751–1760.

46. Prentki, M., and F. M. Matschinsky. 1987. $Ca^{2+}$, cAMP, and phospholipid-derived messengers in coupling mechanisms of insulin secretion. *Physiol. Rev.* 67:1185–1248.

47. Ermentrout, G. B. 2002. Simulating, Analyzing, and Animating Dynamical Systems: A Guide to XPPAUT for Researchers and Students. SIAM Books, Philadelphia, PA.

48. Meissner, H. P. 1976. Electrophysiological evidence for coupling between $\beta$-cells of pancreatic islets. *Nature*. 262:502–504.

49. Eddlestone, G. T., A. Goncalves, and J. A. Bangham. 1984. Electrical coupling between cells in islets of Langerhans from Mouse. *J. Membr. Biol.* 77:1–14.

50. Santos, R. M., L. M. Rosario, A. Nadal, J. Garcia-Sancho, B. Soria, and M. Valdeolmillos. 1991. Widespread synchronous $[Ca^{2+}]_i$ oscillations due to bursting electrical activity in single pancreatic islets. *Pflugers Arch.* 418:417–422.

51. Valdeolmillos, M., A. Gomis, and J. V. Sanchez-Andres. 1996. In vivo synchronous membrane potential oscillations in Mouse pancreatic $\beta$-cells: lack of co-ordination between islets. *J. Physiol.* 493:9–18.

52. Jung, S. K., L. M. Kauri, W. J. Qian, and R. T. Kennedy. 2000. Correlated oscillations in glucose consumption, oxygen consumption, and intracellular free $Ca^{2+}$ in single islets of Langerhans. *J. Biol. Chem.* 275:6642–6650.

53. Sherman, A., and J. Rinzel. 1991. Model for synchronization of pancreatic $\beta$-cells by gap junction coupling. *Biophys. J.* 59:547–559.

54. Sturis, J., K. S. Polonsky, E. Mosekilde, and E. Van Cauter. 1991. Computer model for mechanisms underlying ultradian oscillations of insulin and glucose. *Am. J. Physiol.* 260:E801–E809.

55. Barbosa, R. M., A. M. Silva, A. R. Tomé, J. A. Stamford, R. M. Santos, and L. M. Rosário. 1996. Real time electrochemical detection of 5-HT/insulin secretion from single pancreatic islets: effect of glucose and $K^+$ depolarization. *Biochem. Biophys. Res. Commun.* 228:100–104.

56. Barbosa, R. M., A. M. Silva, A. R. Tomé, J. A. Stamford, R. M. Santos, and L. M. Rosário. 1998. Control of pulsatile 5-HT/insulin secretion from single mouse pancreatic islets by intracellular calcium dynamics. *J. Physiol.* 510:135–143.

57. Pørksen, N., B. Nyholm, J. D. Veldhuis, P. C. Butler, and O. Schmitz. 1997. In humans at least 75% of insulin secretion arises from punctuated insulin secretory bursts. *Am. J. Physiol. Endocrinol. Metab.* 273:E908–E914.

58. Pørksen, N., T. Grofte, J. Greisen, A. Mengel, C. Juhl, J. D. Veldhuis, O. Schmitz, M. Rossle, and H. Vilstrup. 2002. Human insulin release processes measured by intraportal sampling. *Am. J. Physiol. Endocrinol. Metab.* 282:E695–E702.

59. Song, S. H., L. Kjems, R. Ritze, S. M. McIntyre, M. L. Johnson, J. D. Veldhuis, and P. C. Butler. 2002. Pulsatile insulin secretion by human pancreatic islets. *J. Clin. Endocrinol. Metab.* 87:213–221.

60. Goodner, C. J., I. R. Sweet, and H. C. Harrison, Jr. 1988. Rapid reduction and return of surface insulin receptors after exposure to brief pulses of insulin in perfused Rat hepatocytes. *Diabetes*. 37:1316–1323.

61. Sedaghat, A. R., A. Sherman, and M. J. Quon. 2002. A mathematical model of metabolic insulin signaling pathways. *Am. J. Physiol. Endocrinol. Metab.* 283:E1084–E1101.

# *Paper V*

# The Total Quasi-Steady-State Approximation for Fully Competitive Enzyme Reactions

Morten Gram Pedersen *

*Department of Mathematics, Technical University of Denmark, Kgs. Lyngby, Denmark*

Alberto M. Bersani

*Department of Mathematical Methods and Models, "La Sapienza" University, Rome, Italy*

Enrico Bersani

*ISMAC Genova, Genova, Italy*

**Abstract**

The validity of the Michaelis-Menten-Briggs-Haldane approximation for single enzyme reactions has recently been improved by the formalism of the total quasi-steady-state approximation. This approach is here extended to fully competitive systems, and a criterion for its validity is provided. We show that it extends the Michaelis-Menten-Briggs-Haldane approximation for such systems for a wide range of parameters very convincingly, and investigate special cases. It is demonstrated that our method is at least roughly valid in the case of identical affinities. The results presented should be useful for numerical simulations of many *in vivo* reactions.

*Key words:* Michaelis-Menten kinetics, competitive substrates, substrate-inhibitor system, quasi-steady-state assumption.

## 1 Introduction

Biochemistry in general and enzyme kinetics in particular have been heavily influenced by the model of biochemical reactions set forth by Henri (1901a,b, 1902) and

* Corresponding author. Address: Department of Mathematics, Technical University of Denmark, Matematiktorvet, Building 303, DK-2800 Kgs. Lyngby, Denmark, Fax (+45) 4588 1399.

*Email addresses:* m.g.pedersen@mat.dtu.dk (Morten Gram Pedersen), bersani@dmmm.uniroma1.it (Alberto M. Bersani), enrico.bersani@gmail.com (Enrico Bersani).

Michaelis and Menten (1913), and further developed by Briggs and Haldane (1925). This formulation considers a reaction where a substrate $S$ binds reversibly to an enzyme $E$ to form a complex $C$. The complex can decay irreversibly to a product $P$ and the enzyme, which is then free to bind another substrate molecule. This is summarized in the scheme

$$E + S \underset{k_{-1}}{\overset{k_1}{\rightleftarrows}} C \xrightarrow{k_2} E + P, \tag{1}$$

where $k_1, k_{-1}$ and $k_2$ are kinetic parameters (supposed constant) associated with the reaction rates.

Assuming that the complex concentration is approximately constant after a short transient phase leads to the usual Briggs-Haldane approximation (or *standard quasi-steady-state assumption* or *approximation* (standard QSSA, sQSSA)), which is valid when the enzyme concentration is much lower than either the substrate concentration or the Michaelis constant $K_M$ (Segel, 1988). This is usually fulfilled for *in vitro* experiments, but sometimes breaks down *in vivo* (Straus and Goldstein, 1943; Sols and Marco, 1970; Albe et al., 1990). See Schnell and Maini (2003) for a nice and complete review of the kinetics and approximations of scheme (1).

The advantage of a quasi-steady-state approximation is that it reduces the dimensionality of the system, and thus speeds up numerical simulations greatly, especially for large networks as found *in vivo*. Moreover, while the kinetic constants in (1) are usually not known, finding the kinetic parameters characterizing the sQSSA is a standard procedure in *in vitro* biochemistry (Bisswanger, 2002). However, to simulate physiologically realistic *in vivo* scenarios, one faces the problem that the sQSSA might be invalid as mentioned above. Hence, even if the kinetic constants such as $K_M$ are identical *in vivo* and *in vitro*, they need to be implemented in some other approximation which must be valid for the whole system and initial concentrations under investigation.

Approximations such as the *reverse QSSA* (rQSSA) (Segel and Slemrod, 1989; Schnell and Maini, 2000), which is valid for high enzyme concentrations, and the *total QSSA* (tQSSA) (Borghans et al., 1996; Tzafriri, 2003), which is valid for a broader range of parameters covering both high and low enzyme concentrations, have been introduced in the last two decades. Curiously, the rQSSA is equivalent to the *rapid-equilibrium approximation* proposed by Michaelis and Menten (1913), although their names are often connected to the sQSSA introduced by Briggs and Haldane (1925).

Tzafriri (2003) showed that the tQSSA is at least roughly valid for any set of parameters. Also, the tQSSA for reversible reactions has been studied (Tzafriri and Edelman, 2004), i.e. reactions of form (1), but where enzyme and product can recombine to form the complex.

These newer approximations have so far only been found for isolated reactions. However, *in vivo* the reactions are coupled in complex networks or cascades of intermediate, second messengers with successive reactions, competition between substrates, feedback loops etc. Approximations of such scenarios have been carried out within the sQSSA scheme (Bisswanger, 2002), but often without a thorough

investigation of the validity of the approximations. An exception is the case of fully competitive reactions (Segel, 1988; Schnell and Mendoza, 2000), i.e., reactions with competing substrates, also known as substrate-inhibitor systems,

$$\begin{aligned} S_1 + E &\underset{k_{-1}^{(1)}}{\overset{k_1^{(1)}}{\rightleftarrows}} C_1 \xrightarrow{k_2^{(1)}} E + P_1, \\ S_2 + E &\underset{k_{-1}^{(2)}}{\overset{k_1^{(2)}}{\rightleftarrows}} C_2 \xrightarrow{k_2^{(2)}} E + P_2, \end{aligned} \tag{2}$$

where $S_i, C_i$ and $P_i$ represent substrate, enzyme-substrate complex and product $i = 1, 2$, respectively. However, since the sQSSA cannot be expected to be valid *in vivo*, employing the tQSSA to these more complex situations would be beneficial.

This paper investigates the tQSSA for fully competitive reactions and is organized as follows. In Section 2 we recall the most important results in terms of quasi-steady-state approximations for a single reaction and for a fully competitive system. In Section 3 we introduce the tQSSA for a fully competitive system, discuss the timescales of the reactions and introduce a sufficient condition for the validity of the tQSSA. Moreover, the form of the concentrations of the complexes $C_i$ in the quasi-steady-state phase is investigated. In Section 4 we study the special case of identical affinities ($K_M^{(1)} \approx K_M^{(2)}$). The first order approximation is obtained in terms of a perturbation parameter $r$, related to the characteristic constants of the system. Finally, a closed form solution for the total substrate concentrations is obtained in this special case. In Section 5 the situation of very different affinities, for example reflecting a slow or fast competitive inhibitor, is studied. The corresponding approximations for the concentrations of $C_i$ are found and used to obtain a general first order approximation to the tQSSA for fully competitive reactions for any choice of $K_M^{(i)}$, by means of Padé approximant techniques. In Section 6 we show numerically that for a very large range of parameters our tQSSA provides excellent fitting to the solutions of the full system, better than the sQSSA and the single reaction tQSSA, and we discuss the obtained results.

## 2 Theoretical background

We recall briefly the mathematical description of the sQSSA for (1), using the same symbols for the concentrations of the reactants. The reaction (1) can be described by a system of two nonlinear ordinary differential equations. Assuming that the complex is in a quasi-steady-state leads to (Briggs and Haldane, 1925; Segel, 1988; Segel and Slemrod, 1989)

$$\frac{d\,S}{dt} \approx -\frac{V_{max} S}{K_M + S}, \quad S(0) = S_0, \tag{3}$$

Here $V_{max} = k_2\, E_0 = k_2\, E(0)$ is the maximal reaction rate and $K_M = \frac{k_{-1}+k_2}{k_1}$ is the Michaelis constant, identifying the substrate concentration giving the half-max

reaction rate, i.e., $K_M$ reflects the substrate affinity of the enzyme. This approximation is valid whenever (Segel, 1988; Segel and Slemrod, 1989)

$$\frac{E_0}{K_M + S_0} \ll 1, \tag{4}$$

i.e., when the enzyme concentration is low with respect to either the Michaelis constant or to the substrate concentration.

The tQSSA (Borghans et al., 1996; Tzafriri, 2003) arises by changing to the total substrate originally introduced by Straus and Goldstein (1943) $\bar{S} = S + C$. Assuming that the complex is in a quasi-steady-state yields the tQSSA

$$\frac{d\,\bar{S}}{dt} \approx -k_2\, C_-(\bar{S}), \quad \bar{S}(0) = S_0, \tag{5}$$

where

$$C_-(\bar{S}) = \frac{(E_0 + K_M + \bar{S}) - \sqrt{(E_0 + K_M + \bar{S})^2 - 4E_0\bar{S}}}{2}. \tag{6}$$

Tzafriri (2003) showed that the tQSSA is valid whenever

$$\epsilon_{Tz} := \frac{K}{2S_0}\left(\frac{E_0 + K_M + S_0}{\sqrt{(E_0 + K_M + S_0)^2 - 4E_0S_0}} - 1\right) \ll 1, \qquad K = \frac{k_2}{k_1}, \tag{7}$$

and that this is always roughly valid in the sense that

$$\epsilon_{Tz} \leq \frac{K}{4K_M} \leq \frac{1}{4}. \tag{8}$$

The parameter $K$ is known as the Van Slyke-Cullen constant. Tzafriri (2003) found

$$\frac{d\,\bar{S}}{dt} \approx -\frac{V_{max}\bar{S}}{K_M + E_0 + \bar{S}}, \quad \bar{S}(0) = S_0, \tag{9}$$

as a first order approximation to (5). This expression (9) is identical to the formula obtained by Borghans et al. (1996) by means of a two point Padé approximant technique (Baker, 1975), and it is valid at low enzyme concentrations (4) where it reduces to the sQSSA expression (3), but holds moreover at low substrate concentrations $S_0 \ll E_0 + K_M$ (Tzafriri, 2003). We wish to highlight the fundamental fact that performing the substitutions of $S$ by $\bar{S}$ and of $K_M$ by $K_M + E_0$ one obtains a significantly improved sQSSA-like approximation with minimal effort.

The system (2) under investigation in this paper is governed by the coupled ODEs (Rubinow and Lebowitz, 1970; Segel, 1988; Schnell and Mendoza, 2000), $i = 1, 2$,

$$\frac{d\,S_i}{dt} = -k_1^{(i)} E \cdot S_i + k_{-1}^{(i)} C_i, \qquad S_i(0) = S_{i,0}, \tag{10a}$$

$$\frac{d\,C_i}{dt} = k_1^{(i)}(E \cdot S_i - K_M^{(i)} C_i), \qquad C_i(0) = 0, \qquad K_M^{(i)} = \frac{k_{-1}^{(i)} + k_2^{(i)}}{k_1^{(i)}}. \tag{10b}$$

and the conservation laws

$$S_{i,0} = S_i + C_i + P_i, \qquad i = 1, 2, \tag{11}$$
$$E_0 = E + C_1 + C_2. \tag{12}$$

The sQSSA of this system is (Rubinow and Lebowitz, 1970; Segel, 1988)

$$\frac{d\,S_i}{dt} = -\frac{k_2^{(i)} E_0 S_i}{K_M^{(i)}(1 + S_j/K_M^{(j)}) + S_i}\,, \quad S_i(0) = S_{i,0}, \qquad i = 1, 2, \quad j \neq i, \tag{13}$$

which is valid when (Schnell and Mendoza, 2000)

$$\frac{E_0}{K_M^{(i)}(1 + S_{j,0}/K_M^{(j)}) + S_{i,0}} \ll 1\,, \qquad i = 1, 2, \quad j \neq i. \tag{14}$$

Rubinow and Lebowitz (1970) showed that the equations (13), $i = 1, 2$, can be uncoupled when introducing the parameter

$$\delta = \frac{k_2^{(1)} K_M^{(2)}}{k_2^{(2)} K_M^{(1)}},$$

which produces a measure of the competition. This parameter enters when dividing (13) for $i = 1$ with (13) for $i = 2$ and solving, which yields $S_1/S_{1,0} = (S_2/S_{2,0})^{\delta}$. The equations (13), $i = 1, 2$, then become

$$\frac{d\,\bar{S}_1}{dt} \approx -\frac{k_2^{(1)} E_0 \bar{S}_1}{K_M^{(1)}(1 + S_{2,0}(\bar{S}_1/S_{1,0})^{1/\delta}/K_M^{(2)}) + S_1}, \qquad \bar{S}_1(0) = S_{1,0}, \tag{15a}$$
$$\frac{d\,\bar{S}_2}{dt} \approx -\frac{k_2^{(2)} E_0 \bar{S}_2}{K_M^{(2)}(1 + S_{1,0}(\bar{S}_2/S_{2,0})^{\delta}/K_M^{(1)}) + S_2}, \qquad \bar{S}_2(0) = S_{2,0}. \tag{15b}$$

These expressions were used by Schnell and Mendoza (2000) to find analytic, closed form solutions for the cases $\delta \approx 1$ and $\delta \ll 1$ using the so-called Lambert $W$-function.

## 3 Total quasi-steady-state approximation of the competitive system

Following Borghans et al. (1996), we introduce the total substrates

$$\bar{S}_i = S_i + C_i, \qquad i = 1, 2, \tag{16}$$

and rewrite equations (10) in terms of these, obtaining the system of ODEs, $i = 1, 2$,

$$\frac{d\,\bar{S}_i}{dt} = -k_2^{(i)}\, C_i, \qquad \bar{S}_i(0) = S_{i,0}, \tag{17a}$$
$$\frac{d\,C_i}{dt} = k_1^{(i)}\Big((E_0 - C_1 - C_2) \cdot (\bar{S}_i - C_i) - K_M^{(i)} C_i\Big), \qquad C_i(0) = 0. \tag{17b}$$

We require $0 < C_i < \bar{S}_i$, $i = 1, 2$, because of (16), and apply the quasi-steady-state assumption (Borghans et al., 1996; Tzafriri, 2003),

$$\frac{d\,C_i}{dt} \approx 0, \qquad i = 1, 2,$$

which is equivalent to the system

$$C_1 = E_0 - C_2\Big(1 + \frac{K_M^{(2)}}{\bar{S}_2 - C_2}\Big), \tag{18a}$$

$$C_2 = E_0 - C_1\Big(1 + \frac{K_M^{(1)}}{\bar{S}_1 - C_1}\Big), \tag{18b}$$

which should hold for any time $t$ after the initial transient. From this system, it follows that $C_i < E_0$, $i = 1, 2$, in agreement with (12). As shown in Appendix A, the system (18) has a unique solution with $0 < C_i < \min\{\bar{S}_i, E_0\}$. For $C_1$ it is given by finding the appropriate root of the third degree polynomial

$$\begin{aligned}\psi_1(C_1) = &-(K_M^{(1)} - K_M^{(2)})C_1^3 \\ &+ \Big[(E_0 + K_M^{(1)} + \bar{S}_1)(K_M^{(1)} - K_M^{(2)}) - (\bar{S}_1 K_M^{(2)} + \bar{S}_2 K_M^{(1)})\Big]C_1^2 \\ &+ \Big[ - E_0(K_M^{(1)} - K_M^{(2)}) + (\bar{S}_1 K_M^{(2)} + \bar{S}_2 K_M^{(1)}) + K_M^{(2)}(E_0 + K_M^{(1)})\Big]\bar{S}_1 C_1 \\ &- E_0 K_M^{(2)} \bar{S}_1^2.\end{aligned} \tag{19}$$

When $K_M^{(1)} = K_M^{(2)} = K_M$, $\psi_1$ becomes a second degree polynomial, and the root is given by

$$C_1 = \frac{\bar{S}_1(\bar{S}_1 + \bar{S}_2 + K_M + E_0)}{2(\bar{S}_1 + \bar{S}_2)}\left(1 - \sqrt{1 - \frac{4E_0(\bar{S}_1 + \bar{S}_2)}{(\bar{S}_1 + \bar{S}_2 + K_M + E_0)^2}}\right). \tag{20}$$

An analogous polynomial $\psi_2$ for $C_2$ can be found by interchanging the indexes 1 and 2 in (19), because of the symmetry of the system (17), and $C_2$ is again found as the appropriate root.

### *3.1 Validity of the tQSSA*

We expect that after a short transient phase the complex concentrations equal at any time $t$ the instantaneous quasi-steady-state concentrations, $C_i(t) = C_i(\bar{S}_1(t), \bar{S}_2(t))$, given by the roots in the respective polynomials as discussed above. Then the evolution of the system can be studied by means of the tQSSA

$$\frac{d\,\bar{S}_i}{dt} \approx -k_2^{(i)} C_i(\bar{S}_1, \bar{S}_2), \qquad \bar{S}_i(0) = S_{i,0}. \tag{21}$$

Segel (1988) proposed the following two criteria for the validity of a QSSA.

(i) The timescale for the complex(es) during the transient phase, $t_C$, should be much smaller than the timescale for changes in the substrate(s) in the beginning of the quasi-steady-state phase, $t_S$.

(ii) The substrate(s) should be nearly constant during the transient phase.

In our case, (ii) can be translated to (Segel, 1988; Tzafriri, 2003)

$$\frac{S_{i,0} - \bar{S}_i}{S_{i,0}} \leq \frac{t_C}{S_{i,0}} \max \left| \frac{d\,\bar{S}_i}{dt} \right| = \frac{k_2^{(i)} t_C}{S_{i,0}} C_i(S_{1,0}, S_{2,0}) \ll 1, \quad i = 1, 2, \tag{22}$$

where the maximum is taken over the transient phase, i.e., with $\bar{S}_i \approx S_{i,0}$. Since $C_i$ is increasing during the transient phase, the maximum is given by $k_2^{(i)} C_i(S_{1,0}, S_{2,0})$. The substrate timescale (Segel, 1988; Tzafriri, 2003) is estimated from (21) to be

$$t_{\bar{S}_i} \approx \frac{S_{i,0}}{k_2^{(i)} C_i(S_{1,0}, S_{2,0})}, \tag{23}$$

and we see that (22) translates into (i), i.e.,

$$\max_{i=1,2} \frac{t_C}{t_{\bar{S}_i}} = \frac{\max\{t_{C_1}, t_{C_2}\}}{\min\{t_{\bar{S}_1}, t_{\bar{S}_2}\}} \ll 1. \tag{24}$$

The timescale for the complexes is estimated following Borghans et al. (1996):

$$t_{C_i} \approx \frac{C_i(S_{1,0}, S_{2,0})}{\max \left| \frac{dC_i}{dt} \right|} = \frac{C_i(S_{1,0}, S_{2,0})}{k_1^{(i)} E_0 S_{i,0}}, \tag{25}$$

where the maximum is again taken during the transient phase. The timescale for the transient phase is then the maximum of the two individual scales; we want both complexes to be in the quasi-steady-state at the end of the transient phase, and both substrates to be nearly constant during it.

Hence, we propose the following *sufficient* condition for the validity of our tQSSA (21),

$$\epsilon := \max_{i=1,2} \left( \frac{k_2^{(i)} C_i(S_{1,0}, S_{2,0})}{S_{i,0}} \right) \max_{i=1,2} \left( \frac{C_i(S_{1,0}, S_{2,0})}{k_1^{(i)} E_0 S_{i,0}} \right) \ll 1. \tag{26}$$

Whenever the two maxima occur for the same $i$, (26) simplifies to

$$\bar{\epsilon} = \max_{i=1,2} \left( \frac{K_i}{E_0} \left( \frac{C_i(S_{1,0}, S_{2,0})}{S_{i,0}} \right)^2 \right) \ll 1, \tag{27}$$

where we introduced the Van Slyke-Cullen constants $K_i = k_2^{(i)}/k_1^{(i)}$.

## 4 Identical affinity, $K_M^{(1)} \approx K_M^{(2)}$.

When $K_M^{(1)} \neq K_M^{(2)}$ the roots of $\psi_1$ are given by a very complicated formula in contrast to the formula (20) when $K_M^{(1)} \approx K_M^{(2)} = K_M$. To deepen our understanding of the problem we follow this latter case further. It should be noted that the situation is biologically realistic, for example for bacterial carbohydrate sulfotransferase (NodST) with chitotriose and chitopentose as competitive substrates (Pi and

Leary, 2004), for I$\kappa$B kinase (IKK-2) phosphorylation of I$\kappa$B$\alpha$ and p65, which is of importance in inflammatory diseases (Kishore et al., 2003) and for the double phosphorylation of MAPK by MAPKK (Huang and Ferrell, 1996; Bhalla and Iyengar, 1999; Kholodenko, 2000). Following Tzafriri (2003) we let

$$r(X) = \frac{4E_0X}{(X + K_M + E_0)^2},$$

where $X$ is some unspecified substrate concentration. Then we can rewrite (20) as

$$C_1(\bar{S}_1, \bar{S}_2) = \frac{\bar{S}_1(\bar{S}_1 + \bar{S}_2 + K_M + E_0)}{2(\bar{S}_1 + \bar{S}_2)} \left(1 - \sqrt{1 - r(\bar{S}_1 + \bar{S}_2)}\right). \tag{28}$$

Setting

$$K = \frac{\max\{k_2^{(1)}, k_2^{(2)}\}}{\min\{k_1^{(1)}, k_1^{(2)}\}}, \qquad S_0 = S_{1,0} + S_{2,0}, \qquad r_0 = r(S_0), \tag{29}$$

we get from (26) and (28) that

$$\begin{aligned}
\epsilon &= \frac{K}{E_0}\left(\frac{S_0 + K_M + E_0}{2S_0}\left(1 - \sqrt{1 - r_0}\right)\right)^2 \\
&= \frac{K}{S_0}\frac{(1 - \sqrt{1 - r_0})^2}{1 - (1 - r_0)} \\
&= \frac{K}{S_0}\frac{1 - \sqrt{1 - r_0}}{2}\frac{2}{1 + \sqrt{1 - r_0}} \\
&\leq \frac{K}{2S_0}\frac{1 - \sqrt{1 - r_0}}{\sqrt{1 - r_0}} \\
&= \epsilon_{Tz},
\end{aligned}$$

where $\epsilon_{Tz}$ is the expression from (7). Let us remark that the constant $K$ in (29) is different from the Van Slyke - Cullen constant appearing in a single reaction. We can now use the result (8) to get

$$\epsilon \leq \epsilon_{Tz} \leq \frac{K}{4K_M}. \tag{30}$$

Inequality (30) tells us that, for identical affinities, we have that, the smaller the ratio $K/K_M$, the better the tQSSA approximation (21). If $K = k_2^{(i)}/k_1^{(i)}$ (same $i$), then $K \leq K_M$, and hence, $\epsilon \leq \frac{1}{4}$, such that in this case the tQSSA (21) is at least roughly valid. However, this is not necessarily true if $K = k_2^{(i)}/k_1^{(j)}$ ($j \neq i$).

### *4.1 First order tQSSA for identical affinities*

Developing (28) in $r$ yields

$$C_1 = \frac{E_0\bar{S}_1}{\bar{S}_1 + \bar{S}_2 + K_M + E_0} + O(r^2). \tag{31}$$

In this case (compare with Borghans et al. (1996))

$$\epsilon = \frac{KE_0}{(S_{1,0} + S_{2,0} + K_M + E_0)^2} + O(r^2), \qquad K = \frac{\max\{k_2^{(1)}, k_2^{(2)}\}}{\min\{k_1^{(1)}, k_1^{(2)}\}}. \tag{32}$$

When $r \ll 1$ *and* the tQSSA is valid ($\epsilon \ll 1$), we obtain the *first order* tQSSA (with respect to $r$) for competing substrates with identical affinity

$$\frac{d\,\bar{S}_i}{dt} \approx -\frac{k_2^{(i)} E_0 \bar{S}_i}{\bar{S}_1 + \bar{S}_2 + K_M + E_0}, \qquad \bar{S}_i(0) = S_{i,0}, \qquad i = 1, 2. \tag{33}$$

The sufficient conditions for $r \ll 1$ from Tzafriri (2003) translate into either of

$$S_{1,0} + S_{2,0} + K_M \gg E_0, \tag{34}$$

$$E_0 + K_M \gg S_{1,0} + S_{2,0}. \tag{35}$$

The condition (34) also guarantees $\epsilon \ll 1$ because of (32), unless $K \gg K_M + S_{1,0} + S_{2,0}$. As noted above, $K \leq K_M$ if $K = k_2^{(i)}/k_1^{(i)}$ (same $i$), and then indeed $\epsilon \ll 1$.

However, (35) does not imply $\epsilon \ll 1$ but must be accompanied by $K \ll K_M$, in which case (30) guarantees $\epsilon \ll 0.25$. When $K \gtrapprox K_M$ we must require $E_0 \gg K$ such that (32) yields $\epsilon \ll 1$, and in this case (35) simplifies to $E_0 \gg S_{1,0} + S_{2,0}$. In summary, any of the following conditions imply the validity of the first order tQSSA for identical affinities:

$$E_0 \ll S_{1,0} + S_{2,0} + K_M, \quad \text{and} \quad K \lessapprox K_M + S_{1,0} + S_{2,0} \tag{36}$$

$$E_0 + K_M \gg S_{1,0} + S_{2,0}, \quad \text{and} \quad K \ll K_M, \tag{37}$$

$$E_0 \gg S_{1,0} + S_{2,0}, \quad \text{and} \quad E_0 \gg K \gtrapprox K_M. \tag{38}$$

Neglecting $E_0$ in the denominator in (33) we obtain again the sQSSA of competing substrates with identical affinities (see (13) with $K_M^{(1)} = K_M^{(2)} = K_M$). This is valid when (36) holds, as seen from (14). On the other hand, when (37) or (38) is fulfilled, (33) does not reduce to the sQSSA (13). Hence, (37) or (38) extend the parameter region where (33) is valid.

### *4.2 Uncoupled equations and closed form solutions*

When $K_M^{(1)} \approx K_M^{(2)}$ as above, the two equations given by (21) can be uncoupled (Rubinow and Lebowitz, 1970; Segel, 1988; Schnell and Mendoza, 2000) by dividing one by the other and using (20), leading to

$$\frac{d\bar{S}_1}{d\bar{S}_2} = \frac{k_2^{(1)}}{k_2^{(2)}} \frac{\bar{S}_1}{\bar{S}_2},$$

such that

$$\frac{\bar{S}_1}{S_{1,0}} = \left(\frac{\bar{S}_2}{S_{2,0}}\right)^{\delta}, \qquad \delta = \frac{k_2^{(1)}}{k_2^{(2)}}. \tag{39}$$

This relation can then be used to eliminate $\bar{S}_2$ in (20) and, similarly, eliminate $\bar{S}_1$ in the expression for $C_2$. It also shows that when $\delta = 1$, i.e. $k_2^{(1)} = k_2^{(2)} = k_{cat}$, the two substrates behave identically with the only difference given by their initial concentrations. This can also be observed from (21) with (20) inserted.

In the following we assume that the first order tQSSA (33) holds. Using (39) we write (33) as

$$\frac{d\,\bar{S}_1}{dt} \approx -\frac{k_2^{(1)} E_0 \bar{S}_1}{\bar{S}_1 + S_{2,0}(\bar{S}_1/S_{1,0})^{1/\delta} + K_M + E_0}, \qquad \bar{S}_1(0) = S_{1,0}, \tag{40}$$

$$\frac{d\,\bar{S}_2}{dt} \approx -\frac{k_2^{(2)} E_0 \bar{S}_2}{\bar{S}_2 + S_{1,0}(\bar{S}_2/S_{2,0})^{\delta} + K_M + E_0}, \qquad \bar{S}_2(0) = S_{2,0}. \tag{41}$$

These equations are identical to (15) studied by Schnell and Mendoza (2000) setting $K_M^{(1)} = K_M^{(2)}$ and applying the substitution $K_M \to K_M + E_0$. Hence, the same techniques can be used to find closed form solutions.

When $\delta = 1$, (40) and (41) are identical except from the initial conditions and hence the two substrates develop identically, as observed above. The solution is given in closed form by

$$\bar{S}_i(t) \approx S_{i,0}\frac{K_M + E_0}{S_{1,0} + S_{2,0}} \cdot W\left(\frac{S_{1,0} + S_{2,0}}{K_M + E_0}\exp\left(\frac{S_{1,0} + S_{2,0} - k_{cat}E_0 t}{K_M + E_0}\right)\right), \tag{42}$$

where $W$ is the Lambert $W$-function introduced in enzyme kinetics by Schnell and Mendoza (1997a). It is defined as the real valued solution to $W(x)\exp(W(x)) = x$.

The case when $\delta \ll 1$ corresponds to a slow (resp. fast) competitor, when $\bar{S}_1$ is regarded as the competitor (resp. substrate) and $\bar{S}_2$ as the substrate (resp. competitor). The closed form solution can again be found following Schnell and Mendoza (2000), giving

$$\begin{aligned}
\bar{S}_2(t) &\approx (S_{1,0} + K_M + E_0)W\left(\frac{S_{2,0}}{S_{1,0} + K_M + E_0}\exp(\frac{S_{2,0} - k_2^{(2)}E_0 t}{S_{1,0} + K_M + E_0})\right), \\
\bar{S}_1(t) &\approx S_{1,0}\Big(\frac{\bar{S}_2(t)}{S_{2,0}}\Big)^{\delta}.
\end{aligned} \tag{43}$$

At low substrate concentrations (see formula (35)), the argument of $W$ in (42) and (43) is small and the approximation $W(x) \approx x$ holds. Hence, for both $\delta \approx 1$ and $\delta \ll 1$ we find after some algebra

$$\bar{S}_i(t) \approx S_{i,0}\exp\Big(-\frac{k_2^{(i)}E_0}{K_M + E_0}\,t\Big), \tag{44}$$

which is identical to the expression for the tQSSA of an isolated reaction (Tzafriri, 2003). Hence, the two substrates behave completely independently as if they were isolated. The same result is found directly by neglecting $\bar{S}_1 + \bar{S}_2$ in the denominator of (33). This is due to either $K_M$ or the enzyme concentration being much greater than the substrate concentrations, such that the fraction of free enzyme in the sys-

tem is near to unity. Schnell and Mendoza (1997b,c) studied this scenario for the sQSSA.

## 5 $K_M^{(1)} \gg K_M^{(2)}$ and the general first order approximation

We now turn to the case of very different affinities as stated by $K_M^{(1)} \gg K_M^{(2)}$. To investigate this situation closer we perform a perturbation around $K_M^{(2)} = 0$. When $K_M^{(2)} = 0$, we see from (17b) that in the quasi-steady-state, $C_2 \approx \bar{S}_2$ or $E_0 - C_1 - C_2 \approx 0$. In the former case, $C_2 \approx S_{2,0}$ since $k_2^{(2)} = 0$. In the latter case, again from (17b), but now for $i = 1$, it follows that $C_1 \approx 0$, $C_2 \approx E_0$. Since $C_2 \leq \min\{S_{2,0}, E_0\}$ we get that, when $K_M^{(2)} = 0$,

$$C_2 \approx \min\{S_{2,0}, E_0\}. \tag{45}$$

We study these two cases independently, and by means of their corresponding solutions we build a two point Padé approximant (TPPA) (Baker, 1975) in $\eta = S_{2,0}/E_0$ developed around $\eta = 0$ ($E_0 \gg S_{2,0}$) and $\eta = \infty$ ($E_0 \ll S_{2,0}$).

When $E_0 \gg S_{2,0}$ (i.e., $\eta \ll 1$), we expect that after the transient phase the system evolves as two independent reactions: $S_2$ binds with a part of the enzyme during the transient phase as seen from (45), $C_2 \approx S_{2,0}$, leaving $E_0^* = E_0 - S_{2,0}$ to react with $S_1$. Hence, we obtain from (5) and (9)

$$\frac{d\,\bar{S}_1}{dt} \approx -k_2^{(1)} \frac{(E_0^* + K_M^{(1)} + \bar{S}_1) - \sqrt{(E_0^* + K_M^{(1)} + \bar{S}_1)^2 - 4E_0^*\bar{S}_1}}{2} \tag{46}$$

$$\approx -\frac{k_2^{(1)} E_0^* \bar{S}_1}{K_M^{(1)} + E_0^* + \bar{S}_1}. \tag{47}$$

Note that here $K_M^{(2)} = 0$, such that (18a) is not valid. The solution can also be found by setting $C_2 = S_{2,0}$ in (17b) with $i = 1$.

In the case when $0 < K_M^{(2)} \ll K_M^{(1)}$, we neglect terms involving $K_M^{(2)}$ in (19) and obtain that $C_1$ should satisfy

$$\Big(C_1^2 - (E_0 + K_M^{(1)} + \bar{S}_1 - \bar{S}_2)C_1 + (E_0 - \bar{S}_2)\bar{S}_1\Big) \cdot C_1 = 0.$$

Since $C_2 \leq S_{2,0} < E_0$, $C_1 = 0$ is in contradiction with (18b). Thus, $C_1$ solves the second degree polynomial which is exactly the polynomial given from the tQSSA for an isolated reaction, i.e., $\bar{S}_1$ follows again (46) but now with $E_0^* = E_0 - \bar{S}_2$.

We now turn to the case when $C_2 \approx E_0 \ll S_{2,0}$ (i.e., $\eta \gg 1$). Recall that this is the case of the usual *in vitro* experiments. From the conservation law (12) $C_1 \approx 0$. We expand $\psi_1/K_M^{(1)}$ in terms of the small parameter $\rho = K_M^{(2)}/K_M^{(1)}$ and find that the first order term for the root is given by

$$C_1 = \rho \frac{E_0\bar{S}_1}{\bar{S}_2 - E_0} = \frac{K_M^{(2)}}{K_M^{(1)}} \times \frac{E_0\bar{S}_1}{\bar{S}_2 - E_0}. \tag{48}$$

Using (48) for $1/\eta \approx 0$, and the first order approximation (47) for $\eta \approx 0$, the TPPA in $\eta = \bar{S}_2/E_0$ is

$$C_1 = \frac{E_0\bar{S}_1}{K_M^{(1)} + \bar{S}_1 + E_0 + \bar{S}_2/\rho} = \frac{E_0\bar{S}_1}{K_M^{(1)}(1 + \bar{S}_2/K_M^{(2)}) + \bar{S}_1 + E_0}. \quad (49)$$

Plugging (49) into (21) (for $i = 1$) yields then

$$\frac{d\,\bar{S}_i}{dt} = -\frac{k_2^{(i)}E_0\bar{S}_i}{K_M^{(i)}(1 + \bar{S}_j/K_M^{(j)}) + \bar{S}_i + E_0}, \quad \bar{S}_i(0) = S_{i,0}, \quad j \neq i. \quad (50)$$

where $i = 1, j = 2$. Similar computations can be performed for $C_2$, when $K_M^{(1)} \ll K_M^{(2)}$, yielding the same equation (48), where $i = 2, j = 1$.

The two approximations hold for two different regions of parameter space, $K_M^{(1)} \gg K_M^{(2)}$ and $K_M^{(1)} \ll K_M^{(2)}$, respectively. However, let us observe that they reduce not only to the case of identical affinities, (33), for $K_M^{(1)} = K_M^{(2)}$, but also to the sQSSA (13) whenever this approximation holds as guaranteed by (14), and to the single reaction first order tQSSA (9) when $\bar{S}_j/K_M^{(j)}$ can be neglected.

Motivated by this and further encouraged by numerical simulations (see the following section), we propose the expression (50) (for $i = 1, 2$) as the general first order approximation to the tQSSA for fully competitive reactions.

Although not strictly theoretically founded, the above considerations using the TPPA can be seen as the motivation for the formula. However, as shown in Appendix B, we can indeed expect $C_1$ from (49) (and $C_2$ in the corresponding expression) to be a good approximation to the true root of $\psi_1$ ($\psi_2$ for $C_2$) when either (14) holds, or when

$$K_M^{(i)} \gg S_{1,0} + S_{2,0} \quad \text{or} \quad E_0 \gg K_M^{(i)}(1 + S_{j,0}/K_M^{(j)}) + S_{i,0}, \quad i = 1, 2,\ j \neq i.$$

Hence, (50) extends both the sQSSA (13) as well as the single reaction tQSSA (5).

The considerations in Appendix B tell us only when the first order tQSSA (50) is a good approximation of the full tQSSA (21), but neither might be a good representation of the full system. To assure that, $\epsilon$ must be small.

When (49) approximates the full tQSSA we have from (26)

$$\begin{aligned} \epsilon &= \max_{i=1,2} \frac{k_2^{(i)}E_0}{\tilde{K}_{M,0}^{(i)} + S_{i,0} + E_0} \max_{i=1,2} \frac{1}{k_1^{(i)}(\tilde{K}_{M,0}^{(i)} + S_{i,0} + E_0)} \\ &\leq K \max_{i=1,2} \frac{E_0}{\tilde{K}_{M,0}^{(i)} + S_{i,0} + E_0} \max_{i=1,2} \frac{1}{\tilde{K}_{M,0}^{(i)} + S_{i,0} + E_0} \\ &= \max_{i=1,2} \frac{K\,E_0}{(\tilde{K}_{M,0}^{(i)} + S_{i,0} + E_0)^2} \end{aligned} \quad (51)$$

where

$$K = \frac{\max\{k_2^{(1)}, k_2^{(2)}\}}{\min\{k_1^{(1)}, k_1^{(2)}\}}, \qquad \tilde{K}_{M,0}^{(i)} = K_M^{(i)}(1 + S_{j,0}/K_M^{(j)}), \quad i = 1, 2,\ j \neq i. \quad (52)$$

The above considerations yield that either one of the following conditions guarantees the validity of the first order approximation (50) ($i = 1, 2$):

$$E_0 \ll S_{i,0} + \tilde{K}_{M,0}^{(i)}, \qquad \text{and} \qquad K \lessapprox \tilde{K}_{M,0}^{(i)} + S_{i,0}, \quad (53)$$

$$K_M^{(i)} \gg S_{1,0} + S_{2,0}, \qquad \text{and} \qquad K \ll \tilde{K}_{M,0}^{(i)}, \quad (54)$$

$$K_M^{(i)} \gg S_{1,0} + S_{2,0}, \qquad \text{and} \qquad E_0 \gg K \gtrapprox \tilde{K}_{M,0}^{(i)}, \quad (55)$$

$$E_0 \gg \tilde{K}_{M,0}^{(i)} + S_{i,0}, \qquad \text{and} \qquad E_0 \gg K. \quad (56)$$

## 6 Numerical Results and Discussion

*In vivo* reactions are usually modelled by ordinary differential equations using the concentrations of the involved biochemical species. This idea has been questioned to hold for a low number of involved molecules or in a crowded environment, where stochastic methods should be used (Turner et al., 2004). However, in a comparison between the deterministic (sQSSA) and stochastic approaches it was found that the two approaches agreed reasonably well for as few as 100 molecules, and thus it was concluded that intracellular enzyme reactions as a rule are well described by the deterministic approach using concentrations (Turner et al., 2004).

The introduction of the recent total quasi-steady-state approximation (tQSSA) (Borghans et al., 1996; Tzafriri, 2003) is motivated by the need to extend the sQSSA to situations where the enzyme concentration is comparable to or greater than both the substrate concentration and the Michaelis constant. Albe et al. (1990) found that the enzyme concentration was greater than the corresponding substrate concentration in 12% of investigated substrate-enzyme pairs was, and the two concentrations comparable were in other 13%, such that the enzyme concentration was more than ten times lower than the substrate concentration in only 75% of the substrate-enzyme pairs. For comparison, Stayton and Fromm (1979) found that for the sQSSA to hold, one needs that the enzyme concentration is at least 100 times lower than the substrate concentration. However, it should be noted that we find excellent fits for the competitive sQSSA, when the enzyme to substrate ratio is 0.1 (Fig. 2A). Nonetheless, even though the majority of the enzyme-reaction pairs investigated by Albe et al. (1990) could be expected to be well-approximated by the sQSSA, a significant number cannot, and such an approximation would break down in particular in the glycolytic pathway (Albe et al., 1990). It seems reasonable to expect that the same conclusion might hold for other pathways. And even in pathways where a few steps are badly approximated by the sQSSA, the inappropriate use of the sQSSA through out the pathway could yield erroneous predictions of the overall behavior (Pedersen et al., 2006).

In the present manuscript we have extended the total quasi-steady-state assumption to competing substrates, investigating its validity and deepening some special cases.

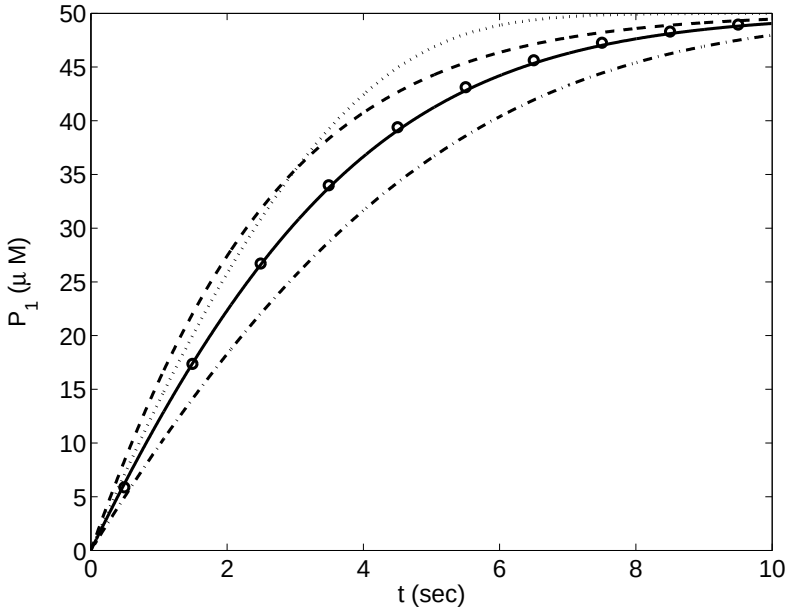


Figure 1. The competitive tQSSA ((21), full curve) approximates the full system ((10), circles) very well ($R^2 = 0.9997$), also when both the competitive sQSSA ((13), dotted curve, $R^2 = 0.9321$) and the single reaction tQSSA ((5), dashed curve, $R^2 = 0.9531$) do not. However, in this case we can not obtain that the competitive first order approximation ((50), dash-dotted curve, $R^2 = 0.9298$) is good. Parameters (based on Pi and Leary (2004)): $K_M^{(1)} = 23\,\mu$M, $K_M^{(2)} = 25\,\mu$M, $k_2^{(1)} = 42\,\text{min}^{-1}$, $k_2^{(2)} = 25\,\text{min}^{-1}$, $S_{1,0} = S_{2,0} = E_0 = 50\,\mu$M ($\epsilon = 0.022$). To fix $k_j^{(i)}$ we have used the constraint $k_{-1}^{(i)} = 4k_2^{(i)}$ (Bhalla and Iyengar, 1999).

As seen in Fig. 1, the approximation (21) is indeed excellent as long as $\epsilon$ is small. This figure is based on the data from Pi and Leary (2004) for carbohydrate sulfotransferase (NodST) with chitopentaose and chitotriose as competing substrates. Of importance, our approximation (21) captures the competition as does the sQSSA (13) and in contrast with the single reaction tQSSA (5), but also at intermediate or high enzyme concentrations where the sQSSA (13) does not hold anymore (Fig. 1). However, when the competition can be neglected due to, e.g., low substrate concentrations, the single reaction tQSSA (5) does indeed estimate the full system well (see, e.g., Fig. 2, panels B and C).

A crucial step of our analysis is finding the roots of the third degree polynomials $\psi_i$. Although we have shown that there is exactly one physically possible root for each complex, and that there exists, e.g., Cardano's formula for this root, the formula is hard to interpret and even to implement. We have used a differential-algebraic equations (DAE) approach, i.e., finding the roots numerically. Such a DAE approach is easier to implement than using the closed form for the root, but increases the time needed for computations.

These problems can partly be resolved by using approximations of the roots of $\psi_i$. Compared to the full solution, such an approximation should preferably be easier

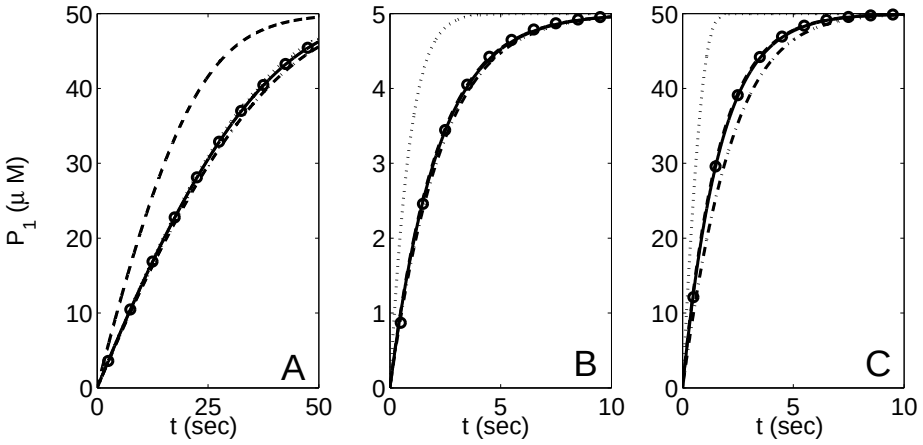


Figure 2. The first order approximation (dash-dot curve) coincides with the competitive sQSSA (dotted curve) when it is valid (panel A), and with the single reaction tQSSA (dashed curve) when the competition is negligible (panel B). However, at high enzyme concentrations the single reaction tQSSA is often a better approximation than the first order tQSSA (panel C). Parameters are as in Fig. 1, except: In A: $E_0 = 5\,\mu$M ($\epsilon = 0.0027$). $R^2$ values (in the following order [*competitive tQSSA* (21), *competitive sQSSA* (13), *single reaction tQSSA* (5), *competitive first order approximation* (50)]): $[1.0000, 0.9994, 0.6485, 0.9967]$. In B: $S_{1,0} = S_{2,0} = 5\,\mu$M ($\epsilon = 0.0694$). $R^2$ values: $[0.9985, 0.5113, 0.9980, 0.9969]$. In C: $E_0 = 200\,\mu$M ($\epsilon = 0.029$). $R^2$ values: $[0.9998, 0.4736, 0.9992, 0.9637]$.

to interpret and to relate to previously known formulas. Furthermore, it should be clearly stated when it is valid. We found a first order approximation (50), which is valid when the sQSSA approach (13) is as stated in (53), and in this case they coincide (Fig. 2A). Moreover, it is valid for high $K_M^{(i)}$ values (conditions (54) and (55)), where it reduces to the single reaction first order approximation (5), see Fig. 2B. Hence, it extends these two approximations beyond the regions where they are known to hold. Finally, the first order approximation is valid at high enzyme concentrations (56), but it is not always accurate if the enzyme concentration is only moderately high. In this case, the single reaction tQSSA (5) is often a better approximation (Fig. 2C).

The case of very different affinities was used to derive the first order approximation (50) using a two-point Padé approximant. However, it is of its own biological interest as seen for example from the data by Pi and Leary (2004) for carbohydrate sulfotransferase (NodST) with chitopentaose as substrate ($K_M^{(1)} = 23\ \mu$M), and chitobiose as a competing substrate ($K_M^{(2)} = 240\ \mu$M). Fig. 3 shows that the full tQSSA (21) approximates the full system very well also in this specific example of $K_M^{(1)} \ll K_M^{(2)}$, even when all other approximations fail. For $P_2$ (Fig. 3B) it is seen that the sQSSA (13) overestimates the transient phase in which mainly $P_1$ (Fig. 3A) is produced, where after it is accelerated, such that the overall behavior is not only quantitatively, but also qualitatively wrongly estimated in this example. Curiously, the single reaction tQSSA (5) estimates $P_1$ well. The reason is the low degree of competition felt by the first reaction as seen from $\tilde{K}_{M,0}^{(1)} \approx 2K_M^{(1)} \ll E_0$, so both

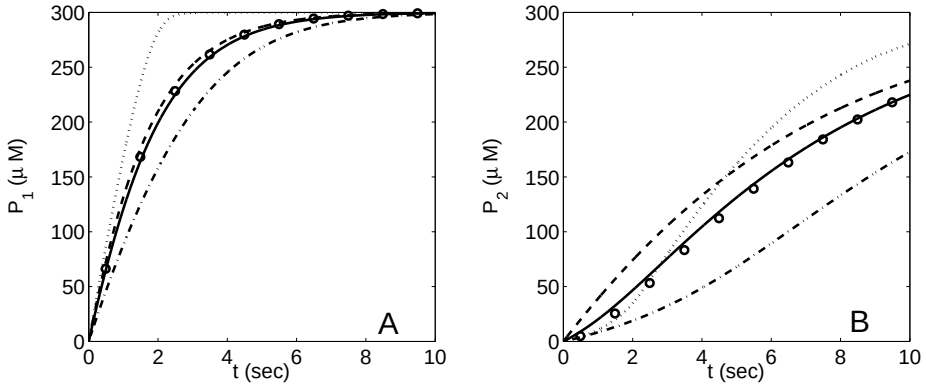


Figure 3. Also $K_M^{(1)} \ll K_M^{(2)}$ is captured well by the competitive tQSSA (21). Legends and kinetic parameters for reaction 1 are as in Fig. 1, but $K_M^{(2)} = 240\,\mu$M, $k_2(2) = 19.5\,\text{min}^{-1}$ and $S_{1,0} = S_{2,0} = E_0 = 300\,\mu$M ($\epsilon = 0.0387$). $R^2$ values; panel A: $[0.9992, 0.7778, 0.9974, 0.8858]$; panel B: $[0.9954, 0.7641, 0.8556, 0.5321]$.

$\tilde{K}_{M,0}^{(1)}$ and $K_M^{(1)}$ are negligible compared to $E_0$. This is not true for the second reaction as illustrated in Fig. 3B.

The fractional errors associated with the different approximations are estimated as $\sqrt{1-R^2}$, where $R^2 = 1 - \sum_i (y_i - \hat{y}_i)^2 / \sum_i (y_i - \bar{y})^2$ represents the goodness of fit (Kvålseth, 1985; Tzafriri and Edelman, 2004, 2005). Here $y_i$ are the data points extracted from the full system (10), $\bar{y}$ is the average of $y_i$ and $\hat{y}_i$ is the fitted (approximated) value corresponding to $y_i$ for each $i$. $R^2 = 1$ for a perfect fit, lower $R^2$ value indicates a worse fit, and $R^2 < 0$ represents that the constant $\bar{y}$ is a better fit than the approximating curve. It should be remarked that $R^2$ values must be used with great care for nonlinear models, and that there exist several definitions of the $R^2$ value. However, the definition applied here seems to be preferable (Kvålseth, 1985).

Fig. 4A show the fractional errors for different enzyme to substrate ratios $E_0/S_0$, $S_0 = S_{1,0} = S_{2,0}$ and for comparable affinities. Our competitive tQSSA (21) gives very low errors for the full range of ratios, and is consistently better than all the other approximations. The figure also show that the first order approximation (50) is a decent fit for all values of $E_0/S_0$, but that it is inferior to the competitive sQSSA (13) at low enzyme to substrate ratios, and to the single reaction tQSSA (5) at high ratios. Hence, the advantage of the first order approximation (50) is, that we have an approximation giving reasonable predictions for a wider range of parameters, rather than an approximation, which is more accurate than the best of the competitive sQSSA (13) and the single reaction tQSSA (5).

When varying the ratio of the affinities $K_M^{(1)}/K_M^{(2)}$, we obtain again that the competitive tQSSA (21) is an excellent approximation for all values of this ratio (Fig. 4B), and it is again superior to the other approximations. The fractional errors associated with both the competitive sQSSA (13) and the single reaction tQSSA (5) are almost unchanged for different $K_M^{(1)}/K_M^{(2)}$ ratios, and for low ratios they are both comparable to the error related to the first order approximation (50). For high val-

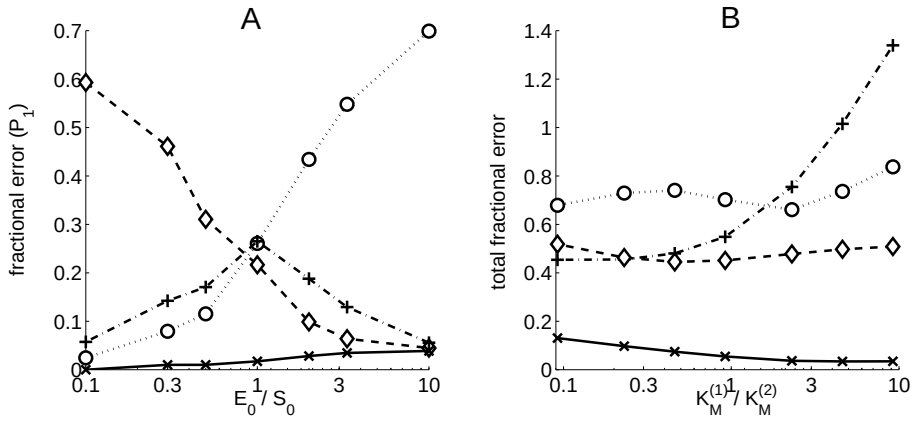


Figure 4. The fractional errors associated with the different approximations. Panel A shows the effect of varying the enzyme to substrate ratio $E_0/S_0$, where $S_0 = S_{1,0} = S_{2,0}$, measured by the fractional errors of $P_1$. Panel B shows the total fractional error, i.e, for the sum of the fractional errors for $P_1$ and $P_2$, when varying $K_M^{(2)}$ reflected in the ratio $K_M^{(1)}/K_M^{(2)}$. Line styles correspond to Fig. 1 with markers: Competitive tQSSA (21) ($\times$); competitive sQSSA (13) ($\circ$); single reaction tQSSA (5) ($\diamondsuit$) and first order approximation (50) ($+$). Parameters are as in Fig. 1 except: Panel A: $S_0 = 5, 15, 25$ $\mu$M for $E_0/S_0 > 1$ and $E_0 = 5, 15, 25$ $\mu$M for $E_0/S_0 < 1$. Panel B: $K_M^{(2)} = 2.5, 5, 10, 25, 50, 100, 250$ $\mu$M. The points in panel A for $E_0/S_0 = 0.1, 1$ and 10 correspond to Figs. 1, 2A and 2B, respectively. The case $K_M^{(2)} = 25$ $\mu$M ($K_M^{(1)}/K_M^{(2)} \approx 1$) correspond to Fig. 1.

ues of $K_M^{(1)}/K_M^{(2)}$, or more precisely low $K_M^{(2)}$ values, the first order approximation breaks apparently down. This is due to large fractional errors with respect to $P_1$, and is related to the large value of $\tilde{K}_{M,0}^{(1)}$ compared to $K_M^{(1)}$. This is not the case for the low $K_M^{(1)}/K_M^{(2)}$ ratio in Fig. 4B, since these are for high $K_M^{(2)}$ values and since $K_M^{(1)}$ and $S_{1,0}$ are of the same magnitude, and hence $\tilde{K}_{M,0}^{(2)}$ and $K_M^{(2)}$ are of similar magnitude.

In the special case of identical affinities we saw that our approach should be at least roughly valid if only $K \leq K_M$. This last assumption seems to be reasonable, since if $K_M^{(1)} \approx K_M^{(2)}$, we expect that the kinetic parameters $k_1^{(i)}$ and $k_2^{(i)}$ are similar for the two substrates. This would imply $K \approx k_2^{(i)}/k_1^{(i)}$ for the same $i$ and consequently $K \lessapprox K_M$. Interestingly, for many metabolic enzymes $k_2 \ll k_{-1}$, i.e. $K \ll K_M$ (Atkinson, 1977). This implies that for competing substrates with identical affinities the relation $K \leq K_M$ is even more reasonable, and even $K \ll K_M$ can be expected, in which case the tQSSA (21) is a very good approximation, as seen from (30). Based on the above mentioned fact that often $k_2^{(i)} \ll k_{-1}^{(i)}$, Bhalla and Iyengar (1999) use the relation $k_{-1}^{(i)} = 4k_2^{(i)}$. Then for identical affinities $k_1^{(i)} = 5k_2^{(i)}/K_M^{(i)} = 5k_2^{(i)}/K_M$, such that

$$K = \frac{\max_i k_2^{(i)}}{\min_i k_1^{(i)}} = \frac{\max_i k_2^{(i)}}{(5/K_M)\min_i k_2^{(i)}} = \frac{K_M}{5}\frac{\max_i k_2^{(i)}}{\min_i k_2^{(i)}},$$

from which it is seen that $K \leq K_M$ unless $k_2^{(1)}$ and $k_2^{(2)}$ differ by more than a factor

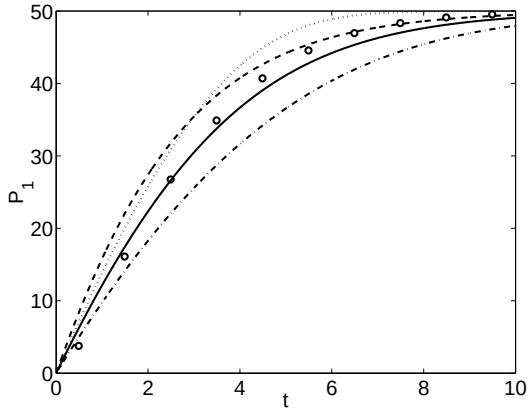


Figure 5. When $\epsilon$ becomes large also the tQSSA (21) fails. Parameters and legends are as in Fig. 1, but with the constraint $k_{-1}^{(i)} = 0.1k_2^{(i)}$, such that $K = 38.18 > K_M^{(i)}$, to force a large $\epsilon = 0.1005$ ($\bar{\epsilon} = 0.0580$ from (27)). $R^2$ values: $[0.9907, 0.9555, 0.9568, 0.9119]$.

5. This is not the case for any of the IKK-2 data with $K_M^{(1)} \approx K_M^{(2)}$ from Kishore et al. (2003), nor for carbohydrate sulfotransferase (NodST) with chitotriose and chitopentaose as substrates (Pi and Leary, 2004). In fact, their $k_{cat}$ (our $k_2^{(i)}$) values differ by less than a factor 2.

The assumption $K \leq K_M^{(i)}$ cannot be expected to hold when $K_M^{(1)} \ll K_M^{(2)}$, as illustrated by Fig. 3. Assuming again $k_{-1}^{(i)} = 4k_2^{(i)}$, such that $k_1^{(i)} = 5k_2^{(i)}/K_M^{(i)}$, then gives

$$K = \frac{\max_i k_2^{(i)}}{\min_i k_1^{(i)}} = \frac{\max_i k_2^{(i)}}{5 \min_i k_2^{(i)}/K_M^{(i)}} \leq \frac{K_M^{(2)}}{5} \frac{\max_i k_2^{(i)}}{\min_i k_2^{(i)}},$$

so again $K \leq K_M^{(2)}$ unless $k_2^{(1)}$ and $k_2^{(2)}$ differ by more than a factor 5. On the other hand

$$K = \frac{\max_i k_2^{(i)}}{5 \min_i k_2^{(i)}/K_M^{(i)}} \geq \frac{\max_i k_2^{(i)}}{5(\max_i k_2^{(i)})(\min_i 1/K_M^{(i)})} = \frac{K_M^{(2)}}{5},$$

such that if $K_M^{(2)} > 5K_M^{(1)}$ we will have $K > K_M^{(1)}$. The parameters in Fig. 3 are such that $K_M^{(1)} < K < K_M^{(2)}$.

Related to the condition $K \leq K_M^{(i)}$ is the difference between $\epsilon$ from (26) and $\bar{\epsilon}$ from (27), which can be significant. In Fig. 5 the (inaccurate) expression from (27) gives $\bar{\epsilon} = 0.0580$, which is lower than $\epsilon$ in Fig. 2B where the tQSSA (21) is a reasonable approximation. But in Fig. 5 the tQSSA (21) does not fit as well as in the previous figures ($R^2 = 0.9907$), and indeed the correct formula from (26) gives a significantly higher value $\epsilon = 0.1005$.

Our results are immediately applicable to, e.g., successive reactions catalyzed by the same enzyme, such as nonprocessive or distributive double phosphorylation or dephosphorylation processes, as seen for example in the MAPK cascade (Burack and Sturgill, 1997; Ferrell and Bhatt, 1997; Zhao and Zhang, 2001; Markevich et al., 2004). The reaction scheme can be seen as a special case of (2) with $P_1 = S_2$

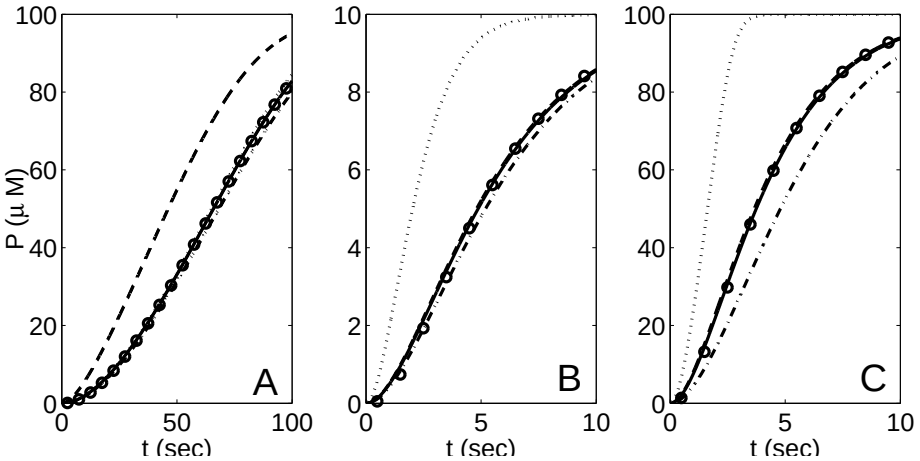


Figure 6. The tQSSA (21) estimates the development of the product of two successive reactions catalyzed by the same enzyme well, and the discussion of the validity of the sQSSA (13), the single reaction tQSSA (5) and the first order tQSSA (50) apparently carries over to this case. Legends are as in Fig. 1, and parameters as in Fig. 2 except for the initial substrate concentrations, which are $S_{2,0} = 0$ in all panels and: In A: $S_{1,0} = 100$ ($R^2 = [1.0000, 0.9988, 0.5759, 0.9949]$). In B: $S_{1,0} = 10$ ($R^2 = [0.9984, -0.3307, 0.9973, 0.9931]$). $E_0 = 5$. $\epsilon = 0.0832$. In C: $S_{1,0} = 100$ ($R^2 = [0.9997, -0.0351, 0.9986, 0.9076]$).

and is summarized as

$$S_1 \xrightarrow{E} S_2 \xrightarrow{E} P,$$

where it is usually assumed that at the beginning only $S_1$ is present. Fig. 6 shows that the results presented here yield a good approximation ($R^2 > 0.998$ in the three examples). This is in great contrast to the competitive sQSSA (13), which in both panels B and C of Fig. 6 gives negative $R^2$ values.

However, it should be remarked that our theoretical investigation of the validity of the tQSSA does not work in the case of successive reactions. The problem is that there is no $S_2$ at time $t = 0$, and hence the timescales can not be found following Segel (1988) because the definition of the transient phase no longer holds. Nevertheless, it seems like the conclusions concerning the validity of the first order approximation from above carry over to this scenario (compare the three panels of Fig. 2 with the panels of Fig. 6). We will present the investigation of such reactions in another paper.

Finding approximations extending the classical sQSSA approach for complex reactions such as successive reactions, open systems, loops such as the Goldbeter-Koshland switch (Goldbeter and Koshland, 1981), feedback systems etc. should be of great interest for further improving investigations and simulations of such reactions *in vivo*, where the sQSSA description breaks down. The alternative is to simulate each step of the reaction, i.e., the full system of ODEs, but for larger systems this can quickly become very computer expensive. Moreover, all of the (often unknown) kinetic parameters are needed for a full simulation, while a QSSA usually needs only $K_M$ and $V_{max}$ values. Furthermore, the QSSA can provide theoretical

insight which is hard to gain from the full system, for example in the way the classical sQSSA (3) explains the saturation curve. We expect that the ideas presented here can be used to extend the tQSSA to the above (and, hopefully, other and more complex) reactions.

**Acknowledgements**

The authors are deeply grateful to the anonymous referees, who gave much appreciated suggestions to several passages of the present paper, which helped clarifying the manuscript greatly. Dr. Giuliana Cortese gave precious suggestions and considerations related to the usage of $R^2$ values. M.G.P. was supported by the European Union through the Network of Excellence BioSim, Contract No. LSHB-CT-2004-005137.

## A Existence and uniqueness of the solution for the complexes

We show the existence and uniqueness of a solution to the system (18) with $0 < C_i < \min\{\bar{S}_i, E_0\}$. First we note that (18) implies

$$\frac{K_M^{(1)} C_1}{\bar{S}_1 - C_1} = \frac{K_M^{(2)} C_2}{\bar{S}_2 - C_2},$$

from which it is seen that $0 < C_1 < \bar{S}_1$ if and only if $0 < C_2 < \bar{S}_2$.

Substituting (18b) into (18a) leads to the following equation in $C_1$

$$C_1 = E_0 - \Big(E_0 - C_1(1 + \frac{K_M^{(1)}}{\bar{S}_1 - C_1})\Big)\Big(1 + \frac{K_M^{(2)}}{\bar{S}_2 - (E_0 - C_1(1 + \frac{K_M^{(1)}}{\bar{S}_1 - C_1}))}\Big) \quad \text{(A.1)}$$

and $C_2$ can then be found from (18b).

Solving (A.1) is equivalent to finding roots of the third degree polynomial

$$\begin{aligned}\psi_1(C_1) = &-(K_M^{(1)} - K_M^{(2)})C_1^3 \\ &+ \Big[(E_0 + K_M^{(1)} + \bar{S}_1)(K_M^{(1)} - K_M^{(2)}) - (\bar{S}_1 K_M^{(2)} + \bar{S}_2 K_M^{(1)})\Big]C_1^2 \\ &+ \Big[ - E_0(K_M^{(1)} - K_M^{(2)}) + (\bar{S}_1 K_M^{(2)} + \bar{S}_2 K_M^{(1)}) + K_M^{(2)}(E_0 + K_M^{(1)})\Big]\bar{S}_1 C_1 \\ &- E_0 K_M^{(2)} \bar{S}_1^2.\end{aligned} \quad \text{(A.2)}$$

An analogous polynomial $\psi_2$ for $C_2$ can be found by interchanging the indexes 1 and 2 in (A.2), because of the symmetry of the system (17). Rearranging the terms, $\psi_1$ can also be written

$$\begin{aligned}\psi_1(C_1) = &K_M^{(2)}(C_1 - E_0)\Big(\bar{S}_1 - C_1\Big)^2 \\ &+ K_M^{(1)} C_1(C_1 + K_M^{(2)} + \bar{S}_2 - E_0))\Big(\bar{S}_1 - C_1\Big) + (K_M^{(1)} C_1)^2.\end{aligned} \quad \text{(A.3)}$$

From (A.2) we see that $\psi_1(0) < 0$, and from (A.3) that $\psi_1(\bar{S}_1) > 0$. Hence, $\psi_1$ has at least one root between $0$ and $\bar{S}_1$, which shows existence.

When $K_M^{(1)} \neq K_M^{(2)}$, we can without loss of generality assume that $K_M^{(1)} > K_M^{(2)}$ because of the symmetry of (2). In this case $\lim_{c\to\pm\infty} \psi_1(c) = \mp\infty$, and we see that $\psi_1$ has one negative root and one root larger than $\bar{S}_1$. Hence, there is a unique root $C_1 \in (0, \bar{S}_1)$, which also solves (A.1). This implies the uniqueness of the solution.

When $K_M^{(1)} = K_M^{(2)} = K_M$, $\psi_1$ becomes a second degree polynomial. Because of (A.2) we have $\lim_{c\to\infty} \psi_1(c) = -\infty$, so the second root is larger than $\bar{S}_1$. Hence, also in this case we have only one root between $0$ and $\bar{S}_1$, given by (20).

The approach to solving (18) taken above helps the theoretical reasoning, but is practically cumbersome, since we need to find the largest $K_M^{(i)}$. In addition, the formula (18b) for finding $C_2$ is numerically imprecise when both $C_1$ and $\bar{S}_1$ are small. Both these problems can be overcome by finding the root of the polynomial $\psi_2$ for $C_2$; $\psi_2$ has a single root in $(0, \bar{S}_2)$ as a consequence of the uniqueness result.

## B Validity of the first order approximation of the root of $\psi_i$

To investigate the validity of (50) we evaluate $\psi_1$ from (19) at $C_1$ given by (49) This yields the remainder

$$\begin{aligned} R_1 := \psi_1(C_1) = -E_0^2 \bar{S}_1^2 K_M^{(2)} \Big[ K_M^{(2)}(E_0 + K_M^{(1)}) + K_M^{(2)} \bar{S}_1 + K_M^{(1)} \bar{S}_2 \Big]^{-3} \times \\ \Big[ K_M^{(1)} K_M^{(2)} \Big( \bar{S}_1 \bar{S}_2 (K_M^{(1)} + K_M^{(2)}) + E_0 (\bar{S}_1 K_M^{(2)} + \bar{S}_2 K_M^{(1)}) \Big) + \\ \bar{S}_1 (K_M^{(2)})^3 (\bar{S}_1 + K_M^{(1)}) + \bar{S}_2 (K_M^{(1)})^3 (\bar{S}_2 + K_M^{(2)}) \Big]. \end{aligned} \quad \text{(B.1)}$$

The term "remainder" is used, since if $R_1$ were zero, then $C_1$ given by (49) would be a true root, not only an approximation. To have a good approximation of the true root, $|R_1|$ must be small compared to typical sizes of $\psi_1$ such as

$$|\psi_1(0)| = E_0 K_M^{(2)} \bar{S}_1^2 \quad \text{and} \quad \psi_1(\bar{S}_1) = (K_M^{(1)} \bar{S}_1)^2.$$

Similar conditions should hold for $C_2$ and $\psi_2$, but calculations and results are identical, and we show them only for $C_1$ in the following.

When (14) holds we expect (50) to hold, and then it reduces to the sQSSA (13). In this case the terms involving $E_0$ in $R_1$ are negligible and the condition $|R_1| \ll |\psi_1(0)|$ implies

$$\frac{E_0}{(\bar{S}_1 + \tilde{K}_M^{(1)})^2} \times \frac{K_M^{(1)}}{K_M^{(2)}} \left( \bar{S}_2 \frac{K_M^{(1)}}{K_M^{(2)}} + \bar{S}_1 \frac{\bar{S}_2 + \tilde{K}_M^{(2)}}{\bar{S}_1 + \tilde{K}_M^{(1)}} \right) \ll 1, \quad \text{(B.2)}$$

where we have introduced the so-called apparent Michaelis constants (see, e.g., Schnell and Mendoza (2000))

$$\tilde{K}_M^{(i)} = K_M^{(i)}(1 + \bar{S}_j / K_M^{(j)}), \quad j \neq i. \quad \text{(B.3)}$$

Similarly $|R_1| \ll \psi_1(S_1)$ can be restated as

$$\left(\frac{E_0}{\bar{S}_1 + \tilde{K}_M^{(1)}}\right)^2 \left(\frac{\bar{S}_2}{K_M^{(2)}} + \frac{\bar{S}_1}{K_M^{(1)}} \frac{\bar{S}_2 + \tilde{K}_M^{(2)}}{\bar{S}_1 + \tilde{K}_M^{(1)}}\right) \ll 1. \tag{B.4}$$

These conditions are both clearly satisfied by (14) as long as $\bar{S}_i$ is not much greater than $K_M^{(i)}$, and $K_M^{(1)}$ and $K_M^{(2)}$ are of similar magnitude.

At high enzyme concentrations, (50) is a good approximation whenever $K_M^{(1)} \approx K_M^{(2)}$, as stated in (35), which stimulates the assumption

$$E_0 + K_M^{(i)} \gg S_{1,0} + S_{2,0}, \quad i = 1, 2. \tag{B.5}$$

Our condition $|R_1| \ll |\psi_1(0)|$ then becomes

$$\frac{E_0}{(E_0 + \tilde{K}_M^{(1)})^2} \times \frac{K_M^{(1)}}{K_M^{(2)}} \left(\bar{S}_2 \frac{K_M^{(1)}}{K_M^{(2)}} + \bar{S}_1 \frac{E_0 + \tilde{K}_M^{(2)}}{E_0 + \tilde{K}_M^{(1)}}\right) \ll 1, \tag{B.6}$$

which is guaranteed by (B.5) if $K_M^{(1)}$ and $K_M^{(2)}$ are of similar magnitude.

The other condition, $|R_1| \ll \psi_1(S_1)$, is now

$$\left(\frac{E_0}{E_0 + \tilde{K}_M^{(1)}}\right)^2 \left(\frac{\bar{S}_2}{K_M^{(2)}} + \frac{\bar{S}_1}{K_M^{(1)}} \frac{E_0 + \tilde{K}_M^{(2)}}{E_0 + \tilde{K}_M^{(1)}}\right) \ll 1. \tag{B.7}$$

This is on the other hand not guaranteed by (B.5); we must require, for example, that

$$K_M^{(i)} \gg S_{i,0}. \tag{B.8}$$

Then (50) reduces to the single reaction first order tQSSA (9).

At high enzyme concentrations, but low $\bar{S}_i$ and $K_M^{(i)}$ values, we can estimate the error that we make by using the first order tQSSA. The remainder $R_1$ from (B.1) is negative, which implies that (49) is an underestimate. The relative error $err_{\text{rel}}$, given as the actual error $err \leq \bar{S}_1 - C_1$ divided by the maximal possible error $\bar{S}_1$, is then bounded by

$$err_{\text{rel}} \leq \frac{\bar{S}_1 - C_1}{\bar{S}_1} = \frac{K_M^{(1)}(1 + \bar{S}_2/K_M^{(2)}) + \bar{S}_1}{K_M^{(1)}(1 + \bar{S}_2/K_M^{(2)}) + \bar{S}_1 + E_0} \leq \frac{\tilde{K}_{M,0}^{(1)} + S_{1,0}}{\tilde{K}_{M,0}^{(1)} + S_{1,0} + E_0},$$

which is indeed small for large $E_0$, say

$$E_0 \gg \tilde{K}_{M,0}^{(i)} + S_{i,0}, \quad i = 1, 2. \tag{B.9}$$

Hence, only for an intermediate range of large, but not too large, values of $E_0$ is the first order approximation bad. When $K_M^{(1)} \approx K_M^{(2)}$, we can use (B.5) instead of (B.8) or (B.9) as a criterion for the first order approximation to be near the full tQSSA in agreement with (35).

**References**

Albe, K. R., Butler, M. H., Wright, B. E., 1990. Cellular concentrations of enzymes and their substrates. J. Theor. Biol. 143, 163–195.

Atkinson, D. E., 1977. Cellular Energy Metabolism and its Regulation. Academic Press, New York.

Baker, Jr., G. A., 1975. Essentials of Padé approximants. Academic Press, London.

Bhalla, U. S., Iyengar, R., 1999. Emergent properties of networks of biological signaling pathways. Science 283, 381–387.

Bisswanger, H., 2002. Enzyme Kinetics. Principles and Methods. Wiley-VCH.

Borghans, J., de Boer, R., Segel, L., 1996. Extending the quasi-steady state approximation by changing variables. Bull. Math. Biol. 58, 43–63.

Briggs, G. E., Haldane, J. B. S., 1925. A note on the kinetics of enzyme action. Biochem. J. 19, 338–339.

Burack, W. R., Sturgill, T. W., 1997. The activating dual phosphorylation of MAPK by MEK is nonprocessive. Biochemistry 36, 5929–5933.

Ferrell, J. E., Bhatt, R. R., 1997. Mechanistic studies of the dual phosphorylation of mitogen-activated protein kinase. J. Biol. Chem. 272, 19008–19016.

Goldbeter, A., Koshland, Jr., D. E., 1981. An amplified sensitivity arising from covalent modification in biological systems. Proc. Natl. Acad. Sci. 78, 6840–6844.

Henri, V., 1901a. Recherches sur la loi de l'action de la sucrase. C. R. Hebd. Acad. Sci. 133, 891–899.

Henri, V., 1901b. Über das gesetz der wirkung des invertins. Z. Phys. Chem. 39, 194–216.

Henri, V., 1902. Théorie générale de l'action de quelques diastases. C. R. Hebd. Acad. Sci. 135, 916–919.

Huang, C.-Y. F., Ferrell, J. E., 1996. Ultrasensitivity in the mitogen-activated protein kinase cascade. Proc. Natl. Acad. Sci. 93, 10078–10083.

Kholodenko, B. N., 2000. Negative feedback and ultrasensitivity can bring about oscillations in the mitogen-activated protein kinase cascades. Eur. J. Biochem. 267, 1583–1588.

Kishore, N., Sommers, C., Mathialagan, S., Guzova, J., Yao, M., Hauser, S., Huynh, K., Bonar, S., Mielke, C., Albee, L., Weier, R., Graneto, M., Hanau, C., Perry, T., Tripp, C. S., 2003. A selective IKK-2 inhibitor blocks NF-$\kappa$B-dependent gene expression in interleukin-1$\beta$-stimulated synovial fibroblasts. J. Biol. Chem. 278, 32861–32871.

Kvålseth, T. O., 1985. Cautionary note about $r^2$. The American Statistician 39, 279–285.

Markevich, N. I., Hoek, J. B., Kholodenko, B. N., 2004. Signaling switches and bistability arising from multisite phosphorylation in protein kinase cascades. J. Cell Biol. 164, 353–359.

Michaelis, L., Menten, M. L., 1913. Die kinetik der invertinwirkung. Biochem. Z. 49, 333–369.

Pedersen, M. G., Bersani, A. M., Bersani, E., 2006. Quasi steady-state approximations in intracellular signal transduction – a word of caution. Preprint

Me.Mo.Mat. no. 3/2006, Department of Mathematical Methods and Models, "La Sapienza" University, Rome, Italy.

Pi, N., Leary, J. A., 2004. Determination of enzyme/substrate specificity constants using a multiple substrate ESI-MS assay. J. Am. Soc. Mass Spectrom. 15, 233–243.

Rubinow, S., Lebowitz, J., 1970. Time-dependent Michaelis-Menten kinetics for an enzyme-substrate-inhibitor system. J. Am. Chem. Soc. 92, 3888–3893.

Schnell, S., Maini, P., 2000. Enzyme kinetics at high enzyme concentrations. Bull. Math. Biol. 62, 483–499.

Schnell, S., Maini, P., 2003. A century of enzyme kinetics: Reliability of the $k_m$ and $v_{max}$ estimates. Comm. Theor. Biol. 8, 169–187.

Schnell, S., Mendoza, C., 1997a. Closed form solution for time-dependent enzyme kinetics. J. Theor. Biol. 187, 207–212.

Schnell, S., Mendoza, C., 1997b. Enzymological considerations for a theoretical description of the quantitative competitive polymerase chain reaction (QC-PCR). J. Theor. Biol. 184, 433–440.

Schnell, S., Mendoza, C., 1997c. Theoretical description of the polymerase chain reaction. J. Theor. Biol. 188, 313–318.

Schnell, S., Mendoza, C., 2000. Time-dependent closed form solutions for fully competitive enzyme reactions. Bull. Math. Biol. 62, 321–336.

Segel, L., 1988. On the validity of the steady state assumption of enzyme kinetics. Bull. Math. Biol. 50, 579–593.

Segel, L. A., Slemrod, M., 1989. The quasi steady-state assumption: a case study in pertubation. SIAM Rev. 31, 446–477.

Sols, A., Marco, R., 1970. Concentration of metabolites and binding sites. Implications in metabolic regulation. In: Current topics in Cellular Regulation. Vol. 2. Academic Press, New York.

Stayton, M. M., Fromm, H. J., 1979. A computer analysis of the validity of the integrated Michaelis-Menten equation. J. Theor. Biol. 78, 309–323.

Straus, O. H., Goldstein, A., 1943. Zone behavior of enzymes. J. Gen. Physiol. 26, 559–585.

Turner, T. E., Schnell, S., Burrage, K., 2004. Stochastic approaches for modelling in vivo reactions. Comp. Biol. Chem. 28, 165–178.

Tzafriri, A. R., 2003. Michaelis-Menten kinetics at high enzyme concentrations. Bull. Math. Biol. 65, 1111–1129.

Tzafriri, A. R., Edelman, E. R., 2004. The total quasi-steady-state approximation is valid for reversible enzyme kinetics. J. Theor. Biol. 226, 303–313.

Tzafriri, A. R., Edelman, E. R., 2005. On the validity of the quasi-steady state approximation of bimolecular reactions in solution. J. Theor. Biol. 233, 343–350.

Zhao, Y., Zhang, Z.-Y., 2001. The mechanism of dephosphorylation of extracellular signal-regulated kinase 2 by mitogen-activated protein kinase phosphatase 3. J. Biol. Chem. 276, 32382–32391.

# *Paper VI*

# THE EFFECT OF NOISE ON $\beta$-CELL BURST PERIOD

MORTEN GRAM PEDERSEN* AND MADS PETER SØRENSEN*

**Abstract.** Bursting electrical behavior is commonly observed in a variety of nerve and endocrine cells, among these in electrically coupled $\beta$-cells located in intact pancreatic islets. However, individual $\beta$-cells usually display either spiking or very fast bursting behavior, and the difference between isolated and coupled cells has been suggested to be due to stochastic fluctuations of the plasma membrane ions channels, which are supposed to have a stronger effect on single cells than on cells situated in clusters (the channel sharing hypothesis). This effect of noise has previously been studied based on numerical simulations. We show here how the application of two recent methods allows an analytic treatment of the stochastic effects on the location of the saddle-node and homoclinic bifurcations, which determine the burst period. Thus, the stochastic system can be analyzed similarly to the deterministic system, but with a quantitative description of the effect of noise. This approach supports previous investigations of the channel sharing hypothesis.

**Key words.** bursting oscillations, stochastic Melnikov method, stochastic bifurcations

**AMS subject classifications.** 37H, 34F05, 60H10, 60H30, 92C

**1. Introduction.** The pancreatic $\beta$-cells are crucial for maintaining the blood sugar levels in a narrow range. When subjected to glucose the $\beta$-cells produce and secrete insulin, and the amount of secreted insulin correlates with the intracellular calcium levels [10].

*In situ* the $\beta$-cells are electrically coupled in the islets of Langerhans where they show bursting electrical activity with burst periods of tens of seconds. Bursting consists of the membrane potential alternating between a silent hyperpolarized phase, and an active phase of spiking rising from a depolarized plateau. During the active phase, calcium enters the cells, raises the intracellular $Ca^{2+}$ concentration and triggers insulin secretion. The plateau fraction, i.e., the ratio of the active phase duration to the burst period, is decisive for the intracellular $Ca^{2+}$ concentrations and for the amount of secreted insulin [2].

However, early recordings of single, isolated pancreatic $\beta$-cells showed that the membrane potential exhibits noisy spiking activity [19], and although it was later found that only approximately one third of isolated cells spike, while half of the single cells are fast bursters with burst period less than 5 seconds [11], there is a fundamental difference in the behavior of single and electrically coupled cells. Importantly, this difference is reflected in intracellular calcium levels [24].

It was early suggested that stochastic fluctuations of ion channels in the plasma membrane were responsible for disrupting the bursting behavior, and transform the isolated cells to spikers, but that the effective sharing of the channels by electrically coupled cells, averages the noise and let the bursting phenomena appear [3]. This was analyzed by Chay and Kang [4] and Sherman, Rinzel and Keizer [21] using mathematical modeling. The burst period and plateau fraction in the deterministic version of the Sherman-Rinzel-Keizer model was later analyzed by bifurcation analysis and Melnikov's method [16].

De Vries and Sherman [6] studied the electrical behavior of coupled pancreatic $\beta$-cells with focus of the *beneficial* influence of noise. It had previously been shown that weak coupling between identical, spiking cells can induce bursting [20], and it is now known that heterogeneous but spiking cells start to burst when coupled with physiologically realistic coupling strengths [7]. The main result presented in [6] is that noise dramatically increases the interval of coupling strengths for which bursting is seen for identical cells, and this observation was supported by analyzing a bifurcation diagram. It was later shown that the beneficial influence is more likely through heterogeneity masqueraded as noise, and that the explanation of the enhancement of emergent bursting must be modified accordingly [14].

The investigations of the effect of noise on beta-cells have so far been done partly by nu-

*Department of Mathematics, Technical University of Denmark, Matematiktorvet Building 303, 2800 Kgs. Lyngby, Denmark (m.g.pedersen@mat.dtu.dk, m.p.soerensen@mat.dtu.dk).

merically solving the stochastic differential equations (SDEs) describing the system, partly by analyzing *deterministic* bifurcation diagrams [1, 4, 6, 14, 21]. The transition from the SDEs to the bifurcation analysis was rather weakly motivated from a theoretical point of view.

We look for a more natural deterministic description of the stochastic system with the aim to characterize how noise shortens or interrupts bursting. This is based on the ideas from Pernarowski et al. [16] using a stochastic version of a polynomial, minimal model [15].

For the transition from the silent to the active phase, we consider the distribution of the solution over time, i.e., we follow the probability that the system is in a certain area of state space over time. The time evolution of the distribution is described by the Fokker-Planck Equation (FPE), which is a partial differential equation. Since bifurcation analysis is better performed on a system of ordinary differential equations (ODEs), and the FPE is computer expensive to solve, we assume that the distribution solving the FPE, and, hence, describing the system, is Gaussian at any point in time. Doing this, we obtain a set of ODEs describing how the the distribution evolves in time. This approach is based on work on models of noisy, spiking neurons [18, 22] and the ODEs describe the evolution of the mean and lower order moments of the assumed Gaussian distribution. A similar approach [12, 13] assumed a Gaussian-like distribution around the deterministic solution, and was used to describe a neural burster [13]. For the transition out of the active phase we use a stochastic Melnikov method [9], thus allowing us to use the ideas from [16] in a stochastic setting.

We find that noise shortens both the active and the silent phase, but has a stronger effect on the exit from the active phase than from the silent phase. Thus, we explain why simulations show that noise shortens the burst period and can transform normal bursters into fast bursters. This supports the idea that stochastic fluctuations in membrane ion channels can disrupt normal bursting and channel sharing restore it [3, 4, 21].

**2. The $\beta$-cell model with noise.** Pernarowski [15] introduced a minimal, deterministic, polynomial model capable of modeling both the spiking and the bursting phenomena seen in $\beta$-cells. The fact that the involved functions are polynomials will be of importance when describing the moments of the distribution [22]. The model is

$$\frac{d\,u}{dt} = f(u) - w - z, \tag{2.1a}$$

$$\frac{d\,w}{dt} = g(u) - w + \sigma\Gamma_t, \tag{2.1b}$$

$$\frac{d\,z}{dt} = \epsilon(h(u) - z), \tag{2.1c}$$

where we have added the white noise term $\Gamma_t$ to include noise, the strength of which is given by $\sigma$. $f$ and $g$ are third order polynomials, while $h$ is a first order polynomial. $u$ mimics the membrane potential of the cell, while $w$ is a fast gating variable. We assume that the ion-channel controlled by $w$ is fluctuating stochastically, and hence we add the noise term to this equation. $z$ is on the other hand a slow gating variable due to the small number $\epsilon$. Thus, we have a fast subsystem $(u, w)$ responsible for the spikes during an active phase of bursting, and a slow $z$ controlling the transition between the silent and active phases.

Following [15] we differentiate (2.1a) with respect to $t$ and then transform system (2.1) to

$$\frac{d^2u}{dt^2} + F(u)\frac{d\,u}{dt} + G(u) + z = -\epsilon(h(u) - z) - \sigma\Gamma_t, \tag{2.2a}$$

$$\frac{d\,z}{dt} = \epsilon(h(u) - z), \tag{2.2b}$$

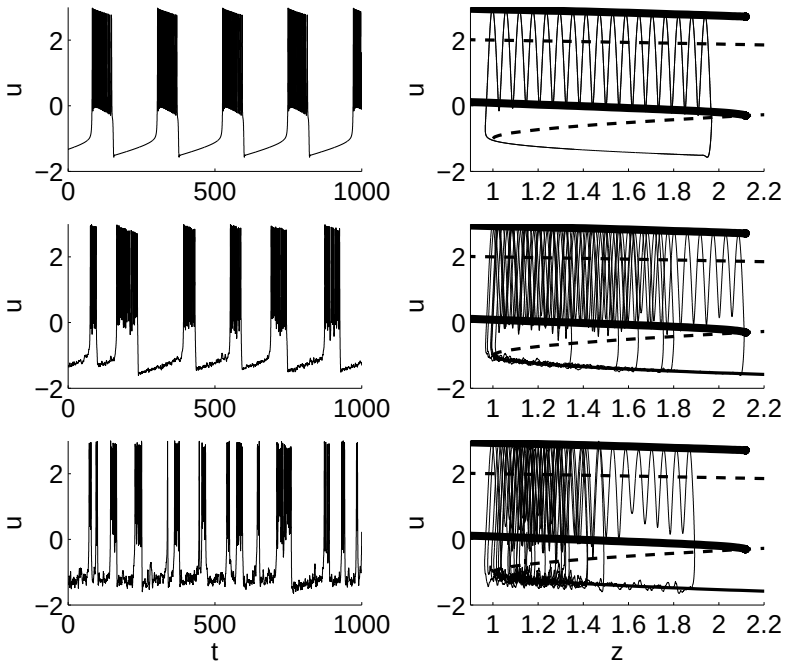


FIGURE 2.1. *Numerical simulations of bursting with different noise strengths. The left panels show time series of the membrane potential $u$, while the right panels show the corresponding projection on the $z-u$ plane and the deterministic bifurcation diagram from figure 2.2. The upper panels show the deterministic case $\sigma = 0$, in the center panels $\sigma = 0.1$, and in the lower panels $\sigma = 0.3$. Other parameters are here and through out the manuscript: $a = 0.25$, $\hat{u} = 1.6$, $\beta = 4$, $u_\beta = -0.954$, $\epsilon = 0.0025$, and $\eta = 0.7$.*

or, equivalently,

$$\frac{d\,u}{dt} = y, \tag{2.3a}$$

$$\frac{d\,y}{dt} = -F(u)y - G(u) - z - \epsilon(h(u) - z) - \sigma\Gamma_t, \tag{2.3b}$$

$$\frac{d\,z}{dt} = \epsilon(h(u) - z), \tag{2.3c}$$

where

$$F(u) = a\big((u-\hat{u})^2 - \eta^2\big), \tag{2.4}$$

$$G(u) = u^3 - 3(u+1), \tag{2.5}$$

$$h(u) = \beta(u - u_\beta). \tag{2.6}$$

With appropriate parameters, the system shows a bursting pattern, but increasing the strength of the noise shortens the bursts, see figure 2.1, left panels.

The deterministic system ($\sigma = 0$) can be analyzed from a bifurcation diagram of the fast subsystem with $z$ as the bifurcation parameter [15, 17]. This is done by setting $\epsilon = 0$. The fixpoints of the fast system falls on the Z-shaped curve $G(u, z) = 0$, see figure 2.2. The fast system is stable for low $z$ values, but increasing $z$, this stability is lost in a Hopf-bifurcation (HB). The fixpoints on the middle branch of the Z-shaped curve are saddle-points, while they are stable on the lower branch. The middle-branch meets the upper and lower branch in saddle-node bifurcations (SN). The Hopf-bifurcation gives rise to stable periodic solutions around the unstable fixpoints on the upper branch, but these periodics disappear in a homoclinic bifurcation (HC) for sufficiently large $z$. The mechanism underlying bursting is

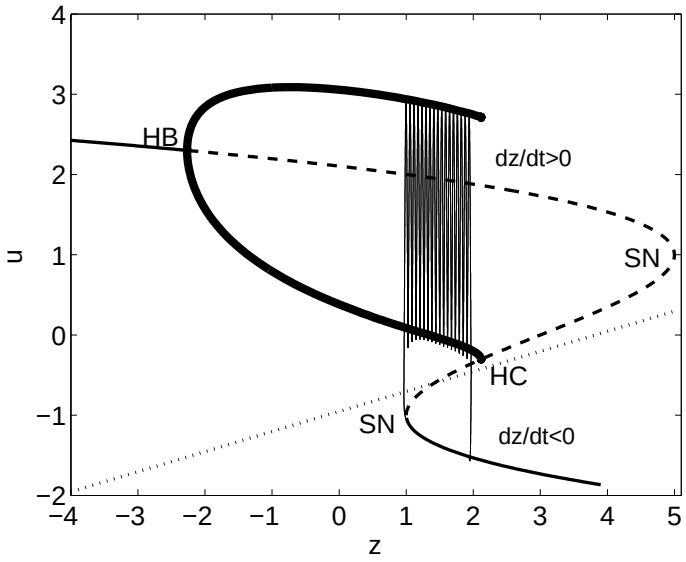


FIGURE 2.2. *Bifurcation diagram of the fast subsystem with $z$ as the bifurcation parameter. Thin, full curves indicate stable fixpoints; thin, broken curve correspond to unstable fixpoints and the thick, full curve shows the extrema of periodic solutions. The dotted curve shows the $z$-nullcline, $\frac{d\,z}{dt} = 0$. A simulation of the deterministic system is projected onto the $z - u$ plane for comparison. See the text for more details.*

based on the bistability between the stable fixpoints on the lower branch and the stable periodics for a range of $z$-values. When we reintroduce the slow variation of $z$ for $0 < \epsilon \ll 1$, we can explain bursting. When the system is near the lower branch, it moves slowly to the left since $u$ is low and thus $\frac{d\,z}{dt} < 0$ here. This continues until the stable branch disappears in the left saddle-node bifurcation. The system now leaves the lower branch (silent phase) and goes to the stable periodics (active phase), where $u$ is high and $\frac{d\,z}{dt} > 0$. Hence, the system now moves to the right until it meets the homoclinic bifurcation and the stable periodics disappear. The system then leaves the active phase and settles on the lower branch and the scenario is repeated.

This explanation gives a hint on how noise shortens the bursts. The random perturbations to the system can make it leave the silent as well as the active phase prematurely when the system is randomly kicked across the corresponding thresholds. When the noise intensity increases, this will happen more often since the kicks are stronger. In figure 2.1, right panels, we see that in general, the noisy system leaves the active phase prematurely, while the early exit from the silent phase is less pronounced. We now aim at understanding this observation better.

**3. Location of the left saddle-node bifurcation.** The exit from the silent phase happens near the left saddle-node bifurcation, see figure 2.2. We expect that for increasing noise, the bifurcation will effectively happen for larger $z$-values, since the noise will tend to push the system across the threshold and into the active phase prematurely.

To analyze this, we look at the distribution of the system under all possible realizations of the noise. Since the fluctuations of $u$ and $w$ are rather small during the active phase, we expect that for fixed $z$ ($\epsilon = 0$) the distribution will be approximately Gaussian. This allows us to use the so-called G-method [22], which is a development of the method from [18].

The idea is that a Gaussian distribution is described completely by its mean and covariance matrix. Hence we follow, for fixed $z$, the means $\bar{u} = \langle u \rangle$ and $\bar{y} = \langle y \rangle$, the variances $S_u = Var(u)$ and $S_v = Var(y)$ and the covariance $C = Cov(u, y)$.

Following [22], we average (2.3a), (2.3b) and the time derivative of the (co)variances $(u-\bar{u})^2$, $(y-\bar{y})^2$ and $(u-\bar{u})(y-\bar{y})$ using Itô's formula and the fact that the odd moments vanish for a Gaussian distribution. To illustrate the procedure, we derive the equation for $C$ in greater details as follows.

$$\begin{aligned}\frac{dC}{dt} &= \frac{d}{dt}\Big\langle (u-\bar{u})(y-\bar{y})\Big\rangle = \Big\langle \frac{d}{dt}[(u-\bar{u})(y-\bar{y})]\Big\rangle \\ &= \Big\langle (u-\bar{u})\frac{d\,(y-\bar{y})}{dt}\Big\rangle + \Big\langle (y-\bar{y})\frac{d\,(u-\bar{u})}{dt}\Big\rangle \\ &= \Big\langle (u-\bar{u})(-F(u)y - G(u) - z - \sigma\Gamma_t)\Big\rangle + \Big\langle (y-\bar{y})^2\Big\rangle \\ &= -\Big\langle (u-\bar{u})F(u)y\Big\rangle - \Big\langle (u-\bar{u})G(u)\Big\rangle + S_y.\end{aligned} \tag{3.1}$$

The first term is found from the Taylor polynomial of $F$ around $\bar{u}$,

$$\begin{aligned}&\Big\langle (u-\bar{u})F(u)y\Big\rangle \\ &= \Big\langle (u-\bar{u})\big((y-\bar{y})+\bar{y}\big)\big(F(\bar{u}) + F'(\bar{u})(u-\bar{u}) + \tfrac{1}{2}F''(\bar{u})(u-\bar{u})^2\big)\Big\rangle \\ &= F(\bar{u})C + F'(\bar{u})\bar{y}S_u + a\Big\langle (u-\bar{u})^3(y-\bar{y})\Big\rangle,\end{aligned} \tag{3.2}$$

where we have again used that the odd moments vanish. Finally, the last term of (3.2) is equal to $3aS_uC$ by the Gaussian joint variable theorem. The second term of (3.1) is treated similarly.

In summary, we obtain the equations,

$$\frac{d\,\bar{u}}{dt} = \bar{y}, \tag{3.3a}$$

$$\frac{d\,\bar{y}}{dt} = -F(\bar{u})\bar{y} - G(\bar{u}) - z - \big(F''(\bar{u})\bar{y} + G''(\bar{u})\big)\frac{S_u}{2} - F'(\bar{u})C, \tag{3.3b}$$

$$\frac{d\,S_u}{dt} = 2\,C, \tag{3.3c}$$

$$\frac{d\,S_y}{dt} = 2\,\big[-F(\bar{u})S_y - \big(F'(\bar{u})\bar{y} + G'(\bar{u})\big)\,C\,\big] + \sigma^2 - 6aS_u^2, \tag{3.3d}$$

$$\frac{d\,C}{dt} = S_y - \big(F'(\bar{u})\bar{y} + G'(\bar{u})\big)S_u - F(\bar{u})C - 3aS_uC. \tag{3.3e}$$

These are exact equations for the means and (co)variances due to $F$ and $G$ being polynomials [22]. Since the system (3.3) is deterministic, we can perform bifurcation analysis on these equations using $z$ as the bifurcation parameter. Starting from the silent phase $\bar{u} \approx -1, \bar{y} = S_u = S_y = C = 0$, we find a branch of stable fixpoints similar to the lower branch of Fig. 2.2 (not shown). This branch ends in a saddle-node bifurcation as for the deterministic case. However, the rest of the bifurcation structure breaks down, and the system (3.3) has, e.g., fixpoints with negative $S_y$ values, which are of course impossible solutions since $S_y$ is a variance. We believe that this break down is because the assumption of a Gaussian distribution holds only in the silent phase, and hence, the system (2.3) is no longer described by system (3.3) after leaving the lower branch. Nevertheless, the saddle-node where the silent phase branch ends can be followed in a two parameter bifurcation diagram with $\sigma$ as the other bifurcation parameter, see Fig. 3.1. For increasing noise intensity $\sigma$ the saddle-node moves to the right, indicating that the noisy system leaves the silent phase earlier for greater noise strength. This corresponds well to direct simulations of the $z$-value for which the noisy system (2.2) leaves the silent phase (Fig. 3.1).

**4. Location of the homoclinic bifurcation.** To follow the exit from the active phase for different noise intensities, we apply a stochastic Melnikov method. The deterministic Melnikov technique was first applied to $\beta$-cell models by Pernarowski et al. [16] and for the model we use here in [15].

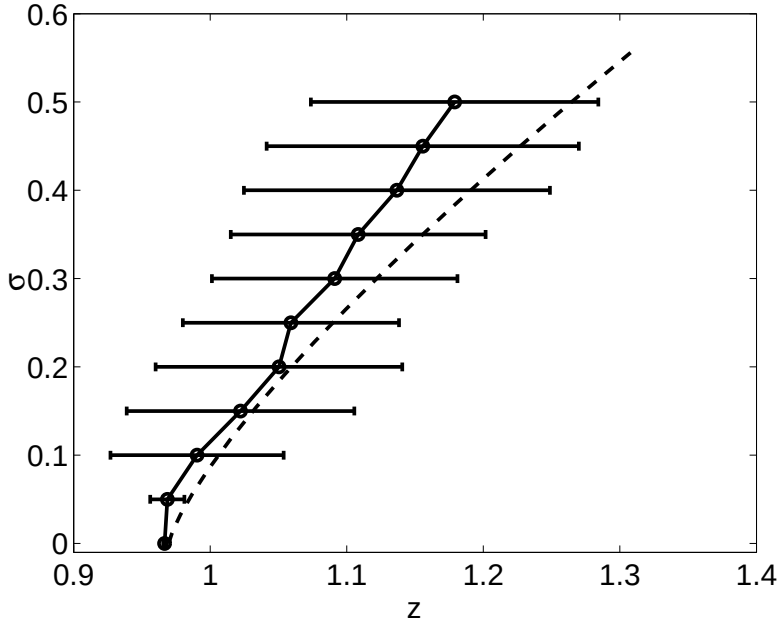


FIGURE 3.1. *Two-parameter bifurcation diagram showing the location of the saddle-node bifurcation where the silent phase branch for system* (3.3) *ends (broken curve). This bifurcation corresponds to the left saddle-node bifurcation in figure 2.2. Direct simulations of the noisy system* (2.2) *shows that the prediction from* (3.3) *is faithful, since the* $z$ *values for which the system* (2.2) *leaves the silent phase (measured as* $u$ *passing through the Poincaré section* $u = -0.55$ *from below) agree well. The bars are mean values of* $z \pm$ *one standard deviation for a simulation until* $t = 10000$*. We have shifted the broken curve 0.03 to the left, since the deterministic version overestimates the* $z$*-value by this amount.*

The Melnikov function is used to determine the distance between the stable and unstable manifolds of a saddle-point for systems, which are perturbations of a Hamiltonian system with a homoclinic saddle-point. In the deterministic case of the $\beta$-cell model, the active phase ends in a homoclinic bifurcation, which happens exactly when the stable and unstable manifolds of the saddle-point coincide, i.e., when the Melnikov function is zero.

We write (2.3) with $\epsilon = 0$ as

$$\frac{d\,u}{dt} = y, \tag{4.1}$$

$$\frac{d\,y}{dt} = -G(u) - z \; + \; [-F(u)y - \sigma\Gamma_t], \tag{4.2}$$

from which it is seen that the term in the square brackets is a perturbation of the Hamiltonian system $\frac{d^2u}{dt^2} + G(u) + z = 0$, which has a saddle-point $(a_s(z), 0)$ with a homoclinic orbit $(u_s, y_s)$ [5, 15]. The Hamiltonian is $H(p, u) = \frac{1}{2}p^2 + V(u; a_s(z))$ with potential

$$V(u, a_s) = \frac{1}{4}(u - a_s)^2[u^2 + 2a_s u + 3a_s^3 - 6]. \tag{4.3}$$

The homoclinic orbit can then be written as

$$(u_s, y_s) = (u_s, \pm\sqrt{-2V(u_s, a_s(z))}\,). \tag{4.4}$$

For the deterministic case, $\sigma = 0$, the square bracket in (4.1) is indeed small and the Melnikov function is [5, 15]

$$M_{det} = -a\left[e_2(a_s(z))(\hat{u}^2 - \eta^2) + e_1(a_s(z))\hat{u} + e_0(a_s(z))\right], \tag{4.5}$$

where

$$e_0(a_s) = -\frac{12}{5}\sqrt{3}(a_s^4 - 2a_s^2 - 4)\sqrt{1-a_s^2} + 6\sqrt{2}a_s(a_s^2-3)\Delta(a_s), \tag{4.6}$$

$$e_1(a_s) = 6\sqrt{3}a_s(3-a_s^2)\sqrt{1-a_s^2} + 3\sqrt{2}(a_s^2-3)(a_s^2+1)\Delta(a_s), \tag{4.7}$$

$$e_2(a_s) = 4\sqrt{3}\sqrt{1-a_s^2} + 2\sqrt{2}a_s(a_s^2-3)\Delta(a_s), \tag{4.8}$$

$$\Delta(a_s) = \cos^{-1}(2a_s/\sqrt{6-2a_s^2}). \tag{4.9}$$

We have changed sign of $M_{det}$ compared to [15] such that $M_{det} > 0$ when the unstable manifold is outside the stable manifold of the saddle-point [23].

The Melnikov function is related to the phase space flux, which is a measure of the transport across the pseudo separatix approximating the separatix of the Hamiltonian system [23]. For the $\beta$-cell model, we are interested in the transport from the inside to the outside of the pseudo separatix, since this will terminate the active phase. The flux is given by the area of the *turnstile lobe* [23], and to first order it is found as

$$\phi_{det} \approx \int_{t_1}^{t_2} M_{det}^+ dt = (t_2 - t_1)M_{det}^+, \tag{4.10}$$

since $M_{det}$ does not depend on $t$. Here and in the following $M^+ = \max\{0, M\}$ is the positive part of $M$, and $t_1$ and $t_2$ are the time points that define the lobe. Note that as long as $M_{det} < 0$, i.e., the unstable manifold lies inside the unstable manifold, $\phi_{det} = 0$ indicating that there is no transport (flux) from inside to outside the separatix, i.e., the system is trapped. For the beta-cell model it then follows the limit cycle characterizing the active phase, see Fig. 2.2.

Another related variable is the average phase space flux. To first order it is approximated by the flux factor given by [9]

$$\Phi_{det} = \lim_{T\to\infty} \frac{1}{2T}\int_{-T}^{T} M_{det}^+ dt = M_{det}^+. \tag{4.11}$$

When $1 \gg \sigma > 0$ in (4.1), we expect that the square bracket in (4.1) is still small, and that the stochastic Melnikov method can be applied. This approach uses a Melnikov process instead of the Melnikov function [9]. It is given by

$$M_{stoch}(t) = M_{det} + \sigma\Xi_t, \tag{4.12}$$

where $\Xi_t$ is a stochastic process with Gaussian distribution in the case of white noise perturbations $\Gamma_t$, which is the case considered here for the $\beta$-cell model. $\Xi_t$ has mean zero and variance

$$\sigma_\Xi^2 = \int_0^\infty |H(k)|^2 dk, \tag{4.13}$$

where $H(k) = \int_{\mathbb{R}} h(t)e^{-ikt}dt$ is the Fourier transform of $h(t) = y_s(-t)$. For the Hamiltonian system (4.1) $y_s$ is odd, and hence, also $h$ and $H$ are odd. By Parseval's equation and (4.4) we then get

$$\sigma_\Xi^2 = \tfrac{1}{2}\int_{\mathbb{R}} |H|^2 = \tfrac{1}{2}\,2\pi\int_{\mathbb{R}} |h|^2 = 2\pi\int_0^\infty |y_s|^2 = 2\pi\int_{a_s}^{b_s} \sqrt{-2V(u, a_s(z))}du, \tag{4.14}$$

where $b_s = -a_s + \sqrt{6-2a_s^2}$ is the largest zero of $V$, corresponding to the point $(b_s, 0)$ on the separatix $(u_s, y_s)$ furthest from the saddle-point [5]. Using standard tables we get the following expression from (4.3)

$$\sigma_\Xi^2 = \sqrt{2}\pi\Big(2\sqrt{6-6a_s^2} + a_s(a_s^2-3)(\pi - 2\sin^{-1}\frac{2a_s}{\sqrt{6-2a_s^2}}\,)\Big). \tag{4.15}$$

The saddle-point $a_s = a_s(z)$ can be determined analytically. Thus, we have a complete description of the Melnikov process (4.12).

The unstable and stable manifolds of the saddle-point intersect when $M_{stoch}(t_0)$ changes sign and becomes positive, and then the system can escape from the inside of the pseudo-separatix. Hence, we expect that the probability of terminating the active phase at $t_0$ is proportional to the probability $Pr(M_{stoch}(t_0) > 0)$.

Now, $X = \frac{M_{stoch}(t_0) - M_{det}}{\sigma\sigma_\Xi} \sim N(0,1)$ is a standard Gaussian variable, so the probability of ending the active phase at $t_0$ is roughly proportional to $Pr(X > \frac{-M_{det}}{\sigma\sigma_\Xi})$. It seems plausible that we need at least a certain probability $\alpha$ in order to effectively end the active phase during a spike period, and there seems to be no *a priori* reason why this probability should depend on $\sigma$. Note that for increasing $\sigma$ and $M_{det} < 0$, the probability $Pr(X > \frac{-M_{det}}{\sigma\sigma_\Xi})$ increases (for fixed $z$, and hence, $M_{det}$ and $\sigma_\Xi$), such that there is a higher probability of ending the active phase prematurely for higher noise strengths as expected (see Fig. 2.1). In the deterministic limit $\sigma \to 0$, this probability is either 0 (for $M_{det} < 0$) or 1 (for $M_{det} > 0$) in accordance with the above observations for the deterministic scenario.

Continuing this idea, we look for the $z$ value for which the active phase terminates. This is a stochastic event, but on average we expect it to be closely related to the probability discussed above. Since the relation $Pr(X > \frac{-M_{det}}{\sigma\sigma_\Xi}) = \alpha$ determines a fixed $\frac{-M_{det}}{\sigma\sigma_\Xi}$, we get that for larger $\sigma$, a larger value of $-M_{det}/\sigma_\Xi$ will be needed for the system to effectively leave the active phase. $-M_{det}/\sigma_\Xi$ is a decreasing function of $z$ (Fig. 4.1), so the escape from the active phase will happen before.

These considerations are supported by numerical simulations, which also confirm that the end of the active phase on average happens for a fixed value of $\frac{-M_{det}}{\sigma\sigma_\Xi} \approx 0.45$ (Fig. 4.1), corresponding to $Pr(X > \frac{-M_{det}}{\sigma\sigma_\Xi}) \approx 0.32$. However, for very low or high $\sigma$ this is not true. For high $\sigma$, the reason is that the system enters the active phase at $z > 1$, e.g., $z \approx 1.1$ for $\sigma = 0.3$ (Fig. 3.1). Hence, there is a lower limit on the $z$ value for which the escape can occur, and thus, the average value will be higher than predicted by the considerations above. For high $\sigma$ we are near the case where $M_{det} = 0$, and hence the considerations above might break down in this deterministic limit, especially considering the probability considerations. Moreover, the Melnikov approach predicts a too large $z$-value for which the system leaves the active phase, even for the deterministic case. This imprecision could be more important for low noise strengths.

The instant flux

$$\phi_{stoch} \approx M^+_{stoch} = (M_{det} + \sigma\Xi_t)^+ \tag{4.16}$$

is at every time $t$ a truncated normal distribution. It has mean equal to the (nonrandom) flux factor $\Phi_{stoch}$ given by [9]

$$\Phi_{stoch} = M_{det} + \sigma\sigma_\Xi f(-M_{det}/(\sigma\sigma_\Xi)) - M_{det}F(-M_{det}/(\sigma\sigma_\Xi)), \tag{4.17}$$

where $f = \frac{1}{\sqrt{2\pi}}e^{-z^2/2}$ is the standard Gaussian density, and $F(z) = \int_\infty^z f(x)dx$ is the corresponding distribution function. We remark that $\Phi_{stoch} \to M^+_{det} = \Phi_{det}$ for $\sigma \to 0$.

However, it is the flux during a finite interval that is relevant for the transition out of the active phase. This finite time flux varies randomly, and hence the mean flux $\Phi_{stoch}$ needs to be held against the variance of $\phi_{stoch}$ in order to determine when the system escapes from the active phase, in the same spirit as for $M_{stoch}$ above. The variance of $\phi_{stoch}$ is given by

$$\begin{aligned} Var\,(\phi_{stoch}) = \\ (\sigma\sigma_\Xi)^2\Bigg[\Big(1 + \big(\frac{M_{det}}{\sigma\sigma_\Xi}\big)^2\Big)\Big(1 - F\big(-\frac{M_{det}}{\sigma\sigma_\Xi}\big)\Big) + \frac{M_{det}}{\sigma\sigma_\Xi}f\big(-\frac{M_{det}}{\sigma\sigma_\Xi}\big) \\ - \Big(f\big(-\frac{M_{det}}{\sigma\sigma_\Xi}\big) + \frac{M_{det}}{\sigma\sigma_\Xi}\Big(1 - F\big(-\frac{M_{det}}{\sigma\sigma_\Xi}\big)\Big)\Big)^2\Bigg], \end{aligned} \tag{4.18}$$

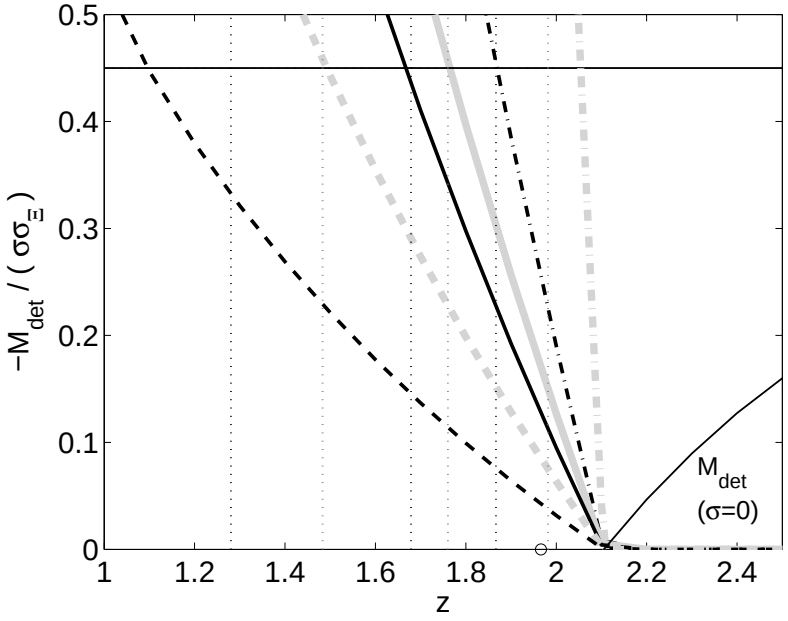


FIGURE 4.1. *Stochastic escape from the active phase is explained by the condition* $Pr(X > -\frac{-M_{det}}{\sigma\sigma_\Xi}) \approx 0.32$ *for* $X \sim N(0,1)$. *This corresponds to* $\frac{-M_{det}}{\sigma\sigma_\Xi} \approx 0.45$ *(horizontal, black line). The decreasing curves are* $\frac{-M_{det}}{\sigma\sigma_\Xi}$ *calculated for different* $z$*-values using* (4.5) *and* (4.15) *for different values of* $\sigma$*:* $0.3$ *(dashed, black curve),* $0.15$ *(dashed, grey curve),* $0.1$ *(full, black curve),* $0.075$ *(full, grey curve),* $0.05$ *(dash-dotted, black curve),* $0.01$ *(dash-dotted, grey curve). Each of the dotted vertical lines indicate for a value of* $\sigma$ *(from left to right:* $\sigma = 0.3, 0.15, 0.1, 0.075, 0.05, 0.01$*) the mean value of a series of* $z$ *values for which the system left the active phase, defined as passing from above to below* $u = -0.8$*, in a simulation of system* (2.3) *until* $t = 40000$*. For comparison, the full, increasing curve is the deterministic* $M_{det}$*. Note that* $M_{det}$ *does not pass through zero at the* $z$ *value (*$\circ$*) for which the deterministic system leaves the active phase. This mismatch between the homoclinic bifurcation and the simulated escape from the active phase is also seen in Figs. 2.1 and 2.2.*

and it is readily seen that $Var(\phi_{stoch}) \to 0$ for $\sigma \to 0$.

From simulations, it again appears that the end of the active phase happens for a roughly constant value of $\Phi_{stoch}/\sqrt{Var(\phi_{stoch})} \approx 0.182$ (Fig. 4.2). Thus, as seen above for the Melnikov process, the related approach using phase space flux predicts that the exit from the active phase occurs for a fixed value of the standardized variable $\frac{\phi_{stoch}-\Phi_{stoch}}{\sqrt{Var(\phi_{stoch})}}$.

**5. Discussion.** We have shown that the escape from the silent as well as from the active phase of the noisy $\beta$-cell model can be studied analytically. For the silent phase we used a collective coordinate approach by assuming a Gaussian distribution and the G-method [18, 22]. We could then follow the saddle-node bifurcation at which the silent phase terminates as the noise strength $\sigma$ varies (Fig. 3.1). For the active phase we used a stochastic Melnikov approach [9], which is new in the context of noisy bursting. We gave an explanation of why a fixed value of $\frac{-M_{det}}{\sigma\sigma_\Xi}$ would predict the $z$ value, for which the system would leave the active phase for different values of $\sigma$. The value of $Pr(X > -\frac{-M_{det}}{\sigma\sigma_\Xi}) \approx 0.32$ is not obvious, and it should be interesting to see if it holds for other stochastic systems that are nearly Hamiltonian.

Noise has a bigger influence on the exit from the active phase than on the escape from the silent phase. However, the plateau fraction is roughly unchanged, since a faster escape from the active phase corresponds to the system entering the silent phase later and vice versa. This is in agreement with the fact that although single cells have shorter burst periods, the plateau fraction is similar to that of intact islets [11].

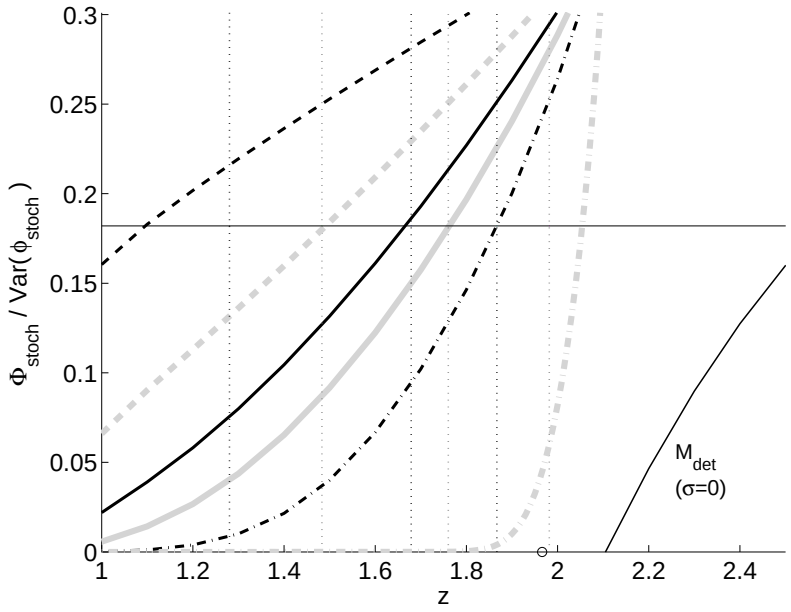


FIGURE 4.2. *Stochastic escape from the active phase is explained by* $\Phi_{stoch}/Var(\phi_{stoch}) \approx 0.182$ *(horizontal, black line). The thick curves show* $\Phi_{stoch}/Var(\phi_{stoch})$ *with the same legends and range of* $\sigma$ *values as in Fig. 4.1. They were calculated from* (4.15), (4.17) *and* (4.18)*. The full curve is* $M_{det}$ *and vertical lines are means of simulated* $z$ *values as in Fig. 4.1.*

Assuming that single cells and small clusters of $\beta$-cells have shorter burst periods due to noise, the channel sharing hypothesis can explain why. As seen in both simulations as well as the treatment presented here, the stronger the noise intensity, the lower the burst period. If we assume that the cells are coupled with infinite coupling strength (the super-cell hypothesis) [4, 21], then in larger groups of cells, the noisy channels will be shared among several cells, and the individual cell would feel smaller fluctuations than if it was isolated, leading to longer burst periods. Extending the methods presented here to groups of coupled cells with finite coupling strength would be interesting in an attempt to gain deeper insight in previously published results [1, 6, 14].

All simulations and bifurcation diagrams were done using XPPAUT [8].

REFERENCES

[1] J. AGUIRRE, E. MOSEKILDE, AND M.A. SANJUAN, *Analysis of the noise-induced bursting-spiking transition in a pancreatic beta-cell model*, Phys. Rev. E, 69 (2004), p. 041910.
[2] F.M. ASHCROFT AND P. RORSMAN, *Electrophysiology of the pancreatic $\beta$-cell*, Prog. Biophys. Mol. Biol., 54 (1989), pp. 87–143.
[3] I. ATWATER, L. ROSARIO, AND E. ROJAS, *Properties of the Ca-activated K+ channel in pancreatic beta-cells.*, Cell Calcium, 4 (1983), pp. 451–461.
[4] T. R. CHAY AND H. S. KANG, *Role of single-channel stochastic noise on bursting clusters of pancreatic $\beta$-cells*, Biophys. J., 54 (1988), pp. 427–435.
[5] G. DE VRIES, *Multiple bifurcations in a polynomial model of bursting oscillations*, J. Nonlinear Sci., 8 (1998), pp. 281–316.
[6] G. DE VRIES AND A. SHERMAN, *Channel sharing in pancreatic $\beta$-cells revisited: Enhancement of emergent bursting by noise*, J. Theor. Biol., 207 (2000), pp. 513–530.
[7] ———, *From spikers to bursters via coupling: Help from heterogeneity.*, Bull. Math. Biol., 63 (2001), pp. 371–391.
[8] G.B. ERMENTROUT, *Simulating, analyzing, and animating dynamical systems: A guide to XPPAUT for researchers and students*, SIAM Books, Philadelphia, 2002.
[9] M. FREY AND E. SIMIU, *Noise-induced chaos and phase space flux*, Physica D, 63 (1993), pp. 321–340.
[10] J.C. JONAS, P. GILON, AND J.C. HENQUIN., *Temporal and quantitative correlation between insulin*

*secretion and stably elevated or oscillatory cytoplasmic $Ca^{2+}$ in mouse pancreatic $\beta$-cells*, Diabetes, 47 (1998), pp. 1266–1273.

[11] T.A. KINARD, G. DE VRIES, A. SHERMAN, AND L.S. SATIN, *Modulation of the bursting properties of single mouse pancreatic beta-cells by artificial conductances*, Biophys. J., 76, pp. 1423–1435.

[12] R. KUSKE, *Probability densities for noisy delay bifurcations*, J. Stat. Phys., 96 (1999), pp. 797–816.

[13] R. KUSKE AND S.M. BAER, *Asymptotic analysis of noise sensitivity in a neuronal burster*, Bull. Math. Biol, 64 (2002), pp. 447–481.

[14] M.G. PEDERSEN, *A comment on noise enhanced bursting in pancreatic beta-cells*, J. Theor. Biol., 235 (2005), pp. 1–3.

[15] M. PERNAROWSKI, *Fast subsystem bifurcations in a slowly varying Liénard system exhibiting bursting*, SIAM J. Appl. Math., 54 (1994), pp. 814–832.

[16] M. PERNAROWSKI, R.M. MIURA, AND J. KEVORKIAN, *Perturbation techniques for models of bursting electrical activity in pancreatic $\beta$-cells*, SIAM J. Appl. Math., 52 (1992), pp. 1627–1650.

[17] J. RINZEL, *Bursting oscillations in an excitable membrane model*, in Ordinary and Partial Differential Equations, B.D. Sleeman and R.J. Jarvis, eds., Springer-Verlag, New York, 1985, pp. 304–316.

[18] R. RODRIGUEZ AND H.C. TUCKWELL, *Statistical properties of stochastic nonlinear dynamical models of single spiking neurons and neural networks*, Phys. Rev. E, 54 (1996), pp. 5585–5590.

[19] P. RORSMAN AND G. TRUBE, *Calcium and delayed potassium currents in mouse pancreatic $\beta$-cells under voltage clamp conditions*, J. Physiol. (London), 374 (1986), pp. 531–550.

[20] A. SHERMAN AND J. RINZEL, *Model for synchronization of pancreatic beta-cells by gap junction coupling*, Biophys. J., 59 (1991), pp. 547–559.

[21] A. SHERMAN, J. RINZEL, AND J. KEIZER, *Emergence of organized bursting in clusters of pancreatic $\beta$-cells by channel sharing*, Biophys. J., 54 (1988), pp. 411–425.

[22] S. TANABE AND K. PAKDAMAN, *Dynamics of moments of FitzHugh-Nagumo neuronal models and stochastic bifurcations*, Phys. Rev. E, 63 (2001), p. 031911 (9 pages).

[23] S. WIGGINS, *Chaotic Transport in Dynamical Systems*, Springer-Verlag, New York, 1992.

[24] M. ZHANG, P. GOFORTH, R. BERTRAM, A. SHERMAN, AND L. SATIN., *The $Ca^{2+}$ dynamics of isolated mouse $\beta$-cells and islets: Implications for mathematical models*, Biophys. J., 84 (2003), pp. 2852–2870.

# *Paper VII*

# A Simplified Model for Mitochondrial ATP Production

Richard Bertram[a], Morten Gram Pedersen[b], Dan S. Luciani[c], and Arthur Sherman[d]

May 16, 2006

[a] Department of Mathematics and Programs in Neuroscience and Molecular Biophysics, Florida State University, Tallahassee, Florida, [b] Department of Mathematics, Technical University of Denmark, Kgs. Lyngby, Denmark, [c] Department of Cellular and Physiological Sciences, University of British Columbia, Vancouver, Canada, [d] Laboratory of Biological Modeling, National Institutes of Health, Bethesda, Maryland

**Corresponding Author:**

Richard Bertram
Department of Mathematics
Florida State University
Tallahassee, Florida 32306, USA
email: bertram@math.fsu.edu
tel: (850)-644-7195
fax: (850)-644-4053

**Abstract**

Most of the adenosine triphosphate (ATP) synthesized during glucose metabolism is produced in the mitochondria through oxidative phosphorylation. This is a complex reaction powered by the proton gradient across the mitochondrial inner membrane, which is generated by mitochondrial respiration. A detailed model of this reaction, which includes dynamic equations for the key mitochondrial variables, was developed earlier by Magnus and Keizer. However, this model is extraordinarily complicated. We develop a simpler model that captures the behavior of the original model but is easier to use and to understand. We then use it to investigate the mitochondrial responses to glycolytic and calcium input. We use the model to explain experimental observations of the opposite effects of raising cytosolic $Ca^{2+}$ in low and high glucose, and to predict the effects of a mutation in the mitochondrial enzyme nicotinamide nucleotide transhydrogenase (Nnt) in pancreatic $\beta$-cells.

**Keywords**: metabolism, calcium, mathematical model

# 1 Introduction

The mitochondria are the primary location for the production of energy-carrying molecules in most cells. Metabolism begins in the cytoplasm with glycolysis, where glucose is metabolised to the primary product pyruvate. The pyruvate enters the mitochondria through shuttles, where it is processed by the citric acid cycle. The coenzymes nicotinamide adenine dinucleotide ($NAD^+$) and flavin adenine dinucleotide (FAD) are reduced during the citric acid cycle, yielding NADH and $FADH_2$ (some NADH is also generated during glycolysis). These electron carriers are used by the electron transport chain, which supplies the energy to establish a proton gradient across the inner membrane of the mitochondria. The gradient is used to power the last stage of metabolism, oxidative phosphorylation. Protons flowing down this gradient through the ATP synthase complex provide the energy to phosphorylate adenosine diphosphate (ADP) to adenosine triphosphate (ATP). This is the primary means through which the energy molecule ATP is produced in most eukaryotic cells.

In a series of papers in the late 1990's, Magnus and Keizer developed mathematical models of oxidative phosphorylation (Magnus and Keizer, 1997; Magnus and Keizer, 1998a; Magnus and Keizer, 1998b). These models were developed in the context of the insulin-secreting pancreatic $\beta$-cell, and were coupled to models of the cell's electrical activity and cytosolic $Ca^{2+}$ handling. The Magnus-Keizer model includes most of the processes thought to be important for mitochondrial oxidative phosphorylation, and indeed, the completeness of the Magnus-Keizer model is one of its strengths. The model was later used and modified by Cortassa *et al.* (2003) to describe metabolism in cardiac cells. The Cortassa model also makes some improvements to the Magnus-Keizer (M-K) model and includes a model for the citric acid cycle (which we do not use here).

The M-K model was derived from first principles, and as a result it is very complex. Many of the properties of the model, such as whether a flux term increases or decreases when the value of a variable or parameter is changed, are masked

by this complexity. Our first goal is to develop a simplified model for oxidative phosphorylation that retains the key features of the M-K model, yet is more intuitive. A description of this simplified model, and comparison with the M-K model as modified by Cortassa *et al.*, is the focus of the first portion of the article.

In the second portion, we use the simplified model to study the response of the mitochondrial variables to pulses of calcium and a variable reflecting glycolytic flux, both of which are inputs to mitochondrial metabolism. This yields predictions about whether the mitochondrial variables increase or decrease in response to the input. Measurements have been made of the levels of NAD(P)H, oxygen, and the mitochondrial inner membrane potential in, for example, pancreatic $\beta$-cells. Besides the clinical significance of these insulin-secreting cells, they are interesting since glucose metabolism is important not only for the survival of the $\beta$-cell, but also for its electrical activity and patterned insulin release.

We next use the model to investigate a recent experimental result from mouse pancreatic islets that has been hard to explain. It was found that elevations in the intracellular $Ca^{2+}$ concentration increase the intracellular NADH concentration when the islet is maintained in a low glucose bath. In higher glucose, a $Ca^{2+}$ concentration increase results in a reduction in the NADH concentration (Luciani *et al.*, 2006). Our model provides a plausible mechanism for this.

Finally, we consider the effects of a negative mutation in the mitochondrial enzyme nicotinamide nucleotide transhydrogenase (Nnt). Such a mutation causes glucose intolerance and impaired $\beta$-cell function in the widely-used C57BL/6J mouse strain (Toye *et al.*, 2005). In the simplified model, simulation of the Nnt mutation is accomplished by increasing the proton leak across the mitochondrial inner membrane. Increase of this single parameter results in changes in the mitochondrial variables that would not be obvious without a mathematical model. This illustrates one of the strengths of the simplified model: its relative simplicity makes it possible to predict and understand the effects of changes in one or more parameters or

variables. This is particularly important when the mitochondrial model is just one component of a larger cellular model.

## 2 Dynamic Equations

We begin by describing the dynamic equations for the mitochondrial variables $NADH_m$, $ADP_m$, $\Delta\Psi$, and $Ca_m$. These equations are themselves simple. However, the flux and reaction terms that make up the equations are quite complex in the M-K model, and it is those that we simplify in the following section.

The first stage of glucose metabolism in eucaryotic cells is glycolysis, which takes place in the cytoplasm. Although this produces some ATP and NADH, its primary output is pyruvate. The pyruvate is transported into the mitochondria where it is rapidly decarboxylated by the pyruvate dehydrogenase complex (PDH). The products of PDH are a molecule of $CO_2$, a molecule of NADH, and acetyl coenzyme A (acetyl CoA). The NADH concentration is decreased by the action of the electron transport chain, during which NADH is converted to $NAD^+$ and oxygen is consumed:

$$\frac{d\,NADH_m}{d\,t} = \gamma(J_{PDH} - J_o) \ , \tag{1}$$

where $NADH_m$ is the mitochondrial NADH concentration, $J_{PDH}$ is the PDH reaction rate, and $J_o$ is the oxygen consumtion rate. Both rates have units of $\mu$M/ms. The time $t$ is measured in ms, and $\gamma = 0.001$ converts $NADH_m$ to units of mM.

The mitochondrial ADP concentration increases due to the action of the adenine nucleotide transporter, which transports ATP out of and ADP into the mitochondria. ADP concentration decreases due to the action of the ATP synthase, which phosphorylates ADP to ATP. Thus,

$$\frac{d\,ADP_m}{d\,t} = \gamma(J_{ANT} - J_{F1F0}) \ , \tag{2}$$

where $ADP_m$ is the mitochondrial ADP concentration (with units of mM), $J_{ANT}$

is the nucleotide transport rate, and $J_{F1F0}$ is the ATP synthase rate (both in $\mu$M/ms). We assume that the mitochondrial concentrations of adenine and pyridine nucleotides are conserved:

$$NAD_m + NADH_m = NAD_{tot} \quad (3)$$

$$ADP_m + ATP_m = A_{tot} \ , \quad (4)$$

where $NAD_{tot}$ and $A_{tot}$ are the total concentrations (in mM, see Table 1).

The inner membrane potential, $\Delta\Psi$, is influenced by many fluxes and reactions:

$$\frac{d\,\Delta\Psi}{d\,t} = \left(J_{H,res} - J_{H,atp} - J_{ANT} - J_{H,leak} - J_{NaCa} - 2J_{uni}\right)/C_m \quad (5)$$

where $J_{H,res}$ is the respiration-driven proton flux, $J_{H,atp}$ is the proton flux through the ATP synthase, $J_{H,leak}$ is the proton leak across the mitochondrial inner membrane, $J_{NaCa}$ is the $Ca^{2+}$ efflux through the electrogenic $Na^+/Ca^{2+}$ exchanger, and $J_{uni}$ is the $Ca^{2+}$ influx through the $Ca^{2+}$ uniporter. The mitochondrial capacitance is $C_m$, and $\Delta\Psi$ has units of mV.

Finally, the $Ca^{2+}$ concentration in the mitochondria ($Ca_m$) is increased by the $Ca^{2+}$ uniporter and decreased by the Na/Ca exchanger:

$$\frac{d\,Ca_m}{d\,t} = f_m(J_{uni} - J_{NaCa}) \ , \quad (6)$$

where $f_m$ is the fraction of free $Ca^{2+}$.

Rather than using pyruvate concentration as input to PDH, the glyceraldehyde 3-phosphate dehydrogenase (GPDH) activity is used in our description. This is a glycolytic enzyme downstream of the key allosteric enzyme phosphofructokinase (PFK) in the glycolytic pathway. Thus, the GPDH reaction rate reflects the flux through the glycolytic pathway. We assume that the GPDH reaction is in rapid equilibrium (Tornheim, 1979), so it can be described by an algebraic function of the substrate fructose 1,6-bisphosphate (FBP),

$$J_{GPDH} = k_{GPDH}\sqrt{(FBP)/(1\mu M)} \quad (7)$$

where FBP has units of $\mu$M and $J_{GPDH}$ has units of $\mu$M ms$^{-1}$. The cytosolic $Ca^{2+}$ concentration, $Ca_c$, is another input to mitochondrial respiration, since cytosolic $Ca^{2+}$ enters the mitochondria through $Ca^{2+}$ uniporters, and affects the mitochondrial dehydrogenases and the inner membrane potential.

The end product of metabolism is ATP. Thus, the output variable for mitochondrial metabolism is the mitochondrial ATP concentration. This is turn determines the cytosolic ATP concentration, through the action of the adenine nucleotide translocator. Input, output, and mitochondrial variables are illustrated in Fig. 1. Also illustrated is the oxygen flux, since this is a measureable quantity.

# 3 Model Simplification

In this section we describe the flux and reaction rates used in the dynamic equations from the previous section. We begin the descriptions of the terms with mathematical expressions from Cortassa *et al.* (2003), which are themselves modifications of expressions from the Magnus-Keizer model (Magnus and Keizer, 1998a; Magnus and Keizer, 1998b). The Cortassa expressions are used since they have been somewhat improved over those from the Magnus-Keizer model. We still, however, refer to these as "M-K expressions" or "M-K functions" since the orginal formulation was by Magnus and Keizer.

We begin with the pyruvate dehydrogenase (PDH) reaction rate, $\hat{J}_{PDH}$. (The hat superscript is used here to distinguish the M-K expression from our simplified expression.) This reaction decarboxylates pyruvate, but since we use GPDH as input to the mitochondria, we use the GPDH reaction rate (Eq. 7) as input to PDH. PDH is also known to be stimulated by mitochondrial $Ca^{2+}$. We modify the M-K expression for $\hat{J}_{PDH}$ by adding an explicit dependence on the ratio of product NADH to substrate $NAD^+$. The modified expression for the PDH reaction rate (in

units of $\mu$M/ms) is:

$$\hat{J}_{PDH} = (V_{PDH} F_{PDH} J_{GPDH})/\gamma_2 \tag{8}$$

where $V_{PDH} = 77$ $\mu$M/s, $\gamma_2 = 0.1$ is the mitochondria/cytosol volume ratio, and $J_{GPDH}$ is the GPDH reaction rate. (Cortassa *et al.* converted M-K parameter values to SI units. We use these parameter values, and convert from mM to $\mu$M.) Finally,

$$F_{PDH} = \frac{1}{1 + u_2 \left[ (1 + u_1 (1 + \frac{Ca_m}{K_{PDHca}})^{-2}) / (\frac{NADH_m}{NAD_m} + K_{PDHnad}) \right]} \quad . \tag{9}$$

Here $u_1 = 1.5$, $u_2 = 1.0$, $K_{PDHca} = 0.05$ $\mu$M and $K_{PDHnad} = 1$.

The simplified PDH reaction rate function that we use is:

$$J_{PDH} = \left( \frac{p_1}{p_2 + \frac{NADH_m}{NAD_m}} \right) \left( \frac{Ca_m}{p_3 + Ca_m} \right) J_{GPDH} \quad . \tag{10}$$

Values for the three parameters ($p_1$, $p_2$, $p_3$), as well as other parameter values for the simplified model, are given in Table 1. The PDH reaction rate computed with the two models is shown in Fig. 2. The top panel shows that $J_{PDH}$ increases linearly with $J_{GPDH}$, and $J_{PDH}$ computed with Eq. 10 (dashed curve) closely matches that computed with Eq. 8 (solid curve). The dependence on NADH is shown in Fig. 2B, with the total NAD concentration ($NADH_m$+$NAD_m$) held constant at 10 mM. The PDH rate decreases when $NADH_m$ is increased (and $NAD_m$ decreased) since $NAD^+$ is a substrate for PDH. The dependence of $J_{PDH}$ on the mitochondrial $Ca^{2+}$ concentration is shown in Fig. 2C. The dehydrogenase rate increases with $Ca_m$, but saturates at relatively low values of $Ca_m$. This $Ca^{2+}$ dependence becomes important later, when we study the effects of input pulses on the mitochondrial variables.

Oxygen is consumed during the final stage of electron transport, and this reflects conversion of NADH to $NAD^+$ by the loss of electrons. The expression for $O_2$ consumption ($J_o$) is quite complex in the M-K model, with dependency on $NAD^+$, NADH, and the proton motive force ($\Delta\mu_H$):

$$\hat{J}_o = \frac{0.5\rho_{res}(A - B + C)}{D} \tag{11}$$

where

$$A = K_{res}(r_a + r_{c1}e^{6\Delta\Psi_B FRT})\sqrt{NADH_m/NAD_m} \quad (12)$$

$$B = r_a e^{6g\Delta\mu_H FRT} \quad (13)$$

$$C = r_{c2}K_{res}e^{6g\Delta\mu_H FRT}\sqrt{NADH_m/NAD_m} \quad (14)$$

$$D = (1 + r_1 K_{res}\sqrt{NADH_m/NAD_m})e^{6\Delta\Psi_B FRT} + (r_2 + r_3 K_{res}\sqrt{NADH_m/NAD_m})e^{6g\Delta\mu_H FRT} \quad . \quad (15)$$

Here $\rho_{res} = 0.6036$ $\mu$M, $K_{res} = 1.35 \times 10^{18}$, $r_a = 6.394 \times 10^{-13}$ ms$^{-1}$, $r_{c1} = 2.656 \times 10^{-22}$ ms$^{-1}$, $r_{c2} = 8.632 \times 10^{-30}$ ms$^{-1}$, $\Delta\Psi_B = 50$ mV, $FRT = \frac{F}{RT} = 0.037$ $mV^{-1}$ is Faraday's constant divided by the gas constant and temperature, $g = 0.85$, $r_1 = 2.077 \times 10^{-18}$, $r_2 = 1.728 \times 10^{-9}$, and $r_3 = 1.059 \times 10^{-26}$. See Magnus and Keizer (1998a) or Cortassa *et al.* (2003) for a description of parameters. The proton motive force, $\Delta\mu_H$, includes both the membrane potential, $\Delta\Psi$, and a contribution due to the proton concentration gradient, $\Delta pH$:

$$\Delta\mu_H = \Delta\Psi + \frac{\Delta pH}{FRT} \quad , \quad (16)$$

where $\Delta pH = -0.6$.

Our simplified expression for $J_o$ is:

$$J_o = \left(\frac{p_4 NADH_m}{p_5 + NADH_m}\right)\left(\frac{1}{1 + \exp((\Delta\Psi - p_6)/p_7)}\right) \quad . \quad (17)$$

Figure 3 shows the $O_2$ consumption rates calculated from Eq. 11 and Eq. 17, with $p_4$–$p_7$ adjusted to match the M-K curves. The consumption rate declines for large $\Delta\Psi$ (Fig. 3A), since it is more difficult to pump protons against a large potential (metabolic control). The consumption rate increases with the NADH concentration (Fig. 3B), since NADH is an electron donor.

As oxygen is consumed by the electron transport chain, protons are pumped across the inner mitochondrial membrane. Thus, the respiration-driven proton flux, $J_{H,res}$, is linked to $O_2$ consumption. Both NADH and FADH are electron donors, but

in the M-K model NADH is the primary donor. We therefore omit the contribution to $J_{H,res}$ from FADH. The M-K expression for the contribution to $J_{H,res}$ from NADH is:

$$\hat{J}_{H,res} = \frac{6\rho_{res}(E-F)}{D} \tag{18}$$

where

$$E = r_a K_{res}\sqrt{NADH_m/NAD_m} \tag{19}$$

$$F = (r_a + r_b)e^{(6g\Delta\mu_H FRT)} \tag{20}$$

and $D$ is given by Eq. 15. The simplified expression for $J_{H,res}$ is similar to that for $J_o$,

$$J_{H,res} = \left(\frac{p_8 NADH_m}{p_9 + NADH_m}\right)\left(\frac{1}{1+\exp((\Delta\Psi - p_{10})/p_{11})}\right) \quad . \tag{21}$$

Figure 4 shows $J_{H,res}$ calculated from both Eq. 18 and Eq. 21. As expected, the dependence of this flux term on $\Delta\Psi$ and $NADH_m$ is similar to that of $J_o$ (Fig. 3).

Adenosine diphosphate is converted to adenosine triphosphate using the energy provided by the flow of protons down their concentration gradient through the $F_1F_0$ ATP-synthase. This is the step at which most of the ATP is formed during glucose metabolism. Proton flux through the ATP-synthase in the M-K model is:

$$\hat{J}_{H,atp} = -3\rho^{F1}\frac{G-H}{K+L} \tag{22}$$

where $\rho^{F1} = 1.787$ mM is the concentration of the ATP-synthase, and

$$G = 100p_a(1+e^{A_{F1}FRT}) \tag{23}$$

$$H = -(p_a + p_b)\, e^{3\Delta\mu_H FRT} \tag{24}$$

$$K = (1+q_1 e^{A_{F1}FRT})\, e^{3\Delta\Psi_B FRT} \tag{25}$$

$$L = (q_2 + q_3 e^{A_{F1}FRT})\, e^{3\Delta\mu_H FRT} \tag{26}$$

and where

$$A_{F1} = \ln\left(K_{F1}\frac{ADP_m}{P_i\, ADP_m}\right)/FRT \quad . \tag{27}$$

Parameter values are $p_a = 1.656 \times 10^{-8}$ ms$^{-1}$, $p_b = 3.373 \times 10^{-10}$ ms$^{-1}$, $q_1 = 1.346 \times 10^{-8}$, $q_2 = 7.739 \times 10^{-7}$, $q_3 = 6.65 \times 10^{-15}$, $K_{F1} = 1.71 \times 10^{6}$, and $P_i = 20$ mM is the inorganic phosphate concentration.

In the simplified expression for $J_{H,atp}$ there is an increasing sigmoidal dependence on $\Delta\Psi$ and a weak decreasing dependence on $ATP_m$:

$$J_{H,atp} = \left(\frac{p_{13}}{p_{13} + ATP_m}\right)\left(\frac{p_{12}}{1 + \exp((p_{14} - \Delta\Psi)/p_{15})}\right) . \quad (28)$$

Graphs of the M-K (Eq. 22) and simplified (Eq. 28) expression are compared in Fig. 5.

The M-K expression for the phosphorylation rate of ADP by the ATP-synthase, $J_{F1F0}$, is:

$$\hat{J}_{F1F0} = -\rho^{F1}\frac{M - N}{K + L} \quad (29)$$

where

$$M = (100p_a + p_{c1}e^{3\Delta\Psi_B FRT})e^{A_{F1}FRT} \quad (30)$$

$$N = p_a e^{3\Delta\mu_H FRT} + p_{c2}e^{A_{F1}FRT}e^{3\Delta\mu_H FRT} \quad (31)$$

and $K$ and $L$ are given by Eq. 25, 26. Because the phosphorylation rate of ADP is determined by the proton flux through the synthase, the simplified expression for $J_{F1F0}$ is similar to that of $J_{H,atp}$. In fact, $J_{F1F0}$ is a constant multiple of $J_{H,atp}$:

$$J_{F1F0} = \left(\frac{p_{13}}{p_{13} + ATP_m}\right)\left(\frac{p_{16}}{1 + \exp((p_{14} - \Delta\Psi)/p_{15})}\right) . \quad (32)$$

The ADP phosphorylation rates computed with Eqs. 29 and 32 are shown in Fig. 6.

There is a small leak of protons across the inner mitochondrial membrane, which is larger for larger values of the electrical potential. This is linear in the M-K model:

$$\hat{J}_{H,leak} = g_H\Delta\mu_H , \quad (33)$$

where $g_H = 2 \times 10^{-3}$ $\mu$M ms$^{-1}$ mV$^{-1}$. In our model we use the linear function

$$J_{H,leak} = p_{17}\Delta\Psi + p_{18} . \quad (34)$$

Note that we have replaced the pH dependence with a constant factor $p_{18}$. The fluxes computed using Eqs. 33 and 34 are shown in Fig. 7.

The ATP produced in the mitochondria is transported to the cytosol through the adenine nucleotide translocator. This is a carrier that exchanges one molecule of mitochondrial $ATP^{4-}$ for one molecule of cytosolic $ADP^{3-}$. It tends to keep the ATP/ADP ratio in the cytosol equal to that in the mitochondria. In the M-K formulation the flux rate, $J_{ANT}$, is:

$$\hat{J}_{ANT} = V_{maxANT} \frac{RAT_m - 0.8\, RAT_c}{(1 + 0.11 RAT_c)(RAT_m + 7.2) e^{(-0.5\, FRT\, \Delta\Psi)}} \tag{35}$$

where $V_{maxANT} = 5\ \mu\text{Mms}^{-1}$ is the maximum flux rate, and

$$RAT_m = \frac{ATP_m}{ADP_m} \tag{36}$$

$$RAT_c = \frac{ATP_c}{ADP_c} \tag{37}$$

are the nucleotide ratios in the mitochondria and the cytosol, respectively. Figure 8 shows the dependence of $J_{ANT}$ on the mitochondrial nucleotide ratio and on the inner membrane potential. Since the transporter maintains $RAT_c \approx RAT_m$, we assume that $RAT_c = RAT_m$ in the figure. The transporter is driven at a higher rate when the mitochondrial ATP/ADP ratio is larger (Fig. 8A), and the transport rate increases with the inner membrane potential (Fig. 8B). In the simplified expression, we set $RAT_c = RAT_m$ and replace the dependence on $RAT_m$ with a simpler functional form:

$$J_{ANT} = p_{19} \left( \frac{RAT_m}{RAT_m + p_{20}} \right) e^{0.5 FRT\, \Delta\Psi} \quad . \tag{38}$$

The $Ca^{2+}$ uniporter carries $Ca^{2+}$ from the cytosol into the mitochondrion and depends on the electrical driving force $\Delta\Psi$. This is described in the M-K model by:

$$\hat{J}_{uni} = V_{maxUni} \left( \frac{O}{P + Q} \right) \quad , \tag{39}$$

where

$$O = 2FRT\,(\Delta\Psi_m - \Delta\Psi^o)\frac{Ca_c}{K_{trans}}\left(1+\frac{Ca_c}{K_{trans}}\right)^3 \quad (40)$$

$$P = \left(1+\frac{Ca_c}{K_{trans}}\right)^4 \quad (41)$$

$$Q = \frac{L_1(1-e^{-2FRT\,(\Delta\Psi_m-\Delta\Psi^o)})}{\left(1+\frac{Ca_c}{K_{act}}\right)^{n_a}} \ . \quad (42)$$

The maximum transport rate is $V_{maxUni} = 10$ $\mu$Mms$^{-1}$, and $K_{trans} = 19$ $\mu$M, $K_{act} = 0.38$ $\mu$M, $L = 110$, $\Delta\Psi^o = 91$ mV is the offset membrane potential, and $Ca_c$ is the cytosolic $Ca^{2+}$ concentration. The uniporter flux is greatly simplified with the expression

$$J_{uni} = (p_{21}\Delta\Psi - p_{22})\,Ca_c^2 \ . \quad (43)$$

The original and simplified expressions for the uniporter rate are shown in Fig. 9. The rate increases when either the inner membrane potential or the cytosolic $Ca^{2+}$ concentration increase.

The final flux term is for the $Na^+/Ca^{2+}$ exchanger, which transports $Ca^{2+}$ out of the mitochondria while bringing $Na^+$ in. The original M-K expression for $\hat{J}_{NaCa}$ was modified by Cortessa *et al.* to include a dependence on the mitochondrial $Ca^{2+}$ concentration. The reformulated expression for $\hat{J}_{NaCa}$ is

$$\hat{J}_{NaCa} = V_{maxNaCa}\frac{\left(\frac{Ca_m}{Ca_c}\right)\,e^{b\,FRT\,(\Delta\Psi-\Delta\Psi^o)}}{\left(1+\frac{K_{Na}}{Na_c}\right)^3\left(1+\frac{K_{Ca}}{Ca_m}\right)} \quad (44)$$

where $Na_c = 10$ mM is the $Na^+$ concentration in the cytosol, $V_{maxNaCa} = 0.06$ $\mu$Mms$^{-1}$, $b = 0.5$, $K_{Na} = 9.4$ mM, and $K_{Ca} = 3.75 \times 10^{-4}$ mM. The simplified expression retains the dependence on $Ca_c$, $Ca_m$, and $\Delta\Psi$:

$$J_{NaCa} = p_{23}\left(\frac{Ca_m}{Ca_c}\right)e^{p_{24}\Delta\Psi} \ . \quad (45)$$

Figure 10 shows $J_{NaCa}$ over a range of values of its three variables. It is assumed that the cytosolic $Na^+$ concentration is constant. There is a positive dependence on the inner membrane potential (Fig. 10A). As expected from the nature

of the $Na^+/Ca^{2+}$ exchanger, the flux is greater when the cytosolic $Ca^{2+}$ concentration is lower (Fig. 10B), or when the mitochondrial $Ca^{2+}$ concentration is greater (Fig. 10C).

# 4 Mitochondrial Responses to Input

An increase in the glucose concentration increases the glycolytic flux, leading to an increase in the FBP concentration. In addition, glycolysis has been shown to be oscillatory in some cases (Tornheim and Lowenstein, 1974; Longo *et al.*, 1991), resulting in periodic pulses of FBP. We next examine the affect that a single FBP pulse has on the mitochondrial variables.

Figure 11 shows the responses to steps in the FBP concentration to 5, 10, or 15 $\mu$M (Fig. 11A), with the cytosolic $Ca^{2+}$ concentration held constant at 0.1 $\mu$M. Each step provides fuel for the mitochondria, so there is a resulting increase in $NADH_m$ (Fig. 11C). The elevated $NADH_m$ increases respiration, increasing the oxygen consumption (Fig. 11E). The increased respiration hyperpolarizes the inner membrane (Fig. 11D), resulting in increased ATP production through the $F_1F_0$ ATP synthase (Fig. 11F). The hyperpolarized membrane also increases the $Ca^{2+}$ uniporter flux rate (Fig. 9), leading to a slight increase in the mitochondrial $Ca^{2+}$ concentration (Fig. 11B). Since respiration saturates at large NADH concentrations (Fig. 4), reflecting metabolic control, there is a saturation of $J_o$, $\Delta\Psi$, and $ATP_m$ for the higher FBP concentrations.

Calcium concentration changes in the cytosol typically occur as the result of ion channel openings or $Ca^{2+}$ release from the endoplasimic reticulum. In many cases, $Ca_c$ is elevated due to bursts of action potentials. In Figure 12 we show the response of the model to three 30-sec $Ca_c$ pulses, with FBP concentration held constant at 5 $\mu$M. Each pulse could reflect a burst of action potentials, which is typically tens of seconds in duration in pancreatic $\beta$-cells (Zhang *et al.*, 2003).

The entry of $Ca^{2+}$ across the inner mitochondrial membrane affects the mitochondria in two ways: the flux of positive ions depolarizes the inner membrane (the electrical effect), and the increase in $Ca_m$ activates PDH, increasing $NADH_m$ and leading to hyperpolarization of the membrane (the dehydrogenase effect). In Fig. 12 we show the results of these combined actions (solid curves), as well as the electrical effect in isolation (dashed curves), obtained by setting $p_3 = 0$, which removes the dehydrogenase effect. Panel C shows that the $Ca^{2+}$ pulses increase $NADH_m$ (solid curve), as expected from the dehydrogenase effect. This transiently enhances respiration, as shown by increases in the oxygen consumption (Fig. 12E). The enhanced respiration hyperpolarizes the inner membrane (Fig. 12D), increasing the ATP production (Fig. 12F). Thus, the $Ca^{2+}$ pulses produce upward "teeth" in the mitochondrial variables and the $O_2$ flux. However, when $p_3 = 0$, isolating the electrical effect, the $Ca^{2+}$ pulses transiently depolarize the inner membrane (Fig. 12D, dashed) and reduce ATP production (Fig. 12F, dashed). Thus, the teeth in the mitochondrial variables are reversed when the dehydrogenase effect is removed, and measurements of $\Delta\Psi$ or $ATP_m$ in response to $Ca^{2+}$ pulses could be used to determine which of the two competing effects of $Ca^{2+}$ flux dominates within the mitochondria.

The direction of the teeth in $\Delta\Psi$ and $ATP_m$ can also be flipped from up to down by increasing the flux rate of the $Ca^{2+}$ uniporter $J_{uni}$. In Fig. 13 we show the response of the system to $Ca^{2+}$ pulses with the default parameter values (solid curves, the control) and with the uniporter flux parameter $p_{21}$ increased from 0.01 to 0.02 $\mu M^{-1} ms^{-1} mV^{-1}$ (dashed curves). This two-fold increase in the parameter value results in an approximately four-fold increase in $Ca_m$ during the sequence of $Ca_c$ pulses (Fig. 13B). The basal level of $Ca_m$ is also elevated, so that the basal level of $NADH_m$ is higher than the control. In fact, the stimulatory effect of $Ca^{2+}$ on PDH is nearly saturated even at the basal level of $Ca_m$, so the size of the upward $NADH_m$ teeth is significantly less than the control (Fig. 13C). This is reflected in the oxygen consumption (Fig. 13E), since the smaller $NADH_m$ teeth stimulate less respiration.

Along with the blunted stimulatory effect of $Ca^{2+}$ on PDH, there is now greater $Ca^{2+}$ flux across the membrane during the $Ca^{2+}$ pulses. Hence, the depolarizing electrical effect of $Ca^{2+}$ is enhanced while the hyperpolarizing dehydrogenase effect is reduced. The net effect is that the $\Delta\Psi$ teeth are now downward (depolarizing) rather than upward (Fig. 13D). Consequently, the $ATP_m$ teeth are also downward (Fig. 13F). In summary, any maneuver that saturates the stimulatory effect of $Ca^{2+}$ on PDH while increasing $Ca^{2+}$ influx across the inner membrane has the potential of reversing the $\Delta\Psi$ and $ATP_m$ teeth from upward to downward.

In a recent *in vitro* experimental study of metabolism in pancreatic islets, the NAD(P)H level was measured simultaneously with the cytosolic $Ca^{2+}$ concentration (Luciani *et al.*, 2006). (NAD(P)H is the sum of the NADH and NADPH concentrations.) When islets were maintained in a low glucose concentration (3 mM) and then depolarized by adding 30 mM KCl to the bath, both the $Ca^{2+}$ concentration and the NAD(P)H concentration (measured through autofluorescence) increased. An example is shown in Fig. 14A. The experiment was repeated in islets maintained in a high glucose concentration (10 mM). At this level of glucose the islet $Ca^{2+}$ concentration oscillates due to bursting electrical activity, so the pharmacological agent diazoxide was added to the bath to hyperpolarize the islets and thus bring $Ca_c$ to a steady low level. When the islets were then depolarized with 30 mM KCl the $Ca^{2+}$ concentration increased as expected. However, the NAD(P)H concentration decreased (Fig. 14B). Thus, an increase in the cytosolic $Ca^{2+}$ concentration elevates the NAD(P)H concentration in low glucose, but lowers it in high glucose.

The small decreases in $NADH_m$ during $Ca^{2+}$ pulses in Fig. 12C in the case where the dehydrogenase effect was removed provides some hope that the model may be able to explain the results of Fig. 14. That is, if the electrical effect of $Ca^{2+}$ dominates the dehydrogenase effect, then an increase in $Ca_m$ should be able to produce downward $NADH_m$ teeth, consistent with Fig. 14B. To accentuate the electrical effect we used larger pulses of $Ca_c$ than in previous simulations (pulsing

from 0.1 $\mu$M to 2 $\mu$M). From the $NADH_m$ differential equation (Eq. 1), we see that $NADH_m$ can decline only if the change in $J_o$ is greater than the change in $J_{PDH}$ during the $Ca^{2+}$ pulses. Figure 15E shows that in the low glucose simulation (FBP=1 $\mu$M), the downward $\Delta\Psi$ teeth have little effect on $J_o$. In fact, the change in $J_{PDH}$ is larger, so the $NADH_m$ teeth are upward (Fig. 15A). In contrast, in the high glucose simulation (FBP=10 $\mu$M), the downward $\Delta\Psi$ teeth cause a significantly greater increase in $J_o$ (Fig. 15F), so that now the change in $J_o$ is greater than the change in $J_{PDH}$ during a $Ca^{2+}$ pulse. As a result, the $NADH_m$ teeth are downward (Fig. 15B). Thus, the model is able to account for the experimental data in Fig. 14. The model is also consistent with the finding that the $Ca^{2+}$-induced decline in NAD(P)H in high glucose is converted to an increase in NAD(P)H when the electron trasport chain (ETC) is blocked (Luciani *et al.*, 2006). Blocking the ETC depolarizes the mitochondrial inner membrane and reduces the magnitude of the $Ca^{2+}$-induced increase in $J_o$.

Given the complexity of mitochondrial metabolism, it is hard to predict the effects of genetic mutations in mitochondrial enzymes without a mathematical model. The current model facilitates such predictions. As an example, we consider the nuclear-encoded mitochondrial enzyme Nicotinamide Nucleotide Transhydrogenase (Nnt). This enzyme detoxifies reactive oxygen species (ROS) which, when elevated, can reduce mitochondrial ATP production (Hoek and Rydstrom, 1988). The accumulation of ROS increases the activity of uncoupling protein 2, resulting in enhanced proton leakage across the inner membrane (Remedi *et al.*, 2006). Thus, mutations in Nnt that diminish its activity will lead to an increase in proton leakage.

How would a mutation in Nnt affect the $Ca^{2+}$ response of the mitochondrial variables? To simulate a negative Nnt mutation we increased the proton leak rate tenfold by increasing $p_{17}$ from 0.002 to 0.02 $\mu Mms^{-1}mV^{-1}$. As expected, one effect is to reduce the inner membrane potential, and thus the mitochondrial ATP concentration. What is not so obvious is that the Nnt mutation also increases the size

of the teeth in $\Delta\Psi$ and $ATP_m$ (Fig. 16). Thus, the effect of $Ca^{2+}$ feedback onto metabolism is amplified in this mutation. This effect, which is due to metabolic control, would likely have been overlooked without a mathematical model.

# 5 Discussion

The simplified model for mitochondrial ATP production that we have described has several advantages over the original Magnus-Keizer or Cortassa *et al.* models upon which it was based. The relative simplicity of the model makes it possible to readily determine the effects of the mitochondrial input on each of the flux and reaction terms. This facilitates comprehension of the model. It is also clear from the new model how changes in parameter values will affect the flux and reaction terms. This helped considerably when trying to reproduce the reversal of the $NADH_m$ teeth in low vs. high glucose (Figs. 14, 15). Also, the simplicity of the model facilitates model studies of mitochondrial gene mutations, and the effects of pharmacological agents that target the mitochondria. Finally, the simplified model may be preferable to more complex models when it forms only a portion of a larger cellular model. Indeed, this was part of our motivation, since our long-term goal is to incorporate all stages of glucose metabolism into a model of metabolic and calcium oscillations in the pancreatic $\beta$-cell.

Our model simulations focused largely on the response of the mitochondrial variables to pulses of $Ca^{2+}$. Our interest in this is driven by several studies in which mitochondrial variables (or oxygen consumption) were measured in pancreatic islets. In one study, the mitochondrial membrane potential was measured with rhodamine 123 simultaneously with the cytosolic $Ca^{2+}$ concentration, which was measured using fura-2/AM (Krippeit-Drews *et al.*, 2000). During glucose stimulation a series of $Ca_c$ pulses were observed, corresponding to bursts of action potentials. Teeth in $\Delta\Psi$ were clearly evident, with each $\Delta\Psi$ deflection correlated with a $Ca_c$ pulse. In this

case, the $\Delta\Psi$ teeth were downward, suggesting that the electrical effect of $Ca^{2+}$ on the mitochondria dominated the dehydrogenase effect. In another study in which $Ca^{2+}$ and $\Delta\Psi$ were measured simultaneously, elevations in the $Ca^{2+}$ concentration through various means depolarized the mitochondrial membrane when the glucose concentration was at a stimulatory level. In basal glucose, elevations in the $Ca^{2+}$ concentration had the opposite effect (Kindmark *et al.*, 2001). Again, this suggests that the teeth are upward (hyperpolarizing) when the dehydrogenase effect dominates, and downward (depolarizing) when the electrical effect dominates (e.g., when the dehydrogenase is saturated, as could occur when the glucose concentration is high). In another study (Jung *et al.*, 2000), an oxygen microsensor was used to measure oxygen levels in mouse islets. The cytosolic $Ca^{2+}$ concentration was measured simultaneously. Teeth in the oxygen consumption were observed, with each tooth (increase in oxygen consumption) corresponding to a $Ca_c$ pulse. Each $Ca_c$ pulse is likely due to a burst of action potentials. Oxygen teeth were again seen in a later study by the same lab (Dahlgren *et al.*, 2005).

Finally, we point out that while our simplified mitochondrial model has many applications, the more complex models of Magnus-Keizer or Cortassa *et al.* have the advantage that the parameters represent specific biophysical rates. Thus, one could develop improved models by obtaining more accurate measurements of the various rate constants. Our parameters, in contrast, are based on curve fitting to the model of Cortassa *et al.* If an improved detailed mitochondrial model were developed, one could again use a curve-fitting approach to develop a simplified model that is more physiologically accurate than ours. We believe that both detailed and simplified mitochondrial models are useful in understanding the function of mitochondria and how they interact with other components of the cell.

**Acknowledgments** R.B. was partially supported by National Science Foundation grant DMS-0311856. M.G.P. and D. S. L. were partially supported by the European

Union through the Network of Excellence BioSim, LSHB-CT-2004-005137. A.S. was supported by the intramural research program of the National Institutes of Health, National Institute of Diabetes and Digestive and Kidney Diseases.

## References

[1] Cortassa, S., M. A. Aon, E. Marban, R. L. Winslow and B. O'Rourke. 2003. An integrated model of cardiac mitochondiral energy metabolism and calcium dynamics. *Biophys. J.* **84**, 2734–2755.

[2] Dahlgren, G. M., L. M. Kauri and R. T. Kennedy. 2005. Substrate effects on oscillations in metabolism, calcium and secretion in single mouse islets of langerhans. *Biochem. Biophys. Res. Commun.* **1724**, 23–36.

[3] Hoek, J. B. and J. Rydstrom. 1988. Physiological roles of nicotinamide nucleotide transhydrogenase. *Biochem. J.* **254**, 1–10.

[4] Jung, S.-K., L. M. Kauri, W.-J. Qian and R. T. Kennedy. 2000. Correlated oscillations in glucose consumption, oxygen consumption, and intracellular free $Ca^{2+}$ in single islets of Langerhans. *J. Biol. Chem.* **275**, 6642–6650.

[5] Kindmark, H., M. Köhler, G. Brown, R. Bränström, O. Larsson and P.-O. Berggren. 2001. Glucose-induced oscillations in cytoplasmic free $ca^{2+}$ concentration precede oscillations in mitochondrial membrane potential in the pancreatic $\beta$-cell. *J. Biol. Chem.* **276**, 34530–34536.

[6] Krippeit-Drews, P., M. Düfer and G. Drews. 2000. Parallel oscillations of intracellular calcium activity and mitochondrial membrane potential in mouse pancreatic $\beta$-cells. *Biochem. Biophys. Res. Commun.* **267**, 179–183.

[7] Longo, E. A., K. Tornheim, J. T. Deeney, B. A. Varnum, D. Tillotson, M. Prentki and B. E. Corkey. 1991. Oscillations in cytosolic free $Ca^{2+}$, oxygen con-

sumption, and insulin secretion in glucose-stimulated rat pancreatic islets. *J. Biol. Chem.* **266**, 9314–9319.

[8] Luciani, D. S., S. Misler and K. S. Polonsky. 2006. $Ca^{2+}$ controls slow NAD(P)H oscillations in glucose-stimulated mouse pancreatic islets. *J. Physiol.* **572**, 379–392.

[9] Magnus, G. and J. Keizer. 1997. Minimal model of $\beta$-cell mitochondrial $Ca^{2+}$ handling. *Am. J. Physiol.* **273**, C717–C733.

[10] Magnus, G. and J. Keizer. 1998a. Model of $\beta$-cell mitochondrial calcium handling and electrical activity. I. Cytoplasmic variables. *Am. J. Physiol.* **274**, C1158–C1173.

[11] Magnus, G. and J. Keizer. 1998b. Model of $\beta$-cell mitochondrial calcium handling and electrical activity. II. Mitochondrial variables. *Am. J. Physiol.* **274**, C1174–C1184.

[12] Remedi, M. S., C. G. Nichols and J. C. Koster. 2006. The mitochondria and insulin release: Nnt just a passing relationship. *Cell Metab.* **3**, 5–7.

[13] Tornheim, K. 1979. Oscillations of the glycolytic pathway and the purine nucleotide cycle. *J. theoret. Biol.* **79**, 491–541.

[14] Tornheim, K. and J. M. Lowenstein. 1974. The purine nucleotide cycle. IV. Interactions with oscillations of the glycolytic pathway in muscle extracts. *J. Biol. Chem.* **249**, 3241–3247.

[15] Toye, A. A., J. D. Lippiat, P. Proks, K. Shimomura, L. Bentley, A. Hugill, V. Mijat, M. Goldsworthy, L. Moir, A. Haynes, J. Quarterman, H. C. Freeman, F. M. Ashcroft and R. D. Cox. 2005. A genetic and physiological study of impaired glucose homeostasis control in C57BL/6J mice. *Diabetologia* **48**, 675–686.

[16] Zhang, M., P. Goforth, R. Bertram, A. Sherman and L. Satin. 2003. The $Ca^{2+}$ dynamics of isolated mouse $\beta$-cells and islets: Implications for mathematical models. *Biophys. J.* **84**, 2852–2870.

**Fig. 1:** Input and output of mitochondrial respiration, and mitochondrial variables present in the model. Oxygen consumption, $J_o$, is also illustrated since it is an observable quantity.

**Fig. 2:** PDH reaction rate computed with Eq. 8 (solid curves) and the simplified expression (Eq. 10, dashed curves). **(A)** $J_{PDH}$ increases linearly with $J_{GPDH}$. ($NADH_m$ = 0.3 mM, $Ca_m$ = 0.2 $\mu$M.) **(B)** The reaction rate decreases when $NADH_m$ is increased and $NAD_m$ is decreased, maintaining $NADH_m + NAD_m$ = 10 mM ($J_{GPDH}$ = 1.5 $\mu$M/s, $Ca_m$ = 0.2 $\mu$M). **(C)** The dehydrogenase saturates at higher values of $Ca_m$ ($NADH_m$ = 0.3 mM, $J_{GPDH}$ = 1.5 $\mu$M/s).

**Fig. 3:** Oxygen consumption rate, calculated with the M-K expression (Eq. 11, solid curves) and with the simplified expression (Eq. 17, dashed curves). **(A)** $J_o$ declines with $\Delta\Psi$, reflecting metabolic control ($NADH_m$ = 0.3 mM). **(B)** $J_o$ increases with NADH, the electron donor to the electron transport chain ($\Delta\Psi$ = 160 mV).

**Fig. 4:** Proton flux across the inner mitochondrial membrane due to respiration, calculated with the M-K expression (Eq. 18) and the simplified expression (Eq. 21). **(A)** $J_{H,res}$ decreases with $\Delta\Psi$, reflecting metabolic control ($NADH_m$ = 0.3 mM). **(B)** Proton flux increases with an increase in the concentration of the electron donor to the electron transport chain. ($\Delta\Psi$ = 160 mV.)

**Fig. 5:** Proton flux through the ATP-synthase, calculated with the M-K expression (Eq. 22, solid curves) and with the simplified expression (Eq. 28, dashed curves). **(A)** $J_{H,atp}$ increases with the electrical gradient, $\Delta\Psi$. ($ATP_m$ = 3 mM.) **(B)** $J_{H,atp}$ declines as the concentration of the reaction product increases. ($\Delta\Psi$ = 160 mV.)

**Fig. 6:** Phosphorylation rate of the ATP synthase, calculated with the M-K ex-

pression (Eq. 29, solid curves) and with the simplified expression (Eq. 32, dashed curves). **(A)** Phosphorylation is powered by the electrical gradient, and thus increases with $\Delta\Psi$. ($ATP_m = 3$ mM.) **(B)** $J_{F1F0}$ declines as the concentration of the reaction product is increased. ($\Delta\Psi = 160$ mV.)

**Fig. 7:** Proton leakage across the inner membrane increases with the electrical potential. Computed with Eq. 33 (solid curves), and with Eq. 34 (dashed curves).

**Fig. 8:** Flux through the adenine nucleotide translocator, calculated with the M-K expression (Eq. 35, solid curves) and the simplified expression (Eq. 38, dashed curves). **(A)** Flux increases with the ATP concentration, and thus with the ATP/ADP ratio. ($\Delta\Psi = 160$ mV.) **(B)** Flux increases with the inner membrane potential ($\mathrm{RAT}_m = 5$).

**Fig. 9:** The uniporter transport rate, calculated with the M-K expression (Eq. 39, solid curves) and the simplified expression (Eq. 43, dashed curves). **(A)** The transport rate increases with the inner membrane potential ($\mathrm{Ca}_c$=0.2 $\mu$M), and **(B)** with the cytosolic $Ca^{2+}$ concentration ($\Delta\Psi = 160$ mV).

**Fig. 10:** The $Na^+/Ca^{2+}$ exchanger flux, calculated with the M-K expression (Eq. 44, solid curves) and the simplified expression (Eq. 45, dashed curves). **(A)** The flux has a positive dependence on the inner membrane potential. ($\mathrm{Ca}_c$=0.2 $\mu$M, $\mathrm{Ca}_m$=0.2 $\mu$M.) **(B)** $J_{NaCa}$ decreases with the cytosolic $Ca^{2+}$ concentration ($\mathrm{Ca}_m$=0.2 $\mu$M, $\Delta\Psi = 160$ mV), and increases with the mitochondrial $Ca^{2+}$ concentration ($\mathrm{Ca}_c$=0.2 $\mu$M, $\Delta\Psi = 160$ mV).

**Fig. 11:** The effects of FBP steps on the mitochondrial variables. The cytosolic $Ca^{2+}$ concentration is 0.1 $\mu$M.

**Fig. 12:** The effects of $Ca^{2+}$ steps on the mitochondrial variables. The dashed curves show the result when the stimulatory effect of $Ca^{2+}$ on PDH activity is saturated by setting $p_3 = 0$ in Eq. 10. The FBP concentration is 5 $\mu$M.

**Fig. 13:** The effects of $Ca^{2+}$ steps on the mitochondrial variables. In one simulation the uniporter flux is doubled ($p_{21} = 0.02$ $\mu M^{-1} ms^{-1} mV^{-1}$, dashed curves). This reverses the direction of the $\Delta\Psi$ and $ATP_m$ teeth. The FBP concentration is 5 $\mu$M.

**Fig. 14:** Experimental simultaneous measurements of NAD(P)H autofluorescence (top) and cytosolic $Ca^{2+}$ concentration (bottom) in pancreatic islets. These data are similar to those reported in an earlier study (Luciani *et al.*, 2006). (A) When the islet was maintained in a low glucose concentration (3 mM), depolarization with 30 mM KCl increased the cytosolic $Ca^{2+}$ concentration and the NAD(P)H autofluorescence (indicative of an increase in concentration). (B) When the islet was maintained in a high glucose concentration (10 mM) and the $Ca^{2+}$ oscillations were abolished with the hyperpolarizing agent diazoxide, subsequent depolarization with 30 mM KCl increased the cytosolic $Ca^{2+}$ concentration, but decreased the NAD(P)H autofluorescence.

**Fig. 15:** Model illustration of how the $NADH_m$ teeth can be upward in low glucose (FBP=1 $\mu$M, left column) and downward in high glucose (FBP=10 $\mu$M, right column). Large pulses of $Ca_c$ are used ($Ca_c$ is pulsed from 0.1 to 2 $\mu$M) to accentuate the electrical effect. The bottom panels show the $J_o$ vs. $\Delta\Psi$ curve (as in Fig. 3A) at the $NADH_m$ levels corresponding to low (panel E) and high (panel F) glucose. (The curve has been shifted to the left in both cases by setting $p_6 = p_{10} = 165$ mV.) The open circle represents the values of $\Delta\Psi$ and $J_o$ prior to a $Ca^{2+}$ pulse. The

closed circle represents the values during a $Ca^{2+}$ pulse. The change in $J_o$ during a pulse is much greater in high glucose than in low glucose, causing the $NADH_m$ teeth to be downward in high glucose (panel B) and upward in low glucose (panel A).

**Fig. 16:** In the Nnt mutant, proton leakage across the inner mitochondrial membrane is increased. This is simulated by increasing $p_{17}$ from 0.002 $\mu$Mms$^{-1}$mV$^{-1}$ (wild type, solid curves) to 0.02 $\mu$Mms$^{-1}$mV$^{-1}$ (mutant, dashed curves). This lowers the membrane potential and basal level of ATP, but also increases the size of the teeth in $\Delta\Psi$ and $ATP_m$. The FBP concentration is 5 $\mu$M.

**Table 1. Parameter Values for the Simplified Model**

| | | |
|---|---|---|
| $p_1 = 400$ | $p_2 = 1$ | $p_3 = 0.01\ \mu$M |
| $p_4 = 0.6\ \mu\text{Mms}^{-1}$ | $p_5 = 0.1$ mM | $p_6 = 177$ mV |
| $p_7 = 5$ mV | $p_8 = 7\ \mu M\text{ms}^{-1}$ | $p_9 = 0.1$ mM |
| $p_{10} = 177$ mV | $p_{11} = 5$ mV | $p_{12} = 120\ \mu\text{Mms}^{-1}$ |
| $p_{13} = 10$ mM | $p_{14} = 190$ mV | $p_{15} = 8.5$ mV |
| $p_{16} = 35\ \mu\text{Mms}^{-1}$ | $p_{17} = 0.002\ \mu\text{Mms}^{-1}\ \text{mV}^{-1}$ | $p_{18} = -0.03\ \mu\text{Mms}^{-1}$ |
| $p_{19} = 0.35\ \mu\text{Mms}^{-1}$ | $p_{20} = 2$ | FRT=0.037 $\text{mV}^{-1}$ |
| $p_{21} = 0.01\ \mu\text{M}^{-1}\text{ms}^{-1}\text{mV}^{-1}$ | $p_{22} = 1.1\ \mu\text{M}^{-1}\text{ms}^{-1}$ | $p_{23} = 0.001\ \mu\text{Mms}^{-1}$ |
| $p_{24} = 0.016\ \text{mV}^{-1}$ | $NAD_{tot} = 10$ mM | $A_{tot} = 15$ mM |
| $C_m = 1.8\ \mu\text{M mV}^{-1}$ | $f_m = 0.01$ | $k_{GPDH} = 5 \times 10^{-4}\ \mu\text{Mms}^{-1}$ |

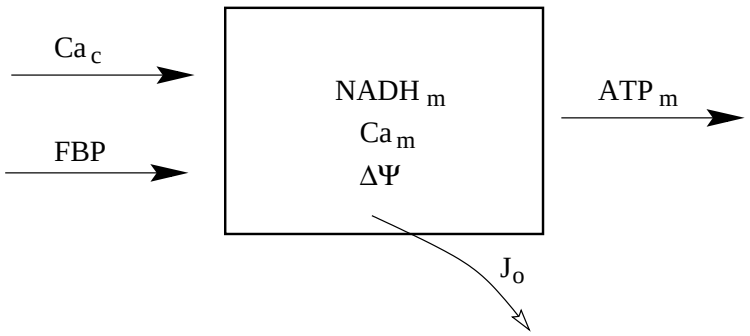


Figure 1:

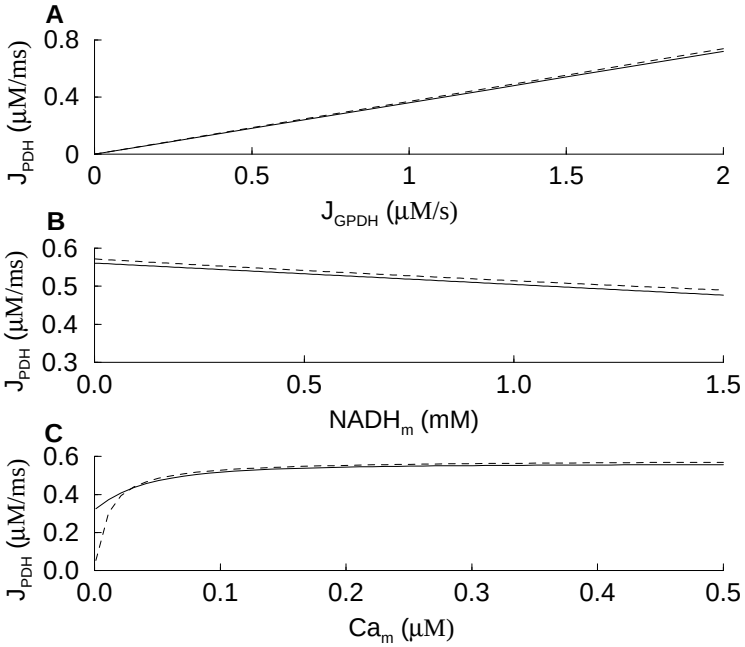
A
0.8
0.4
0
$J_{PDH}$ (μM/ms)
0
0.5
1
1.5
2
$J_{GPDH}$ (μM/s)
B
0.6
0.5
0.4
0.3
$J_{PDH}$ (μM/ms)
0.0
0.5
1.0
1.5
$NADH_m$ (mM)
C
0.6
0.4
0.2
0.0
$J_{PDH}$ (μM/ms)
0.0
0.1
0.2
0.3
0.4
0.5
$Ca_m$ (μM)

Figure 2:

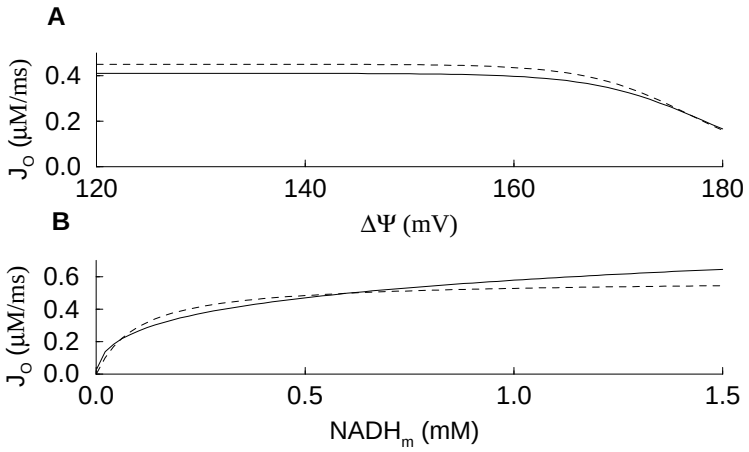
A
0.4
0.2
0.0
$J_O$ (μM/ms)
120
140
160
180
ΔΨ (mV)
B
0.6
0.4
0.2
0.0
$J_O$ (μM/ms)
0.0
0.5
1.0
1.5
$NADH_m$ (mM)

Figure 3:

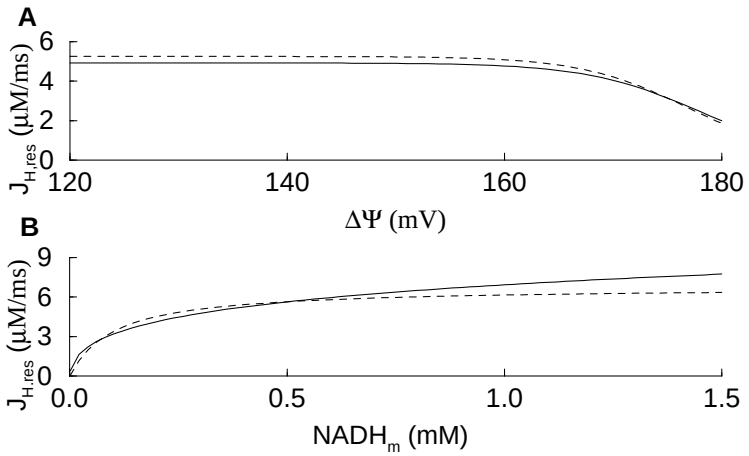
A
6
4
2
0
$J_{H,res}$ (μM/ms)
120
140
160
180
ΔΨ (mV)
B
9
6
3
0
$J_{H,res}$ (μM/ms)
0.0
0.5
1.0
1.5
$NADH_m$ (mM)

Figure 4:

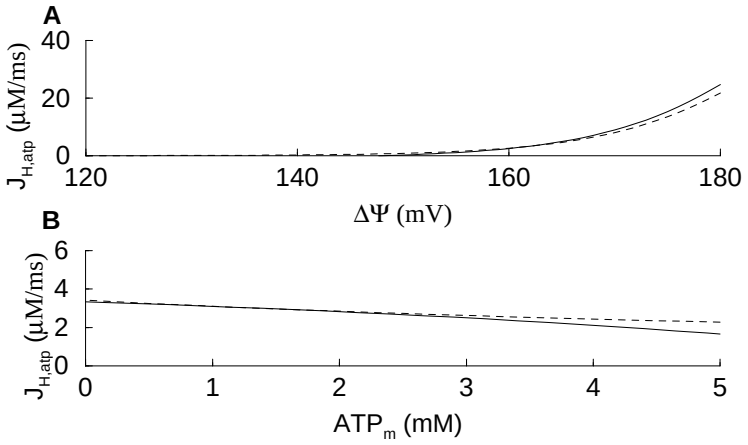
A
40
20
0
$J_{H,atp}$ (μM/ms)
120
140
160
180
ΔΨ (mV)
B
6
4
2
0
$J_{H,atp}$ (μM/ms)
0
1
2
3
4
5
$ATP_m$ (mM)

Figure 5:

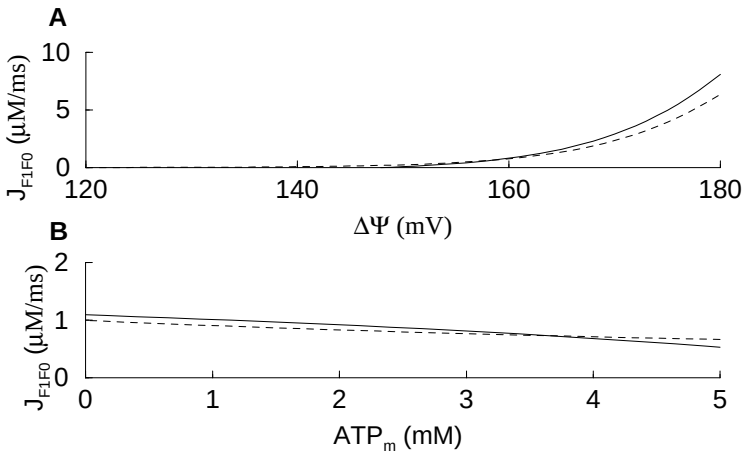
A
10
5
0
$J_{F1F0}$ (μM/ms)
120
140
160
180
ΔΨ (mV)
B
2
1
0
$J_{F1F0}$ (μM/ms)
0
1
2
3
4
5
$ATP_m$ (mM)

Figure 6:

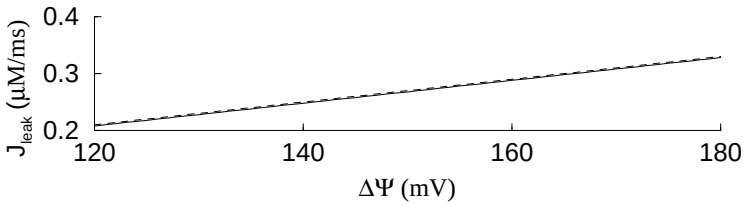


Figure 7:

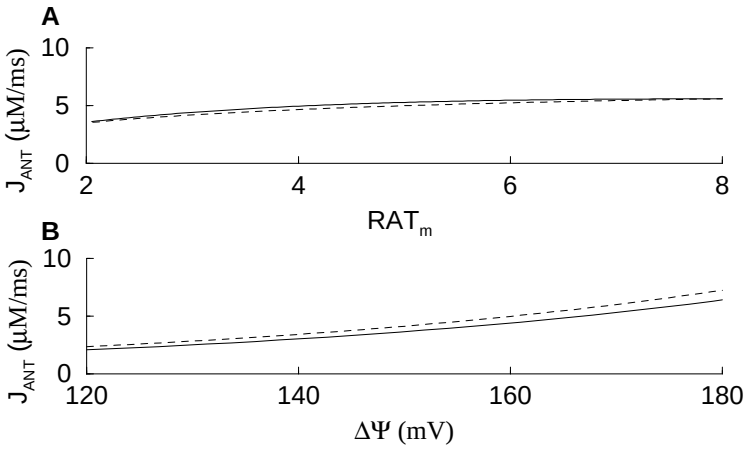
A
10
5
0
$J_{ANT}$ (μM/ms)
2
4
6
8
$RAT_m$
B
10
5
0
$J_{ANT}$ (μM/ms)
120
140
160
180
ΔΨ (mV)

Figure 8:

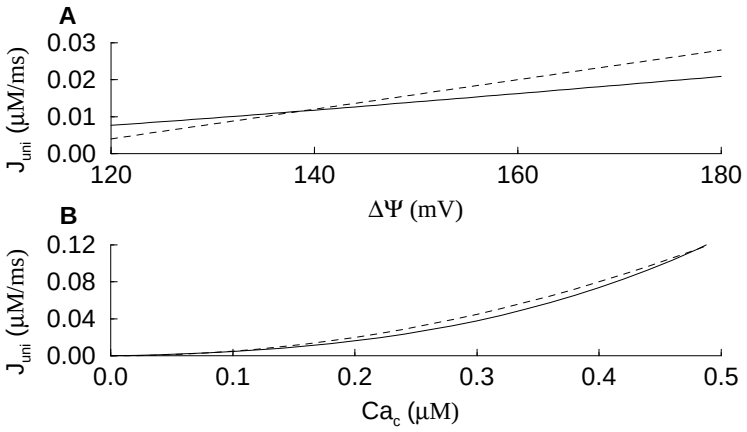
A
0.03
0.02
0.01
0.00
$J_{uni}$ (μM/ms)
120
140
160
180
ΔΨ (mV)
B
0.12
0.08
0.04
0.00
$J_{uni}$ (μM/ms)
0.0
0.1
0.2
0.3
0.4
0.5
$Ca_c$ (μM)

Figure 9:

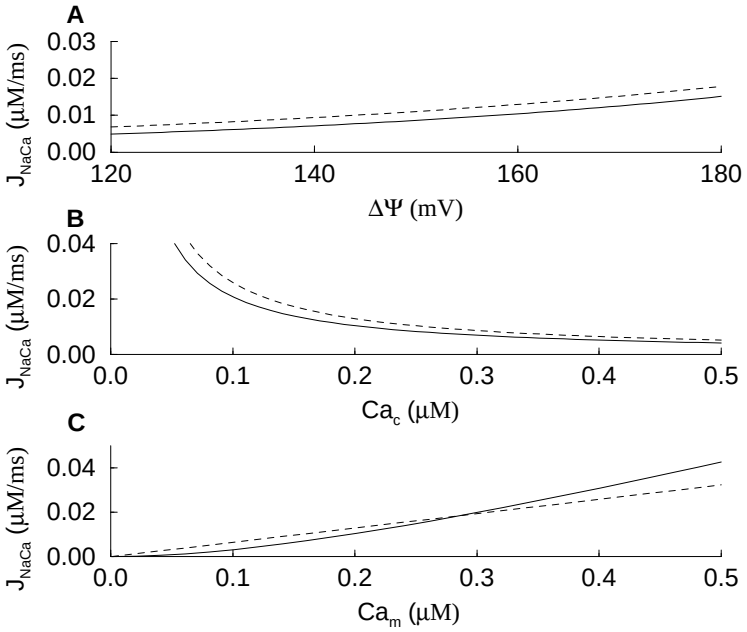
A
0.03
0.02
0.01
0.00
$J_{NaCa}$ (μM/ms)
120
140
160
180
ΔΨ (mV)
B
0.04
0.02
0.00
$J_{NaCa}$ (μM/ms)
0.0
0.1
0.2
0.3
0.4
0.5
$Ca_c$ (μM)
C
0.04
0.02
0.00
$J_{NaCa}$ (μM/ms)
0.0
0.1
0.2
0.3
0.4
0.5
$Ca_m$ (μM)

Figure 10:

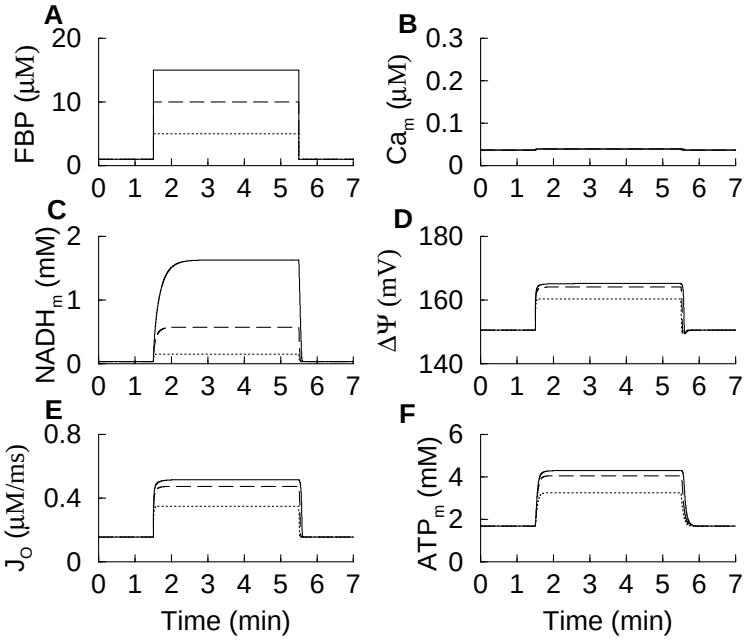
A
FBP (μM)
20
10
0
B
$Ca_m$ (μM)
0.3
0.2
0.1
0
C
$NADH_m$ (mM)
2
1
0
D
ΔΨ (mV)
180
160
140
E
$J_O$ (μM/ms)
0.8
0.4
0
F
$ATP_m$ (mM)
6
4
2
0
0 1 2 3 4 5 6 7
Time (min)

Figure 11:

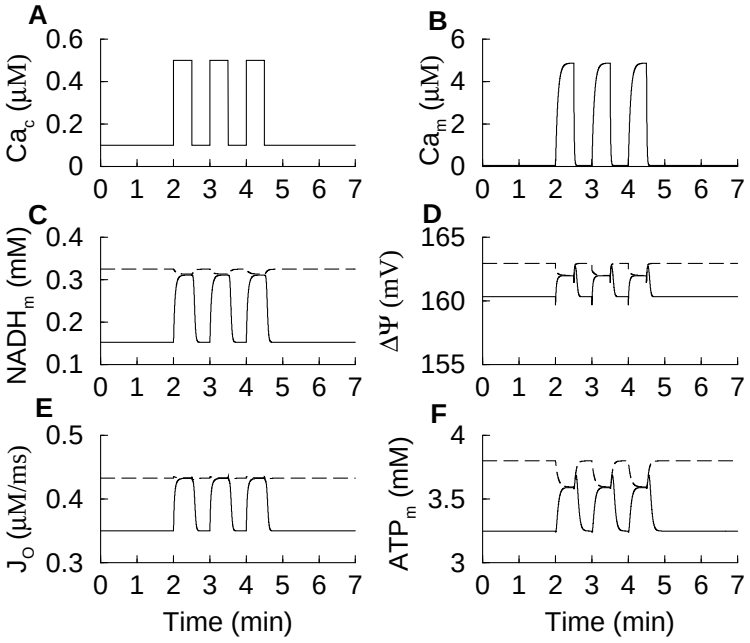
A
B
C
D
E
F
$Ca_c$ (μM)
$Ca_m$ (μM)
$NADH_m$ (mM)
ΔΨ (mV)
$J_O$ (μM/ms)
$ATP_m$ (mM)
Time (min)
Time (min)

Figure 12:

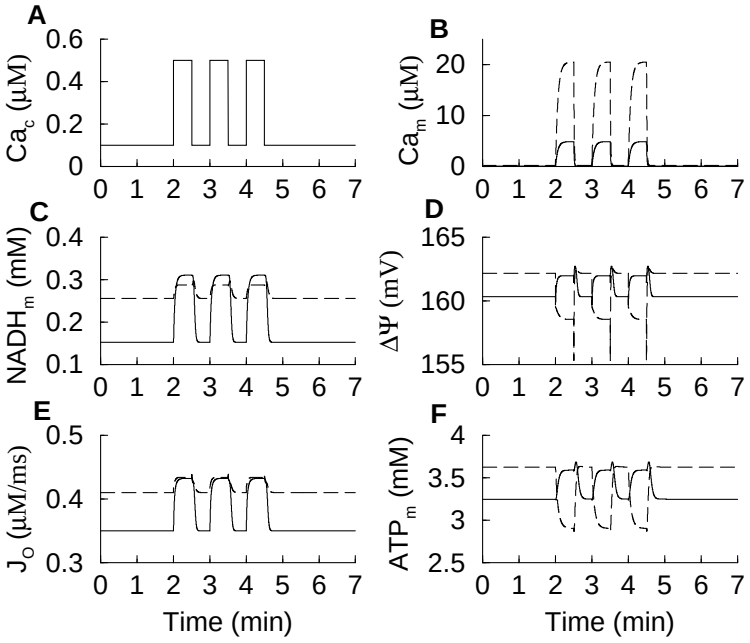
A
B
C
D
E
F
$Ca_c$ (μM)
$Ca_m$ (μM)
$NADH_m$ (mM)
ΔΨ (mV)
$J_O$ (μM/ms)
$ATP_m$ (mM)
Time (min)
Time (min)

Figure 13:

41

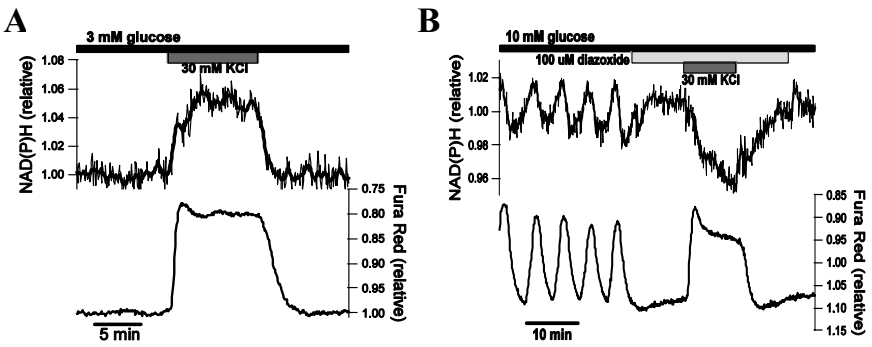
A
3 mM glucose
30 mM KCl
NAD(P)H (relative)
1.08
1.06
1.04
1.02
1.00
0.75
0.80
0.85
0.90
0.95
1.00
Fura Red (relative)
5 min
B
10 mM glucose
100 uM diazoxide
30 mM KCl
NAD(P)H (relative)
1.02
1.00
0.98
0.96
0.85
0.90
0.95
1.00
1.05
1.10
1.15
Fura Red (relative)
10 min

Figure 14:

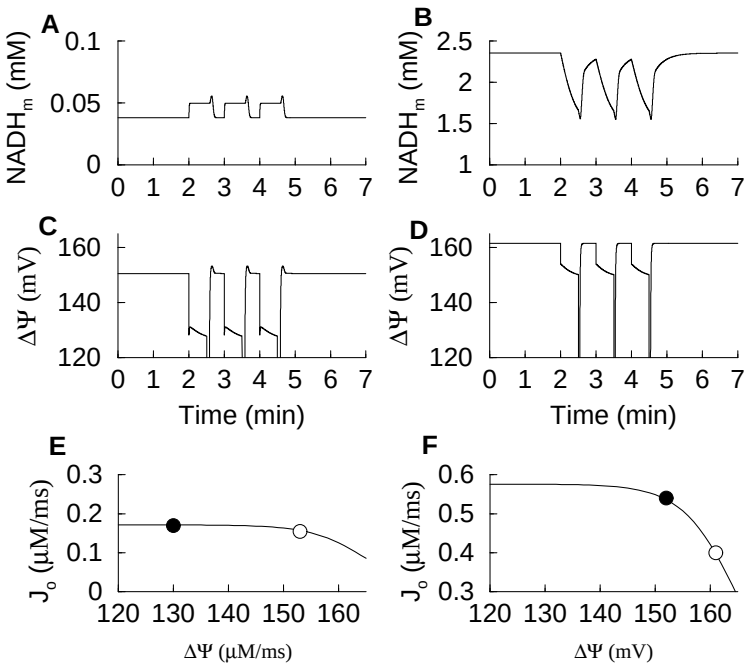


Figure 15:

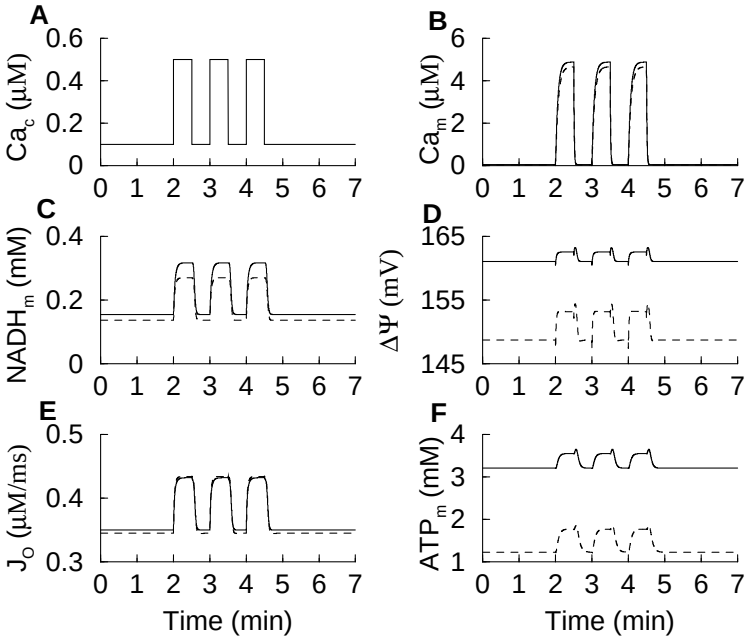
A
B
C
D
E
F
$Ca_c$ (μM)
$Ca_m$ (μM)
$NADH_m$ (mM)
ΔΨ (mV)
$J_O$ (μM/ms)
$ATP_m$ (mM)
Time (min)
Time (min)

Figure 16:

# *Paper VIII*

# Quasi Steady-State Approximations in Intracellular Signal Transduction – a Word of Caution

Morten Gram Pedersen[1], Alberto M. Bersani[2], and Enrico Bersani[3].

1. Department of Mathematics, Technical University of Denmark, Kgs. Lyngby, Denmark,
2. Department of Mathematical Methods and Models (Me.Mo.Mat.), "La Sapienza" University, Rome, Italy,
3. Datalink Informatica, Rome, Italy.

*Running Title:* QSSA in Intracellular Signal Transduction

*Subdivision*: Systems Biology

*Corresponding author:*
Morten Gram Pedersen
Department of Mathematics, Technical University of Denmark
Matematiktorvet, Building 303
DK-2800 Kgs. Lyngby, Denmark
Fax: (+45) 4588 1399
e-mail: `m.g.pedersen@mat.dtu.dk`.

*Abbreviations*:
QSSA, Quasi steady-state approximation; sQSSA, standard QSSA; tQSSA, total QSSA; MM, Michaelis-Menten; MAPK, mitogen activated protein kinase; MAPKK, MAPK kinase; MKKK, MAPK kinase kinase; MKP, MAPK phosphatase; ERK, extracellular signal-regulated kinase; MEK, MAPK and ERK kinase; NGF, nerve growth factor; EGF, epidermal growth factor.

Keywords: Michaelis-Menten kinetics, quasi steady-state assumption, enzyme signaling networks, double phosphorylation, MAPK cascade.

## Summary

The main goal of computational biology, and in particular of Systems Biology, is to define a comprehensive model that can accurately represent the experimental data and serve as a tool to generate and test hypotheses. Consequently, a high accuracy of the model is necessary in order to give a satisfactory prediction, both by a qualitative and quantitative point of view. Enzyme reactions play a pivotal role in intracellular signal transduction. Many enzymes are known to possess Michaelis-Menten (MM) kinetics and the MM approximation is often used when modeling enzyme reactions. However, it is known that the MM approximation is only valid at low enzyme concentrations, a condition not fulfilled in many *in vivo* situations. Thus, using the MM approximation with its parameter values obtained from *in vitro* experiments will often lead to false conclusions when simulating *in vivo* systems. Recently several other mathematical approaches, such as the total quasi steady-state approximation (tQSSA), have been developed for enzymes with MM kinetics. These new approximations are valid not only whenever the MM approximation is, but moreover in a greatly extended parameter range. Starting from a single reaction and arriving at the mitogen activated protein kinase (MAPK) cascade, we give several examples of biologically realistic scenarios where the MM approximation leads to quantitatively as well as qualitatively wrong conclusions, and show that the tQSSA improves the accuracy of the simulations greatly. Moreover, we discuss the use of approximations in reverse engineering and the biological importance of our findings.


## Introduction

Every living cell responds to external stimuli, like hormones, ions, heat shock, etc., which are transduced by a complex intracellular molecular network. When an external ligand binds a plasma membrane receptor, intracellular second messengers interacting with membrane receptors are activated, and by means of biochemical reactions

transduce the signal.

In the last decade many mathematical models have been formulated to investigate the behavior of complex intracellular biochemical networks. Many of those are based on the well-studied MAPK cascade (see for example [1–5]), and although not crucial for the results presented here, this ubiquitous signalling pathway will be given special attention in the following.

The aim of such modeling (which is an integral part of the 'Systems Biology' large scale project) is roughly twofold: to reproduce and study some particular phenomena observed experimentally (like bistability, oscillations, ultrasensitivity, hysteresis, etc.) and to investigate the properties of these networks as information processing and transducing devices. As a hope for the future, this modeling could be used for pharmaceutical scopes (first of all drug discovery) as a reliable tool to make predictions about the effects of drugs on the biochemical networks, thus shortening the preclinical phase. This goal is related to the ambitious project of a "Virtual Cell" ( [6], http://www.vcell.org/) or "Silicon Cell" ( [7], http://www.siliconcell.net/), which aims at simulating the behavior of whatever cell as closely as possible to the physiological reality: "A silicon cell is a precise replica of (part of) a living cell" (cited from http://www.siliconcell.net/).

Surprisingly, the mathematical formulation of these highly interconnected enzyme reactions is usually based on *in vitro* studies of isolated reactions, without a serious criticism of the delicate passage from the kinetics of simple reactions to the kinetics of a network of reactions shared by several cascades in a crowded molecular environment [8]. This can be justified when analyzing underlying mechanisms (e.g., the importance of feedback or the creation of oscillations), where the exact kinetic expressions and parameters are less important since one is usually only interested in the qualitative behavior that the system can perform. However, in the light of the Silicon Cell project, which aims at being a both qualitative as well as quantitative precise representation of the living cell, the use of correct parameters, kinetic expressions and initial conditions (i.e., steady-state concentrations of molecular species) becomes cru-

cial. This is the subject of the present work.

One of the principal components of the mathematical approach to Systems Biology is the model of biochemical reactions set forth by Henri in 1901 [9–11] and Michaelis and Menten in 1913 [12], and further developed by Briggs and Haldane in 1925 [13]. This formulation considers a reaction where a substrate $S$ binds an enzyme $E$ reversibly to form a complex $C$. The complex can then decay irreversibly to a product $P$ and the enzyme, which is then free to bind another molecule of the substrate. This process is summarized in the scheme

$$E + S \underset{d}{\overset{a}{\rightleftarrows}} C \xrightarrow{k} E + P, \tag{1}$$

where $a, d$ and $k$ are kinetic parameters (supposed constant) associated with the reaction rates.

This scheme is mathematically represented by a system of two nonlinear ordinary differential equations (ODEs), corresponding initial conditions and two conservation laws as shown in the Methods section. The initial conditions give the concentrations of $S$ and $C$ at the beginning of the reaction, and their time development is described by the ODEs, while $E$ and $P$ are linked to $S$ and $C$ through the conservation laws.

Assuming that the complex concentration is approximately constant after a short transient phase leads to the usual Michaelis-Menten (MM) approximation (or *standard quasi steady-state assumption* or *approximation* (standard QSSA, sQSSA)), which is valid when the enzyme concentration is much lower than either the substrate concentration or the Michaelis constant $K_M$ [14, 15]. This condition is usually fulfilled for *in vitro* experiments, but often breaks down *in vivo* [16, 17]. We refer to the Methods section for the mathematical formulation of scheme (1), and to [18] for a nice, general review of the kinetics and approximations of (1).

The advantage of a quasi steady-state approximation is that it reduces the dimensionality of the system, passing from two equations (*full system*) to one ( *MM approximation or sQSSA)* and thus speeds up numerical simulations greatly, especially for large networks as found *in vivo*. Moreover, the kinetic constants in (1) are usually not known,

whereas finding the kinetic parameters for the MM approximation is a standard *in vitro* procedure in biochemistry [19]. However, to simulate physiologically realistic *in vivo* scenarios, one faces the problem that the MM approximation is no longer valid as mentioned above. Hence, even though the kinetic constants such as $K_M$ are identical *in vivo* and *in vitro*, they need to be implemented in an approximation which is valid for the system under investigation.

Approximations such as the *total QSSA* (tQSSA) [20, 21], which is valid for a broader range of parameters covering both high and low enzyme concentrations, have been introduced recently. Tzafriri [21] showed that the tQSSA is at least roughly valid for any set of parameters in the case of the reaction in (1). Importantly, the tQSSA uses the same parameters ($V_{max}, K_M$) as the sQSSA. Hence, the parameters found *in vitro* from the MM approach can be used by the tQSSA for modeling *in vivo* scenarios.

The roles of $V_{max}$, the maximal reaction velocity, and $K_M$, the Michaelis constant describing the concentration of the substrate at which the reaction rate is half maximal, become essential when characterizing biochemical reactions *in vitro* as well as *in vivo*. Moreover, descriptions of cooperative reactions, inhibition and many other biochemical processes have exploited the fundamental ideas of the MM scheme, i.e., the sQSSA and the parameters $V_{max}$ and $K_M$ (see, e.g., [19]). However, since these approximations cannot be expected to be valid *in vivo*, employing the tQSSA to these more complex situations would be preferable. Tzafriri & Edelman [22] studied the completely reversible enzyme reaction in terms of the tQSSA. We have recently derived the tQSSA for fully competitive reactions [23].

In this paper we show that the use of the sQSSA can lead to gross quantitative as well as qualitative wrong conclusions even in the case of simple networks. The tQSSA is shown to estimate the behavior significantly better, and therefore we propose to use this approximation when modeling intracellular signalling networks.

# Results

Our investigation applies to every biochemical network which includes enzyme reaction cascades. Many mathematical models have been applied to the phosphorylation and dephosphorylation reactions with special attention to the MAPK cascade, for which there exist many experimental [24–26] and theoretical results [1–5]. We discuss the validity limits of the sQSSA and the advantage of the tQSSA, starting from subcomponents of this cascade and finally arriving at the full cascade including feedback. To fully appreciate the differences between the sQSSA and the tQSSA we recall the simpler and very general cases of, firstly, a single reaction, and then two reactions with substrates competing for the same enzyme. All mathematical expressions are given in the Methods section or the Appendix.

For the single reaction represented in (1) it has been known for many years that the sQSSA (MM approximation) holds when the initial substrate concentration is much higher than the initial enzyme concentration ($S_T \gg E_T$), but it was later realized that this is not a necessary condition; if the enzyme concentration is much less than the Michaelis constant, then the sQSSA also holds [14, 15]. This is summarized in the validity criterion $E_T \ll S_T + K_M$, which loosely says that the sQSSA holds at low enzyme concentrations (with respect to either the substrate concentration or the $K_M$ value).

This can not be expected to hold *in vivo*, and the tQSSA has been introduced in order to have an approximation applicable to *in vivo* reactions as well [20, 21]. This approximation holds for a much larger region of parameter space, and is in fact always roughly valid [21]. Importantly, the tQSSA coincides with the sQSSA when the latter is expected to hold, i.e., at low enzyme concentrations. Fig. 1 shows that the tQSSA approximates the full system very well also for high enzyme concentrations where the sQSSA fails.

[Figure 1 about here.]

## Competing substrates and the double phosphorylation mechanism

A theoretically well-studied example of a slightly more complicated network is the case of fully competitive reactions [14, 23, 27], i.e., reactions with competing substrates, $S_1$ and $S_2$, also known as substrate-inhibitor systems,

$$\begin{aligned} S_1 + E &\underset{d_1}{\overset{a_1}{\rightleftarrows}} C_1 \xrightarrow{k_1} E + P_1, \\ S_2 + E &\underset{d_2}{\overset{a_2}{\rightleftarrows}} C_2 \xrightarrow{k_2} E + P_2, \end{aligned} \tag{2}$$

where $S_i, C_i$ and $P_i$ represent substrate, enzyme-substrate complex and product ($i = 1, 2$) for the two competing reactions. Note that this reaction scheme also covers competitive inhibition (for $k_2 = 0$ with $S_2$ being the inhibitor).

The validity criterion of the sQSSA for (2) is known [14,27], and says basically that the sQSSA holds at low enzyme concentrations as in the case of a single, noncompetitive reaction, which can be seen as a special case of (2) which negligible inhibitor concentration. We [23] extended the region of validity by employing the tQSSA to (2), and as shown in Fig. 2 it approximates the full system very well. We have not found any values of the parameters for which numerical simulations show that our tQSSA breaks down dramatically. Of importance, our approximation captures the competition as does the competitive sQSSA (18) and in contrast with the single reaction tQSSA (10), but also at intermediate or high enzyme concentrations where the sQSSA does not hold anymore (Fig. 2). However, when the competition can be neglected due to, e.g., low substrate concentrations, the single reaction tQSSA does indeed estimate the full system well (not shown).

Our results are immediately applicable to, e.g., successive reactions catalyzed by the same enzyme, such as nonprocessive or distributive double phosphorylation or dephosphorylation processes, as seen for example in the MAPK cascade [28–32]. The reaction scheme can be seen as a special case of (2) with $P_1 = S_2$ and is summarized as

$$S_1 \xrightarrow{E} S_2 \xrightarrow{E} P, \tag{3}$$

where it is usually assumed that at the beginning only $S_1$ is present. Here $S_1$ and $S_2$ compete for the same enzyme, $E$. For the case of the MAPK cascade one can think of, e.g., diphosphorylated and thus activated MAPKK (MAPKK-PP, here $E$) phosphorylating MAPK (here $S_1$) twice, producing first mono-phosphorylated MAPK (MAPK-P, here $S_2$) and then double-phosphorylated MAPK (MAPK-PP, here $P$). See also scheme (4) below.

In the MAPK cascade literature every single reaction is often treated by a MM approximation for an isolated reaction of the form (1), not only without any *a priori* examination of its applicability, but also neglecting the other terms involved in the double reaction and, in particular, the important fact that, for example, MAPK and MAPK-P are competing substrates for MAPKK-P (however, see [31,32]). This means that even when the sQSSA for (3) holds, the neglect of the competition leads to wrong estimations of the behavior, and can only be expected to be an even greater problem when the sQSSA breaks down, in which case the tQSSA should be used. This situation is illustrated in Fig. 2B, which shows that even when both the non-competitive sQSSA and tQSSA as well as the competitive sQSSA fail, the competitive tQSSA is an excellent approximation.

[Figure 2 about here.]

The double phosphorylation as well as double dephosphorylation of MAPK was recently modelled taking into consideration the competition between the pools of MAPK with different phosphorylation states [31,32]. We model this process by assuming that (2) holds for both the phosphorylation as well as the dephosphorylation processes as in [31]. In [32] both (2) as well as a more complicated process of phosphorylation were considered, but this further step is not of our interest here although applying the tQSSA to this more complicated scheme would be interesting. Similarly, we follow [31] and model the dephosphorylation by (2) instead of the slightly more complicated scheme from [32] for the sake of simplicity.

Thus, we are studying the scheme

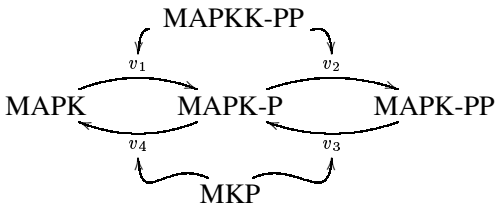


(4)

where the reaction rates $v_1 - v_4$ are assumed to follow Michaelis-Menten kinetics with competition between MAPK and MAPK-P for activated MAPKK (MAPKK-PP), and between MAPK-PP and MAPK-P for the generic phosphatase MKP [33]. Using parameters from [32, Fig.1], we see in Fig. 3A that in this case the competitive sQSSA underestimates the duration of the transient phase before reaching the steady state. Furthermore, it underestimates the steady state level of MAPK-PP. However, this underestimation is not a feature of the sQSSA, since lowering the total MAPK concentration to $[\text{MAPK}]_T = 50$ results in an (even more pronounced) overestimation of the steady state level (Fig. 3B), which of course can be of equal importance as an underestimation. Notably, the tQSSA fits both the dynamic behavior as well as steady state levels very well in both cases. Remark the counter-intuitive result that a ten times *lower* total MAPK concentration in Fig. 3B yields a more than two times *higher* level of activated MAPK, showing the strength and utility of mathematical modeling. To illustrate the importance of a reliable estimation of the MAPK levels, we remark that is has been shown experimentally that the dynamics of MAPK activity is crucial for the fate of the cell [24,34,35]. For example, PC12 cells proliferate in response to transient MAPK activation, while they differentiate when the activated MAPK levels are sustained [36]. We follow this up in the next section and in the discussion.

[Figure 3 about here.]

## The MAPK cascade

[Figure 4 about here.]

In the MAPK pathway, the upstream kinase (denoted MKKK, i.e. MAP kinase kinase kinase; for example Raf) when activated phosphorylates the immediately downstream target, which is also a kinase (MAPKK, i.e. MAP kinase kinase, for example MEK) successively on two specific sites, eventually activating it. This last double-phosphorylated kinase (MAPKK-PP) acts on the MAPK (for example ERK) through specific phosphorylation events on two distinct sites. The activated MAPK is then responsible for further downstream signalling. The activated cascade is shut down by the reverse action of specific phosphatases [33, 37], whose outcome is the time modulation of the signal, probably through the regulation of the active kinase (for example, transient versus sustained activation). Moreover, the phosphatase controls the steady state level of activated MAPK, which, in turn, controls downstream processes as mentioned in the previous section.

Looking at the complete MAPK cascade, shown in Fig. 4, it is clear that all the problems arising in the simpler cases described in the previous sections may occur.

[Figure 5 about here.]

One of the most interesting phenomena in biochemical networks is the appearance of (sustained) oscillations experimentally observed, for example, in glycolysis, in intracellular calcium or in circadian networks. Recently, these oscillatory phenomena have been investigated theoretically for signal transduction networks like MAPK cascade [3].

Several authors suppose that MAPK-PP acts, by means of a feedback mechanism, on the first layer of the MAPK cascade, and in some cases this feedback has been shown experimentally, for example in NIH3T3 cells, where Raf-1, a MKKK, was found to be inactivated by ERK, a MAPK [38]. See also [35, 39] for reviews. Kholodenko [3] introduced a noncompetitive inhibition of this kind. The mathematical model of this complex network (with or without feedback) was built using the non-competitive MM approximation, and it was shown that oscillations could occur for several parameter values.

However, the appearance of oscillations could depend on the way in which the model has been formulated. We compare the network with the full system of reactions to both the competitive sQSSA [31, 32] and the competitive tQSSA [23]. Note that the tQSSA used here is an *ad hoc* approach (see Appendix C), since a truly valid tQSSA has not been found yet for large networks such as the MAPK cascade. In contrast to Kholodenko [3], we model the negative feedback as a competitive inhibition with inhibition constant $K_I$ to allow the use of the competitive tQSSA (see Fig. 4 and Appendix C). Our simulations confirm that the cascade can reach a steady state as well as oscillate also in this case. However, with parameters very similar to [3] the (competitive) sQSSA approximation can lead to qualitatively wrong conclusions such as oscillations when the full system is steady (Figs. 5B and C), or quantitative wrong estimations of, e.g., the amplitude of the oscillations (Fig. 5A), or the steady-state levels of MAPK-PP (Fig. 5D), while the full system is in general much better approximated by the (competitive) tQSSA. However, for some parameters the tQSSA approach also fails qualitatively (Fig. 5B), or with respect to the period of the oscillations (Fig. 5A).

In Table 1 we summarize the ranges of the inhibition constant $K_I$ for which MAPK-PP oscillates in the three cases. It is seen that the solution of the full system undergoes oscillations for a very narrow range of this parameter, while the use of the sQSSA yields oscillations for a much larger range, also for values for which the solution of the full system does not perform rhytmic behavior (Figs. 5B and D). However, the competitive tQSSA also fails to predict the behavior for some parameters, but the range for which this occurs is markedly reduced compared to the sQSSA (Table 1). New improved tQSSAs should be developed in order to get a better representation of the full system.

[Table 1 about here.]

The great majority of authors using the sQSSA usually neglects the concentration of the complexes, as expressed, e.g., in the conservation law $[\text{MAPK}]_T = [\text{MAPK}] + [\text{MAPK-P}] + [\text{MAPK-PP}]$ [3, 32], but this is only valid at low enzyme concentrations.

We suppose that this is the major reason for the poor prediction of the sQSSA. The complex concentrations are indeed significant in our simulations of the full system as shown in Fig. 6A. This figure shows the complex (MAPK-P)-(MAPKK-PP) of reaction 8 in Fig. 4, the substrate MAPK-P and the free enzyme MAPKK-PP. In contrast with the sQSSA, the tQSSA considers the complex concentrations, and it is seen from Fig. 6A that this is necessary, since the total substrate concentration is comparable with the complex concentration.

Taking the complex concentrations into account is not only important for the generation of oscillations, but, as it could be expected, also for the steady-state concentrations obtained for the full system, the sQSSA and the tQSSA at high values of the inhibition constant $K_I$ (Table 1). With the parameters used here the competitive sQSSA overestimates the steady-state level of activated MAPK (Fig. 5D) as in the simpler case considering only the last level of the cascade (Fig. 3B). On the other hand, the competitive tQSSA estimates this level well (Figs. 5C and D). As mentioned in the previous section, the correct estimation of activated MAPK-PP has important implications for predicting further downstream effects. We follow this question up in the discussion.

[Figure 6 about here.]

A second problem of both the QSSAs is the fact that the complex never enters a steady state during the oscillations. In Fig. 6B we show the time derivatives of the concentrations from panel A, which measure the rate of change. The assumption that the complex concentration changes much more slowly than the substrate lies at the heart of the QSSAs, but this does not hold in general; as seen in Fig. 6B the rate of change of the complex is comparable to that of the substrate, the total substrate and the kinase. We believe that this is why the tQSSA also fails for some parameters and, moreover, sometimes estimates the period of the oscillations badly (Fig. 5B). Consequently, it would in some cases be preferable to model the network by means of the full system. The implications of this approach and its flaws will be faced in the discussion.

# Discussion

Far from being a collection of serial chemical reactions, the higher eukaryotic intracellular signal transduction networks are very intricate and highly complex. The increased amount of data and knowledge about these networks has made mathematical modeling and computational methods increasingly important in Systems Biology, and has led to projects such as the Silicon Cell, which aims at being a precise replica of the living cell. This means using experimentally found data and reproducing both qualitative and quantitative behavior of the cell.

So far most of the models describing enzyme reactions, e.g., in the MAPK cascade, have been based on the classical Michaelis-Menten approximation (sQSSA) and many of these did not consider competition between substrates. These approaches were taken, although parameters and initial conditions were chosen so that the validity criterion for the sQSSA no longer held and the competition could not be neglected. As exceptions, we mention Hatakeyama et al. [31] and Markevich et al. [32], who treated the problem of substrate competition in terms of the sQSSA for two substrates competing for the same kinase, but they did not consider the region of validity of the sQSSA and neglected the enzyme-substrate complexes.

Although it was known that the sQSSA will often be invalid *in vivo*, the sQSSA approach was necessary for many years, since no better approximations were known, but this has changed recently with the introduction of the tQSSA. This approach was first applied to the simplest reactions [20, 21], and later to increasingly more complex schemes such as reversible reactions [22] and fully competing systems [23].

We have here presented the application of the tQSSA to biologically realistic networks, and shown that it is superior to the sQSSA in all the presented cases. We did not formally investigate the validity of the tQSSA for all the reaction networks examined, and found in fact that the tQSSA has its limitations as well (Table 1), probably related to the fact that the complexes do not always enter a quasi-steady state (Fig. 6B). However, based on our simulations we feel confident in saying that compared to the

sQSSA it provides a more accurate estimate of the behavior of enzyme networks. For example, it was found that the tQSSA estimates the steady state levels of activated MAPK very well (Figs. 3 and 5A), while the sQSSA often fails dramatically. We believe that the main reason for this is the fact that the tQSSA incorporates the complex concentrations while the sQSSA does not, as stated for example in the conservation law $[\text{MAPK}]_T = [\text{MAPK}] + [\text{MAPK-P}] + [\text{MAPK-PP}]$ [3, 32].

To illustrate the importance of a reliable estimation of the MAPK dynamics and steady-state levels, we remark that is has been suggested that both the duration and intensity of the activated MAPK is crucial for the fate of the cell ( [40] and references therein). For example, rat PC12 cells differentiate if stimulated by NGF and proliferate if stimulated by EGF [41, 42], although the cognate receptors use the same signaling cytoplasmic network to transduce the signal to the nucleus. In the two cases, the most evident difference is that NGF induces a sustained MAPK (ERK) activity, while EGF induces a transient MAPK (ERK) activity (see [36] for a review). Recently, it was also shown that PC12 [42] and Kaposi Sarcoma [43] cells are sensitive to the strength of the MAPK signal indicating a threshold phenomenon, which means that even minor changes in the levels of activated MAPK can have dramatic consequences.

We showed that the choice of the approximation scheme could dramatically change the size of the parameter range in which oscillations occur in the MAPK cascade with a competitive, negative feedback (Fig. 5A and Table 1).

If any Silicon Cell should help to discover pharmaceutically sensitive targets and reproduce the effects of drugs on these targets, the quantitative aspects of the model would have to be carefully studied and resolved, for example in estimating the size of the above parameter windows. For instance, continuing the example of the MAPK cascade with inhibitory feedback, assume that we wish to apply a drug in order to create oscillations. Lowering the $K_I$ value would appear promising on the basis of the model using the sQSSA, since this model predicts oscillations in a rather wide parameter range (Table 1). However, this could encourage a waste of resources searching for an appropriate pharmaceutical compound, since the drug would have to be very finely

tuned and, hence, difficult to find, because the full system has a very narrow parameter range yielding oscillations. Thus, one might be better off looking for a drug acting elsewhere in the network.

Since the tQSSA, although superior to the sQSSA, also does not always work, one could suggest to use the alternative of simulating each step of the reaction by means of the full system of ODEs, which means describing every reaction in terms of two equations, and facing three instead of two parameters for every reaction, as it has been done for example for the MAPK cascade [4]. However, more equations would mean, especially for larger systems, that this approach quickly would become computer expensive.

A more serious problem is the fact that the three rate constants ($a, d$ and $k$ in (1)) are usually unknown, while finding the QSSA parameters $K_M$ and $V_{max}$ (or $k_{cat} = V_{max}/E_T$) is a standard procedure in biochemistry. Thus, the reduction obtained from the QSSA is in this sense an advantage compared to the full system. We could in any case rebuild the parameters $a, d, k$ starting from the MM parameters, but as shown in Appendix B, we then introduce a degree freedom. Bhalla and Iyengar [2] try to overcome this problem supposing that $d = 4k$, but this hypothesis seems to us a bit arbitrary without any strong experimental support, as already remarked by the authors. However, we have applied this assumption through out this work when modeling the full system.

The validity of the tQSSA depends on the precise values of $a, d$ and $k$ as stated for example in (13) for the case of a single reaction: The smaller the ratio $K/K_M$, i.e., the larger the ratio $d/k$, the better the approximation. However, for any choice with a large ratio $d/k$, the tQSSA holds. A similar result holds for fully competitive reactions [23]. This is consistent with the choice of $d = 4k$ and supported by the fact that for many enzymes the parameter $d$ is much greater than $k$ [44, 45].

From a theoretical point of view, the application of the tQSSA in this way makes the actual parameter values of $a, d$ and $k$ less important. When we *a priori* know that

the system can be well-approximated by the tQSSA, all the possible choices of $a, d, k$ will give approximations near each other, and hence, near the true solution, assuming that the true parameters are such that the tQSSA is valid. This can be used in cases where only the parameters $K_M$ and $V_{max}$ are available, the sQSSA is known not to hold, and only a very complicated tQSSA, too complicated to implement effectively on a computer, exists. One can then choose any relation between $a, d$ and $k$ giving the correct values for $K_M$ and $V_{max}$, check that the tQSSA holds using a theoretically founded validity criteria, and then do the simpler implementation of the full system of equations.

Related to the above, but from another point of view, is the lack of reliable experimental data about the kinetic constants of the intracellular biochemical reactions, including $K_M$ and $V_{max}$ values. To reconstruct these missing parameter values, some authors rely on the so-called reverse engineering (or inverse problem). The classical approach to reverse engineering is based on least square techniques with the aim to find the set of parameters that gives the best fitting curve, i.e., the curve passing "as close as possible" to the experimental data. This is done searching for the global minimum of a function of as many variables as there are unknown parameters. To find the global minimum of these functions is in general far from trivial, for example due to the risk of finding only local, not global, minima. Furthermore the uniqueness of this minimum cannot, in general, be guaranteed; several sets of parameters could give the global minimum. This is the question of *a priori identifiability* [46].

As shown in the present work, the misuse of the sQSSA can lead to large quantitative and qualitative errors. However, even when the sQSSA is not a good approximation of the system, we can still find parameters for which the sQSSA does fit the data (the full system), by minimizing, e.g., the least square error. This would inevitably lead to wrongly estimated parameters, since the original ones did not provide a good approximation.

From these considerations it follows that the ability of the model to fit a certain data set can not be used to test whether a certain approximation holds. Applying reverse

engineering for the sQSSA, without any *a priori* examination of its validity, one could argue that the (mis)use of the sQSSA causes no problems, since we obtain a good fit anyway. However, one would prefer to have a model that works under many different conditions, not only in a certain experimental setting. If fitting the sQSSA model to the data yields wrong estimates of the parameters, then it is likely that the predicted behavior using these parameters would be far from the true behavior. The same would be true if the model was later used as a subsystem of an enlarged model. For example, the estimation of the Michaelis or inhibition constant relying on a wrong model formulation could be crucial as seen in the following example.

Assume that all the parameters except the inhibition constant $K_I$ were known for the model illustrated by Fig. 4. If we had a data set for this model showing stable behavior, according to Table 1, using the sQSSA we would estimate a value of $K_I$ greater than 3.02, even though the true value of $K_I$ could be between 0.18 and 3.02. Assume now that we obtain a drug capable of lowering the $K_I$ value according to some known mechanisms, and that we decide to administrate the drug to lower $K_I$ with the aim to let the system oscillate. Believing that the sQSSA estimated $K_I$ is the true value, we would apply a certain amount of the drug in order to get below the threshold value at $K_I = 3.02$. But the actual value of $K_I$ could be completely different from the wrongly estimated one and such that the drug administration, though lowering $K_I$, would leave the system stable.

Similar problems can be expected to occur in metabolic control analysis [47–49], which is used to find the steps in the network that controls some output behavior, e.g., the concentration of a certain biochemical species. It seems likely that an invalid sQSSA model might predict that a certain step is the most important, while the full system or the corresponding tQSSA model finds that step to be less important. In the light of applications for the pharmaceutical industry, this could lead to a waste of money and energy focusing on an apparently sensitive target, which then turns out to be unimportant or, viceversa, the neglect of an important target that apparently seems unimportant.

In conclusion, we have shown that the use of the classical MM approach (sQSSA) should be done with much care, since it can lead to both quantitative and qualitative errors. This has further impact on techniques such as reverse engineering and metabolic control analysis. Finding approximations improving the sQSSA for complex reactions such as successive reactions, open systems, loops such as the Goldbeter-Koshland switch [50], feedback systems etc., and investigating their validity, should be of great interest for further investigations and simulations of such reactions *in vivo*, where the MM description can be expected to break down.

### Acknowledgements

M. G. Pedersen was supported by BioSim (EU contract No. 005137).

## Methods

We compare various approximation schemes of the time concentration development of the chemical species involved in the reactions. This is done by numerically solving the system of ordinary differential equations (ODEs) derived from the reaction scheme using the methods and approximations within the various approaches. To illustrate this idea we use the example of an isolated reaction

$$E + S \underset{d}{\overset{a}{\rightleftarrows}} C \xrightarrow{k} E + P. \tag{5}$$

The fundamental step is modeling all of the intermediate steps including binding, dissociation and release of the product using mass action and conservation laws. This leads to an ODE for each involved complex and substrate. We refer to this as the full system. For (5) the equations are

$$\frac{dS}{dt} = -a(E_T - C)S + d\,C, \tag{6a}$$

$$\frac{dC}{dt} = a(E_T - C)S - (d + k)C\,. \tag{6b}$$

with the initial conditions

$$S(0) = S_T, \quad C(0) = 0, \tag{7}$$

and the conservation laws

$$E + C = E_T, \quad S + C + P = S_T. \tag{8}$$

Here $E_T$ is the total enzyme concentration assumed to be free at time $t = 0$. Also the total substrate concentration, $S_T$, is free at $t = 0$. This is the so-called Michaelis-Menten (MM) kinetics [12, 14, 19]. Let us observe that this system (6) admits an asymptotic solution for $t \to \infty$ obtained by setting the derivatives equal to zero. This solution is given by $C = S = 0$, so that from the conservation laws $P = S_T$ and $E = E_T$. This means that all the substrate eventually becomes product due to the irreversibility, while the enzyme eventually is free and the complex concentration tends to zero.

The next, well-known and widely used step is that of the Henri-Michaelis-Menten-Briggs-Haldane approximation [9–15]. It leads to an ODE for each substrate while the complexes are assumed to be in a quasi-steady state (i.e., $\frac{dC}{dt} \approx 0$). See e.g. [19] for a general introduction to this approach. We stress here that this is an approximation to the full system, and that (for (5)) it is only valid at low enzyme concentrations, i.e., $E_T \ll S_T + K_M$ [14, 15]. We refer to this as the standard quasi-steady state approximation (sQSSA). For (5) it is given by

$$\begin{aligned} \frac{d\,S}{dt} &\approx -\frac{V_{max}\,S}{K_M + S}, \quad S(0) = S_T, \\ E(0) = E_T, \quad V_{max} &= k\,E_T, \quad K_M = \frac{d+k}{a}. \end{aligned} \tag{9}$$

When we have more than one reaction in the system we denote the MM constant for reaction $i$ by $K_i^M$, and the reaction constants by $a_i, d_i$ and $k_i$.

As mentioned in the introduction, *in vivo* we cannot in general assume a low enzyme concentration and hence, the MM approximation can not be expected to hold. A recent approach to resolve this problem is that of the total quasi-steady state assumption

(tQSSA). It was introduced by Borghans et al. [20] and refined by Tzafriri [21] for isolated reactions. We have recently extended it to fully competitive reactions [23]. The tQSSA [20, 21] arises by introducing the total substrate

$$\bar{S} = S + C,$$

and assuming that the complex is in a quasi-steady state as for the sQSSA. For (5) it gives [21]

$$\frac{d\,\bar{S}}{dt} \approx\ -k\,C_{-}(\bar{S}), \quad \bar{S}(0) = S_T, \tag{10}$$

where

$$C_{-}(\bar{S}) = \frac{(E_T + K_M + \bar{S}) - \sqrt{(E_T + K_M + \bar{S})^2 - 4E_T\bar{S}}}{2}. \tag{11}$$

Numerical integration of (10) easily gives the time behavior of $\bar{S}, C$ (by (11)) and $S$ (by the relation $S = \bar{S} - C$).

Tzafriri [21] showed that the tQSSA (10) is valid whenever

$$\epsilon_{Tz} := \frac{K}{2S_T}\left(\frac{E_T + K_M + S_T}{\sqrt{(E_T + K_M + S_T)^2 - 4E_T S_T}} - 1\right) \ll 1, \quad \text{where} \quad K = \frac{k}{a}, \tag{12}$$

and that this is always roughly valid in the sense that

$$\epsilon_{Tz} \leq \frac{K}{4K_M} \leq \frac{1}{4}. \tag{13}$$

This means that for *any* combination of parameters and initial conditions (10) is a decent approximation to the full system (6). The parameter $K$ is known as the Van Slyke-Cullen constant.

As a first order approximation to (10), Tzafriri [21] found the expression, obtained originally in [20] by different techniques,

$$\frac{d\,\bar{S}}{dt} \approx\ -\frac{V_{max}\,\bar{S}}{K_M + E_T + \bar{S}}, \quad \bar{S}(0) = S_T. \tag{14}$$

This approximation is valid at low enzyme concentrations $E_T \ll S_T + K_M$, where it reduces to the MM expression (9), but holds moreover at low substrate concentrations $S_T \ll E_T + K_M$ [21]. Thus, with minimal effort performing the substitutions

of $S$ by $\bar{S}$ and of $K_M$ by $K_M + E_T$ one obtains a significantly improved MM-like approximation, without any need of more advances mathematics.

We refer to the Appendix for the full system of differential equations describing the different networks investigated in the Results section.

The parameter values used for the MAPK cascade are given in figure captions or Appendix C (online material), Table 1. As shown in Appendix B, when going from experimentally obtained (MM) parameters ($V_{max}, K_M$) to the full system, there is one degree of freedom with respect to the choice of parameters $(a, d, k)$. We have used the constraint proposed in [2, supplementary, on-line material] that $d = 4k$. This is consistent with the fact that for many enzymes the parameter $d$ is much greater than $k$ [44].

# A The tQSSA for fully competitive enzyme reactions

The system (2) is governed by the coupled ODEs [14, 27, 51], $i = 1, 2$,

$$\frac{d\,S_i}{dt} = -a_i E \cdot S_i + d_i C_i, \qquad S_i(0) = S_{i,T}, \tag{15a}$$

$$\frac{d\,C_i}{dt} = a_i(E \cdot S_i - K_i^M C_i), \qquad C_i(0) = 0, \qquad K_i^M = \frac{d_i + k_i}{a_i}. \tag{15b}$$

and the conservation laws

$$S_{i,T} = S_i + C_i + P_i, \qquad i = 1, 2, \tag{16}$$

$$E_T = E + C_1 + C_2. \tag{17}$$

The sQSSA of this system is [14, 51]

$$\frac{d\,S_i}{dt} \approx -\frac{k_i E_T S_i}{K_i^M(1 + S_j/K_j^M) + S_i}\,, \quad S_i(0) = S_{i,T}, \qquad i = 1, 2, \quad j \neq i, \tag{18}$$

which is valid when [27]

$$\frac{E_T}{K_i^M(1 + S_{j,T}/K_j^M) + S_{i,T}} \ll 1\,, \qquad i = 1, 2, \quad j \neq i. \tag{19}$$

As in the non-competitive case, it says that the sQSSA holds at low enzyme concentrations.

We have improved these results [23], applying the tQSSA to both reactions and showing that the tQSSA is given by finding $C_1$ as the unique biologically acceptable root ($0 < C_1 < \min\{E_T, \bar{S}_1\}$) of the third degree polynomial

$$\begin{aligned}\psi_1(C_1) = &-(K_1^M - K_2^M)C_1^3 \\ &+ \big[(E_T + K_1^M + \bar{S}_1)(K_1^M - K_2^M) - (\bar{S}_1 K_2^M + \bar{S}_2 K_1^M)\big]C_1^2 \\ &+ \big[ - E_T(K_1^M - K_2^M) + (\bar{S}_1 K_2^M + \bar{S}_2 K_1^M) + K_2^M(E_T + K_1^M)\big]\bar{S}_1 C_1 \\ &- E_T K_2^M \bar{S}_1^2,\end{aligned} \tag{20}$$

and similarly finding $C_2$ as the root in the polynomial $\psi_2$ obtained by interchanging the indices 1 and 2 in (20). After a short transient phase the complex concentrations are assumed to equal the quasi steady-state concentrations, $C_i = C_i(\bar{S}_1, \bar{S}_2)$, given by the roots in the respective polynomials as discussed above. Then the evolution of the system can be studied by means of the tQSSA

$$\frac{d\,\bar{S}_i}{dt} \approx -k_i C_i(\bar{S}_1, \bar{S}_2), \qquad \bar{S}_i(0) = S_{i,T}. \tag{21}$$

This approach extends both the sQSSA for competitive reactions (18) as well as the tQSSA for isolated reactions (10) as shown in [23].

# B Relationship among the kinetic parameters

While every reaction is characterized by three constant rates $(a, d, k)$, its QSSA works with only two parameters: $V_{max}$ and $K_M$. Since $K_M = \frac{k+d}{a}$ and $V_{max} = kE_T$, we have

$$k = \frac{V_{max}}{E_T}, \qquad a = \frac{k+d}{K_M} = \frac{V_{max} + dE_T}{E_T K_M}. \tag{22}$$

Posing $d = 4k$ [2, on-line material] we uniquely obtain the values of $a, d$ and $k$ from $K_M$ and $V_{max}$ as

$$k = \frac{V_{max}}{E_T}, \qquad d = \frac{4V_{max}}{E_T}, \qquad a = \frac{5V_{max}}{E_T K_M}. \tag{23}$$

In general, posing $d = \alpha k$ we have

$$k = \frac{V_{max}}{E_T}, \qquad d = \frac{\alpha V_{max}}{E_T}, \qquad a = \frac{k+d}{K_M} = \frac{(1+\alpha)V_{max}}{E_T K_M}, \tag{24}$$

with a freedom degree, related to the value of $\alpha$. Consequently, it is possible to vary the triplet $(a, d, k)$ obtaining the same pair $(V_{max}, K_M)$.

However, the different choices of $(a, d, k)$ could produce significantly different outputs, and thus predict completely different behavior in the solutions of the full system and of its QSSAs, respectively.

# References

1. Huang C.-Y. F. & Ferrell J. E. (1996) Ultrasensitivity in the mitogen-activated protein kinase cascade. *Proc. Natl. Acad. Sci.* **93**, 10078–10083.

2. Bhalla U. S. & Iyengar R. (1999) Emergent properties of networks of biological signaling pathways. *Science* **283**, 381–387.

3. Kholodenko B. N. (2000) Negative feedback and ultrasensitivity can bring about oscillations in the mitogen-activated protein kinase cascades. *Eur. J. Biochem.* **267**, 1583–1588.

4. Schoeberl B., Eichler-Jonsson C., Gilles E. D. & Muller G. (2002) Computational modeling of the dynamics of the MAP kinase cascade activated by surface and internalized EGF receptors. *Nat. Biotechnol.* **20**, 370–375.

5. Sasagawa S., Ozaki Y.-I., Fujita K. & Kuroda S. (2005) Prediction and validation of the distinct dynamics of transient and sustained ERK activation. *Nat. Cell Biol.* **7**, 365–373.

6. Loew L. & Schaff J. (2001) The virtual cell: a software environment for computational cell biology. *Trends Biotechnol.* **19**, 401–406.

7. Snoep J. L. (2005) The Silicon Cell initiative: working towards a detailed kinetic description at the cellular level. *Curr Opin Biotechnol.* **16**, 336–343.

8. Ellis R. J. (2001) Macromolecular crowding: obvious but underappreciated. *Trends Biochem. Sci.* **26**, 597–604.

9. Henri V. (1901) Recherches sur la loi de l'action de la sucrase. *C. R. Hebd. Acad. Sci.* **133**, 891–899.

10. Henri V. (1901) Über das gesetz der wirkung des invertins. *Z. Phys. Chem.* **39**, 194–216.

11. Henri V. (1902) Théorie générale de l'action de quelques diastases. *C. R. Hebd. Acad. Sci.* **135**, 916–919.

12. Michaelis L. & Menten M. L. (1913) Die kinetik der invertinwirkung. *Biochem. Z.* **49**, 333–369.

13. Briggs G. E. & Haldane J. B. S. (1925) A note on the kinetics of enzyme action. *Biochem. J.* **19**, 338–339.

14. Segel L. A. (1988) On the validity of the steady state assumption of enzyme kinetics. *Bull. Math. Biol.* **50**, 579–593.

15. Segel L. A. & Slemrod M. (1989) The quasi steady-state assumption: a case study in perturbation. *SIAM Rev.* **31**, 446–477.

16. Straus O. H. & Goldstein A. (1943) Zone behavior of enzymes. *J. Gen. Physiol.* **26**, 559–585.

17. Sols A. & Marco R. (1970) Concentration of metabolites and binding sites. Implications in metabolic regulation. In Current topics in Cellular Regulation, volume 2. Academic Press, New York.

18. Schnell S. & Maini P. K. (2003) A century of enzyme kinetics: Reliability of the $K_M$ and $v_{max}$ estimates. *Comm. Theor. Biol.* **8**, 169–187.

19. Bisswanger H. (2002) Enzyme Kinetics. Principles and Methods. Wiley-VCH, Weinheim.

20. Borghans J., de Boer R. & Segel L. (1996) Extending the quasi-steady state approximation by changing variables. *Bull. Math. Biol.* **58**, 43–63.

21. Tzafriri A. R. (2003) Michaelis-Menten kinetics at high enzyme concentrations. *Bull. Math. Biol.* **65**, 1111–1129.

22. Tzafriri A. R. & Edelman E. R. (2004) The total quasi-steady-state approximation is valid for reversible enzyme kinetics. *J. Theor. Biol.* **226**, 303–313.

23. Pedersen M. G., Bersani A. M. & Bersani E. (2005) The total quasi-steady-state approximation for fully competitive enzyme reactions. *Submitted* .

24. Chang L. & Karin M. (2001) Mammalian MAP kinase signalling cascades. *Nature* **410**, 37–40.

25. Pearson G., Robinson F., Gibson T. B., Xu B. E., Karandikar M., Berman K. & Cobb M. H. (2001) Mitogen-activated protein (MAP) kinase pathways: regulation and physiological functions. *Endocr. Rev.* **22**, 153–183.

26. Chen Z., Gibson T. B., Robinson F., Silvestro L., Pearson G., Xu B., Wright A., Vanderbilt C. & Cobb M. H. (2001) MAP kinases. *Chem. Rev.* **101**, 2449–2476.

27. Schnell S. & Mendoza C. (2000) Time-dependent closed form solutions for fully competitive enzyme reactions. *Bull. Math. Biol.* **62**, 321–336.

28. Burack W. R. & Sturgill T. W. (1997) The activating dual phosphorylation of MAPK by MEK is nonprocessive. *Biochemistry* **36**, 5929–5933.

29. Ferrell J. E. & Bhatt R. R. (1997) Mechanistic studies of the dual phosphorylation of mitogen-activated protein kinase. *J. Biol. Chem.* **272**, 19008–19016.

30. Zhao Y. & Zhang Z.-Y. (2001) The mechanism of dephosphorylation of extracellular signal-regulated kinase 2 by mitogen-activated protein kinase phosphatase 3. *J. Biol. Chem.* **276**, 32382–32391.

31. Hatakeyama M., Kimura S., Naka T., Kawasaki T., Yumoto N., Ichikawa M., Kim J. H., Saito K., Saeki M., Shirouzu M., Yokoyama S. & Konagaya A. (2003) A computational model on the modulation of mitogen-activated protein kinase (MAPK) and Akt pathways in heregulin-induced ErbB signalling. *Biochem. J.* **373**, 451–463.

32. Markevich N. I., Hoek J. B. & Kholodenko B. N. (2004) Signaling switches and bistability arising from multisite phosphorylation in protein kinase cascades. *J. Cell Biol.* **164**, 353–359.

33. Camps M., Nichols A. & Arkinstall S. (2000) Dual specificity phosphatases: a gene family for control of MAP kinase function. *FASEB J.* **14**, 6–16.

34. Ebisuya M., Kondoh K. & Nishida E. (2005) The duration, magnitude and compartmentalization of ERK MAP kinase activity: mechanisms for providing signaling specificity. *J. Cell Sci.* **118**, 2997–3002.

35. Lewis T. S., Shapiro P. S. & Ahn N. G. (1998) Signal transduction through MAP kinase cascades. *Adv. Cancer Res.* **74**, 49–139.

36. Marshall C. J. (1995) Specificity of receptor tyrosine signaling: transient versus sustained extracellular signal-regulated kinase activation. *Cell* **80**, 179–185.

37. Zhan X. L., Wishart M. J. & Guan K. L. (2001) Nonreceptor tyrosine phosphatases in cellular signaling: regulation of mitogen-activated protein kinases. *Chem. Rev.* **101**, 2477–2496.

38. Dougherty M. K., Muller J., Ritt D. A., Zhou M., Zhou X. Z., Copeland T. D., Conrads T. P., Veenstra T. D., Lu K. P. & Morrison D. K. (2005) Regulation of Raf-1 by direct feedback phosphorylation. *Mol. Cell* **17**, 215–224.

39. Ferrell, Jr., J. E. (2002) Self-perpetuating states in signal transduction: positive feedback, double-negative feedback and bistability. *Curr. Opin. Cell Biol.* **14**, 140–148.

40. Hill C. S. & Treisman R. (1995) Transcriptional regulation by extracellular signals: Mechanisms and specificity. *Cell* **80**, 199–211.

41. Traverse S., Seedorf K., Paterson H., Marshall C. J., Cohen P. & Ullrich A. (1994) EGF triggers neuronal differentiation of PC12 cells that overexpress the EGF receptor. *Curr. Biol.* **4**, 694–701.

42. New L., Li Y., Ge B., Zhong H., Mansbridge J., Liu K. & Han J. (2001) SB203580 promote EGF-stimulated early morphological differentiation in PC12 cell through activating ERK activity. *J. Cell. Biochem.* **83**, 585–596.

43. Bardelli C., Sala M., Cavallazzi U. & Prat M. (2005) Agonist met antibodies define the signalling threshold required for a full mitogenic and invasive program of Kaposi's Sarcoma cells. *Biochem. Biophys. Res. Comm.* **334**, 1172–1179.

44. Atkinson D. (1977) Cellular Energy Metabolism and its Regulation. Academic Press, New York.

45. Cao Y., Gillespie D. T. & Petzold L. R. (2005) Accelerated stochastic simulation of the stiff enzyme-substrate reaction. *J. Chem. Phys.* **123**, 144917.

46. Saccomani M. P., D'Angio L., Audoly S. & Cobelli C. (2001) *A priori* identifiability of physiological parametric models. In E. Carson & C. Cobelli, (ed.), Modelling Methodology for Physiology and Medicine, chapter 4, pp. 77–105. Academic Press, San Diego.

47. Hornberg J., Binder B., Bruggeman F., Schoeberl B., Heinrich R. & Westerhoff H. (2005) Control of MAPK signalling: from complexity to what really matters. *Oncogene* **24**, 5533–5542.

48. Hornberg J. J., Bruggeman F. J., Binder B., Geest C. R., de Vaate A. J. M. B., Lankelma J., Heinrich R. & Westerhoff H. V. (2005) Principles behind the multifarious control of signal transduction. ERK phosphorylation and kinase/phosphatase control. *FEBS J.* **272**, 244–258.

49. Cascante M., Boros L. G., Comin-Anduix B., de Atauri P., Centelles J. J. & Lee P. W.-N. (2002) Metabolic control analysis in drug discovery and disease. *Nat. Biotechnol.* **20**, 243–249.

50. Goldbeter A. & Koshland, Jr., D. E. (1981) An amplified sensitivity arising from covalent modification in biological systems. *Proc. Natl. Acad. Sci.* **78**, 6840–6844.

51. Rubinow S. I. & Lebowitz J. L. (1970) Time-dependent Michaelis-Menten kinetics for an enzyme-substrate-inhibitor system. *J. Am. Chem. Soc.* **92**, 3888–3893.

# List of Tables

| Method | Oscillations |
|---|---|
| Full system | $K_I < 0.18$ |
| Competitive tQSSA | $K_I < 0.86$ |
| Competitive sQSSA | $K_I < 3.02$ |

Table 1: Regions of oscillations for the MAPK cascade with feedback expressed by the inhibition constant $K_I$.

# List of Figures

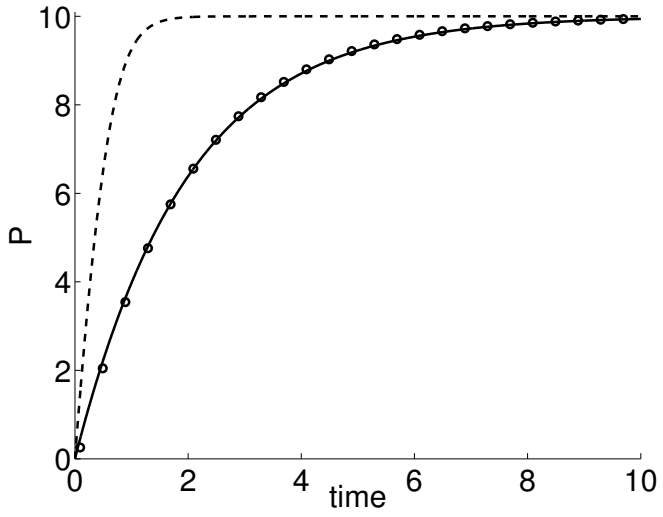


Figure 1: Temporal evolution of the product $P$ at high enzyme concentrations for the single reaction (1). In this case, the solution of the full system (circles) is badly approximated by the MM approximation (sQSSA, dashed curve), while the tQSSA (full curve) estimates the behavior very well. Parameters are $k = 0.6, K_M = 8, E(0) = E_T = 50$, and $S(0) = S_T = 10$, all in arbitrary units.

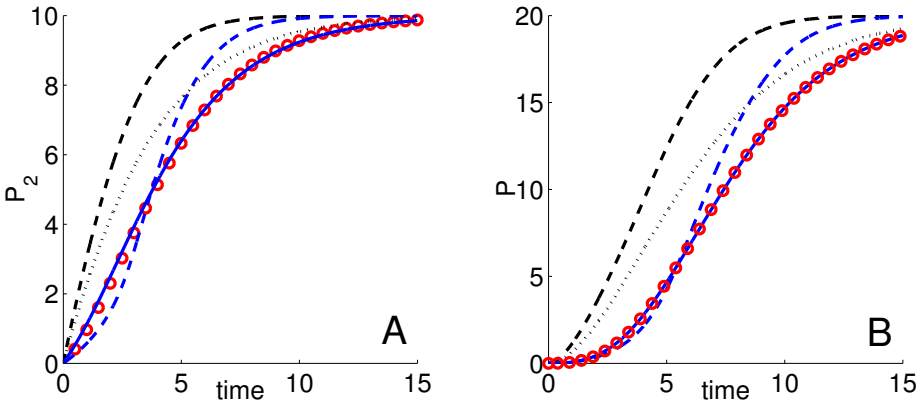


Figure 2: Competitive systems. Panel A: A simulation of competing substrates (scheme (2)). Panel B: A simulation of two successive reactions catalyzed by the same enzyme (scheme (3)). In both cases the full system (red circles) is estimated very well by the competitive tQSSA (blue, full curve), while the competitive sQSSA (blue, dashed curve) as well as the non-competitive sQSSA (black, dashed curve) and tQSSA (black, dotted curve) do not fit. The parameters are in both panels: $k_1 = 0.5, k_2 = 0.6, K_1^M = 0.75, K_2^M = 8, E_{tot} = 10$, and $S_1(0) = S_2(0) = 10$ in panel A, $S_1(0) = 20, S_2(0) = 0$ in panel B. All units are arbitrary.

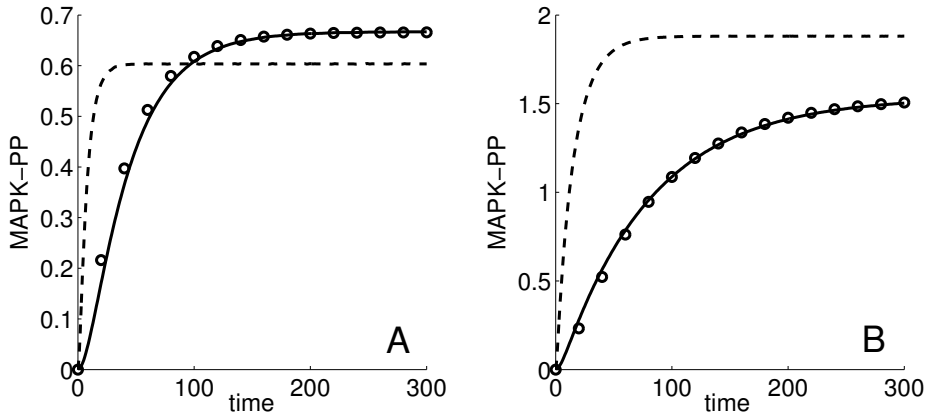


Figure 3: Phosphorylation and dephosphorylation. The sQSSA (dashed line) leads to a wrong estimation of both the transient behavior as well as steady state levels, while the tQSSA (full line) fits well, for the double phosphorylation/dephosphorylation (4) modelled with MM kinetics. The full system is shown as circles. Parameters: $[\text{MAPK}]_T = 500$ (panel A), $[\text{MAPK}]_T = 50$ (panel B), $[\text{MKP}]_T = 100, [\text{MAPKK}]_T = 50,\ K_1^M = 50,\ K_2^M = 500,\ K_3^M = 22,\ K_4^M = 18,$ $k_1 = 0.01,\ k_2 = 15,\ k_3 = 0.084,\ k_4 = 0.06$. (Concentrations and time in arbitrary units, but for consistence with [32] one can think of nM and seconds).

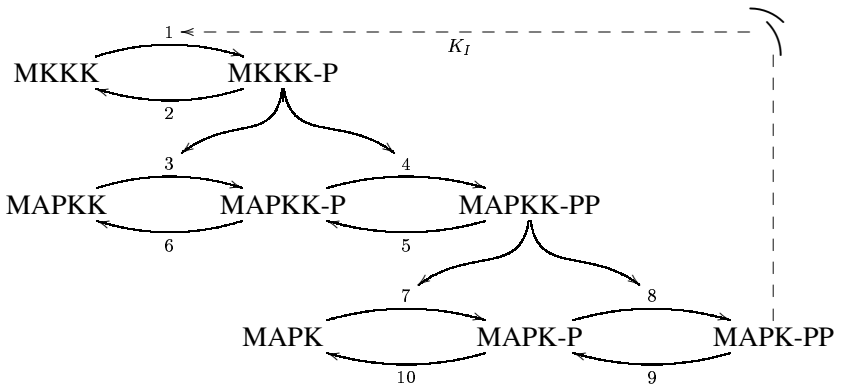


Figure 4: The MAPK cascade. The diagram is based on [3]. Each of the reactions is assumed to follow MM kinetics, but there are competitive reactions since MKKK-P catalyzes both reactions 3 and 4 and MAPKK-PP catalyzes both reactions 7 and 8. Similarly, reactions 5 and 6 are assumed to compete for a phosphatase, and both reactions 9 and 10 to be catalyzed by another phosphastase (MKP in (4)). The phosphatases are not shown for clarity of the figure. The dashed line indicates inhibition of reaction 1 by MAPK-PP as in [3]. However, we assume that this inhibition is competitive. *M*-P and *M*-PP represent, respectively, monophosphorylated and diphosphorylated *M*, where *M* is either MKKK, MAPKK or MAPK.

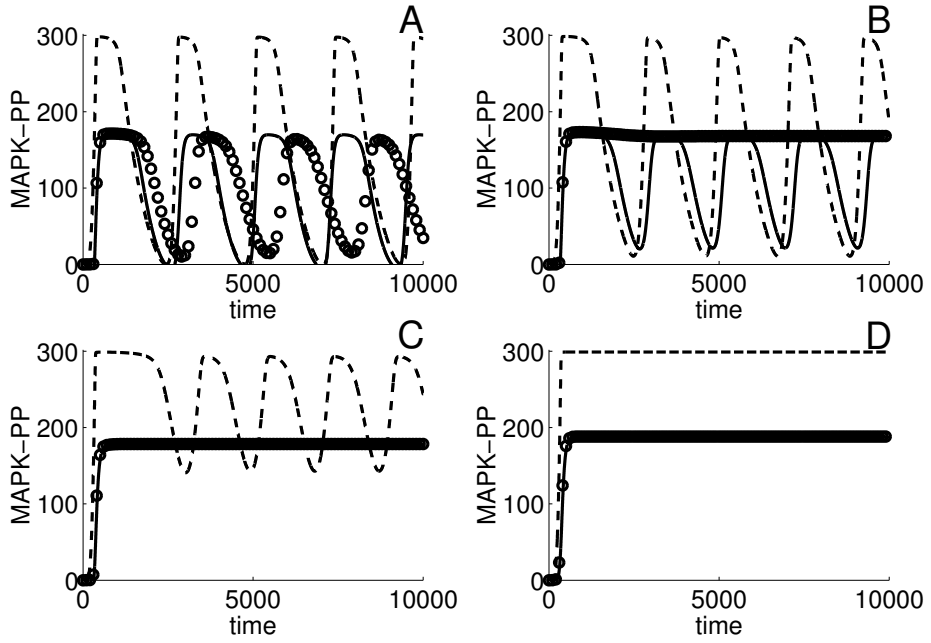


Figure 5: Simulations of the MAPK cascade with feedback as in Fig. 4. The computed MAPK-PP concentration is shown following the legends in Fig. 3. The values of the inhibition constant are as follows: Panel A: $K_I = 0.1$. Panel B: $K_I = 0.5$. Panel C: $K_I = 2.5$. Panel D: $K_I = 20$. At low values of $K_I$ (panel A), all the three schemes, full system (circles), tQSSA (full curve) and sQSSA (dashed curve), produce oscillations, but the tQSSA follows the solution much better than the sQSSA, especially with respect to the amplitude of the oscillations. In panel C, although the MAPK-PP modelled by the full system (circles) almost immediately reaches a steady-state, the sQSSA (dashed curve) shows oscillations. On the other hand, the full system is followed very well by the tQSSA (full curve). However, this is not always the case, since the tQSSA can also predict oscillations when the full system is stable (panel B). Finally, at high values of $K_I$ all the three approaches go to a steady state, but the sQSSA overestimates the MAPK-PP level significantly (panel D).

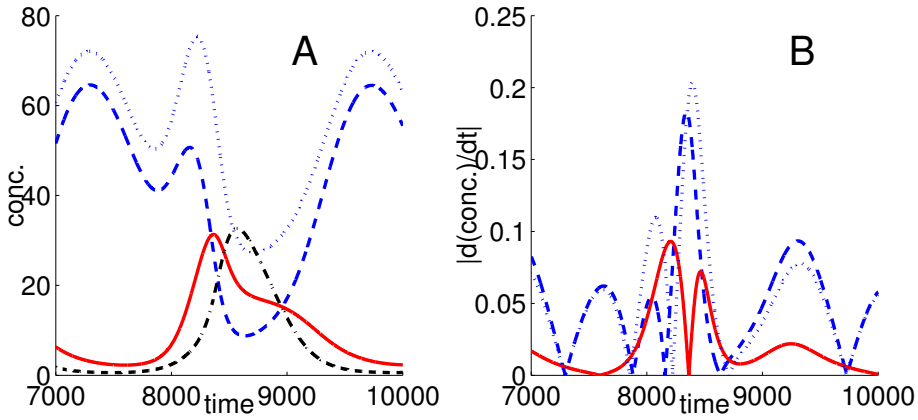


Figure 6: Non-neglectible and non-constant complex concentrations in the MAPK cascade. In the full system describing the MAPK cascade with feedback, the complex (MAPK-P)–(MAPKK-PP) is neither negligible (panel A) nor approximately constant (panel B). Panel A shows the concentrations of the complex (MAPK-P)–(MAPKK-PP) (red, full curve), MAPK-P (blue, dashed curve), "total MAPK-P" ($\overline{\text{MAPK-P}}$ ; blue, dotted curve) and MAPKK-PP (black, dash-dot curve) during the last part of the simulation of the full system from figure 5B. Panel B shows the absolute value of the time derivative of the complex, MAPK-P and $\overline{\text{MAPK-P}}$ (same legends as in panel A).

# *Paper IX*

# A MATHEMATICAL APPROACH TO THE STUDY OF SIGNAL TRANSDUCTION PATHWAYS IN MAPK CASCADE

A. M. BERSANI

*Dept. Mathematical Methods and Models - University "La Sapienza"*
*via A. Scarpa, 16 - 00161 Rome (Italy)*
*E-mail: bersani@dmmm.uniroma1.it*

M. G. PEDERSEN

*Department of Mathematics - Technical University of Denmark*
*Matematiktorvet, Building 303 - 2800 Kgs. Lyngby (Denmark)*
*E-mail: M.G.Pedersen@mat.dtu.dk*

E. BERSANI

*DataLink Informatica s.r.l. - via V. Cortese, 147/F - 00128 Rome (Italy)*
*E-mail: e.bersani@datalinkinformatica.com*

F. BARCELLONA

*Dept. INFOCOM - University "La Sapienza"*
*via Eudossiana, 18 - 00184 Rome (Italy)*
*E-mail: francesco.barcellona@uniroma1.it*

Mathematical modelling of signal transduction pathways is a very useful approach for understanding molecular mechanisms. Without this theoretical framework, it is, in general, difficult to understand the high complexity of metabolic phenomena. The main goal of computational biology, and in particular of systems biology, is to define a comprehensive model that can accurately represent the experimental data and, mainly, serve as a fundamental tool to generate and test hypotheses. In this work we reexamine the mathematical model of MAP kinase cascade.

## 1. Introduction

In the last decade, more and more interest has been paid to the mathematical models of intracellular phenomena and in particular of signal transduction.

Every cell responds to external signals, like hormones, metals, heat

shocks and so on, which are transduced by a complex protein network. When a signal arrives at the cell membrane, some proteins, starting from membrane receptors, are activated and by means of biochemical reactions transduce the signal. At each step of the network, the signal can be modulated, damped, or amplified. The most important enzymes which are involved in the transduction are the so-called kinases, which activate the proteins of the network, by means of phosphorylation[14,25]. Viceversa, the role of the phosphatases is to inactivate the proteins by dephosphorylation. Although other kinds of biochemical reactions can happen, phosphorylation is an important intracellular reaction.

The mitogen activated protein kinase (MAPK) cascade is the most investigated of these signal transduction pathways, evolutionarily conserved from yeast to man and involved in many different physiological functions[10,24]. In the experimental investigations of the MAPK cascade signal transduction, many interesting properties have emerged; among these, the existence of feedback loops (positive and negative), ultrasensitivity and hysteresis [2,5,6,12,13,18,19,20,32].

All these phenomena have attracted the attention of biomathematicians, interested in theoretical investigation of signal transduction by means of dynamical systems, based on the tenets of enzyme kinetics (see, for example, Refs. [3, 5, 16, 18, 19, 29]). These models, although not realistic because of incomplete experimental data related to the model parameters, have been successful in reproducing all these features and are very promising in doing quantitative predictions in the future (see Ref. [35] for a recent review).

Surprisingly, the mathematical formulation of these highly interconnected enzyme reactions is based on *in vitro* studies of isolated reactions, without a serious criticism of the delicate passage from the kinetics of simple reactions to the kinetics of a network of reactions shared by several cascades, in a crowded molecular environment[11].

The main goal of a mathematical approach to the intracellular biochemical interactions is related to the ambitious project of a virtual cell, with the aim to simulate satisfactorily the behaviour of whatever cell. One of the principal components of these models is the so-called Michaelis-Menten (MM) kinetics[21,8,4,14,35], which describes enzyme reactions by means of ordinary differential equations.

Biochemists often use the MM approximation, or *standard quasi-steady-state* approximation (sQSSA) to simplify the model under suitable hypotheses. This approach is very useful in the case of isolated reactions, but it is not always reasonable, in particular when we have to face with many

interconnected reactions. In this paper we investigate the applicability of the MM approximation, showing some (even simple) counterexamples.

## 2. The Michaelis-Menten approximation

The phosphorylation reaction is characterized by the following events: an enzyme $E$ (in this case a kinase) binds reversibly with a substrate $S$, forming a complex $C$ (also denoted $E$-$S$). The complex is assumed to break irreversibly down into the original enzyme and a product $P$ (e.g. a phosphorylated form of the substrate). The enzyme $E$ becomes free again, ready to bind with other molecules of the substrate. In other terms, we can present the reaction by means of the following scheme:

$$E + S \underset{d}{\overset{a}{\rightleftarrows}} C = E\text{-}S \xrightarrow{V} E + P. \tag{1}$$

From a mathematical point of view, every of these individual reactions can be represented by the mass action principle, where the rate of the reaction is proportional to the concentrations of the reactants. The proportionality constant indicates how fast the reaction is. From the above scheme, the reaction is characterized by a system of four ordinary differential equations

$$\frac{d[S]}{dt} = -a[E][S] + d[C] \ , \tag{2}$$

$$\frac{d[C]}{dt} = a[E][S] - d[C] - V[C] \ , \tag{3}$$

$$\frac{d[E]}{dt} = -a[E][S] + d[C] + V[C] \ , \tag{4}$$

$$\frac{d[P]}{dt} = V[C] \ , \tag{5}$$

where $[S]$, $[E]$, $[C]$, $[P]$ represent the absolute concentrations of the different enzymes involved in the reaction, subject to the initial conditions

$$\begin{aligned} [E](0) := E_0 = [E_{tot}] \ ; \quad [S](0) := S_0 = [S_{tot}] \ ; \\ [C](0) := C_0 = 0 \ ; \qquad [P](0) := P_0 = 0 \ , \end{aligned} \tag{6}$$

and to the mass balance (conservation) laws

$$[E_{tot}] = [E] + [C] \qquad ; \qquad [S_{tot}] = [S] + [C] + [P] \ . \tag{7}$$

4

It follows that there are only two independent equations and we can rewrite the system in the form

$$\frac{d[S]}{dt} = -a([E_{tot}] - [C])[S] + d[C], \tag{8}$$

$$\frac{d[C]}{dt} = a([E_{tot}] - [C])[S] - (d+V)[C] \ . \tag{9}$$

This is the Michaelis-Menten (MM) kinetics[21,8,4,35]. For simplicity, we will in the following leave out the brackets, when no confusion could occur.

In order to simplify the model and reduce the number of parameters, Michaelis and Menten[21] proposed an approximation, which is known as the Michaelis-Menten, or standard quasi-steady-state approximation (sQSSA). It is based on the hypothesis that, after a short transient phase, the complex $C$ is approximately in a state of dynamically equilibrium. Consequently, putting the right hand side of Eq. (9) equal to zero, we obtain the following relationships

$$C = \frac{E_0 \ S}{K_m + S} \ , \tag{10}$$

$$\frac{dS}{dt} = -\frac{V_{max} S}{K_m + S} \ . \tag{11}$$

where $K_m = \frac{d+V}{a}$ and $V_{max} = V \cdot E_0$.

Already Michaelis and Menten realized that this approximation is guaranteed when the enzyme concentration is much less than the substrate concentration. Actually, in [21] the authors found a less precise formula. Formulas (10) and (11) were obtained by Briggs and Haldane in 1925[8].

Even though the MM approximation is based on a qualitative assumption ("the complex is more or less in equilibrium, so its derivative is *close* to zero"), several biochemical books and papers interpret the approximation as the case in which the derivative of the complex *is* null. This interpretation is obviously incorrect. In fact it is very simple to show, from (2) – (5), that setting $\frac{dC}{dt} = 0$ implies that every concentration is constant. In other words, the strict condition $\frac{dC}{dt} = 0$ can be applied only for the asymptotic analysis of the system (2) – (5). Many authors have studied the MM kinetics by a mathematical point of view (see, e.g., Refs. [17, 31, 7, 28, 26, 34], and the review paper [27]), by means of asymptotic expansions and singular perturbation techniques. In fact, in these articles the authors introduce a parameter $\epsilon$, which is related to the biochemical quantities involved in the reaction, and develop an asymptotic expansion in terms of

that parameter, showing that, when $\epsilon \ll 1$, the MM approximation may be applied. The Michaelis-Menten curve of the temporal evolution of the product $P$ is always concave, while, in general, the solution $P$ of the system (2) – (5) passes from a first convex phase to a second concave one, as seen in Fig. 1D.

In 1967 Heineken et al.[17] proposed an asymptotic expansion in terms of the parameter $\epsilon_{HTA} = \frac{E_0}{S_0}$, obtaining, at the zeroth order, the Michaelis-Menten approximation.

In 1989 Segel and Slemrod[31], using the parameter $\epsilon_{SS} = \frac{E_0}{S_0+K_m}$, showed that an appropriate steady state approximation can be applied to more general cases. In fact, the Segel-Slemrod approximation (*reverse quasi-steady-state approximation*, rQSSA), may be applied even when $E_0 \gg S_0$ or $E_0 \approx S_0$, provided $K_m \gg E_0$. This can occur in many biochemical reactions (see Refs. [22] and [15] for a practical example). The final equation for $S$ is the same as in the sQSSA.

The above mentioned results, published on journals of applied mathematics or of theoretical biology, have become "classical" issues in many books devoted to mathematical biology (see, for example, Refs. [22], [23]). In spite of this fact, it seems that the great majority of biologists and biochemists ignore all the contributions after 1925 and consider only the original theory by Michaelis and Menten and by Briggs and Haldane.

Furthermore, other authors have extended the results obtained in Ref. [31]. In particular, we want to mention the paper by Borghans, de Boer and Segel[7]. Introducing the new variable $\overline{S}(t) = S(t) + C(t)$ and working on asymptotic expansions in terms of the parameter $\epsilon_{BBS} = \frac{K \cdot E_0}{(K_m+E_0+S_0)^2}$, where $K = \frac{d}{a}$, the authors arrive at the approximation

$$C \approx C_-(\overline{S}), \tag{12}$$

$$\frac{d\overline{S}}{dt} = -VC_-(\overline{S}) \ , \tag{13}$$

where

$$C_-(\overline{S}) = \frac{(E_0 + K_m + \overline{S}) - \sqrt{(E_0 + K_m + \overline{S})^2 - 4E_0\overline{S}}}{2}.$$

This approximation is usually denoted the *total quasi-steady-state approximation* (tQSSA). Very recently, Tzafriri[34] showed that

$$\epsilon_{BBS} \leq \frac{K}{4K_m} \leq \frac{1}{4}\,. \tag{14}$$

6

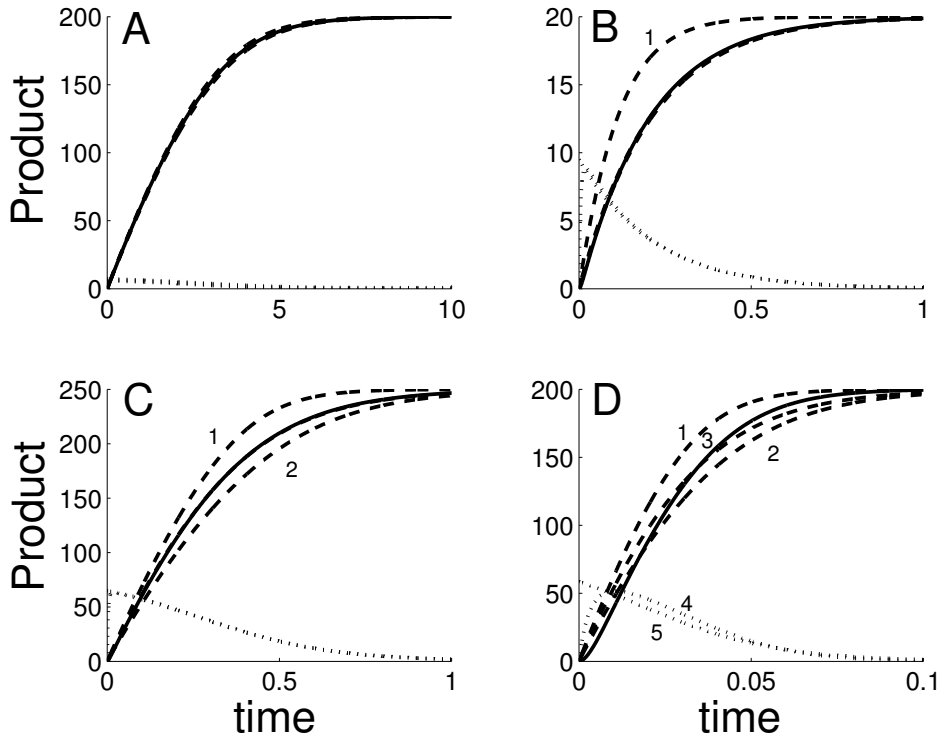


Figure 1. A: $\epsilon_{SS} = 0.03, \epsilon_{Tz} = 1.81$. The complex (dotted curve) is more or less constant and all approximations fit. B: $\epsilon_{SS} = 0.83, \epsilon_{Tz} = 0.10$. Note that MM (dashed curve indicated by 1) does not approximate anymore, and that the complex (dotted curve) is no longer constant. C: $\epsilon_{SS} = 0.29, \epsilon_{Tz} = 1.25$. MM (dashed curve, 1) and Tzafriri's 1st order tQSSA (dashed curve, 2) are both bad approximations, but tQSSA is still good. D: $\epsilon_{SS} = 0.33, \epsilon_{Tz} = 1.00$. Note that also the full tQSSA (dashed curve, 3) now fails to approximate well. This is best seen from the fact that the complex level (dotted curve, 4) is badly approximated by the tQSSA complex level (dotted curve, 5). In A-C: $K/K_m = 0.025$, while in D: $K/K_m = 0.2475$.

Consequently, the Borghans approximation may be considered a reasonable good approximation for every values of the parameters, especially when $\frac{K}{K_m} \ll 1$. Tzafriri also obtained the first order approximation of tQSSA, arriving at the equation for the total substrate

$$\frac{d\overline{S}}{dt} \approx \frac{-VE_0\overline{S}}{E_0 + K_m + \overline{S}} \,. \tag{15}$$

This approximation of the tQSSA is valid when either $\epsilon_{SS} \ll 1$ or $\epsilon_{Tz} := \frac{S_0}{K_m + E_0} \ll 1$.

In Fig. 1 we can clearly see how the different approximations are valid for much more general situations than the original work by Michaelis and Menten. As far as we know, no authors use the Borghans nor the Tzafriri

approximations, even though their formulas are very simple to implement, and clearly are more precise for a larger parameter range than the sQSSA.

## 3. The double phosphorylation mechanism

We move on to the MAPK cascade continuing the discussion of the risk of using the sQSSA. In this pathway, the upstream kinase (denoted Raf or MKKK, i.e. MAP kinase kinase kinase) phosphorylates the immediately downstream target, which is also a kinase (MEK, or MKK, i.e. MAP kinase kinase) successively on two specific sites, eventually activating it. This last double-phosphorylated kinase (MKK-PP or MKK**) acts on the MAPK (or ERK) through specific phosphorylation events on two sites. The activated MAPK is the last effector which usually enters the cell nucleus, where the signal is translated in the appropriate gene expression program. The activated cascade is shut down by the reverse action of specific phosphatases[9,36], whose outcome is the time modulation of the signal, probably through the regulation of the active kinase (for example, transient versus sustained activation).

As mentioned above and shown in Fig. 2 the kinase MKK can be phosphorylated twice by MKKK*. The MKK dephosphorylations are done by a phosphatase (PPase). In this case the equations regulating the reaction and the conservation laws become more complicated. As an example we consider the isolated diphosphorylation mechanism of MKK. Using the notation $E$-$S$ for the complexes, we can write the corresponding system

$$\begin{aligned}[MKK^*]' = {} & V_3[MKK - MKKK^*] + V_6[MKK^{**} - PPase] \\ & + d_4[MKK^* - MKKK^*] + d_5[MKK^* - PPase] \\ & - a_4[MKK^*][MKKK^*] - a_5[MKK^*][PPase],\end{aligned} \tag{16}$$

$$\begin{aligned}[MKK - MKKK^*]' = {} & a_3[MKK][MKKK^*] \\ & -(V_3 + d_3)[MKK - MKKK^*],\end{aligned} \tag{17}$$

$$\begin{aligned}[MKK^{**}]' = {} & V_4[MKK^* - MKKK^*] \\ & +d_6[MKK^{**} - PPase] - a_6[MKK^{**}][PPase],\end{aligned} \tag{18}$$

$$\begin{aligned}[MKK^* - PPase]' = {} & a_5[MKK^*][PPase] \\ & -(V_5 + d_5)[MKK^* - PPase],\end{aligned} \tag{19}$$

8

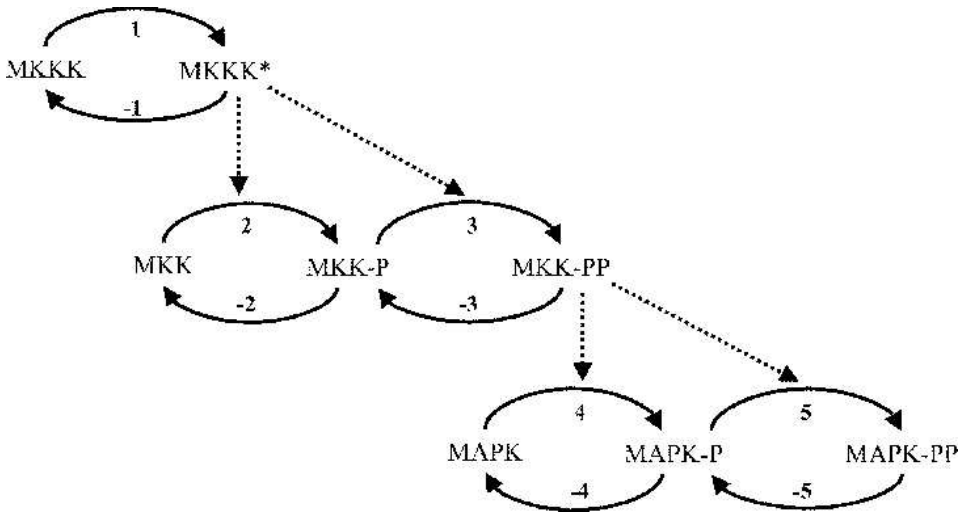


Figure 2. The MAPK cascade. The picture has been taken from the paper by Aguda and Sauro. MKKK* means monophosphorylated MKKK; MKK-P and MKK-PP represent, respectively, monophosphorylated and diphosphorylated MKK; MAPK-P and MAPK-PP represent, respectively, monophosphorylated and diphosphorylated MAPK.

$$[MKK^* - MKKK^*]' = a_4[MKK^*][MKKK^*] \quad (20)$$
$$-(V_4 + d_4)[MKK^* - MKKK^*],$$
$$[MKK^{**} - PPase]' = a_6[MKK^{**}][PPase] \quad (21)$$
$$-(V_6 + d_6)[MKK^{**} - PPase],$$

with the conservation laws

$$[MKKK^*] = [MKKK_{tot}] - [MKK - MKKK^*] \quad (22)$$
$$-[MKK^* - MKKK^*],$$
$$[MKK] = [MKK_{tot}] - [MKK^*] - [MKK - MKKK^*] \quad (23)$$
$$-[MKK^* - MKKK^*] - [MKK^{**}]$$
$$-[MKK^{**} - PPase] - [MKK^* - PPase],$$
$$[PPase] = [PPase_{tot}] - [MKK^{**} - PPase] \quad (24)$$
$$-[MKK^* - PPase].$$

Since phosphatase PPase catalyzes two reactions, more variables must be taken into account in the conservation law for MKK as shown in equation (23). Consequently, any steady-state approximation will result in more complicated expressions than in the case of a monophosphorylation reaction.

In fact, imposing a Michaelis-Menten condition for all the complexes, i.e. setting Eqns. (17), (19), (20) and (21) equal to zero, and introducing the parameters $k_j = \frac{d_j+V_j}{a_j}$, we arrive at the following quasi-steady-state relations for $[MKK^* - PPase]$ and $[MKK^{**} - PPase]$:

$$[MKK^* - PPase] = \frac{[MKK^*][PPase_{tot}]}{[MKK^*] + k_5\left(1 + \frac{[MKK^{**}]}{k_6}\right)} , \tag{25}$$

$$[MKK^{**} - PPase] = \frac{[MKK^*][PPase_{tot}]}{[MKK^{**}] + k_6\left(1 + \frac{[MKK^*]}{k_5}\right)} . \tag{26}$$

In the literature every single reaction is usually treated by a MM approximation, neglecting the other terms involved in the double reaction and, in particular, the important fact that, for example, $[MKK^*]$ is involved in the phosphorylation of $[MKK]$ and in the production of $[MKK^{**}]$.

The relations obtained by isolating the single reaction,

$$[MKK^* - PPase] = \frac{[MKK^*][PPase_{tot}]}{[MKK^*] + k_5} , \tag{27}$$

$$[MKK^{**} - PPase] = \frac{[MKK^*][PPase_{tot}]}{[MKK^{**}] + k_6} , \tag{28}$$

can be considered good approximations of (25), (26) only under suitable conditions, like

$$[MKK^*] \ll k_5 \quad , \quad [MKK^{**}] \ll k_6 , \tag{29}$$

which are, in general, not satisfied.

Thanks to equation (23), a sufficient condition to fulfill both conditions (29) is

$$[MKK_{tot}] \ll \min\{k_5, k_6\} . \tag{30}$$

Nevertheless, some of the most popular papers devoted to models of the MAP-kinases cascade use sQSSA, even if the parameters they consider do not satisfy conditions (29). In this case, the approximation leads to results substantially different from the full system of equations. We follow this up in another paper.

## 4. The MAPK cascade

Looking at the complete MAP-kinases cascade, shown in Fig. 2, it is clear that all the problems arising in the simpler cases described in the previous

paragraphs may occur. Nevertheless the above cited authors approximate every isolated reaction in terms of Michaelis-Menten mechanisms, without considering their applicability.

In particular, we want to stress that many authors assume that the concentration of the complexes may be considered not only constant, but even negligible with respect to the substrate and enzyme concentrations. In fact, in the conservation laws of the quasi-steady-state approximation, the complex concentrations disappear.

As an example, in Fig. 3 we compare the asymptotic values of the most important (by a physiological point of view) enzymes: the monophosphorylated MKKK and the diphosphorylated MKK and MAPK, in the Huang-Ferrell model. In fact, as shown in Fig. 2, enzyme MKKK is a substrate for its kinase, but acts as a kinase on MKK*. Similarly, MKK**, which is a substrate for the enzyme PPase, acts as a kinase on MAPK-P. Furthermore, MAPK-PP concentration influences the processes that follow the MAPK cascade in the network. Consequently, the asymptotic values of all the MAP-kinases determine the efficacy of the reactions they are regulating. As seen from Fig. 3 the MM approximation results in different levels than the full system of equations. This is in large part due to the neglect of the complexes.

Finally, several authors suppose that MAPK-PP acts, by means of a feedback mechanism, on the first layer of the MAPK cascade, and in some cases this feedback has been shown experimentally (see Ref. [12] for a review). For example, Kholodenko[19] introduced a noncompetitive inhibition of this kind, showing the oscillatory nature of the cascade for a certain range of parameter values. In the case of feedback, it is harder to decide whether sQSSA can be applied. The investigation of the various types of feedback will be the subject of a future paper.

## 5. Conclusions and perspectives

Every cellular network is very complicated. Due to many different interactions, we cannot *a priori* expect that the network can be represented by some steady-state approximation. Without any further information on the concentrations and the parameter values, the only thing to do seems to describe every reaction in terms of two equations, since the complexes cannot be neglected. This means to face with 4 parameters for every reaction, instead of 2. This fact is, in general, not so cumbersome, because many parameters can be measured experimentally.

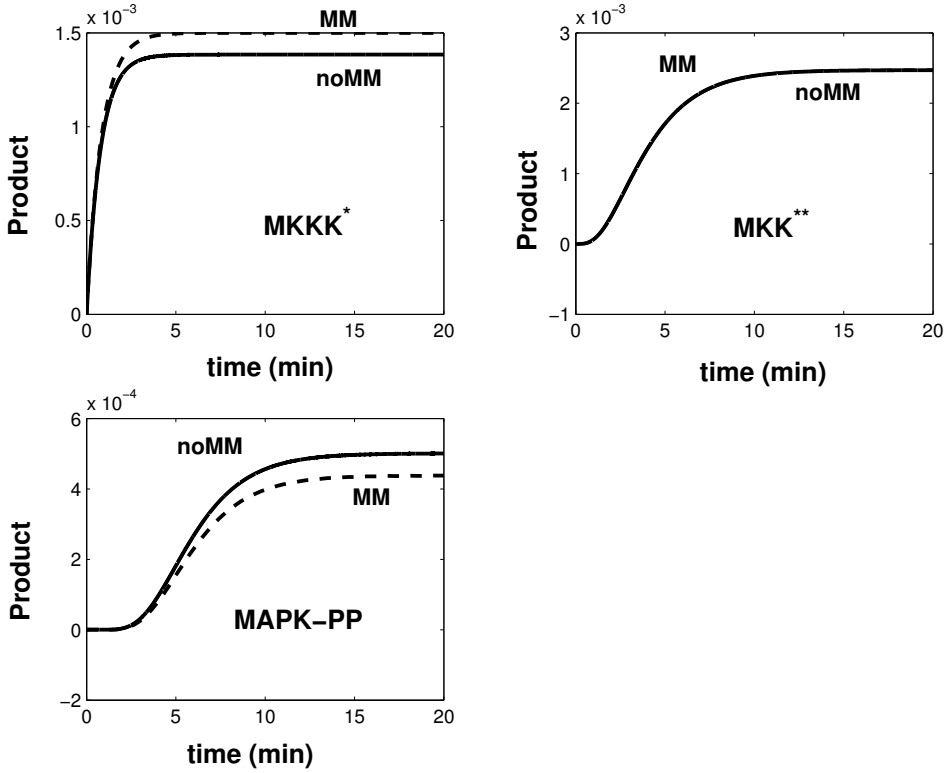


Figure 3. MKKK*, MKK**, and MAPK-PP in the full system (solid line) and in the MM approximation (dashed line). The values of the parameters can be found in [18]. While the plots of MKK** are close, for MKKK* and MAPK-PP the difference is evident.

As we have seen, the classical Michaelis-Menten approximation (sQSSA) is not valid in general, and even when applicable for the isolated single reactions, we cannot be sure that it works in the case of even two consecutive reactions as in the example of the diphosphorylation of MKK. This problem can only be expected to increase with the size of the network under investigation. An obvious and relevant question in this context is if the improved rQSSA and tQSSA approximation can be used as a better approximation than the sQSSA. This investigation of this issue is one of the main goals of our current research. Another important aim is to reexamine the results obtained in the literature in terms of sQSSA, using the full system of equations. In particular, the extremal phenomena, like oscillations, bistability, hysteresis, ultrasensitivity are of special interest for our investigations.

## References

1. B. D. Aguda and H. M. Sauro, *Methods Mol. Biol.* **250**, 167 (2004).
2. D. Angeli, J. E. Ferrell Jr. and E. D. Sontag, *PNAS* **101**, 1822 (2004).

3. U. S. Bhalla, R. Iyengar, *Chaos* **11**, 221 (2001).
4. H. Bisswanger, *Enzyme Kinetics*, Wiley (1999).
5. N. Bluthgen, *PhD thesis* (2003).
6. N. Bluthgen, H. Herzel, *J. Theor. Biol.* **225**, 293 (2003).
7. J. A. M. Borghans, R. J. de Boer and L. A. Segel, *Bull. Math. Biol.* **58**, 43 (1996).
8. G. E. Briggs and J. B. S. Haldane, *Biochem. J.* **19**, 338 (1925).
9. M. Camps, A. Nichols and S. Arkinstall, *FASEB J.* **14**, 6 (2000).
10. Z. Chen et al., *Chem. Rev.* **101**, 2449 (2001).
11. R. J. Ellis, *Trends Biochem. Sci.* **26**, 597 (2001).
12. J. E. Ferrell Jr., *Curr. Opin. Cell. Biol.* **14**, 140 (2002).
13. J. E. Ferrell Jr. and W. Xiong, *Chaos* **11**, 227 (2001).
14. A. Fersht, *Enzyme Structure and Mechanism*, Freeman & Co., (1985).
15. C. L. Frenzen and P. K. Maini, *J. Math. Biol.* **26**, 689 (1988).
16. M. Hakateyama et al., *Biochem. J.* **373**, 451 (2003).
17. F. G. Heineken, H. M. Tsuchiya and A. Aris, *Math. Biosci.* **1**, 95 (1967).
18. C.-Y. F. Huang and J. E. Ferrell Jr., *Proc. Natl. Acad. Sci. USA* **93**, 10078 (1996).
19. B. N. Kholodenko, *Eur. J. Biochem.* **267**, 1583 (2000).
20. N. I. Markevich, J. B. Hoek and B. N. Kholodenko, *J. Cell. Biol.* **164**, 353 (2004).
21. L. Michaelis and M. L. Menten, *Biochem. Z.* **49**, 333 (1913).
22. J. D. Murray, *Mathematical Biology*, Springer-Verlag, (1990).
23. R. E. O'Malley Jr. , *Singular Perturbation Methods for Ordinary Differential Equations*, Springer-Verlag (1991).
24. G. Pearson et al., *Endocr. Rev.* **22**, 153 (2001).
25. N. C. Price and L. Stevens, *Fundamentals of Enzymology*, Oxford Univ. Press, (1989).
26. S. Schnell and P. K. Maini, *Math. Comput. Modelling* **35**, 137 (2002).
27. S. Schnell and P. K. Maini, *Comments Theor. Biol.* **8**, 169 (2003).
28. S. Schnell and C. Mendoza, *J. Theor. Biol.* **187**, 207 (1997).
29. B. Schoeberl et al., *Nature Biotechnol.* **20**, 370 (2002).
30. A. R. Sedaghat, A. Sherman and M. J. Quon, *Am. J. Endocrinol. Metabol.* **283**, E1084 (2002).
31. L. A. Segel and M. Slemrod, *SIAM Rev.* **31**, 446 (1989).
32. P. Smolen, D. A. Baxter and J. H. Byrne, *J. Neurosci.* **21**, 6644 (2001).
33. J. J. Tyson, K. C. Chen and B. Novak, *Curr. Opin. Cell. Biol.* **15**, 221 (2003).
34. A.R. Tzafriri, *Bull. Math. Biol.* **65**, 1111 (2003).
35. S. J. Vaytaden, S. M. Ajay and U. S. Bhalla, *ChemBioChem* **5**, 1365 (2004).
36. X. L. Zhan, M. J. Wishart and K. L. Guan, *Chem. Rev.* **101**, 2477 (2001).

# *Paper X*

# THE TOTAL QUASI-STEADY STATE APPROXIMATION FOR COMPLEX ENZYME REACTIONS

M.G. Pedersen, Technical University of Denmark, Kgs. Lyngby, Denmark
A.M. Bersani, University "La Sapienza", Rome, Italy
E. Bersani, DataLink Informatica, Rome, Italy
G. Cortese, University of Padova, Italy

Corresponding Author: A.M.Bersani,
University "La Sapienza"
Dept. of Mathematical Methods and Models (Me.Mo.Mat.)
Via A. Scarpa 16, 00161 Rome, Italy
Phone: +39 0649766681, Fax: +39 0649766684
email: bersani@dmmm.uniroma1.it

**Abstract.** Biochemistry in general and enzyme kinetics in particular have been heavily influenced by the model of biochemical reactions known as Michaelis-Menten kinetics. Assuming that the complex concentration is approximately constant after a short transient phase leads to the usual Michaelis-Menten (MM) approximation (or standard quasi steady-state approximation (sQSSA)), which is valid when the enzyme concentration is sufficiently small. This condition is usually fulfilled for in vitro experiments, but often breaks down in vivo. The total QSSA (tQSSA), which is valid for a broader range of parameters covering both high and low enzyme concentrations, has been introduced in the last two decades. We extend the tQSSA to more complex reaction schemes, like fully competitive reactions, double phosphorylation, Goldbeter-Koshland switch and we show that for a very large range of parameters our tQSSA provides excellent fitting to the solutions of the full system, better than the sQSSA and the single reaction tQSSA. Finally we discuss the need for a correct model formulation when doing "reverse engineering", which aims at finding unknown parameters by fitting the model to experimentally obtained data. We show that the estimated parameters are much closer to the real values when using the tQSSA rather than the sQSSA, which overestimates the parameter values greatly.

## 1. Introduction

One of the principal components of the mathematical approach to Systems Biology is the model of biochemical reactions set forth by Henri in 1901 [8, 9, 10] and Michaelis and Menten in 1913 [12], and further developed by Briggs and Haldane in 1925 [4]. This formulation considers a reaction where a substrate $S$ binds an enzyme $E$ reversibly to form a complex $C$. The complex can then decay irreversibly to a product $P$ and the enzyme, which is then free to bind another molecule of the substrate. This process is summarized in the scheme

$$E + S \underset{d}{\overset{a}{\rightleftarrows}} C \xrightarrow{k} E + P, \tag{1}$$

where $a, d$ and $k$ are kinetic parameters (supposed constant) associated with the reaction rates.

This scheme is mathematically represented by a system of two nonlinear ordinary differential equations (ODEs), corresponding initial conditions and two conservation laws as shown in the next section. The initial conditions give the concentrations of $S$ and $C$ at the beginning of the reaction, and their time development is described by the ODEs, while $E$ and $P$ are linked to $S$ and $C$ through the conservation laws.

Assuming that the complex concentration is approximately constant after a short transient phase leads to the usual Michaelis-Menten (MM) approximation (or *standard quasi steady-state assumption* or *approximation* (standard QSSA, sQSSA)), which is valid when the enzyme concentration is much lower than either the substrate concentration or the Michaelis constant $K_M$ [18, 19]. This condition is usually fulfilled for *in vitro* experiments, but often breaks down *in vivo* [21, 20]. We refer to the next section for the mathematical formulation of scheme (1), and to [16] for a nice, general review of the kinetics and approximations of (1).

The advantage of a quasi steady-state approximation is that it reduces the dimensionality of the system, passing from two equations (*full system*) to one (*MM approximation or sQSSA)* and thus speeds up numerical simulations greatly, especially for large networks as found *in vivo*. Moreover, the kinetic constants in (1) are usually not known, whereas finding the kinetic parameters for the MM approximation is a standard *in vitro* procedure in biochemistry [2]. However, to simulate physiologically realistic *in vivo* scenarios, one faces the problem that the MM approximation is no longer valid as mentioned above. Hence, even though the kinetic constants such as $K_M$ are identical *in vivo* and *in vitro*, they need to be implemented in an approximation which is valid for the system under investigation.

Approximations such as the *total QSSA* (tQSSA) [3, 22], which is valid for a broader range of parameters covering both high and low enzyme concentrations, have been introduced recently. Tzafriri [22] showed that the tQSSA is at least roughly valid for any set of parameters in the case of the reaction in (1). Importantly, the tQSSA uses the same parameters ($V_{max}, K_M$) as the sQSSA. Hence, the parameters found *in vitro* from the MM approach can be used by the tQSSA for modeling *in vivo* scenarios.

The roles of $V_{max}$, the maximal reaction velocity, and $K_M$, the Michaelis constant describing the concentration of the substrate at which the reaction rate is half maximal, become essential when characterizing biochemical reactions *in vitro* as well as *in vivo*. Moreover, descriptions of cooperative reactions, inhibition and many other biochemical processes have exploited the fundamental ideas of the MM scheme, i.e., the sQSSA and the parameters $V_{max}$ and $K_M$ (see, e.g., [2]). However, since these approximations cannot be expected to be valid *in vivo*, employing the tQSSA to these more complex situations would be preferable. Tzafriri & Edelman [23] studied the completely reversible enzyme reaction in terms of the tQSSA. We have recently derived the tQSSA for fully competitive reactions [13].

In this paper we show that the use of the sQSSA can lead to gross quantitative as well as qualitative wrong conclusions even in the case of simple networks. The tQSSA is shown to estimate the behavior significantly better, and therefore we propose to use this approximation when modeling intra-cellular signalling networks. We refer to [14] for further biological examples. We also discuss the use of reverse engineering as a tool of obtaining missing parameters, and show that the sQSSA can lead to wrong estimates, while the tQSSA finds estimates closer to the real values.

## 2. Theoretical background

We recall briefly the mathematical description of the sQSSA for (1), using the same symbols for the concentrations of the reactants. The reaction (1) can be described by the following system of nonlinear ordinary differential equations

$$\frac{dS}{dt} = -a(E_T - C)\,S + d\,C \tag{2}$$

$$\frac{dC}{dt} = a(E_T - C)\,S - (d+k)\,C \tag{3}$$

with the initial conditions

$$S(0) = S_T, \quad C(0) = 0, \tag{4}$$

and the conservation laws

$$E + C = E_T, \quad S + C + P = S_T. \tag{5}$$

Assuming that the complex is in a quasi-steady state, i.e., $\frac{dC}{dt} \approx 0$, leads to [4, 18, 19]

$$\frac{dS}{dt} \approx -\frac{V_{max}S}{K_M + S}, \quad S(0) = S_T, \tag{6}$$

$$E(0) = E_T, \quad V_{max} = k\,E_T, \quad K_M = \frac{d+k}{a}.$$

Here $V_{max}$ is the maximal reaction rate and $K_M$ is the Michaelis constant, identifying the substrate concentration giving the half-max reaction rate, i.e., $K_M$ reflects the substrate affinity of

the enzyme. This approximation is valid whenever [18, 19]

$$\frac{E_T}{K_M + S_T} \ll 1, \tag{7}$$

i.e., at low enzyme concentrations.

The tQSSA [3, 22] arises by introducing the total substrate

$$\bar{S} = S + C.$$

Assuming that the complex is in a quasi-steady state yields the tQSSA

$$\frac{d\,\bar{S}}{dt} \approx -k\, C_-(\bar{S}), \quad \bar{S}(0) = S_T, \tag{8}$$

where

$$C_-(\bar{S}) = \frac{(E_T + K_M + \bar{S}) - \sqrt{(E_T + K_M + \bar{S})^2 - 4E_T\bar{S}}}{2}. \tag{9}$$

Tzafriri [22] showed that the tQSSA is valid whenever

$$\epsilon_{Tz} := \frac{K}{2S_T}\left(\frac{E_T + K_M + S_T}{\sqrt{(E_T + K_M + S_T)^2 - 4E_T S_T}} - 1\right) \ll 1, \qquad K = \frac{k}{a}, \tag{10}$$

and that this is always roughly valid in the sense that

$$\epsilon_{Tz} \leq \frac{K}{4K_M} \leq \frac{1}{4}. \tag{11}$$

The parameter $K$ is known as the Van Slyke-Cullen constant. Tzafriri [22] expanded equations (9) and (10) in terms of

$$r(\bar{S}) = \frac{4E_T\bar{S}}{(E_T + K_M + \bar{S})^2} < 1 \tag{12}$$

and assuming the validity of the tQSSA ($\epsilon_{Tz} \ll 1$) and $r \ll 1$, he found

$$\frac{d\,\bar{S}}{dt} \approx -\frac{V_{max}\bar{S}}{K_M + E_T + \bar{S}}, \quad \bar{S}(0) = S_T, \tag{13}$$

as a first order approximation to (8). This expression (13) is identical to the formula obtained by Borghans et al. [3] by means of a two point Padé approximant technique [1].

This approximation is valid at low enzyme concentrations (7) where it reduces to the MM expression (6), but holds moreover at low substrate concentrations $S_T \ll E_T + K_M$ [22]. We wish to highlight the fundamental fact that performing the substitutions of $S$ by $\bar{S}$ and of $K_M$ by $K_M + E_T$ one obtains a significantly improved MM-like approximation with minimal effort.

## 3. Total quasi-steady state approximation of the competitive system

In [13] we investigated the system

$$\begin{aligned} S_1 + E &\underset{d_1}{\overset{a_1}{\rightleftarrows}} C_1 \xrightarrow{k_1} E + P_1, \\ S_2 + E &\underset{d_2}{\overset{a_2}{\rightleftarrows}} C_2 \xrightarrow{k_2} E + P_2, \end{aligned} \tag{14}$$

which consists of two reactions catalyzed by the same enzyme, i.e., a system with competing substrates. It is governed by the coupled ODEs [15, 18, 17], $i = 1, 2$,

$$\frac{d\,S_i}{dt} = -a_i E \cdot S_i + d_i C_i, \qquad S_i(0) = S_{i,T}, \tag{15a}$$

$$\frac{d\,C_i}{dt} = a_i(E \cdot S_i - K_i^M C_i), \qquad C_i(0) = 0, \qquad K_i^M = \frac{d_i + k_i}{a_i}. \tag{15b}$$

and the conservation laws

$$S_{i,T} = S_i + C_i + P_i, \qquad i = 1,2, \tag{16}$$
$$E_T = E + C_1 + C_2. \tag{17}$$

The sQSSA of this system is [15, 18]

$$\frac{dS_i}{dt} = -\frac{k_i E_T S_i}{K_i^M(1 + S_j/K_j^M) + S_i}\,, \quad S_i(0) = S_{i,T}, \qquad i = 1,2, \quad j \neq i, \tag{18}$$

which is valid when [17]

$$\frac{E_T}{K_i^M(1 + S_{j,T}/K_j^M) + S_{i,T}} \ll 1\,, \qquad i = 1,2, \quad j \neq i. \tag{19}$$

In [13], following [3], we introduced the total substrates

$$\bar{S}_i = S_i + C_i, \qquad i = 1,2, \tag{20}$$

and rewrote equations (15) in terms of these, obtaining the system of ODEs, $i = 1,2$,

$$\frac{d\bar{S}_i}{dt} = -k_i C_i, \qquad \bar{S}_i(0) = S_{i,T}, \tag{21a}$$
$$\frac{dC_i}{dt} = a_i\big((E_T - C_1 - C_2)\cdot(\bar{S}_i - C_i) - K_i^M C_i\big), \qquad C_i(0) = 0. \tag{21b}$$

where we have introduced the MM constants

$$K_i^M = \frac{d_i + k_i}{a_i}.$$

We required $0 < C_i < \bar{S}_i$, $i = 1,2$, because of (20), and applied the quasi steady-state assumption [3, 22],

$$\frac{dC_i}{dt} \approx 0, \qquad i = 1,2,$$

which is equivalent to the system

$$C_1 = E_T - C_2\big(1 + \frac{K_2^M}{\bar{S}_2 - C_2}\big), \tag{22a}$$
$$C_2 = E_T - C_1\big(1 + \frac{K_1^M}{\bar{S}_1 - C_1}\big). \tag{22b}$$

Then $C_i < E_T$, $i = 1,2$, in agreement with (17).

Substituting (22b) into (22a) leads to the following equation in $C_1$

$$C_1 = E_T - \Big(E_T - C_1(1 + \frac{K_1^M}{\bar{S}_1 - C_1})\Big)\Big(1 + \frac{K_2^M}{\bar{S}_2 - (E_T - C_1(1 + \frac{K_1^M}{\bar{S}_1 - C_1}))}\Big) \tag{23}$$

and $C_2$ can then be found from (22b).

Solving (23) is equivalent to finding roots of the third degree polynomial

$$\begin{aligned}\psi_1(C_1) = &-(K_1^M - K_2^M)C_1^3 \\ &+ \big[(E_T + K_1^M + \bar{S}_1)(K_1^M - K_2^M) - (\bar{S}_1 K_2^M + \bar{S}_2 K_1^M)\big]C_1^2 \\ &+ \big[-E_T(K_1^M - K_2^M) + (\bar{S}_1 K_2^M + \bar{S}_2 K_1^M) + K_2^M(E_T + K_1^M)\big]\bar{S}_1 C_1 \\ &- E_T K_2^M \bar{S}_1^2.\end{aligned} \tag{24}$$

An analogous polynomial $\psi_2$ for $C_2$ can be found by interchanging the indexes 1 and 2 in (24), because of the symmetry of the system (21). Rearranging the terms, $\psi_1$ can also be written

$$\begin{aligned}\psi_1(C_1) = &K_2^M(C_1 - E_T)\big(\bar{S}_1 - C_1\big)^2 \\ &+ K_1^M C_1(C_1 + K_2^M + \bar{S}_2 - E_T)\big)\big(\bar{S}_1 - C_1\big) + (K_1^M C_1)^2.\end{aligned} \tag{25}$$

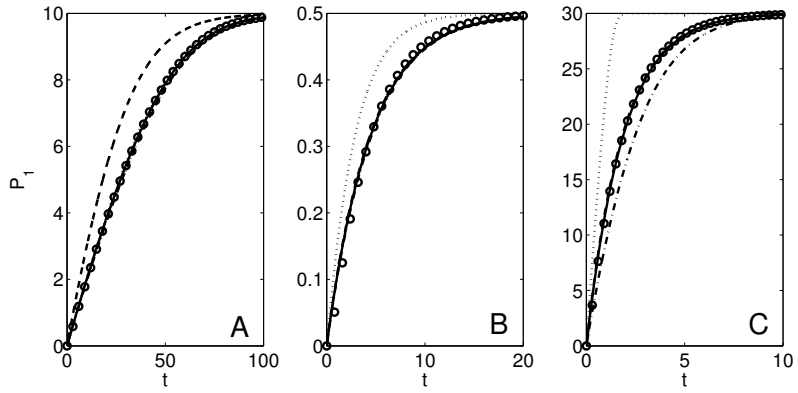


Figure 1: QSSAs for the fully competitive reaction. The first order approximation (dash-dot curve) coincides with the competitive sQSSA (dotted curve) when it is valid (panel A), and with the single reaction tQSSA (dashed curve) when the competition is negligible (panel B). However, at high enzyme concentrations the single reaction tQSSA is often a better approximation than the first order tQSSA (panel C). Parameters are $a_1 = a_2 = 0.2, d_1 = d_2 = 1, k_1 = 0.6, k_2 = 0.5$, $(K_1^M = 8, K_2^M = 7.5, K = 3)$. In A: $S_{1,T} = S_{2,T} = 10$, $E_T = 1$. $\epsilon = 0.0038$. In B: $S_{1,T} = S_{2,T} = 0.5$, $E_T = 5$. $\epsilon = 0.0832$. In C: $S_{1,T} = S_{2,T} = 30$, $E_T = 100$. $\epsilon = 0.0219$. All units are arbitrary.

We have shown the existence and uniqueness of biologically consistent roots of $\psi_1(C_1)$ and $\psi_2(C_2)$, which we will indicate with $C_i = C_i(\bar{S}_1, \bar{S}_2)$. We expect that after a short transient phase the complex concentrations equal the quasi steady-state concentrations, $C_i = C_i(\bar{S}_1, \bar{S}_2)$, given by the roots in the respective polynomials as discussed above. Then the evolution of the system can be studied by means of the tQSSA

$$\frac{d\,\bar{S}_i}{dt} \approx -k_i C_i(\bar{S}_1, \bar{S}_2), \qquad \bar{S}_i(0) = S_{i,T}. \tag{26}$$

Operating approximations for the two different regions of parameter space: $K_1^M \gg K_2^M$ and $K_1^M \ll K_2^M$ and matching them by means of a two point Padé approximant (TPPA) techniques, gives then

$$\frac{d\,\bar{S}_i}{dt} = -\frac{k_i E_T \bar{S}_i}{K_i^M(1 + \bar{S}_j/K_j^M) + \bar{S}_i + E_T}, \quad \bar{S}_i(0) = S_{i,T}, \quad j \neq i. \tag{27}$$

where $i = 1, j = 2$.

This formula reduces not only to the special case of identical affinities but also to the sQSSA (18) whenever this approximation holds as guaranteed by (19), and to the single reaction first order tQSSA (13) when $\bar{S}_j/K_j^M$ can be neglected.

Motivated by this and further encouraged by numerical simulations (see Fig. 1), we proposed the expression (27) (for $i = 1, 2$) as the general first order approximation to the tQSSA for fully competitive reactions.

Although not strictly theoretically founded, the above considerations using the TPPA can be seen as the motivation for the formula.

Our results are immediately applicable to, e.g., successive reactions catalyzed by the same enzyme, such as nonprocessive or distributive double phosphorylation or dephosphorylation processes, as seen for example in the MAPK cascade [5, 6, 24, 11]. The reaction scheme can be seen as a special case of (14) with $P_1 = S_2$ and is summarized as

$$S_1 \xrightarrow{E} S_2 \xrightarrow{E} P,$$

where it is usually assumed that at the beginning only $S_1$ is present. Fig. 2 shows that the results presented here are often a good approximation.

However, it should be remarked that our theoretical investigation of the validity of the tQSSA does not work in the case of successive reactions. The problem is that there is no $S_2$ at time

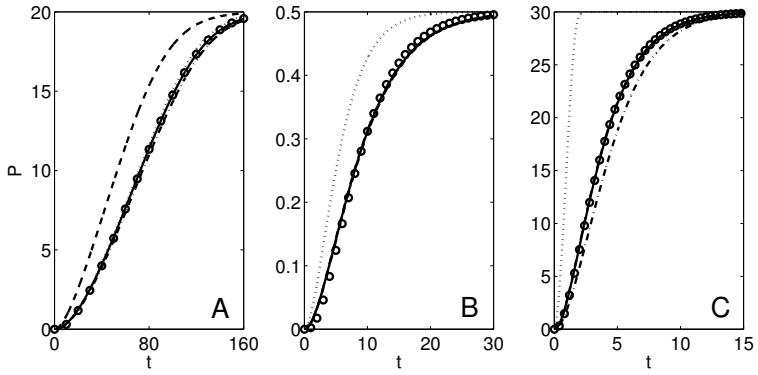


Figure 2: The tQSSA estimates well the development of the product of two successive reactions catalyzed by the same enzyme, and the discussion of the validity of the sQSSA, the single reaction tQSSA and the first order tQSSA apparently carries over to this case. Legends and parameters are as in Fig. 1 except for the initial substrate concentrations, which are $S_{2,T} = 0$ in all panels and: In A: $S_{1,T} = 20$. In B: $S_{1,T} = 0.5$. In C: $S_{1,T} = 30$. All units are arbitrary.

$t = 0$, and hence the time scales can not be found following [18] because the definition of the transient phase no longer holds.

Nevertheless, it seems like the conclusions concerning the validity of the first order approximation from above carries over to this scenario (compare the three panels of Fig. 1 with the panels of Fig. 2).

We will present the investigation of such reactions in another paper.

## 4. Total quasi-steady state approximation of the Goldbeter-Koshland switch

Goldbeter and Koshland [7] considered the following reaction

$$\begin{aligned} S + E_1 &\underset{d_1}{\overset{a_1}{\rightleftarrows}} C_1 \xrightarrow{k_1} E_1 + P, \\ P + E_2 &\underset{d_2}{\overset{a_2}{\rightleftarrows}} C_2 \xrightarrow{k_2} E_2 + S, \end{aligned} \tag{28}$$

which describes, for example, the cycle of phosphorylation and dephosphorylation of a substrate, by means of a kinase $E_1$ and a phosphatase $E_2$. This reaction is very important in every intracellular pathway, because the process of phosphorylation and dephosphorylation is one of the most important to activate and inactivate enzymes.

The reaction is governed by the coupled ODEs

$$\frac{dS}{dt} = -a_1 E_1 \cdot S + d_1 C_1, \qquad S(0) = S_T, \tag{29a}$$

$$\frac{dC_1}{dt} = a_1 E_1 \cdot S - (d_1 + k_1) C_1, \qquad C_1(0) = 0, \tag{29b}$$

$$\frac{dC_2}{dt} = a_2 E_2 \cdot P - (d_2 + k_2) C_2, \qquad C_2(0) = 0. \tag{29c}$$

and the conservation laws

$$S_T = S + C_1 + C_2 + P, \tag{30}$$

$$E_{i,T} = E_i + C_i \quad , \quad i = 1, 2 \; . \tag{31}$$

The sQSSA of this system is given by setting $\frac{dC_1}{dt} \approx \frac{dC_2}{dt} \approx 0$ and neglecting the complex concentrations which yields

$$\frac{dS}{dt} = \frac{k_2 E_{2,T}(S_T - S)}{K_2^M + S_T - S} - \frac{k_1 E_{1,T} S}{K_2^M + S}, \qquad \bar{S}(0) = S_T. \tag{32}$$

Introducing the total substrates $\bar{S} = S + C_1$ , $\bar{P} = P + C_2$, we rewrite the Eqs. (29) in the following way:

$$\frac{d\bar{S}}{dt} = k_2 C_2 - k_1 C_1 = -\frac{d\bar{P}}{dt}, \qquad \bar{S}(0) = S_T, \tag{33a}$$

$$\frac{dC_1}{dt} = a_1(E_{1,T} - C_1)\cdot(\bar{S} - C_1) - (d_1 + k_1)C_1, \qquad C_1(0) = 0, \tag{33b}$$

$$\frac{dC_2}{dt} = a_2(S_T - \bar{S} - C_2)\cdot(E_{2,T} - C_2) - (d_2 + k_2)C_2, \qquad C_2(0) = 0. \tag{33c}$$

Assuming the tQSSA $\frac{dC_i}{dt} \approx 0$ and considering only the biologically significant roots $C_i$, we arrive at the following equation

$$\frac{d\bar{S}}{dt} \approx k_2 C_2^- - k_1 C_1^- \qquad \bar{S}(0) = S_T \tag{34}$$

where

$$C_1^- = \frac{(\bar{S} + E_{1,T} + K_1^M) - \sqrt{(\bar{S} + E_{1,T} + K_1^M)^2 - 4\bar{S}E_{1,T}}}{2}, \tag{35}$$

$$C_2^- = \frac{(S_T - \bar{S} + E_{2,T} + K_2^M) - \sqrt{(S_T - \bar{S} + E_{2,T} + K_2^M)^2 - 4(S_T - \bar{S})E_{2,T}}}{2} \tag{36}$$

and $K_i^M = \frac{d_i + k_i}{a_i}$.

Formulas (35) and (36) show that, differently from the case of a single phosphorylation reaction, in this situation the quasi steady-state does not imply that the complexes tend to be negligible. In Fig. 3 we compare the simulations of the full system and of its sQSSA and tQSSA, and it is seen that the tQSSA is superior to the sQSSA.

The study of the sufficient conditions to guarantee the validity of the tQSSA, the time scales of the transient phases and a deeper comparison with the sQSSA are the subject of a paper in preparation.

## 5. Reverse engineering

Many biochemical systems, especially larger networks, are little understood, and many parameters are often unknown. A common method to obtain these parameters is to fit a mathematical model to experimentally obtained data, for example by least square methods. This is often refered to as reverse engineering. However, a model formulated with the sQSSA can not be expected to be a good representation of the full system as discussed in the previous sections. As for most other approaches, the use of this approximation produces excellent goodness of fit. But for the sQSSA such a good fit will necessarily correspond to parameter values far from the true ones. Indeed, inserting the true values in the sQSSA model does, in general, not approximate the full system. Instead, we expect that the tQSSA will reduce this problem consistently.

To investigate this issue, we compare the results of parameter estimation using the two QSSA approaches for the simplest case of a single reaction (1), which concerns the evaluation of $k$ and $K_M$. This was done using observations of the product $P$, which were generated by simulating the full system with the "true" parameter values $k = 0.6$ and $K_M = 10$, extracting 50 points in time and adding noise from a normal distribution to each of these points. The noise was assumed to be normal with zero mean and standard deviation 2, corresponding to 2% of the total substrate concentration $S_T = 100$. The enzyme concentration was fairly high, $E_T = 50$. For both the sQSSA and the tQSSA we estimated the parameters $k$ and $K_M$ by optimizing the fit of each model to the observations. This was implemented using the "nls" package of the R

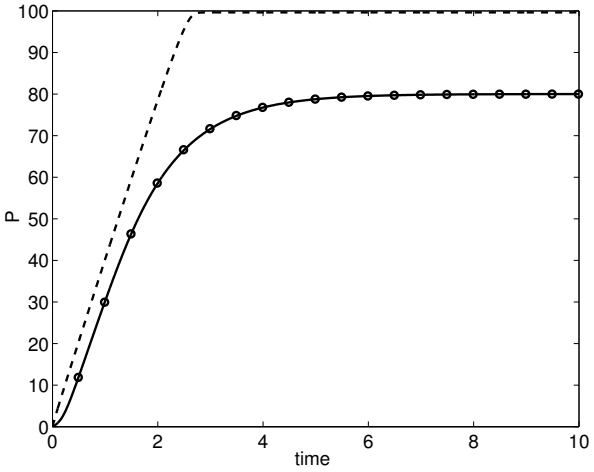


Figure 3: The tQSSA estimates well the development of the product $P$ of the Goldbeter-Koshland switch. Legends are: Full system (circles), sQSSA (dashed line) and tQSSA (full curve), where we show $P_{tQSSA} := \bar{P} - C_2^-$ for a correct comparison for the tQSSA. The parameters are $S_T = 100, E_{1,T} = 50, E_{2,T} = 10, a_1 = a_2 = 4, d_1 = d_2 = 5, k_1 = k_2 = 1$, all in arbitrary units.

program for the nonlinear least square estimates. An output of this procedure is shown in Fig. 4. The obtained values from the sQSSA (Fig. 4A) were $k = 1.21 \pm 0.13$ and $K_M = 103.0 \pm 9.4$, while the tQSSA (Fig. 4B) yielded $k = 0.73 \pm 0.12$ and $K_M = 17.6 \pm 11.6$. We note that when using the sQSSA the parameters are greatly overestimated, especially $K_M$ which is an order of magnitude higher than the real value. On the other hand the estimation obtained from tQSSA is much nearer to the true values. This advantage of the tQSSA is clearly confirmed by the fact that the true values $k = 0.6$ and $K_M = 10$ fall inside one standard deviation from the corresponding estimated values, while the intervals estimated by the sQSSA do not include the true values. Indeed, they are very distant from these values. This is further confirmed by the 95 % confidence intervals $(0.998, 1.551)$ and $(75.3, 147.4)$ for the $k$ and $K_M$, respectively, in the sQSSA.

The wrong estimation by the sQSSA is related to the need to "move" the model with the true parameters (Fig. 4A, dashed curve) in order to make it fit the data points as well as the full system. Since the model with the true parameters was not a good representation of the full system, we had to change the parameters a lot to obtain a good fit. This was not necessary for the tQSSA since already with the true parameters it was a good approximation of the full system, and hence, it fitted the data set well.

From the results we conclude that the confidence interval is important when obtaining parameters from "reverse engineering" rather than a single value. This is reflected by the large standard deviation for the tQSSA estimation of $K_M = 17.6 \pm 11.6$. However, even considering the confidence interval the sQSSA is far from the true value. We continue the study of reverse engineering in a future work.

## 6. Conclusions

Although it was known that the sQSSA will often be invalid *in vivo*, the sQSSA approach was necessary for many years, since no better approximations were known, but this has changed recently with the introduction of the tQSSA. This approach was first applied to the simplest reactions [3, 22], and later to increasingly more complex schemes such as reversible reactions [23] and fully competing systems [13].

We have here presented the application of the tQSSA to biologically realistic reactions, and shown that it is superior to the sQSSA in all the presented cases.

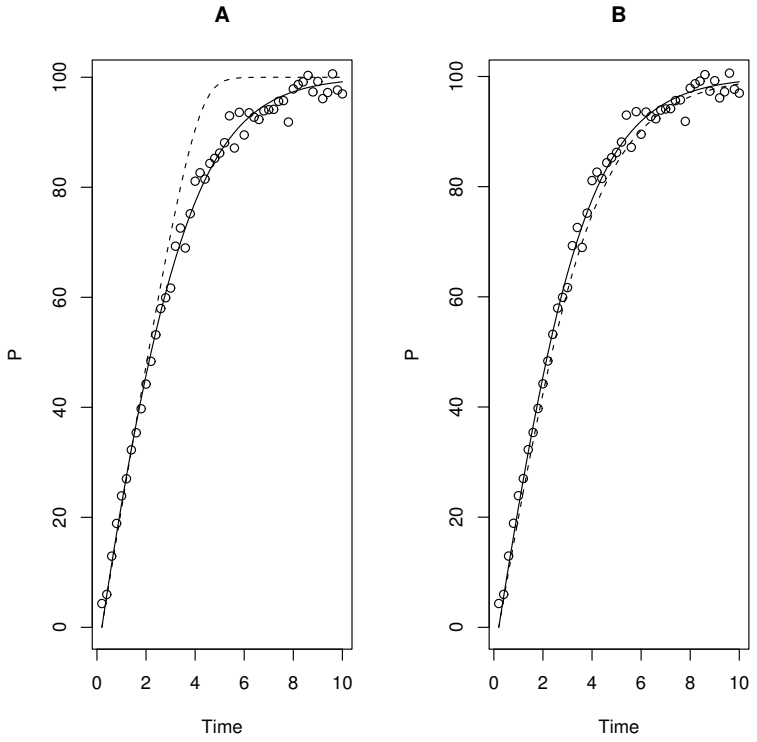


Figure 4: Parameter estimation of $k$ and $K_M$ using perturbed observations from the full system with $k = 0.6$, $K_M = 10$, $S_T = 100$ and $E_T = 50$ with noise from a $N(0, 2^2)$ distribution. Panels A and B show the fitting using the sQSSA and tQSSA, respectively. The generated data points are indicated by circles, the approximation using the true values is the dashed curved, while the fitted approximation is shown by the full curve. The obtained values are: Panel A: $k = 1.21 \pm 0.13, K_M = 103.0 \pm 9.4$. Panel B: $k = 0.73 \pm 0.12, K_M = 17.6 \pm 11.6$. All units are arbitrary.

Related to the above, but from another point of view, is the lack of reliable experimental data about the kinetic constants of the intracellular biochemical reactions, including $K_M$ and $V_{max}$ values. To reconstruct these missing parameter values, some authors rely on the so-called reverse engineering (or inverse problem).

From the considerations of the previous Section it follows that the ability of the model to fit a certain data set can not be used to test whether a certain approximation holds. Indeed, we found a good fit for the sQSSA even though it was known not to hold (Fig. 4A).

Applying reverse engineering for the sQSSA, without any *a priori* examination of its validity, one could argue that the (mis)use of the sQSSA causes no problems, since we obtain a good fit anyway. However, one would prefer to have a model that works under many different conditions, not only in a certain experimental setting. If fitting the sQSSA model to the data yields wrong estimates of the parameters, then it is likely that the predicted behavior using these parameters would be far from the true behavior. Again, the use of the tQSSA shows to be the most correct among all the known approximations.

## References

[1] Baker, Jr., G. A., Essentials of Padé approximants. Academic Press, London, 1975.

[2] Bisswanger, H., Enzyme Kinetics. Principles and Methods. Wiley-VCH, Weinheim, 2002.

[3] Borghans, J. A. M., de Boer, R. J. and Segel, L. A., Extending the quasi-steady state approximation by changing variables. Bull. Math. Biol., 58 (1996), 43–63.

[4] Briggs, G. E. and Haldane, J. B. S., A note on the kinetics of enzyme action. Biochem. J., 19 (1925), 338–339.

[5] Burack, W. R. and Sturgill, T. W., The activating dual phosphorylation of MAPK by MEK is nonprocessive. Biochemistry, 36 (1997), 5929–5933.

[6] Ferrell, J. E. and Bhatt, R. R., Mechanistic studies of the dual phosphorylation of mitogen-activated protein kinase. J. Biol. Chem., 272 (1997), 19008–19016.

[7] Goldbeter, A. and Koshland, Jr., D. E., An amplified sensitivity arising from covalent modification in biological systems. Proc. Natl. Acad. Sci., 78 (1981), 6840–6844.

[8] Henri, V., Recherches sur la loi de l'action de la sucrase. C. R. Hebd. Acad. Sci., 133 (1901), 891–899.

[9] Henri, V., Über das gesetz der wirkung des invertins. Z. Phys. Chem., 39 (1901), 194–216.

[10] Henri, V., Théorie générale de l'action de quelques diastases. C. R. Hebd. Acad. Sci., 135 (1902), 916–919.

[11] Markevich, N. I., Hoek, J. B. and Kholodenko, B. N., Signaling switches and bistability arising from multisite phosphorylation in protein kinase cascades. J. Cell Biol., 164 (2004), 353–359.

[12] Michaelis, L. and Menten, M. L., Die kinetik der invertinwirkung. Biochem. Z., 49 (1913), 333–369.

[13] Pedersen, M. G., Bersani, A. M. and Bersani, E., The total quasi-steady-state approximation for fully competitive enzyme reactions. (2005). Submitted.

[14] Pedersen, M. G., Bersani, A. M. and Bersani, E., Quasi steady-state approximations in intracellular signal transduction – a word of caution. (2006). Submitted.

[15] Rubinow, S. I. and Lebowitz, J. L., Time-dependent Michaelis-Menten kinetics for an enzyme-substrate-inhibitor system. J. Am. Chem. Soc., 92 (1970), 3888–3893.

[16] Schnell, S. and Maini, P. K., A century of enzyme kinetics: Reliability of the $K_M$ and $v_{max}$ estimates. Comm. Theor. Biol., 8 (2003), 169–187.

[17] Schnell, S. and Mendoza, C., Time-dependent closed form solutions for fully competitive enzyme reactions. Bull. Math. Biol., 62 (2000), 321–336.

[18] Segel, L. A., On the validity of the steady state assumption of enzyme kinetics. Bull. Math. Biol., 50 (1988), 579–593.

[19] Segel, L. A. and Slemrod, M., The quasi steady-state assumption: a case study in perturbation. SIAM Rev., 31 (1989), 446–477.

[20] Sols, A. and Marco, R., Concentration of metabolites and binding sites. Implications in metabolic regulation. In: Current topics in Cellular Regulation, volume 2, (Eds.: Horecker, B. L. and Stadtman, E. R.) Academic Press, New York, 1970.

[21] Straus, O. H. and Goldstein, A., Zone behavior of enzymes. J. Gen. Physiol., 26 (1943), 559–585.

[22] Tzafriri, A. R., Michaelis-Menten kinetics at high enzyme concentrations. Bull. Math. Biol., 65 (2003), 1111–1129.

[23] Tzafriri, A. R. and Edelman, E. R., The total quasi-steady-state approximation is valid for reversible enzyme kinetics. J. Theor. Biol., 226 (2004), 303–313.

[24] Zhao, Y. and Zhang, Z.-Y., The mechanism of dephosphorylation of extracellular signal-regulated kinase 2 by mitogen-activated protein kinase phosphatase 3. J. Biol. Chem., 276 (2001), 32382–32391.

# Bibliography

Ainscow, E. K., Rutter, G. A., 2002. Glucose-stimulated oscillations in free cytosolic ATP concentration imaged in single islet $\beta$-cells: evidence for a $Ca^{2+}$ -dependent mechanism. Diabetes 51, S162–S170.

Albe, K. R., Butler, M. H., Wright, B. E., 1990. Cellular concentrations of enzymes and their substrates. J. Theor. Biol. 143, 163–195.

Alberts, B., Johnson, A., Lewis, J., Raff, M., Roberts, K., Walter, P., 2002. Molecular Biology of the Cell, 4th Edition. Garland Science.

Andreu, E., Bernat, S., Sanchez-Andres, J. V., 1997. Oscillation of gap junction electrical coupling in the mouse pancreatic islets of Langerhans. J. Physiol. 498, 753–761.

Arredouani, A., Henquin, J. C., Gilon, P., 2002. Contribution of the endoplasmic reticulum to the glucose-induced $[Ca^{2+}]_c$ response in mouse pancreatic islets. Am. J. Physiol. Endocrinol. Metab. 282, E982–E991.

Ashcroft, F., Rorsman, P., 1989. Electrophysiology of the pancreatic $\beta$-cell. Prog. Biophys. Mol. Biol. 54, 87–143.

Aslanidi, O. V., Mornev, O., Skyggebjerg, O., Arkhammar, P., Thastrup, O., M.P. Sørensen, P. C., Conradsen, K., Scott, A., 2001. Excitation wave propagation as a possible mechanism for signal transmission in pancreatic islets of langerhans. Biophys. J. 80, 1195–1209.

Atwater, I., Dawson, C., Scott, A., Eddlestone, G., Rojas, E., 1980. The nature of the oscillatory behaviour in electrical activity from pancreatic $\beta$-cell. Horm. Metab. Res. Suppl. 10, 100–107.

Atwater, I., Rosario, L., Rojas, E., 1983. Properties of the Ca-activated $K^+$ channel in pancreatic $\beta$-cells. Cell Calcium 4, 451–461.

Barbosa, R. M., Silva, A., Tomé, A., Stamford, J., Santos, R., Rosário, L., 1998. Control of pulsatile 5-HT/insulin secretion from single mouse pancreatic islets by intracellular calcium dynamics. J. Physiol. 510, 135–143.

Beauvois, M. C., Merezak, C., Jonas, J. C., Ravier, M. A., Henquin, J. C., Gilon, P., 2006. Glucose-induced mixed $[Ca^{2+}]_c$ oscillations in mouse $\beta$-cells are controlled by the membrane potential and the SERCA3 $Ca^{2+}$-ATPase of the endoplasmic reticulum. Am. J. Physiol. Cell Physiol. 290, C1503–C1511.

Bensoussan, A., Lions, J., Papanicolaou, G., 2002. Asymptotic analysis for periodic structures. North Holland, New York.

Bergsten, P., Grapengiesser, E., Gylfe, E., Tengholm, A., Hellman, B., 1994. Synchronous oscillations of cytoplasmic $Ca^{2+}$ and insulin release in glucose-stimulated pancreatic islets. J. Biol. Chem. 269, 8749–8753.

Berman, N., Chou, H. F., Berman, A., Ipp, E., 1993. A mathematical model of oscillatory insulin secretion. Am. J. Physiol. 264, R839–R851.

Bertram, R., Previte, J., Sherman, A., Kinard, T. A., Satin, L. S., 2000. The phantom burster model for pancreatic $\beta$-cells. Biophys. J. 79, 2880–2892.

Bertram, R., Satin, L., Zhang, M., Smolen, P., Sherman, A., 2004. Calcium and glycolysis mediate multiple bursting modes in pancreatic islets. Biophys. J. 87, 3074–3087.

Bertram, R., Sherman, A., 2004a. A calcium-based phantom bursting model for pancreatic islets. Bull. Math. Biol. 66, 1313–1344.

Bertram, R., Sherman, A., 2004b. Filtering of calcium transients by the endoplasmic reticulum in pancreatic $\beta$-cells. Biophys. J. 87, 3775–3785.

Bertram, R., Smolen, P., Sherman, A., Mears, D., Atwater, I., Martin, F., Soria, B., 1995. A role for calcium release-activated current (CRAC) in cholinergic modulation of electrical activity in pancreatic $\beta$-cells. Biophys. J. 68, 2323–2332.

Bertuzzi, F., Davalli, A. M., Nano, R., Socci, C., Codazzi, F., Fesce, R., Di Carlo, V., Pozza, G., Grohovaz, F., 1999. Mechanisms of coordination of $Ca^{2+}$ signals in pancreatic islet cells. Diabetes 48, 1971–1978.

Bokvist, K., Eliasson, L., Ammälä, C., Renström, E., Rorsman, P., 1995. Co-localization of L-type $Ca^{2+}$ channels and insulin-containing secretory granules and its significance for the initiation of exocytosis in mouse pancreatic B-cells. EMBO J. 14, 50–57.

Borghans, J., de Boer, R., Segel, L., 1996. Extending the quasi-steady state approximation by changing variables. Bull. Math. Biol. 58, 43–63.

Briggs, G. E., Haldane, J. B. S., 1925. A note on the kinetics of enzyme action. Biochem. J. 19, 338–339.

Brissova, M., Fowler, M. J., Nicholson, W. E., Chu, A., Hirshberg, B., Harlan, D. M., Powers, A. C., 2005. Assessment of human pancreatic islet architecture and composition by laser scanning confocal microscopy. J. Histochem. Cytochem. 53, 1087–1097.

Cabrera, O., Berman, D. M., Kenyon, N. S., Ricordi, C., Berggren, P.-O., Caicedo, A., 2006. The unique cytoarchitecture of human pancreatic islets has implications for islet cell function. Proc. Natl. Acad. Sci. 103, 2334–2339.

Calabrese, A., Zhang, M., Serre-Beinier, V., Caton, D., Mas, C., Satin, L. S., Meda, P., 2003. Connexin 36 controls synchronization of $Ca^{2+}$ oscillations and insulin secretion in MIN6 cells. Diabetes 52, 417–424.

Cao, D., Lin, G., Westphale, E. M., Beyer, E. C., Steinberg, T. H., 1997. Mechanisms for the coordination of intercellular calcium signaling in insulin-secreting cells. J. Cell. Sci. 110, 497–504.

Chay, T. R., 1997. Effects of extracellular calcium on electrical bursting and intracellular and luminal calcium oscillations in insulin secreting pancreatic $\beta$-cells. Biophys. J. 73, 1673–1688.

Chay, T. R., Kang, H. S., 1988. Role of single-channel stochastic noise on bursting clusters of pancreatic $\beta$-cells. Biophys. J. 54, 427–435.

Chay, T. R., Keizer, J., 1983. Minimal model for membrane oscillations in the pancreatic $\beta$-cell. Biophys. J. 42, 181–190.

Chen, L., Koh, D. S., Hille, B., 2003. Dynamics of calcium clearance in mouse pancreatic $\beta$-cells. Diabetes 52, 1723–1731.

Chou, H.-F., Ipp, E., 1990. Pulsatile insulin secretion in isolated rat islets. Diabetes 39, 112–117.

Corkey, B. E., Deeney, J. T., Yaney, G. C., Tornheim, K., Prentki, M., 2000. The role of long-chain fatty acyl-CoA esters in $\beta$-cell signal transduction. J. Nutr. 130, 299S–304S.

Cortassa, S., Aon, M. A., Marban, E., Winslow, R. L., O'Rourke, B., 2003. An integrated model of cardiac mitochondrial energy metabolism and calcium dynamics. Biophys. J. 84, 2734–2755.

De Vries, G., Sherman, A., 2000. Channel sharing in pancreatic $\beta$-cells revisited: Enhancement of emergent bursting by noise. J. Theor. Biol. 207, 513–530.

De Vries, G., Sherman, A., 2001. From spikers to bursters via coupling: Help from heterogeneity. Bull. Math. Biol. 63, 371–391.

Düfer, M., Haspel, D., Krippeit-Drews, P., Aguilar-Bryan, L., Bryan, J., Drews, G., 2004. Oscillations of membrane potential and cytosolic $Ca^{2+}$ concentration in $SUR1^{-/-}$ beta cells. Diabetologia 47, 488–498.

Eddlestone, G. T., Goncalves, A., Bangham, J., 1984. Electrical coupling between cells in islets of Langerhans from mouse. J. Membr. Biol. 77, 1–14.

Eto, K., Tsubamoto, Y., Terauchi, Y., Sugiyama, T., Kishimoto, T., Takahashi, N., Yamauchi, N., Kubota, N., Murayama, S., Aizawa, T., Akanuma, Y., Aizawa, S., Kasai, H., Yazaki, Y., Kadowaki, T., 1999. Role of NADH shuttle system in glucose-induced activation of mitochondrial metabolism and insulin secretion. Science 283, 981–985.

Fisher, R. A., 1937. The wave of advance of advantageous genes. Ann. Eugen. 7, 355–369.

Fransson, U., Rosengren, A. H., Schuit, F. C., Renström, E., Mulder, H., 2006. Anaplerosis via pyruvate carboxylase is required for the fuel-induced rise in the ATP:ADP ratio in rat pancreatic islets. Diabetologia 49, 1578–1586.

Gilon, P., Arredouani, A., Gailly, P., Gromada, J., Henquin, J. C., 1999. Uptake and release of $Ca^{2+}$ by the endoplasmic reticulum contribute to the oscillations of the cytosolic $Ca^{2+}$ concentration triggered by $Ca^{2+}$ influx in the electrically excitable pancreatic B-cell. J. Biol. Chem. 274, 20197–20205.

Gilon, P., Ravier, M., Jonas, J., Henquin, J., 2002. Control mechanisms of the oscillations of insulin secretion in vitro and in vivo. Diabetes 51, S144–S151.

Goforth, P., Bertram, R., Khan, F., Zhang, M., Sherman, A., Satin, L., 2002. Calcium-activated $K^+$ channels of mouse $\beta$-cells are controlled by both store and cytoplasmic $Ca^{2+}$: Experimental and theoretical studies. J. Gen. Physiol. 120, 307–322.

Goodner, C., Hom, F., Koerker, D., 1982. Hepatic glucose production oscillates in synchrony with the islet secretory cycle in fasting rhesus monkeys. Science 215, 1257–1260.

Goodner, C., Koerker, D., Stagner, J., Samols, E., 1991. In vitro pancreatic hormonal pulses are less regular and more frequent than in vivo. Am. J. Physiol. Endocrinol. Metab. 260, E422–E429.

Grodsky, G., Landahl, H., Curry, D., Bennett, L., 1970. A two-compartmental model for insulin secretion. Adv. Metab. Disord. 1, 45–50.

Grodsky, G. M., 1972. A threshold distribution hypothesis for packet storage of insulin and its mathematical modeling. J. Clin. Invest. 51, 2047–2059.

Göpel, S. O., Kanno, T., Barg, S., Eliasson, L., Galvanovskis, J., Renström, E., Rorsman, P., 1999a. Activation of $Ca^{2+}$-dependent $K^+$ channels contributes to rhythmic firing of action potentials in mouse pancreatic $\beta$ cells. J. Gen. Physiol. 114, 759–770.

Göpel, S. O., Kanno, T., Barg, S., Galvanovskis, J., Rorsman, P., 1999b. Voltage-gated and resting membrane currents recorded from B-cells in intact mouse pancreatic islets. J. Physiol. 521, 717–728.

Haspel, D., Krippeit-Drews, P., Aguilar-Bryan, L., Bryan, J., Drews, G., Düfer, M., 2005. Crosstalk between membrane potential and cytosolic $Ca^{2+}$ concentration in beta cells from $Sur1^{-/-}$ mice. Diabetologia 48, 913–921.

Hellman, B., Dansk, H., Grapengiesser, E., 2004. Pancreatic $\beta$-cells communicate via intermittent release of ATP. Am. J. Physiol. Endocrinol. Metab. 286, E759–E765.

Henquin, J.-C., 2000. Triggering and amplifying pathways of regulation of insulin secretion by glucose. Diabetes 49, 1751–1760.

Henri, V., 1901a. Recherches sur la loi de l'action de la sucrase. C. R. Hebd. Acad. Sci. 133, 891–899.

Henri, V., 1901b. Über das Gesetz der Wirkung des Invertins. Z. Phys. Chem. 39, 194–216.

Henri, V., 1902. Théorie générale de l'action de quelques diastases. C. R. Hebd. Acad. Sci. 135, 916–919.

Hollingdal, M., Juhl, C., Pincus, S., Sturis, J., Veldhuis, J., Polonsky, K., Pørksen, N., Schmitz, O., 2000. Failure of physiological plasma glucose excursions to entrain high-frequency pulsatile insulin secretion in type 2 diabetes. Diabetes 49, 1334–1340.

Jonkers, F. C., Jonas, J.-C., Gilon, P., Henquin, J.-C., 1999. Influence of cell number on the chracteristics and synchrony of $Ca^{2+}$ oscillations in clusters of mouse pancreatic islet cells. J. Physiol. 520, 839–849.

Jung, S., Kauri, L., Qian, W., Kennedy., R., 2000. Correlated oscillations in glucose consumption, oxygen consumption, and intracellular free $Ca^{2+}$ in single islets of Langerhans. J. Biol. Chem. 275, 6642–6650.

Kanno, T., Rorsman, P., Göpel, S., 2002. Glucose-dependent regulation of rhythmic action potential firing in pancreatic $\beta$-cells by $K_{ATP}$-channel modulation. J. Physiol. 545, 501–507.

Keizer, J., Magnus, G., 1989. ATP-sensitive potassium channel and bursting in the pancreatic beta cell. A theoretical study. Biophys. J. 56, 229–242.

Khoo, S., Gibson, T. B., Arnette, D., Lawrence, M., January, B., McGlynn, K., Vanderbilt, C. A., Griffen, S. C., German, M. S., Cobb, M. H., 2004. MAP kinases and their roles in pancreatic beta-cells. Cell Biochem. Biophys. 40, 191–200.

Kinard, T., De Vries, G., Sherman, A., Satin, L., 1999. Modulation of the bursting properties of single mouse pancreatic $\beta$-cells by artificial conductances. Biophys. J. 76, 1423–1435.

Kindmark, H., Köhler, M., Arkhammar, P., Efendic, S., Larsson, O., Linder, S., Nilsson, T., Berggren, P. O., 1994. Oscillations in cytoplasmic free calcium concentration in human pancreatic islets from subjects with normal and impaired glucose tolerance. Diabetologia 37, 1121–1131.

Kindmark, H., Köhler, M., Brown, G., Bränström, R., Larsson, O., Berggren, P. O., 2001. Glucose-induced oscillations in cytoplasmic free $Ca^{2+}$ concentration precede oscillations in mitochondrial membrane potential in the pancreatic $\beta$-cell. J. Biol. Chem. 276, 34530–34536.

Kindmark, H., Köhler, M., Nilsson, T., Arkhammar, P., Wiechel, K. L., Rorsman, P., Efendic, S., Berggren, P. O., 1991. Measurements of cytoplasmic free $Ca^{2+}$ concentration in human pancreatic islets and insulinoma cells. FEBS Lett. 291, 310–314.

Krippeit-Drews, P., Düfer, M., Drews, G., 2000. Parallel oscillations of intracellular calcium activity and mitochondrial membrane potential in mouse pancreatic B-cells. Biochem. Biophys. Res. Commun. 267, 179–183.

Kulkarni, R. N., 2004. The islet $\beta$-cell. Int. J. Biochem. Cell Biol. 36, 365–371.

Kwan, E., Gaisano, H., 2005. Glucagon-like peptide 1 regulates sequential and compound exocytosis in pancreatic islet $\beta$-cells. Diabetes 54, 2734–2743.

Lang, D., Matthews, D., Peto, J., Turner, R., 1979. Cyclic oscillations of basal plasma glucose and insulin concentrations in human beings. N. Engl. J. Med. 301, 1023–1027.

Larsson, O., Kindmark, H., Bränström, R., Fredholm, B., Berggren, P. O., 1996. Oscillations in $K_{ATP}$ channel activity promote oscillations in cytoplasmic free $Ca^{2+}$ concentration in the pancreatic $\beta$ cell. Proc. Natl. Acad. Sci. 93, 5161–5165.

Liu, Y. J., Tengholm, A., Grapengiesser, E., Hellman, B., Gylfe, E., 1998. Origin of slow and fast oscillations of $Ca^{2+}$ in mouse pancreatic islets. J. Physiol. 508, 471–481.

Longo, E. A., Tornheim, K., Deeney, J., Varnum, B., Tillotson, D., Prentki, M., Corkey, B., 1991. Oscillations in cytosolic free $Ca^{2+}$, oxygen consumption, and insulin secretion in glucose-stimulated rat pancreatic islets. J. Biol. Chem. 266, 9314–9319.

Luciani, D. S., 2004. Oscillations of cytosolic $Ca^{2+}$ and metabolism studied in murine pancreatic islets. Ph.D. thesis, Department of Physics, Technical University of Denmark.

Luciani, D. S., Misler, S., Polonsky, K. S., 2006. $Ca^{2+}$ controls slow NAD(P)H oscillations in glucose-stimulated mouse pancreatic islets. J. Physiol. 572, 379–392.

MacDonald, M. J., Fahien, L. A., Brown, L. J., Hasan, N. M., Buss, J. D., Kendrick, M. A., 2005. Perspective: Emerging evidence for signaling roles of mitochondrial anaplerotic products in insulin secretion. Am. J. Physiol. Endocrinol. Metab. 288, E1–E15.

MacDonald, M. J., Fahien, L. A., Buss, J. D., Hasan, N. M., Fallon, M. J., Kendrick, M. A., 2003. Citrate oscillates in liver and pancreatic beta cell mitochondria and in INS-1 insulinoma cells. J. Biol. Chem. 278, 51894–51900.

Magnus, G., Keizer, J., 1997. Minimal model of $\beta$-cell mitochondrial $Ca^{2+}$ handling. Am. J. Physiol. 273, C717–C733.

Magnus, G., Keizer, J., 1998a. Model of $\beta$-cell mitochondrial calcium handling and electrical activity. I. Cytoplasmic variables. Am. J. Physiol. Cell Physiol. 274, C1158–C1173.

Magnus, G., Keizer, J., 1998b. Model of $\beta$-cell mitochondrial calcium handling and electrical activity. II. Mitochondrial variables. Am. J. Physiol. Cell Physiol. 274, C1174–C1184.

Mao, C., Berman, N., Roberts, K., Ipp., E., 1999. Glucose entrainment of high-frequency plasma insulin oscillations in control and type 2 diabetic subjects. Diabetes 48, 714–721.

Martin, F., Soria, B., 1996. Glucose-induced $[Ca^{2+}]_i$ oscillations in single human pancreatic islets. Cell Calcium 20, 409–414.

Matschinsky, F. M., Glaser, B., Magnuson, M. A., 1998. Pancreatic $\beta$-cell glucokinase: closing the gap between theoretical concepts and experimental realities. Diabetes 47, 307–315.

McCormack, J. G., Halestrap, A. P., Denton, R. M., 1990. Role of calcium ions in regulation of mammalian intramitochondrial metabolism. Physiol. Rev. 70, 391–425.

Meissner, H., 1976. Electrophysiological evidence for coupling between beta cells of pancreatic islets. Nature 262, 502–504.

Meissner, H. P., Schmelz, H., 1974. Membrane potential of beta-cells in pancreatic islets. Pflügers Arch. 351, 195–206.

Michaelis, L., Menten, M. L., 1913. Die Kinetik der Invertinwirkung. Biochem. Z. 49, 333–369.

Miura, Y., Henquin, J. C., Gilon, P., 1997. Emptying of intracellular $Ca^{2+}$ stores stimulates $Ca^{2+}$ entry in mouse pancreatic $\beta$-cells by both direct and indirect mechanisms. J. Physiol. 503, 387–398.

Nadal, A., Quesada, I., Soria, B., 1999. Homologous and heterologous asynchronicity between identified $\alpha$-, $\beta$- and $\delta$-cells within intact islets of Langerhans in the mouse. J. Physiol. 517, 85–93.

Niki, I., Niwa, T., Yu, W., Budzko, D., Miki, T., Senda, T., 2003. $Ca^{2+}$ influx does not trigger glucose-induced traffic of the insulin granules and alteration of their distribution. Exp. Biol. Med. 228, 1218–1226.

Nilsson, T., Schultz, V., Berggren, P. O., Corkey, B. E., Tornheim, K., 1996. Temporal patterns of changes in ATP/ADP ratio, glucose 6-phosphate and cytoplasmic free $Ca^{2+}$ in glucose-stimulated pancreatic $\beta$-cells. Biochem. J. 314, 91–94.

O'Connor, M., Landahl, H., Grodsky, G., 1980. Comparison of storage- and signal-limited models of pancreatic insulin secretion. Am. J. Physiol. 238, R378–R389.

Orci, L., 1985. The insulin factory: a tour of the plant surroundings and a visit to the assembly line. The Minkowski lecture 1973 revisited. Diabetologia 28, 528–546.

Palti, Y., David, G. B., Lachov, E., Mida, Y. H., Schatzberger, R., 1996. Islets of Langerhans generate wavelike electric activity modulated by glucose concentration. Diabetes 45, 595–601.

Pernarowski, M., 1994. Fast subsystem bifurcations in a slowly varying Liénard system exhibiting bursting. SIAM J. Appl. Math. 54, 814–832.

Pørksen, N., 2002. The in vivo regulation of pulsatile insulin secretion. Diabetologia 45, 3–20.

Pørksen, N., Grofte, T., Greisen, J., Mengel, A., Juhl, C., Veldhuis, J., Schmitz, O., Rossle, M., Vilstrup, H., 2002. Human insulin release processes measured by intraportal sampling. Am. J. Physiol. Endocrinol. Metab. 282, E695–E702.

Pørksen, N., Juhl, C., Hollingdal, M., Pincus, S., Sturis, J., Veldhuis, J., Schmitz, O., 2000. Concordant induction of rapid in vivo pulsatile insulin secretion by recurrent punctuated glucose infusions. Am. J. Physiol. Endocrinol. Metab. 278, E162–E170.

Pørksen, N., Nyholm, B., Veldhuis, J., Butler, P., Schmitz, O., 1997. In humans at least 75% of insulin secretion arises from punctuated insulin secretory bursts. Am. J. Physiol. Endocrinol. Metab. 273, E908–E914.

Quesada, I., Martin, F., Soria, B., 2000. Nutrient modulation of polarized and sustained submembrane $Ca^{2+}$ microgradients in mouse pancreatic islet cells. J. Physiol. 525, 159–167.

Ravier, M. A., Guldenagel, M., Charollais, A., Gjinovci, A., Caille, D., Sohl, G., Wollheim, C. B., Willecke, K., Henquin, J. C., Meda, P., 2005. Loss of connexin36 channels alters $\beta$-cell coupling, islet synchronization of glucose-induced $Ca^{2+}$ and insulin oscillations, and basal insulin release. Diabetes 54, 1798–1807.

Rinzel, J., 1985. Bursting oscillations in an excitable membrane model. In: Sleeman, B., Jarvis, R. (Eds.), Ordinary and Partial Differential Equations. Springer-Verlag, New York, pp. 304–316.

Ritzel, R. A., Veldhuis, J., Butler, P., 2003. Glucose stimulates pulsatile insulin secretion from human pancreatic islets by increasing secretory burst mass: dose-response relationships. J. Clin. Endocrinol. Metab. 88, 742–747.

Ritzel, R. A., Veldhuis, J., Butler, P., 2006. The mass, but not the frequency, of insulin secretory bursts in isolated human islets is entrained by oscillatory glucose exposure. Am. J. Physiol. Endocrinol. Metab. 290, E750–E756.

Rizzuto, R., Bernardi, P., Pozzan, T., 2000. Mitochondria as all-round players of the calcium game. J. Physiol. 529, 37–47.

Rocheleau, J. V., Remedi, M. S., Granada, B., Head, W. S., Koster, J. C., Nichols, C. G., Piston, D. W., 2006. Critical role of gap junction coupled $K_{ATP}$ channel activity for regulated insulin secretion. PLoS Biol. 4, e26.

Rocheleau, J. V., Walker, G. M., Head, W. S., McGuinness, O. P., Piston, D. W., 2004. Microfluidic glucose stimulation reveals limited coordination of intracellular $Ca^{2+}$ activity oscillations in pancreatic islets. Proc. Natl. Acad. Sci. 101, 12899–12903.

Rorsman, P., Eliasson, L., Renström, E., Gromada, J., Barg, S., Göpel, S., 2000. The cell physiology of biphasic insulin secretion. News Physiol. Sci. 15, 72–77.

Rorsman, P., Trube, G., 1986. Calcium and delayed potassium currents in mouse pancreatic $\beta$-cells under voltage clamp conditions. J. Physiol. (London) 374, 531–550.

Santos, R. M., Rosario, L. M., Nadal, A., Garcia-Sancho, J., Soria, B., Valdeolmillos, M., 1991. Widespread synchronous $[Ca^{2+}]_i$ oscillations due to bursting electrical activity in single pancreatic islets. Pflügers Arch. 418, 417–422.

Schuit, F., De Vos, A., Farfari, S., Moens, K., Pipeleers, D., Brun, T., Prentki, M., 1997. Metabolic fate of glucose in purified islet cells. Glucose-regulated anaplerosis in $\beta$ cells. J. Biol. Chem. 272, 18572–18579.

Segel, L., 1988. On the validity of the steady state assumption of enzyme kinetics. Bull. Math. Biol. 50, 579–593.

Segel, L. A., Slemrod, M., 1989. The quasi steady-state assumption: a case study in pertubation. SIAM Rev. 31, 446–477.

Sha, L., Westerlund, J., Szurszewski, J. H., Bergsten, P., 2001. Amplitude modulation of pulsatile insulin secretion by intrapancreatic ganglion neurons. Diabetes 50, 51–55.

Sherman, A., 1997. Calcium and membrane potential oscillations in pancreatic $\beta$-cells. In: Othmer, H. G., Adler, F. R., Lewis, M. A., Dallon, J. C. (Eds.), Case Studies in Mathematical Modeling – Ecology, Physiology and Cell Biology. Prentice Hall, New Jersey, pp. 199–217.

Sherman, A., Rinzel, J., 1991. Model for synchronization of pancreatic $\beta$-cells by gap junction coupling. Biophys. J. 59, 547–559.

Sherman, A., Rinzel, J., Keizer, J., 1988. Emergence of organized bursting in clusters of pancreatic $\beta$-cells by channel sharing. Biophys. J. 54, 411–425.

Smolen, P., Rinzel, J., Sherman, A., 1993. Why pancreatic islets burst but single $\beta$ cells do not. The heterogeneity hypothesis. Biophys. J. 64, 1668–80.

Song, H., McIntyre, S., Shah, H., Veldhuis, J., Hayes, P., Butler, P., 2000. Direct measurement of pulsatile insulin secretion from the portal vein in human subjects. J. Clin. Endocrinol. Metab. 85, 4491–4499.

Song, S., Kjems, L., Ritze, R., McIntyre, S., Johnson, M., Veldhuis, J., Butler, P., 2002. Pulsatile insulin secretion by human pancreatic islets. J. Clin. Endocrinol. Metab. 87, 213–221.

Stagner, J. I., Samols, E., Weir, G. C., 1980. Sustained oscillations of insulin, glucagon, and somatostatin from the isolated canine pancreas during exposure to a constant glucose concentration. J. Clin. Invest. 65, 939–942.

Sturis, J., Cauter, E. V., Blackman, J., Polonsky, K., 1991. Entrainment of pulsatile insulin secretion by oscillatory glucose infusion. J. Clin. Invest 87, 439–445.

Sturis, J., Knudsen, C., O'Meara, N., Thomsen, J., Mosekilde, E., Cauter, E. V., Polonsky, K., 1995. Phase-locking regions in a forced model of slow insulin and glucose oscillations. Chaos 5, 193–199.

Sturis, J., O'Meara, N., Shapiro, E., Blackman, J., Tillil, H., Polonsky, K., Cauter, E. V., 1993. Differential effects of glucose stimulation upon rapid pulses and ultradian oscillations of insulin secretion. J. Clin. Endocrinol. Metab. 76, 895–901.

Sturis, J., Pugh, W., Tang, J., Ostrega, D., Polonsky, J., Polonsky, K., 1994. Alterations in pulsatile insulin secretion in the Zucker diabetic fatty rat. Am. J. Physiol. Endocrinol. Metab. 267, E250–E259.

Tamarina, N. A., Kuznetsov, A., Rhodes, C. J., Bindokas, V. P., Philipson, L. H., 2005. Inositol (1,4,5)-trisphosphate dynamics and intracellular calcium oscillations in pancreatic $\beta$-cells. Diabetes 54, 3073–3081.

Tengholm, A., Hellman, B., Gylfe, E., 2001. The endoplasmic reticulum is a glucose-modulated high-affinity sink for $Ca^{2+}$ in mouse pancreatic $\beta$-cells. J. Physiol. 530, 533–540.

Tornheim, K., 1997. Are metabolic oscillations responsible for normal oscillatory insulin secretion. Diabetes 46, 1375–1380.

Tornheim, K., Lowenstein, J. M., 1974. The purine nucleotide cycle. IV. Interactions with oscillations of the glycolytic pathway in muscle extracts. J. Biol. Chem. 249, 3241–3247.

Tsaneva-Atanasova, K., Zimliki, C. L., Bertram, R., Sherman, A., 2006. Diffusion of calcium and metabolites in pancreatic islets: killing oscillations with a pitchfork. Biophys. J. 90, 3434–3446.

Tzafriri, A. R., 2003. Michaelis-Menten kinetics at high enzyme concentrations. Bull. Math. Biol. 65, 1111–1129.

Valdeolmillos, M., Gomis, A., Sanchez-Andres, J., 1996. In vivo synchronous membrane potential oscillations in mouse pancreatic beta-cells: lack of co-ordination between islets. J. Physiol. 493, 9–18.

Valdeolmillos, M., Santos, R., Contreras, D., Soria, B., Rosario, L., 1989. Glucose-induced oscillations of intracellular $Ca^{2+}$ concentration resembling bursting electrical activity in single mouse islets of langerhans. FEBS Lett. 259, 19–23.

Westerlund, J., Bergsten, P., 2001. Glucose metabolism and pulsatile insulin release from isolated islets. Diabetes 50, 1785–1790.

Westermark, P., 2005. Models of the metabolism of the pancreatic $\beta$-cell. Ph.D. thesis, Royal Institute of Technology, Stockholm, Sweden.

Wild, S., Roglic, G., Green, A., Sicree, R., King, H., 2004. Global prevalence of diabetes: estimates for the year 2000 and projections for 2030. Diabetes Care 27, 1047–1053.

Zhang, M., Goforth, P., Bertram, R., Sherman, A., Satin., L., 2003. The $Ca^{2+}$ dynamics of isolated mouse $\beta$-cells and islets: Implications for mathematical models. Biophys. J. 84, 2852–2870.

Zimliki, C. L., Mears, D., Sherman, A., 2004. Three roads to islet bursting: emergent oscillations in coupled phantom bursters. Biophys. J. 87, 193–206.